The Economic Case for Bulk Energy Storage in Transmission Systems with High Percentages of Renewable Resources

Final Project Report

Power Systems Engineering Research Center

Empowering Minds to Engineer
the Future Electric Energy System

The Economic Case for Bulk Energy Storage in Transmission Systems with High Percentages of Renewable Resources

Final Project Report

Project Team

Ward Jewell, Project Leader
Zhouxing Hu

Wichita State University

Nan Li
Kory W. Hedman
John R. Ruggiero
Gerald T. Heydt

Arizona State University

PSERC Publication 14-9

September 2014

For information about this project, contact

Ward Jewell
Wichita State University
334 Wallace Hall
Wichita, KS 67260
Ward.Jewell@wichita.edu
316-978-6340

Power Systems Engineering Research Center

The Power Systems Engineering Research Center (PSERC) is a multi-university Center conducting research on challenges facing the electric power industry and educating the next generation of power engineers. More information about PSERC can be found at the Center's website: http://www.pserc.org.

For additional information, contact:

Power Systems Engineering Research Center
Arizona State University
527 Engineering Research Center
Tempe, Arizona 85287-5706
Phone: 480-965-1643
Fax: 480-965-0745

Notice Concerning Copyright Material

Acknowledgements

This is the final report for the Power Systems Engineering Research Center (PSERC) research project titled "The Economic Case for Bulk Energy Storage in Transmission Systems with High Percentages of Renewable Resources" (project T-48). We express our appreciation for the support provided by PSERC's industry members and by the National Science Foundation under the Industry / University Cooperative Research Center program.

The authors also thank the industry advisors for this project: Simon Chiang (PG&E), Paul Myrda (EPRI), Donald Pelley (SRP), James Price (CAISO), James Sehwail (ITC), Jonathan Stahlhut (formerly at Arizona Public Service), Janos Toth (formerly at BC Hydro), Shimo Wang (formerly at Southern California Edison), Helen Whittaker (BC Hydro), and Bill Winston (Southern Company).

Executive Summary

As the penetrations of variable renewable generation increase, the uncertainty and variability of wind and solar require more resources to follow the variations. Energy storage technologies may become an increasing part of the resource mix for following renewables. This final report addresses several aspects of the economics of using energy storage, optimized for multiple objectives, including cost, congestion, and emissions, for increasing levels of renewable resource penetration. The report is presented in three parts.

Part I: Optimal Generation Expansion Planning with Integration of Variable Renewables and Bulk Energy Storage Systems

Pumped-hydroelectric energy storage has proven to be valuable as bulk energy storage for energy arbitrage coordinating with conventional thermal generators. New storage technologies, including compressed air and batteries, are in various stages of development and commercialization. In the future grid there are uncertainties in terms of modeling and optimization in assessing the value of bulk energy storage coordinating less with thermal generators and more with wind and solar. Moreover, the price of natural gas is predicted to have large variations in the next several decades and new environmental regulations may cause the retirement of some coal fired generators. A generation planning model is therefore needed that comprehensively models wind, solar and energy storage under multiple scenarios of energy and environmental policies and natural gas prices.

Part I of this report presents such an optimal planning model using a multi-period optimization formulation that is implemented in MATPOWER's open source extensible optimal power flow structure. Storage, wind, and several types of energy storage are available as resources in the generation expansion model. Storage at multiple locations is co-optimized in hourly simulations using four representative weeks for the four seasons.

Policies are modeled as prices and limits to CO_2 emissions and subsidies to renewable generation. In a cap-and-trade scenario, CO_2 prices begin at 36.94 $/ton and rise to 60.18 $/ton over a 20-year planning horizon. Subsidies for wind and solar were modeled as 22 $/MWh. An emissions cap of 1,000 lbs/MWh was modeled for new generation. A low natural gas price scenario has the price rising from 2.5 $/MBtu to 5.86 $/MBtu over a 20-year planning horizon. A high gas price scenario rises to 14 $/MBtu.

The planning model was first tested and verified on a 3-bus test system. This model was then applied to 20-year planning horizon on a reduced 240-bus model of the Western Electric Coordinating Council (WECC) system. The planning model developed in this work is now available for use on other systems by system planners and researchers.

The implementation of the planning model on the WECC system yielded some interesting results:

- In every case simulated except the case with high natural gas prices, no renewable subsidies, and no price or limit on CO_2 emissions, coal-fired generation is retired. Retirements are greatest for the low gas price case with CO_2 price and renewable incentives.

- Significant natural gas fired generation is retired in every case. New gas-fired generation is built in the low gas price cases with CO_2 price and renewable incentives, and with no incentives or CO_2 price.
- Nuclear generation is built in all of the high-gas-price cases.
- A significant amount of new wind generation is installed in every case except the case with low natural gas prices, no renewable subsidies, and no price or limit on CO_2 emissions.
- Solar generation is installed in the cases with a CO_2 price, regardless of gas price, and in the high-gas-price case when there is a limit on CO_2 emissions for new generation.
- Energy storage is installed in every case except the low-gas-price case when there is a limit on CO_2 emissions for new generation.
- Average production costs, which includes fuel, O&M, emissions, and subsidies, increase in all cases over the first ten years. They then decrease over the second ten years for the cases with high gas prices. They remain approximately constant for the low gas price cases with either a price or limit on CO_2 emissions. Average production costs continue to increase for the case with low gas prices and no price or limit on CO_2 emissions.
- CO_2 emissions only decrease over the 20-year horizon in the cases with a price on CO_2 emissions.

Future research will revise the environmental regulations to those that have been proposed by the US Environmental Protection Agency in 2014. Transmission expansion will be added to the planning model. Unit commitment, ramp rates, and market models will also be added, along with a corresponding reductions from one-hour to shorter simulation time steps.

Part II: The Cost and Benefit of Bulk Energy Storage in the Arizona Power Transmission System

This research project addresses the issue of making an economic case for bulk energy storage in electric power systems. Bulk energy storage has often been suggested for large scale electric power systems in order to levelize load; store energy when it is inexpensive and discharge energy when it is expensive; potentially defer transmission and generation expansion; and provide for generation reserve margins. As renewable energy resource penetration increases, the uncertainty and variability of wind and the diurnal variation of solar energy may be alleviated or even eliminated through the utilization of bulk energy storage technologies. The research considers the utilization of *pumped hydro storage* as the main, credible, and economically feasible energy storage technology. The focus in this report is on pumped hydro energy storage.

The research describes how pumped hydro storage can improve (reduce) operating costs. The intent is to partially justify the commission of large scale pumped hydro energy storage through the reduction of operating costs. Note that the design of large scale storage is done in the long term, typically longer than five years, and economic operation of power systems is done in real time. These are disparate time horizons. The proposal described in

this report is for the design of large scale energy storage using the benefits of economic operation as a partial justification of the project.

From a technical approach, the quadratic programming function in MATLAB termed QUADPROG is used to simulate an economic dispatch that includes energy storage. A program is created that utilizes quadratic programming to analyze various cases using a 2010 summer peak load from the Arizona transmission system, part of the Western Electricity Coordinating Council (WECC). The MATLAB program is used to test the Arizona test bed with a low level of energy storage to study how the storage power limit affects several optimization outputs such as the system wide operating costs. Very high levels of energy storage (e.g., up to 13.6 GW) are then augmented to see how high level energy storage affects peak shaving, load factor, operating costs and other system applications. Various constraint relaxations are made to analyze why the applications tested eventually are limited by the facilities available. That is, the transmission and storage assets that are the operational constraints are identified. Pumped hydro energy storage has two main specifications: power (i.e., MW) and energy (i.e., MWh). The ratio of these two quantities, E/P, is discussed in the report and levels of E/P from 1.0 to 10.0 are discussed and evaluated.

The authors identify strengths and weaknesses of the quadratic programming approach. The main strength is that the software needed for the analysis of efficacy of pumped hydro is readily available and no special data requirements are present. Also, results indicate that the quadratic programming approach gives an accurate answer within the bounds of approximate modeling of active power losses in the transmission system (e.g., about 3 – 5%). The 'DC power flow study' assumption is made for the analysis and the report assesses the accuracy of this approach: there is good / excellent agreement with alternative analyses which use more elaborate models. Advice and experience in the use of QUADPROG are given in an appendix for potential users of these software tools.

A main conclusion of the study is that bulk energy storage using pumped hydro, even in a desert environment such as Arizona, may offer an economically feasible technology to levelize the system load, and thereby reduce operating costs. The analysis includes published data on the costs of development of pumped hydro. Typical figures for Arizona are found to be a reduction of operating costs in the 4 to 8% range is feasible.

The documentation and test cases focus on the potential for six pumped hydro sites in Arizona and adjacent southern California and Nevada:

- Longview Pumped Storage located in Big Chino Valley, Yavapai county, southeast of Seligman, AZ
- Table Mountain Pumped Storage located in Mohave county near the towns of Peach Springs and Kingman, AZ
- Eagle Mountain Pumped Storage located in San Bernardino county, northeast of Palm Springs, CA
- Lake Mead located in Clark county Nevada and Mohave county Arizona, near Boulder City, NV
- Glen Canyon in Coconino county Arizona near Page, AZ
- Horse Mesa in Maricopa county near Globe, AZ.

A discussion of the non-electrical issues in the development of these sites is given. These include regulatory, environmental, and sociological issues. The logical next step in bringing this technology to fruition would be a full scale study of both the economic dispatch and unit commitment of a large scale system with pumped hydro as bulk energy storage. The analysis contained in this study is considered to be preliminary because the following issues are modeled and considered only in approximate terms: the cost to develop a site for pumped hydro; national and international issues relating to water usage (e.g., from the Colorado River); accounting for water losses; accounting for long term environmental phenomena (e.g., drought); approvals required from Native American communities; public acceptance of such proposals (which are by their nature large-scale and publically visible); availability of funds from commercial, private, and state and national sources for the required investment.

From a technical point of view, the detailed inclusion of active power losses in the transmission system were modeled only in an approximate way, and this too deserves greater scrutiny. Suggestions for further work are given in Chapter 6 of the report.

Part III: Economic Assessment of Energy Storage in Systems with High Levels of Renewable Resources

Part III of the final report evaluates the attractiveness of bulk energy storage technologies under high renewable penetration levels. Different energy storage technologies are studied to assess the economic case of energy storage in systems with high renewable penetration levels and identify their appropriate applications.

This report reviews the different types of bulk energy storage technologies. The characteristics of different energy storage technologies, such as power and energy capacities, ramping capabilities, and other characteristics are described. Based on the characteristics and costs, the appropriate applications are identified and summarized for each type of energy storage technology.

To study the economical case for bulk energy storage in transmission system with high renewable penetration, a stochastic unit commitment model is proposed to identify the impact of increasing renewable penetration on the attractiveness of bulk energy storage in comparison to conventional generators. By using a stochastic unit commitment model, both the energy shifting and fast ramping capabilities of energy storage technologies are captured endogenously. The results show that conventional generators will see lower profits and, hence, produce lower returns on investments as the renewable penetration levels increase. However, by integrating energy storage into the system, the average costs of conventional generators decrease, while fewer generators are dispatched in the system with higher capacity factors compared to the cases without energy storage. As such, energy storage improves the utilization of the conventional generators in the system.

Besides providing bulk energy management services, the benefits of energy storage in procuring regulation services in real-time operation are also evaluated in this report. A two-stage optimization framework is used to demonstrate the attractiveness of energy storage in providing high quality of regulation services. By having energy storage in the

system, the system reliability and the capability to integrate high penetration levels of renewable energy are enhanced.

While most forms of energy storage are still considered to be too expensive and not competitive with conventional generators, it is shown in the report that the attractiveness of conventional generators decreases as the renewable penetration levels increase whereas the attractiveness of energy storage increases with the increase in renewable resources. As a result, with new energy storage technologies, it is expected that there will be a break point where energy storage becomes competitive with conventional generating resources, resulting in increased deployment of energy storage technologies.

Project Publications:

N. Li and K. W. Hedman, "Economic assessment of energy storage in systems with high levels of renewable resources," *IEEE Transactions on Sustainable Energy*, accepted for publication.

N. Li and K.W. Hedman, "Economic assessment of bulk energy storage in transmission system with high penetration of renewable energy," *IEEE PES General Meeting 2013*, Vancouver, BC, CA.

J. Ruggiero, G. T. Heydt, "Making the economic case for bulk energy storage in electric power systems," *Proc. North American Power Symposium*, October 2013, Manhattan, KS.

Zhouxing Hu, Ward T. Jewell, Optimal generation expansion planning with integration of variable renewables and bulk energy storage systems. *IEEE Conference on Technologies for Sustainability*, Portland, Oregon, August 2013.

Haneen Aburub, Ward T. Jewell, "Assessment of the use of a wholesale grid state indicator in the distribution system," *Frontiers of Power Conference*, Stillwater, Oklahoma, October 2013.

Haneen Aburub, Ward T. Jewell, James E. Price, "Assessment of the use of CAISO wholesale grid state indicator to schedule storage," *North American Power Symposium*, Manhattan, Kansas, October 2013

Student Theses:

Zhouxing Hu, *Optimal generation expansion planning with integration of variable renewables and bulk energy storage systems*, PhD Dissertation, Wichita State University, Wichita KS, May, 2013.

John R. Ruggiero, "*The cost and benefit of bulk energy storage in the Arizona power transmission system,"* Masters Thesis, Arizona State University, Tempe, AZ, December, 2013.

Part I

Optimal Generation Expansion Planning with Integration of Variable Renewables and Bulk Energy Storage Systems

Zhouxing Hu
Ward Jewell

Wichita State University

For information about Part I, contact

Ward Jewell
Wichita State University
334 Wallace Hall
Wichita, KS 67260
Ward.Jewell@wichita.edu
316-978-6340

Power Systems Engineering Research Center

The Power Systems Engineering Research Center (PSERC) is a multi-university Center conducting research on challenges facing the electric power industry and educating the next generation of power engineers. More information about PSERC can be found at the Center's website: http://www.pserc.org.

For additional information, contact:

Power Systems Engineering Research Center
Arizona State University
527 Engineering Research Center
Tempe, Arizona 85287-5706
Phone: 480-965-1643
Fax: 480-965-0745

Table of Contents

List of Figures

List of Tables

1. Introduction

The research presented in this report is from the PhD dissertation of Dr. Zhouxing Hu [1].

1.1 Research Objectives

The key objective of this research is to develop a generation planning model that considers variable outputs of wind and solar generators and explores optimal investments of energy storage in multiple locations. This research also analyzes the results through application of two test systems—a small 3-bus test system and a reduced 240-bus Western Electric Coordinating Council model. The outcome of this research—a proposed optimal planning model—could be utilized to analyze other power systems for policy-regulated planning or even operation purposes. The general conclusions derived from the test systems may provide limited references to the resource planning engineers and policies makers.

The following tasks are covered in this work:

- Construct the 240-bus WECC model in MATPOWER[1] from raw data, including profiles of loads and renewables, and parameters of the transmission system and generators, provided by Price and Goodin [1].
- Run 24-hour operation simulations using alternating current optimal power flow (AC OPF) to study the impact of increased wind and solar generation to some major transmission paths, as well as locational marginal pricing (LMP) at the pumped-hydro storage buses in the WECC system.
- Develop a methodology that co-optimizes the operations of EES at multiple locations, and extend it to the generation planning model.
- Develop a generation planning model that includes the objective function, variables to be optimized, equality and inequality constraints, and variable bounds.
- Collect the average or levelized cost data of each generator including EES by fuel type or by technology.
- Incorporate the price of CO_2 emissions [3] and renewable incentives into the model inputs according to each study scenario.
- Use MATPOWER's extensible standard direct current optimal power flow (DC OPF) framework to solve the optimal planning problem.
- Analyze the planning results, including assessing the value of different energy storage technologies and the impact of multiple regulatory policies.

[1]An open-source MATLAB-based power system simulation package developed by Zimmerman et al. at Cornell University.

The planning model of this research is relatively detailed concerning energy storage optimization and therefore simplifies other operation criteria, for example, using DC OPF to solve the planning model, applying a linear cost model to all generators except for natural gas, and using an estimated limit for each transmission line where interface flow limits are ignored. When applying regulatory policies to this planning model in order to evaluate the impacts to the test systems, only two of them, in terms of CO_2 emissions and renewable incentives, are used in this research. However, other policies, if designated, are possible to be incorporated into this optimal planning model as well by modifying the data inputs.

1.2 Report Organization

Section 2 of this report introduces the prospective impact of energy regulatory policies, wind and solar generation, and value of EES in the future grid. Section 3 reviews existing algorithms of EES modeling and optimization, generation planning, and simulation platforms. The AC OPF-based operation test of the WECC model to demonstrate the potential value of EES is discussed in Section 4. Section 5 presents the proposed optimal planning model and cost model for the planning simulations in this research. Section 6 introduces two test systems that were prepared for the planning study and analyzes the numerical results. Section 7 presents some general conclusions and future work.

2. Review of Literature

This chapter reviews the literature related to energy storage planning and operation, generation investment planning, and power-flow study tools. Section 2.1 compares the modeling and optimization of bulk energy storage with thermal generators and with renewables. The planning model of generation investment is investigated in Section 2.2. Finally, Section 2.3 introduces the simulation tools and some popular optimization solvers related to this work.

2.1 Modeling and Optimization of Bulk Energy Storage

2.1.1 Coordination with Thermal Units

Essentially, EES could be imagined as a virtual transmission line connected between different time periods of one location rather than a real transmission line connected between two different locations. With EES, a virtual transmission line, surplus (usually cheaper) energy at one period could be transported to another time period when energy is more valuable. With this unique feature, the modeling and optimization of energy storage need to consider the power flow status of multiple time periods in order to find the best solution.

Optimization of EES has been studied for more than a half century, beginning with an early study of hydrothermal coordination in 1963 [4]. Hydroelectric generator scheduling and pumped-hydro scheduling could be similar since both have storage (energy capacity) limitations among certain operating time intervals. Several algorithms have been developed to coordinate pumped-hydro storage and thermal generators, e.g., the gradient method [5], λ-γ iteration [5], dynamic programming [6], and Lagrangian relaxation [7]. However, these algorithms could be more difficult to apply to a more detailed model that has large capacities of renewables and multiple EES units. Replacement of thermal plants by renewable generators causes traditional hydro-thermal coordination to be less applicable in future power systems because approximated cubic or quadratic heat rate curves, on which existing algorithms are based, do not apply to renewable generators such as wind and solar. Thus, a new EES scheduling algorithm needs to be developed.

2.1.2 Coordination with Wind Turbines

In the future grid, the scheduling of EES needs to focus more on renewable generation and the transmission system for at least two reasons: (1) renewable generators are given market preference and often have a lower operating cost than fossil-fuel-fired generators, especially with the added cost of GHG emissions, and (2) transmission congestion or variation occurs more frequently when handling generation from variable renewable resources like wind and solar. The power output of wind and solar units often has more variations and larger deviations compared to traditional generators and other renewables. Operational issues such as deficit of operating reserve, ramping capability, or voltage support are also involved. In general, coordinating with a high penetration level of

renewables, an EES unit could make a profit or reduce the system operating cost, not only through energy arbitrage and congestion relief by participating in an energy market but also through ancillary services or other applications by participating in an ancillary market [8]. Assessing the value of EES providing ancillary service is beyond the scope of this work.

In a future grid dominated by wind and solar generators, which are modeled using flat operation curves instead of cubic or quadratic heat rate curves of thermal units, bulk energy storage appears to be less valuable by operating for energy arbitrage. However, through a short-term operation study of a wind-enriched power system, a larger variation of LMP [9], which measures the marginal value of energy at certain locations, is usually observed. It reveals the potential value of energy arbitrage in such a system by alleviating the variation of wind output and relieving transmission congestion. To relieve transmission congestion, the scheduling of EES will be more economic by following the LMP, also referred to as nodal pricing, at the storage location [10]. In this approach, transmission loss and congestion need to be considered for energy storage scheduling, and therefore, AC OPF would be recommended. The LMP will have much larger and more frequent variance if there is a high penetration of variable renewable generation on the system. For example, in real practice, if wind generators produce more energy than a day-ahead or hour-ahead forecast, LMP will decrease drastically, and vice versa. Another situation is, when a forecast showing that wind will blow hard during the current off-peak period (midnight) but drop off during next the peak period, some slow-start generators (e.g., coal) would prefer to operate at their minimum output instead of completely shutting down during the current off-peak period, and wind generation has to be curtailed to meet the power balancing requirement (generation plus transmission loss equal to demand), which causes a significant drop of LMP (sometimes LMP even drops below zero at buses where wind generations are curtailed). EES operation could be designed intuitively as collecting energy at low-LMP periods and releasing it during high-LMP periods. This is the ideal situation whereby EES could make a profit by providing energy services as a participant in the energy market.

Recently, a multi-period optimization approach was proposed [11] [12] to modeling the energy arbitrage operation and optimal planning of EES coordinating with increasing renewables, especially wind. The methodology of modeling and scheduling EES slightly varies depending on the specific research scope, e.g., operation or planning. The planning study of EES needs to determine the sizes, both power and energy capacity, and even locations of energy storage and analyze their long-term investment, while the operation study uses pre-defined sizes and locations for energy storage and analyzes their short-term impacts. In long-term planning studies, a stochastic model of renewables and load are often adopted, and the effect of a transmission system is often ignored [11] [13]. These studies often focus on the modeling of long-term pricing and the investment rate of generators and EES units, and only utilize economic dispatch or DC OPF to deal with the linear model of the aggregated power system. Operational studies of EES often employ a deterministic model with a detailed AC transmission system and respect the power system reliability [12]. Other studies using a deterministic reliable operation model without considering the effect of the transmission system could be a compromise between

operation and planning [14] [15]. However, it is notable from [15] that the security-constrained unit commitment is considered in the optimization model and solved by using mixed-integer programming.

In this research, the modeling of EES is similar to the planning model proposed by Oh [11], but it is combined with generation expansion planning modeling, which is discussed in Section 2.2. The optimization of the planning problem utilizes linear lossless DC OPF, deterministic renewable and load profiles, and multi-period optimization.

2.2 OPF-Based Generation Planning

Generation expansion planning and transmission expansion planning are two major planning topics in the power industry. Generally, these two topics should be combined because each one closely depends on the other. However, transmission planning is not considered in this research because either of the problems alone is a complex optimization model, and the major scope of this work is on planning for resource and energy storage.

The generation planning model in this work is developed based on the planning algorithm used in the PSERC project M-24 [16] with the SuperOPF planning tool [17]. SuperOPF is a MATLAB-based tool box that further utilizes MATPOWER's extensible OPF structure [18] to deal with stochastic, contingency-based, security-constrained OPF problems. The two-stage solver in the SuperOPF tool is capable of solving both day-ahead and real-time optimal operation problems. The first stage solver, *c3sopf*, can be easily modified to *c3sopfi* for the generation investment planning problem (details can be found in Appendix B in the User's Manual), and it has been tested and applied to the policy-regulated resource planning model developed in the M-24 project.

Except the planning model of energy storage, the generation planning model for wind and solar will be different from the model proposed in the PSERC project, where all wind generators share an identical capacity factor (as well as solar generators) and ignore the hour-by-hour variations. This is a typical planning algorithm that normally applies to traditional generators and is even applicable to hydro units. However, applying this algorithm to wind and solar is found to be unrealistic. It will enrich the value of wind and solar because their outputs are treated as dispatchable, both up and down, during the OPF simulation. In this work, hourly maximum outputs of wind and solar, referred to as profiles, will be applied to each wind and solar unit and will vary according to their locations. The negative side of this modeling algorithm is that the size of the problem is expanded with more simulated time points.

Moreover, the chronologic cost analysis with renewables developed by Poonpun [19] and a CO_2 emissions-incorporated OPF algorithm developed by Shao [3] will be applied to the operations study and the optimal planning model, respectively, in this research.

2.3 Simulation Tool

In order to solve the OPF-based multi-period optimization problem, MATPOWER will be primarily used as the simulation tool. The whole optimization model proposed in this research is solved by utilizing MATPOWER's extensible OPF structure. The key portion of the generation planning model applied in the SuperOPF tool is rebuilt in MATPOWER to achieve faster processing speed because SuperOPF is built on top of MATPOWER and is repurposed to solve the generation investment problem.

MATPOWER's extensible standard OPF structure [18] is as follows:

Objective function:

$$\min_{x,z} \; f(x) + f_u(x,z) \tag{2.1}$$

Constraints:

$$g(x) = 0 \tag{2.2}$$

$$h(x) \leq 0 \tag{2.3}$$

$$x_{min} \leq x \leq x_{max} \tag{2.4}$$

$$l \leq \mathrm{A}\begin{bmatrix} x \\ z \end{bmatrix} \leq u \tag{2.5}$$

$$z_{min} \leq z \leq z_{max} \tag{2.6}$$

For standard AC OPF, the optimization vector x consists of voltage angle θ, voltage magnitude V_m, active power injection P_g, and reactive power injection Q_g. The term $f(x)$ denotes the cost of active and reactive power output of all generators. The term $f_u(x,z)$ could be defined by users and is optional. In a standard AC OPF model, equation (2.2) represents the energy balance constraint; equation (2.3) is the inequality constraint or power flow constraint for each transmission line; equation (2.4) represents the bounded variables θ, V_m, P_g, and Q_g; and equations (2.5) and (2.6) construct the additional variables and constraints associated with the user-defined objective function. For a standard DC OPF, V_m and Q_g are dropped, and transmission losses are ignored.
In contrast to the previously used PowerWorld simulator, MATPOWER utilizes a standard OPF solver rather than primal linear programming (LP) OPF [20]. The LP OPF linearizes non-linear constraints before solving the model. This process improves the solution time but loses accuracy. Upper and lower bus voltage limits are not able to be added to PowerWorld's LP OPF model. PowerWorld is a commercial tool with predefined functions and add-ons whose source code is completely sealed in order to prevent users from adding more variables and constraints into the OPF model. MATPOWER is open source, and its extensible OPF architecture [18] provides more flexibility for modifying the optimization model based on the user's needs. The

MATLAB Interior Point Solver (MIPS) [21] is a powerful nonlinear solver that can be utilized to solve both AC OPF and DC OPF. MATPOWER also has an interface to invoke other powerful nonlinear programming and quadratic programming solvers, e.g., MINOPF [22], TSOPF [23], BPMPD [24], MOSEK [25], CPLEX [26], GUROBI [27], etc., according to different types of optimization models. The sequential hourly simulation of operation study in this work is solved by using the default MIPS, while the long-term planning problem, a much larger one with multi-period optimization and energy-storage model, needs be solved by using more powerful solvers, e.g., GUROBI or CPLEX.

However, MATPOWER, as a power flow study tool, certainly has some drawbacks. It does not have any user-friendly interfaces or windows, which allow input or output data to be sorted easily. Without a one-line diagram display, the power grid parameters and real-time power flow are not easily viewable.

3. Impact of Renewables on WECC System

Before developing the planning study, fundamental analysis of the reduced 240-bus WECC model in terms of AC OPF simulation is necessary to help understand the simulation tool, power network topology, modeling issues, marginal price variations, etc. Details of the WECC model are described in the first section. Section 3.2 introduces the model setup in MATPOWER and discusses some modeling experiences. Section 3.3 provides the numerical results of the WECC model for a 24-hour sequential run using AC OPF. Finally, some discussion is provided in Section 3.4.

3.1 Description of WECC Model

The full network model (FNM) of the WECC coordinated power system is currently not publicly available. The test system of the reduced WECC 240-bus model was provided by Price and Goodin [1] at CAISO. The development of this model was based on a previous 225-bus model for a market operation study [28], where it was extended from a 179-bus model originally built for power system operation analysis [29]. These reduced models were constructed by aggregating the bulk transmission system[2] and generators, and estimating the transmission line parameters at their best effort. Fortunately, the 240-bus model was provided as a validated model for a market study after being verified with the results of the WECC FNM.

The network model of the WECC was received as a raw data file in PTI format [30], the topology of which is displayed in Figure 3.1. The model was first imported into PowerWorld, and the economic dispatch was studied visually by creating a one-line diagram, as shown in Figure 3.2. In order to conduct research in MATPOWER, this WECC model was converted to the MATPOWER format and tailored for operation studies. For example, the interface (i.e., a group of transmission lines connected between two areas) limits could be bounded instead of imposing MVA limits for each transmission line in MATPOWER, but this is not feasible in PowerWorld. System reserves could also be co-optimized with power flow in MATPOWER.

[2]There is no unified definition for a bulk transmission system. Normally, it refers to the transmission system with voltage level of 115 kV or above.

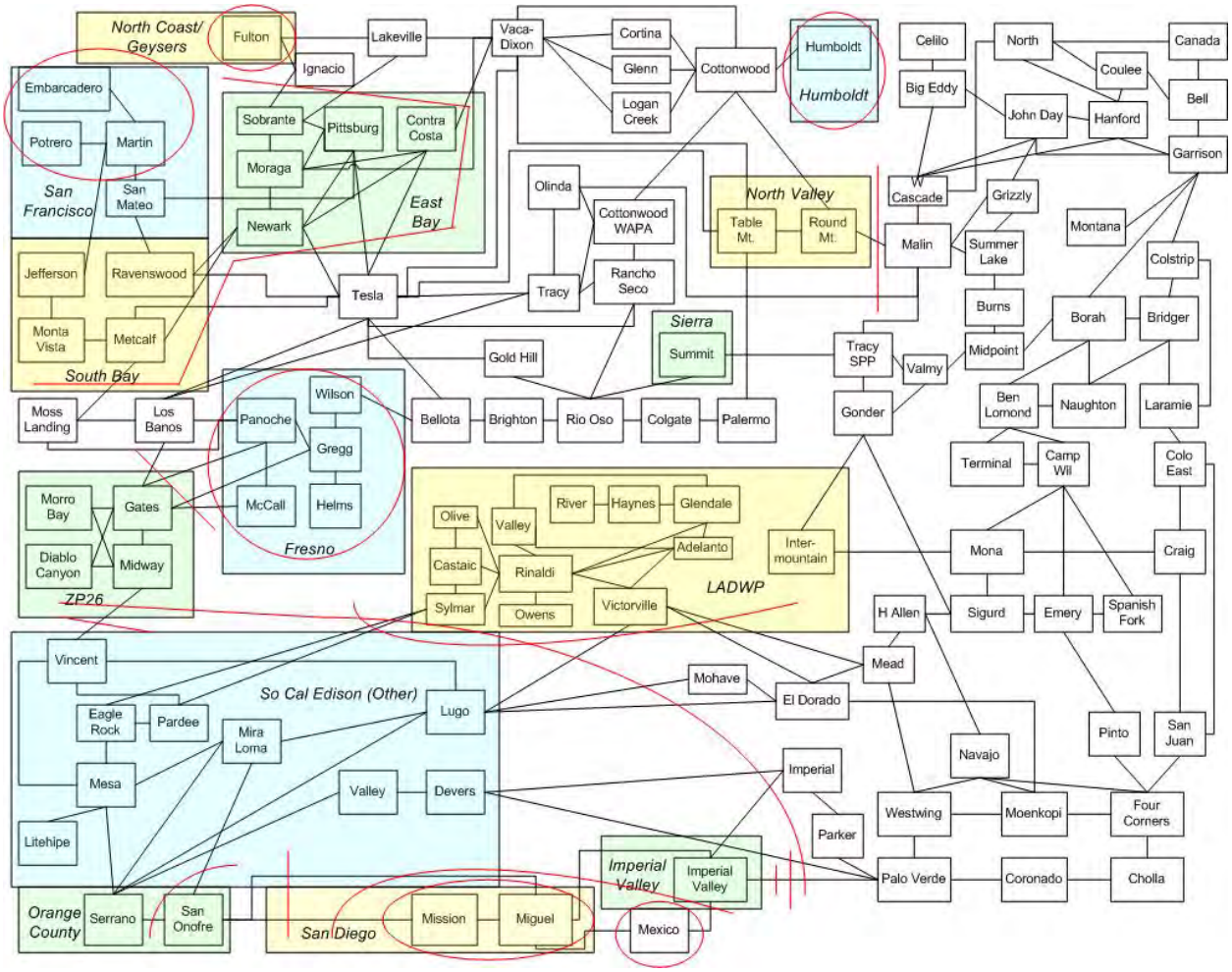

Figure 3.1. Network topology of 240-bus WECC model.

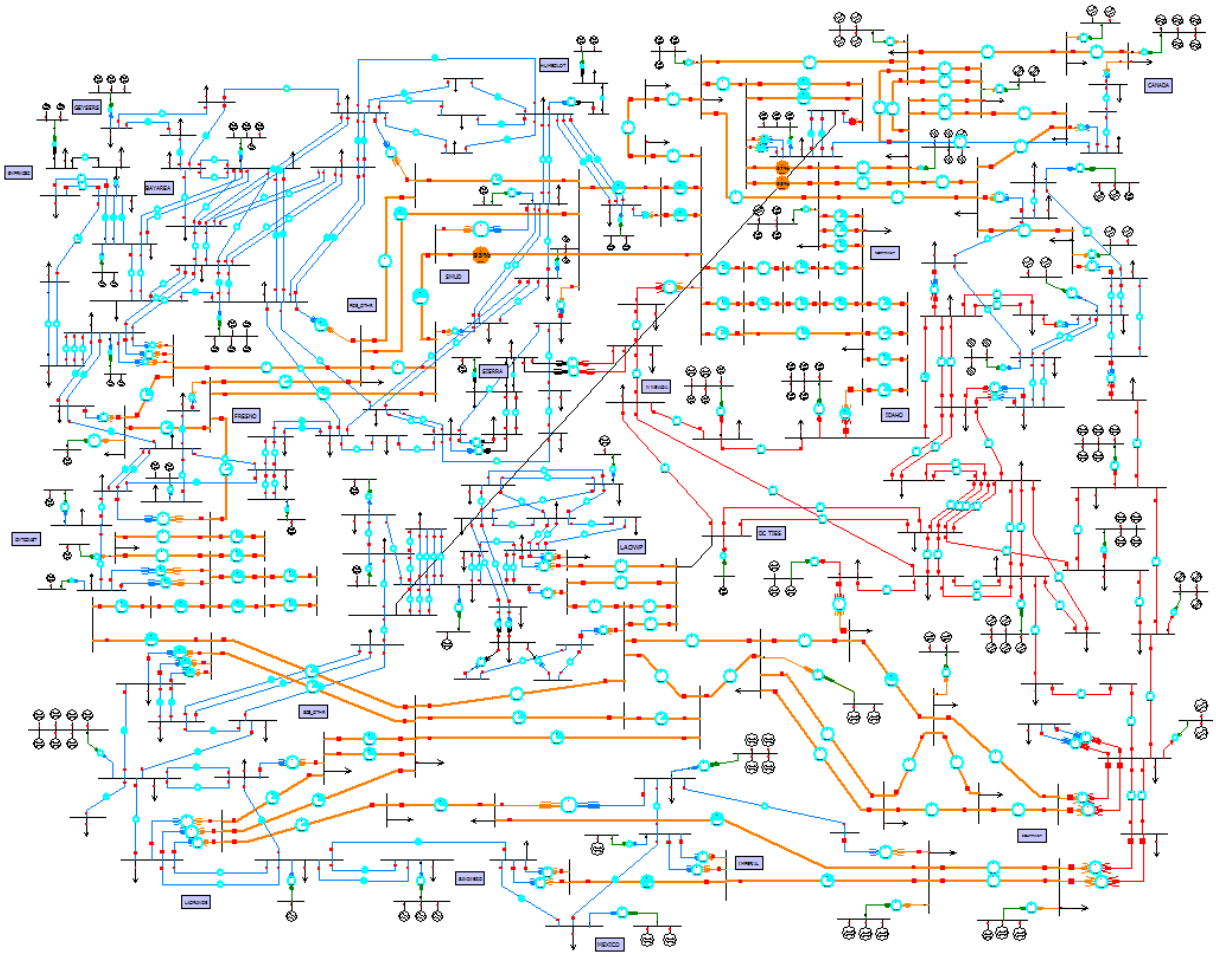

Figure 3.2. One-line diagram of 240-bus WECC model in PowerWorld.

3.2 Model Setup in MATPOWER

The WECC model constructed in MATPOWER is consistent with the settlements of major components as proposed by Price and Goodin [1], except for the added optimization of two high-voltage direct current (HVDC) transmission lines—the Pacific DC Intertie (PDCI) and the Intermountain HVDC (Path 27). Hourly outputs of hydro generators, both coordinating with current renewables and future renewables, are directly applied with the profile data, which is optimized by Price and Goodin [1]. However, in the planning simulation described in the next two chapters, the hydro generators are optimized according to the best investment decision.

Following the PTI file, Bus 3933 "Tesla" is selected as the system reference bus (slack bus). Lower and upper limits of the bus voltages are set at 0.95 and 1.11 *pu*, respectively. Maximum power outputs (P_{max}) of the hydro and renewable generators are imported from hourly profiles. The P_{max} of coal units are set at 85% of maximum capacity, based on average performance of the coal generators. The P_{min} of gas, hydro, and nuclear units are set at 5%, 20%, and 90% of maximum capacity, respectively.

For simplicity in this WECC model, a linear cost model is applied to coal, nuclear, hydro, and renewable generators, with operating costs (linear coefficients) of 16.04, 5, 25, and 5 $/MWh, respectively. Only gas units, with the highest installed capacity by fuel type in the WECC system, have a quadratic cost model. The operating cost of the nuclear, hydro, and renewable generators described above are suggested values from Price and Goodin [1]. The operating costs ($/MWh) of coal and gas generators are calculated by using the fuel price ($/MBTU) multiplied by the heat rate (MBTU/MWh) of each generator. Since heat rate data of coal units in the WECC model is not provided, an annual average operating heat rate of 10.414 MBTU/MWh [32] is assigned to all coal generators in this model. Fuel prices of $1.54/MBTU and $5/MBTU [1] are used for all coal and gas generators, respectively. As a result of this price setting, nuclear and renewable units have top priority to be dispatched, followed by coal, hydro, and gas.

Since thermal limits of all transmission lines are not publicly available, interface (path, corridor) flow limits are suggested to apply to the OPF study. The transmission-constrained interfaces in this model are shown in Figure 3.3. The interface flow is the summation of power flows through a group of transmission lines with a predefined direction. Interface flow often represents a net import to or export from an area or zone. Its limit is derived from a reliability study by operations engineers and is normally lower than the summation of thermal limits of each individual transmission line. Modeling of the transmission system in this study makes a tighter area interchange and looser inner area power flow.

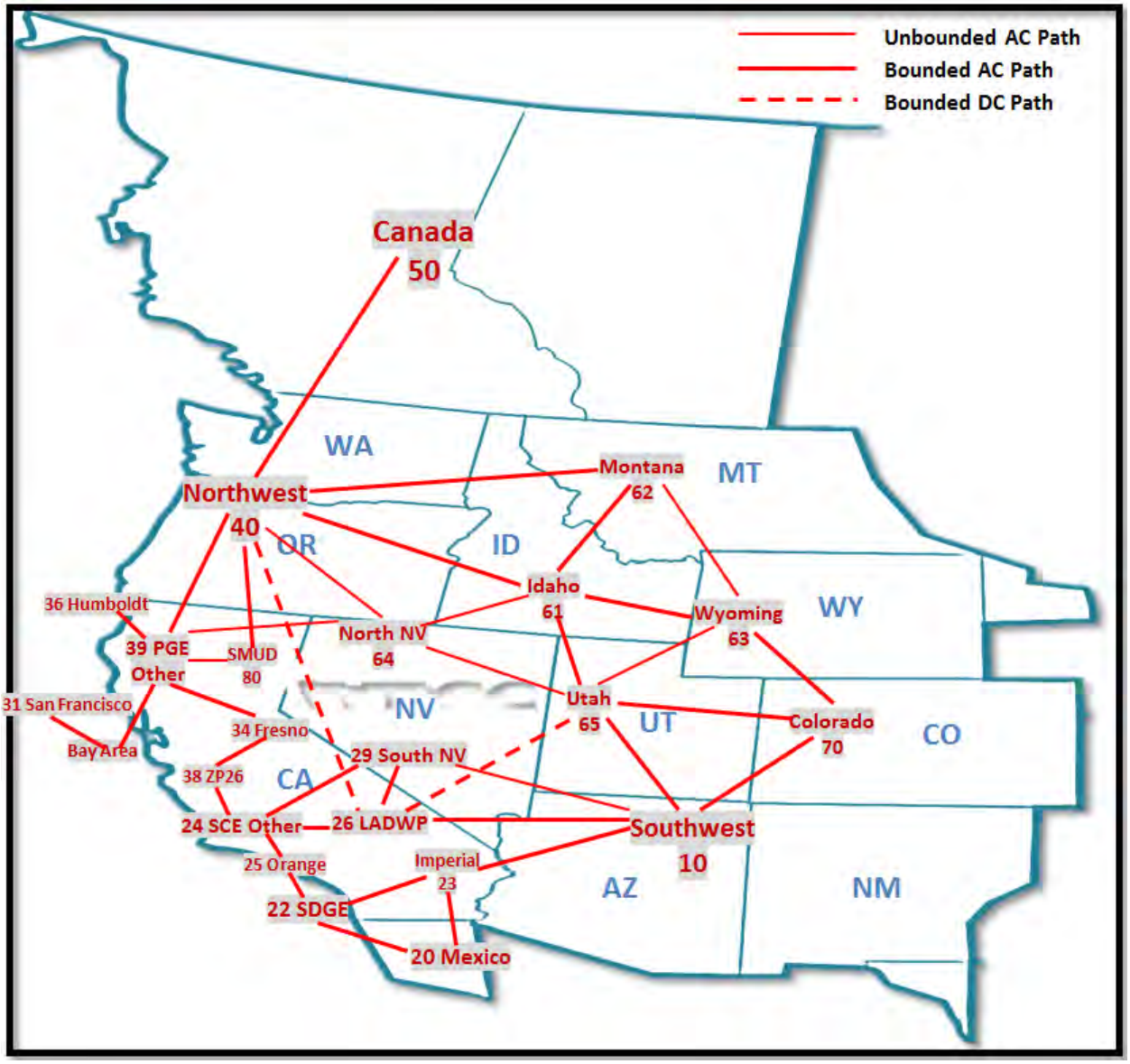

Figure 3.3. Transmission map of WECC 240-bus model.

The reduced 240-bus model is a larger, more-realistic, and detailed model compared to some frequently used small test models, e.g., the IEEE 24-bus reliability test system [31]. It brings more challenges relative to constructing, solving, error checking, and collecting and analyzing results. The specifications, challenges, and suggestions through the model setup for AC OPF operation studies in MATPOWER are summarized as follows:

- 240 Buses: Appropriate voltage range must be assigned for each bus, which could affect the solving time and results of AC OPF. Also, lower and upper voltage limits of each bus can be different.
- 448 Branches: No specific thermal limits are available for all branches including transformers. It is suggested to use interface flow (transmission path or corridor) limits and often reliability limits for the operation study. Two HVDC transmission

lines could be modeled in the lasted version of MATPOWER (v. 4.1) (see User's Manual, Section 6.5.3).

- 145 Generators: Even though hydro generators are optimized in both the base case and the future case according to load and renewables, it is necessary to redo the optimization if a new study scenario is created, for example, further increased renewable generation, less amount of water capacity available for hydro generation, unit commitment with ramp rate and reserve added, etc. Other generators have constant maximum and minimum power output range as specified by Price and Goodin [1].
- Cost: Appropriate cost curves, necessary for all generators, are based on certain study scenarios. The cost curve provided by Price and Goodin [1] is relatively flat for a large portion of the generators, which decreases the benefit of storing electricity and impairs the solver performance. Either generation cost or cycle efficiency of storage, or both, could be modified accordingly to reflect the real values of EES.

3.3 Numerical Study

To test the modeling and OPF solver, a summer day (July 30, 2004) profile is selected to examine the OPF results of this model. All generators are committed online. The load profile is the same for both cases—the first with existing renewable generators and the second with projected future renewables. The generation profile of the base case contains the power output of existing renewable generators and optimized hydro generation, while that of the future case contains the power output of projected future renewable generation and an optimized hydro schedule in the future. There is no restriction or price on CO_2 emissions in this case.

OPF results of 24-hour generation by fuel type in both the base case and the future case are plotted in Figure 3.4. Their comparison shows that generation from gas units decreases as much as 50% due to the increased renewables and almost hits the minimum (93,420 MW) from 2 am to 4 am. With existing renewables, wind and solar (variable) generators have a total capacity of 7,199 MW, but an output of 2,857 ~ 4,519 MW for this daily period. Geothermal, biomass, and small hydro (invariable) generators have a total capacity of 5,145 MW, generating 3,939 ~ 4,078 MW. It is obvious that these "invariable" renewables have a much higher capacity credit and lower output variations. However, they are more resource-limited and therefore expand very slowly compared to wind and solar. In a future profile, the output of invariable renewables is almost the same, but wind and solar generation climbs to 11,559 ~ 19,126 MW, with more observable variations.

In a future case of this study day, generation from variable renewables is negatively correlated with daily demand. It is worse if only considering wind generation because the peak output of solar power is relatively fixed from 12 pm to 5 pm, but wind often blows during the night. In this situation, hydro and gas generators are dispatched almost down to minimum during off-peak hours. If there is more output available from wind with a

lower demand on the system, which likely will occur in the spring or fall, then the output from the coal generators must be lowered or wind generation itself must be curtailed, if transmission is congested.

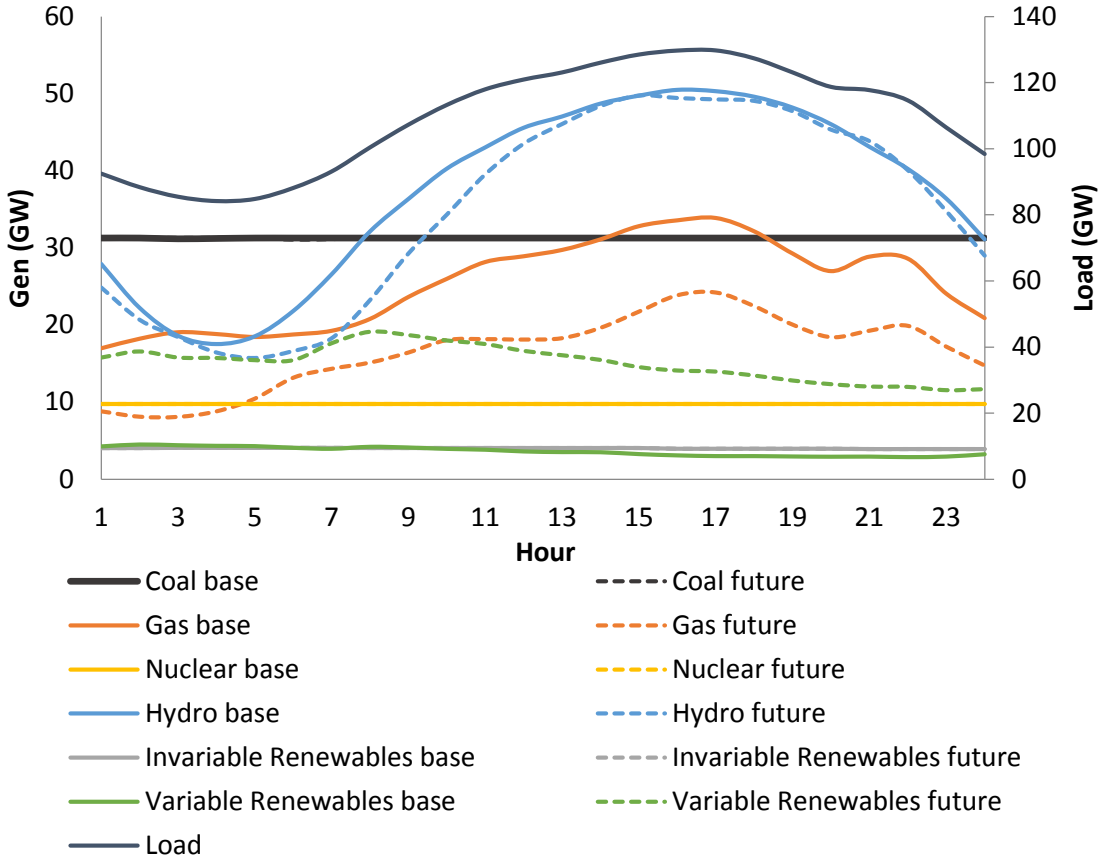

Figure 3.4. Generation dispatch by source type in base case and future case of a summer day (data profile of July 30, 2004).

An increased renewable penetration level leads to decreased LMP with higher deviations in a daily period, as shown in Figure 3.5 and Figure 3.6. LMP is the marginal energy cost with transmission congestion and loss considered at particular location (i.e., bus). Normally, higher LMP indicates insufficient energy, and lower LMP indicates a surplus of energy at that location. This is a good indicator for energy arbitrage by EES. Theoretically, EES makes a profit within an operation cycle if the LMP at charging divided by the LMP at discharging exceeds cycle efficiency. For a particular EES, a higher deviation between lower and higher LMP within a certain period usually provides more profit for an energy-arbitrage operation.

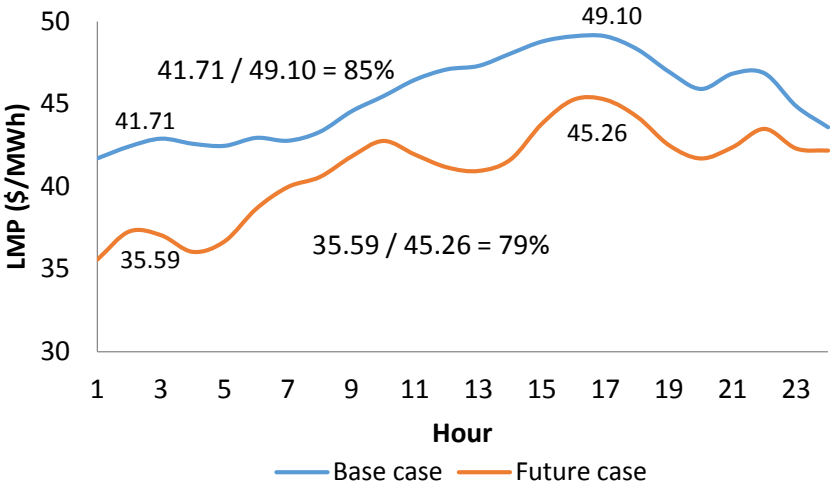

Figure 3.5. LMP at bus 2638.

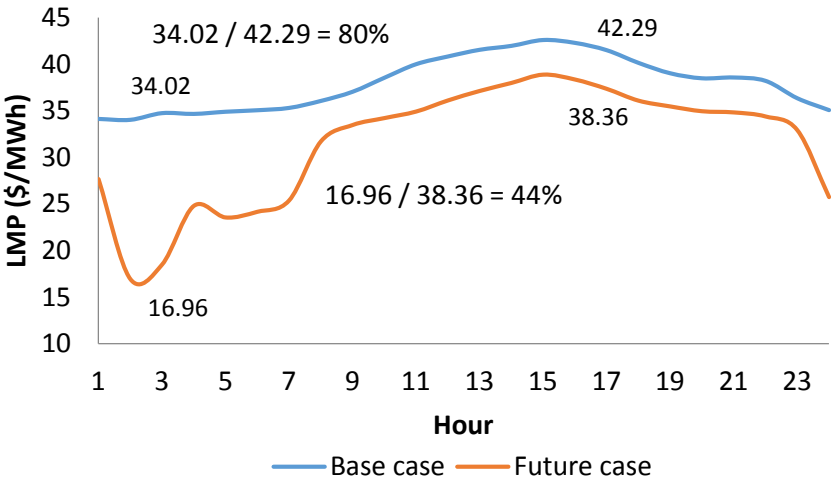

Figure 3.6. LMP at bus 7031.

As shown in both figures, energy arbitrage produces more economic benefits in the future case. For this particular day, pumped-hydro storage at bus 7031, "Colorado East," receives a higher profit in the future case. The LMP at bus 7031 drops as low as 16.96 at midnight because of high wind output and low load in that area (i.e., Colorado).
Figure 3.7 and Figure 3.8 show the results of the impact of future renewables on the interface flow of Southern California Import Transmission (SCIT) and PDCI. SCIT is the largest corridor in this WECC model, containing fifteen 500-kV and three 230-kV AC transmission lines with a reliability limit of 10,000 MW.[3] SCIT connects southern California, including the Los Angeles Department of Water and Power, to northern

[3]The SCIT limit varies with system conditions [1]. It is suggested to use 10,800 MW for June, July, August, and September, and 10,000 MW for a typical week profile.

California via path 26, to the northwest area (Oregon) via PDCI, and to the southwest area (Arizona) via path 46.

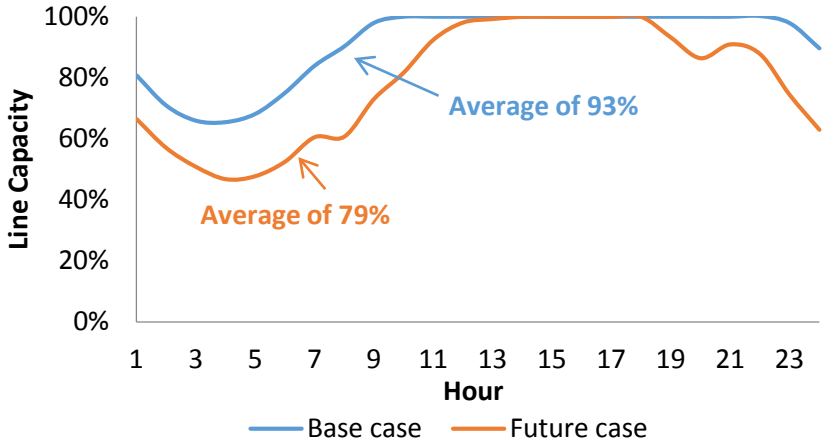

Figure 3.7. Impact of renewables on SCIT import with maximum transmission capacity of 10,000 MW.

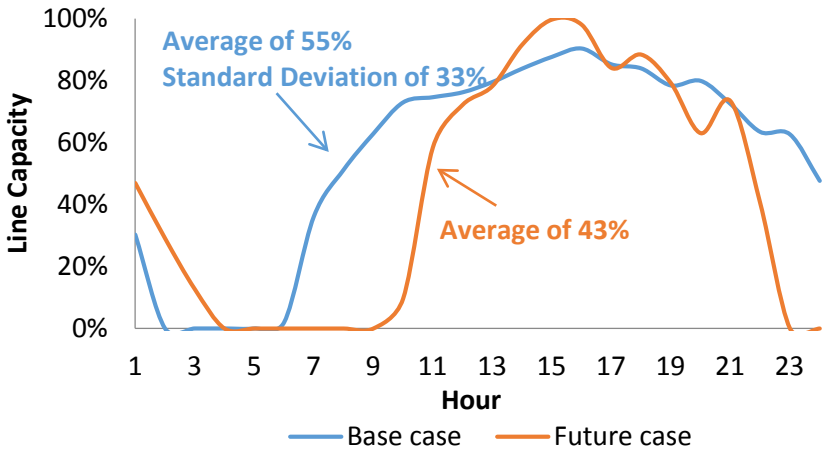

Figure 3.8. Impact of renewables on PDCI with north to south maximum transmission capacity of 3,313 MW.

After analysis, it was found that, as a result of the increased renewable penetration level, the average power transmission level decreases and the deviation increases. However, it is interesting to see that the hours of maximum flow decrease in the future case of SCIT. This is mainly affected by off-peak generation from wind and on-peak generation from solar power at bus 2438 "Mesa" in the Southern California Edison (SCE) footprint.

Other results like daily CO_2 emissions and transmission losses of the WECC model in both cases are listed and compared in Table 3.1. It is worth pointing out that transmission losses are greater in the future case. This is nothing to be concerned about because energy from renewables is cheap and clean. It is better to use the energy rather than curtail it, as long as the system operating cost and CO_2 emissions are lowered.

Table 3.1. OPF Results Comparison for Daily Operation

	Base Case	**Future Case**
Load (GWh)	2,619.2	2,619.2
Renewable penetration level (%)	7	17.5
CO_2 emissions from coal (ton)	746,724.4	746,552.2
CO_2 emissions from gas (ton)	263,616.4	172,029.1
Total CO_2 emissions (ton)	1,010,340.9	918,581.4
Highest LMP of P ($/MWh)	51.27 @ 3301	51.07 @ 3301
Lowest LMP of P ($/MWh)	-21.92 @ 6205	14.60 @ 6205
Highest LMP of Q ($/MWh)	2.75 @ 6104	9.46 @ 5004
Lowest LMP of Q ($/MWh)	-477.3 @ 6235	-53.76 @ 6235
Transmission losses (GWh)	49.4	55.7
Transmission losses (% of generation)	1.85	2.08
Total system operating cost ($ million)	59.2	50.6

3.4 Discussion

With the increased penetration level of renewable energy, mostly wind and solar, the power flow on transmission paths fluctuates more and the usage rate of transmission lines is lowered. Meanwhile, LMP at selected buses experience higher deviations with more wind and solar generation. These observations could be generalized to all buses and transmission lines in the system. The operation analysis of the WECC system provides a hint that energy storage investment is a feasible solution with increased wind and solar penetration in the future grid. The planning study in the next two chapters determines the optimal investment size of EES in selected locations and further analyzes the potential of each technology for bulk storage and impact on the planning model.

4. Modeling Methodology and Data Collection

The planning model begins with this chapter, where formulation of the entire optimization problem and cost parameters that support optimal planning in this research are presented. Section 4.1 describes the construction of the mathematical optimization model that provides optimal operation-based generation expansion planning with EES and hydro optimization. Section 4.2 analyzes the data sources that are used as input parameters of the optimization model.

4.1 Design of Optimization Model

4.1.1 Objective Function

The objective function is to minimize the total cost across the simulated time horizon (*t*), as shown in equation (4.1). The total cost in the optimal operation-based generation expansion planning model here contains variable cost (i.e., C_g^V, including fuel cost and O&M cost) of existing generators (*g*), fixed cost (C_i^F) savings from retired power capacity (R_i) of generators allowed to be retired (*i*); and variable cost (C_j^V), fixed cost (C_j^F), and investment cost (i.e., capital cost recovery, C_j^I) of new generators (*j*) including EES.

$$\min_{\theta_k, P_{ijt}, R_i, I_j, IP_j, IE_j} \left\{ \begin{array}{c} \tau \sum_t C_g^V P_{gt} + \sum_i [C_i^F (P_i^0 - R_i)] + \\ \sum_j \left[\tau \sum_t C_j^V P_{jt} + \left(C_j^I + C_j^F \right) \left(I_j + IP_j + IE_j \right) \right] \end{array} \right\} \tag{4.1}$$

This objective function co-optimizes the hourly operation (i.e., first term), the retirement of generation capacity (i.e., second term), and the operation of optimal-invested capacity (i.e., third term) across the entire planning horizon (*t*). It drives down the total cost by retiring those underused capacities with a higher fixed cost and installing new generators with both lower capital cost and fixed cost. Compared to the objective function used in the PSERC M-24 project (i.e., equation (3.1) on page 47 of the report [16]) this objective function drops the benefit function of demand response (i.e., B_{jk} as expressed in the report) but adds the investment function of energy storage (i.e., IP_j and IE_j in the objective function of equation (4.1).

In MATPOWER, the generator cost function is specified in the *mpc.gencost* struct. It can be expressed in terms of piecewise linear or polynomial. The variable cost C^V ($/MWh) associated with power output and the fixed cost C^F ($/MW) associated with power capacity can be incorporated into either of the two cost models of each generator. For example, the cost of emissions or other penalties could be incorporated into the objective function by adding an extra $/MWh cost to the C^V in the generator cost function, if needed, e.g., CO_2 emissions-incorporated OPF [3].

Other costs associated with user-defined variables (*R*, *I*, *IP*, *IE*), which represent the retired MW capacity, invested MW capacity, invested MW capacity of EES, and invested

MWh capacity of EES, respectively, must be specified in the user-defined cost function. The details of how to add user-defined cost are introduced in Section 5.3.1 of the MATPOWER 4.1 User's Manual.

4.1.2 Variables

The variables in this optimization problem consist of standard variables from MATPOWER's standard AC OPF or DC OPF frame, and user-defined variables that are added in this project using the extended OPF formulation. For faster-solving performance, simulations in this research are based on standard DC OPF with variables θ and P_g, the voltage angle at each generator bus and the power output of each generator, respectively. Voltage magnitude V_m and generator reactive power output Q_g will be dropped to reduce the size of the problem. The user-defined variables added in this research are $R,\ I,\ IP$, and IE, which are vectors with specified upper and lower bounds. Equation (4.2) to equation (4.8) indicate the upper and lower bounds of each variable.

$$\theta_k^{ref} \le \theta_k \le \theta_k^{ref}, \quad k \in [reference\ bus] \tag{4.1}$$

$$\theta_k^{min} \le \theta_k \le \theta_k^{max}, \quad k \notin [reference\ bus] \tag{4.2}$$

$$P_{ij}^{min} \le P_{ij} \le P_{ij}^{max} \tag{4.3}$$

$$R_i^{min} \le R_i \le R_i^{max} \tag{4.4}$$

$$I_j^{min} \le I_j \le I_j^{max} \tag{4.5}$$

$$IP_j^{min} \le IP_j \le IP_j^{max} \tag{4.6}$$

$$IE_j^{min} \le IE_j \le IE_j^{max} \tag{4.7}$$

4.1.3 DC Network Constraints

The standard DC OPF constraints, denoted as equations (2.2) to (2.4) were introduced in Chapter 2. For example, equation (4.9), which enforces power balance in the network, is categorized as the equality constraint in equation (2.2) in the OPF model.

$$\sum_i \sum_j \sum_t P_{ijt} = Total\ Annual\ Demand \tag{4.8}$$

Also, additional constraints are applied to MATPOWER's extensible framework, i.e. constraint equations (2.5) and (2.6), using the callback functions (see Section 6.2 in the MATPOWER 4.1 User's Manual). In this research work, constraints of hydro optimization, generation expansion planning, and energy storage investment are constructed and can be applied to the optimization model separately.

4.1.4 Hydro Optimization Constraints

The constraint used for hydro optimization is written as equation (4.10) which enforces the condition that the total energy output from hydro generators in the simulated time horizon should not exceed the water availability of that period.

$$\sum_t P_t^{hydro} \leq \Delta^{hydro} \sum_t P_t^{hydro,max} \tag{4.9}$$

The water availability is expressed as the total energy capacity of all hydro units multiplied by the capacity factor. To be specific, different capacity factors could be applied to different hydro generators, which require that multiple constraints be added.

4.1.5 Generation Expansion Planning Constraints

Constraints, listed as equations (4.11) to (4.14), are used for generation expansion planning in this optimization model.

$$0 \leq P_{it} + R_i \leq P_i^{max} \tag{4.10}$$

$$P_{jt} \leq \delta_{jt} I_j \tag{4.11}$$

$$\sum I_j^s \leq I^{s,max} \tag{4.12}$$

$$\sum_i \Delta_i R_i \leq \sum_j \Delta_j \left(I_j + IP_j\right) \tag{4.13}$$

Equations (4.11) and (4.12) are constraints of power output from retired generators and invested generators, respectively. In this situation, the results of variable R_i could be any optimal value between $\max[P_i^{min}, R_i^{min}]$ and $\min[P_i^{max}, R_i^{max}]$. In reality, a generator will be retired mostly in terms of an entire unit, which should be considered as a mixed-integer optimization problem. However, when dealing with a heavily reduced power system model with most of the generators aggregated by fuel type and location, e.g., the reduced 240-bus WECC model, it will be much easier to use linear programming method for the generation expansion planning problem without losing much accuracy. For the investment constraint in equation (4.12), δ_{jt} is a vector that reflects the resource availability for each generator *j* at time point *t*. This vector is necessary to represent the hourly variable output of wind and solar. For those generators that are not resource-dependent, δ_{jt} is normally set as 1 for all *t*. Constraint equation (4.13) indicates that the sum of invested generator *j* of fuel type *s* should not exceed the maximum investment allowed for that fuel type. Constraint equation (4.14) enforces the fact that new invested capacity should cover the demand increase and the amount of retired capacity. The capacity factor Δ is considered for each generator according to the fuel type.

Constraint equations (4.11), (4.12), and (4.13) retain similar functions as those developed in the SuperOPF Investment Planning Tool. Constraint equation (4.14) is added to simply ensure the adequacy of resources and reserves. These variables and constraints are

directly defined and added by using MATPOWER's callback functions in order to minimize the computational overheads in terms of both execution time and memory consumption. In SuperOPF, the planning problem solver *c3sopfi* is modified from the day-ahead problem solver *c3sopf* and, therefore, contains more variables and constraints than needed for investment planning simulations. When running *c3sopfi*, those unnecessary variables and constraints are automatically relaxed to eliminate their functions yet generate extra computational overhead.

4.1.6 Energy Storage Optimal Planning Constraints

As stated previously, EES has unique operation features like limited power capacity and energy capacity. To respect these features, all time periods within an operation cycle of the EES should be incorporated into one single model to find the optimal operation schedule of the EES. The user-added *A* matrix in constraint equation (2.5) associated with the storage variables is not as sparse as that with the generation planning variables and, of course, is much larger in size. In other words, if it is applied, the EES model will generate most of the constraints in this optimization model due to the time-related and energy-limited operation feature of EES.

The EES operation-related constraints are listed as equations (4.15) to (4.21).

$$0 \le P_{jt}^{c} \le IP_j \tag{4.14}$$

$$0 \le P_{jt}^{d} \le IP_j \tag{4.15}$$

$$0 \le P_{jt}^{c} \le \frac{IE_j - E_j^{t-1}}{\eta_j^{c}} \tag{4.16}$$

$$0 \le P_{jt}^{d} \le \eta_j^{d} E_j^{t-1} \tag{4.17}$$

$$E_j^{t} = E_j^{t-1} + \eta_j^{c} P_{jt}^{c} - \frac{P_{jt}^{d}}{\eta_j^{d}} \tag{4.18}$$

$$0 \le E_j^{t} \le IE_j \tag{4.19}$$

$$E_j^{T} = E_j^{0} = \alpha IE_j \tag{4.20}$$

Constraint equations (4.15) and (4.16) indicate that the power input (i.e., charge) and the power output (i.e., discharge) at any time period should not exceed the installed power capacity of the EES. Equation (4.17) realizes the fact that charging power should not exceed the amount of empty capacity left from the previous time period. Similarly, equation (4.18) denotes that discharging power should not exceed the amount of energy remain from the previous time period. Equation (4.19) calculates the remaining energy in the EES for each time period. Equation (4.20) is a physical limit of the remaining energy for each time period. In order to maintain a fair economic analysis of energy storage, it is

necessary to implement the binding equation (4.21), whereby the amount of energy left after one operation cycle should be equal to that at the initial status. Among these equality and inequality constraints, equations (4.17), (4.18), (4.19), and (4.21) are cross-period constraints that reflect the operational feature of the EES.

4.1.7 Additional Operation Constraints

There might be other constraints used to represent normal operation conditions. For example, equations (4.22) and (4.23) indicate that conventional hydro generators and natural gas generators often hold a portion of their capacity, 13% and 10%, respectively, as assumed in this research, for spinning reserves.

$$P_{hydro} \leq P_{hydro}^{max} \times 87\% \tag{4.21}$$

$$P_{gas} \geq P_{gas}^{max} \times 90\% \tag{4.22}$$

4.2 Data Preparation

4.2.1 Generation and Load Profile

Load profile, which represents the instant power demand at specific buses of each time point, is preloaded to the optimization model for each simulation. Generation profile is typically used to set the maximum output of wind and solar generators according to the amount of wind and solar energy available at each time point.

In this research work, a sequence of hourly time periods will be applied to the optimal planning simulation for all testing cases. In order to minimize the optimization model size and solving time, a typical week profile will be used instead of running through all 8,760 hours of one year. Generally, this work uses four typical weeks, each week representing a season in a year. The typical week profile of generation and load will preserve the peaks, minimums, and averages of each season, and represent the changes between neighboring hours [1]. Another method of reducing problem size is by using typical hours to represent each operation scenario in a year. For example, as used in the project report of Schulze et al. [16], an annual operation could be divided into 16 scenarios, with peak, high, medium, and low of each season, which are represented by 16 hours accordingly. However, using contiguous hours in typical days or weeks could better represent the operational behavior of EES interact with wind and solar generation. The tradeoff will be the augmented problem size.

4.2.2 Variable Cost

The variable cost, also known as production cost, is defined as the cost associated with the energy output of each generator, expressed as $/MWh. In the MATPOWER simulation tool, the variable cost of each generator (including user-added generators

employing callback functions) could be added into the *mpc.gencost* matrix directly. Depending on the design of the experiment, the variable cost could incorporate fuel cost, variable O&M cost, emissions cost, and any subsidy for wind and solar generation.

Fuel price usually has a large impact on the results of generation expansion planning. It is difficult to predict the future fuel price because this is determined by the market of commodities. Normally, fuel prices will be slightly increasing over a typical planning horizon (i.e., 20 to 30 years) due to currency inflation and increased energy consumption. The natural gas price has a relative larger divergence since 1997 according to archived data from the U.S. Energy Information Administration (EIA) (Figure 4.1). The natural gas price is believed to remain uncertain for the future prospective. Therefore, it is necessary to simulate a set of diverse prices to examine their impacts on different planning scenarios.

In this planning study, the levelized cost of energy (LCOE) of fuel cost (if any) and O&M cost is utilized as an average variable cost for each generation technology. Listed in Table 4.1 are the LCOE data derived by NREL-SEAC[4] in the report by Tidball et al. [34], which are selected as variable costs in the simulation, except for the fuel costs of natural gas generators.

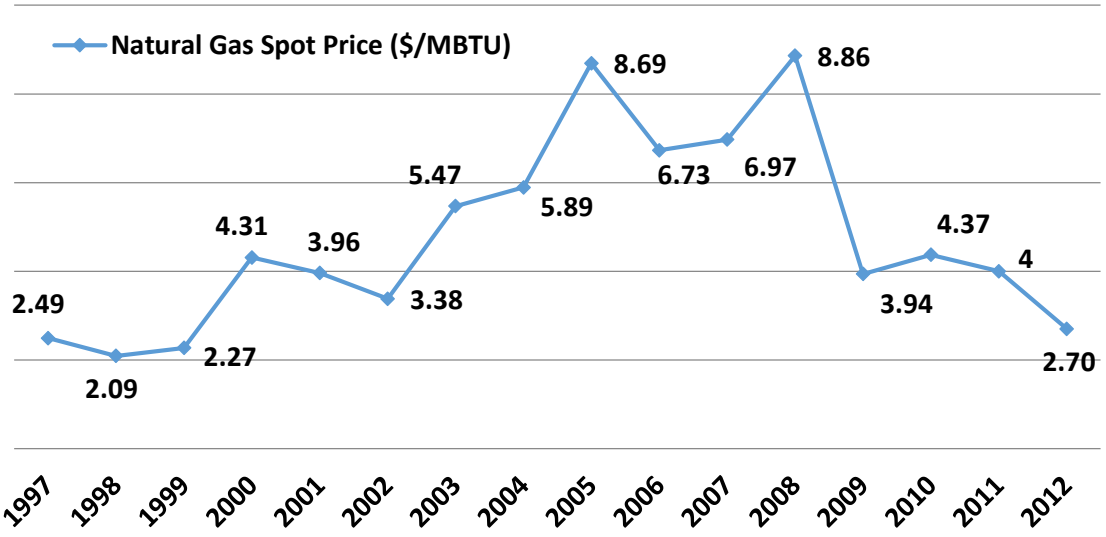

Figure 4.1. Henry Hub Gulf Coast Natural Gas Spot Price.

[4]NREL-SEAC: National Renewable Energy Laboratory Strategic Energy Analysis Center

Table 4.1. Levelized Fuel Cost and O&M Cost

Technology	**Fuel Cost ($/MWh)**		**O&M Cost ($/MWh)**	
	2015	**2030**	**2015**	**2030**
Coal	18.70	20.49	6.54	6.54
Natural Gas	as specified	as specified	5.00	5.00
Nuclear	9.92	12.90	12.02	12.02
Wind (onshore)	0	0	8.08	7.31
Solar Thermal	0	0	17.03	17.03
Photovoltaic (utility scale)	0	0	5.76	3.43
Geothermal	0	0	22.86	22.86
Biomass	29.35	31.11	19.73	19.73

To simulate a policy-regulated CO_2 emissions reduction, e.g., the Kerry-Lieberman Bill, a variable emissions cost (in $/MWh) is added to each coal or natural gas generator model. According to the emissions-incorporated OPF algorithm developed by Shao [3], it is more accurate to incorporate the CO_2 emissions rate in ton/MBTU to the heat rate function, which is usually nonlinear and unique, of each generator. To reduce problem size in the planning study, an average CO_2 emissions rate expressed in ton/MWh is designated to each type of generator, listed in Table 4.2, which is calculated as the product of average CO_2 emission factors, in ton/MBTU, of coal and natural gas [3] and average heat rates, in MBTU/MWh, of each type of generator [32].

Table 4.2. Average CO_2 Emission Rate (ton/MWh)

Generator Type	**CO2 Emission Rate**
Coal	0.8333
Natural gas (combustion turbine)	0.5117
Natural gas (combined cycle)	0.3411

4.2.3 Fixed Cost

The fixed cost of each generator may include startup cost, fixed O&M cost, tax, and insurance. The startup cost is often considered in the unit commitment process, which is not included in this planning work. Land rental cost, tax, and insurance are usually expressed as $/MW cost, which is related to the power capacity of each generator. These costs vary by states and will be ignored in this model. The annual fixed O&M costs from NREL-SEAC data are listed in Table 4.3 for different types of generators [34]. The fixed O&M cost are assumed to be constant throughout the planning horizon.

Table 4.3. Annual Fixed O&M Cost in 2015 ($/MW)

Fuel Type	**Annual Fixed O&M Cost**
Coal	36,780
Natural gas (combustion turbine)	6,880
Natural gas (combined cycle)	15,000
Nuclear	93,770
Wind (onshore)	11,980
Solar thermal	48,790
Photovoltaic (utility scale)	9,920

4.2.4 Capital Cost

Except for the fixed O&M cost, capital cost is another major part of the investment cost for new generators. The overnight capital cost (OCC) is considered a total cost for the overall construction of a power plant. In this study, it is broken down into an annual cost, denoted as annual capital recovery (ACR). The ACR of each power plant is the product of the OCC and the capital recovery factor (CRF), which is normally derived by

$$CRF = \frac{i(1+i)^n}{(1+i)^n-1} \tag{4.23}$$

where n is the number of years for the loan, and i is the interest rate. In this study, the interest rates for coal and nuclear plants are assumed to be higher due to the longer loan duration and higher financial risk, as shown in Table 4.4. The OCC data of 2022 and 2032 are derived from the long-term capital cost forecasted by NREL-SEAC [34].

Table 4.4. Capital Cost by Fuel Type

Technology	***n***		***i*** **(%)**	**CRF (%)**	**OCC in 2022 ($/kW)**	**OCC in 2032 ($/kW)**	**ACR in 2022 ($/MW)**	**ACR in 2032 ($/MW)**
Coal	60		14.57	14.57	2400	2400	349,780	349,780
Natural Gas (CC)	30		12	12.41	820	820	101,798	101,798
Nuclear	60		14.57	14.57	3200	3100	466,373	451,799
Wind (onshore)	20		12	13.39	1600	1500	214,206	207,512
Solar Thermal	30		12	12.41	4600	4600	571,061	571,061
Photovoltaic (utility scale)	30		12	12.41	2200	1800	273,116	223,459

4.2.5 Energy Storage Data

The input data of each EES applied in this planning model involves location, minimal and maximum investment allowance (for both power and energy capacity), initial rate, charging and discharging efficiency, ACR of power, ACR of energy, and O&M cost. Only five technologies that have been used or proven to be potentially applicable as bulk energy storage for energy management are considered in this planning simulation. According to the cost analysis in different study reports [34] [35] [36] [37], capital costs as well as cycle efficiencies always present a wide range of variation. In order to explore the average planning results of each EES technology, the capital cost and efficiency are divided into two levels of situation—the best and the worst. Summarized from two reports [36] and [37], the best situation consists of the lowest capital cost and the highest efficiency, and vice versa. Similar to the ACR calculation of generation technologies, under assumptions of 250 cycles per year operation and the 3% interest rate shown in Table 4.5 the ACR of EES are calculated and presented in Table 4.6.

Table 4.5. EES Parameters

Technology	**Cycles in Life**	**Average Cycles per Year**	***n***	***i* (%)**	**CRF (%)**
Pumped Hydro (PH)	25,000	250	50†	3.00	3.89
Compressed Air Energy Storage (CAES)	25,000	250	50†	3.00	3.89
Sodium Sulfur (Na-S)	3,000	250	12	3.00	10.05
Vanadium Redox (VR)	5,000	250	20	3.00	6.72
Lithium-ion (Li-ion)	4,000	250	16	3.00	7.96

†Life cycle of pumped hydro and CAES are assumed to be limited by other components.

Table 4.6. Calculated ACR of EES

Technology	**Level**	**Capital Cost ($/kW)**	**Capital Cost ($/kWh)**	**ACR ($/MW)**	**ACR ($/MWh)**	**O&M ($/MWh)**	**Cycle Efficiency (%)**
PH	Worst	2440	10	94,832	389	4	81
	Best	1500	10	58,298	389	4	85
CAES	Worst	1140	3	44,307	117	3	50
	Best	500	3	19,433	117	3	70
Na-S	Worst	305	491	30,641	49,327	7	75
	Best	200	181	20,092	18,184	7	78
VR	Worst	1280	257	86,036	17,274	1	65
	Best	608	88	40,867	5,915	1	75
Li-ion	Worst	305	1000	24,281	79,611	7	80
	Best	200	290	15,922	23,087	7	85

5. Test Systems and Simulation Results

In this chapter, two test systems are applied to the planning model proposed in Chapter 4, with summarized cost data and multiple simulating scenarios. Section 5.1 introduces the small 3-bus test system, the formulation of study scenarios, and the simulation results. The organization of Section 5.2 is similar to that of Section 5.1. The simulating scenarios in Section 5.2 aim to verify the practical policies with the validated 240-bus WECC model following the model stress test in Section 5.1.

5.1 Simple 3-Bus Test System

5.1.1 Test System Setup

As shown in Figure 5.1, a simple 3-bus model is applied to the proposed optimal planning model to test the sensitivity of future energy investment responding to different anticipated energy policies and natural gas prices. The solid lines represent existing transmission lines and generators, and the dashed lines represent new types of generators—solar (S), wind (W) and storage (EES), potentially to be built in the future. Future investments of existing types of generators are assumed to be only invested at the bus where that type of generator is located. For example, future investments of coal (C), natural gas (G), and nuclear (N) generators are placed at bus 1, bus 2, and bus 1, respectively. The reactance of each transmission line is assumed to be j0.1 p.u. with identical transmission capacity of 300 MW. Transmission line losses and reactive power in the system will not be considered in the DC OPF model. The peak demand of the system is 600 MW, with one-third distributed at bus 2 and two-thirds distributed at bus 3.

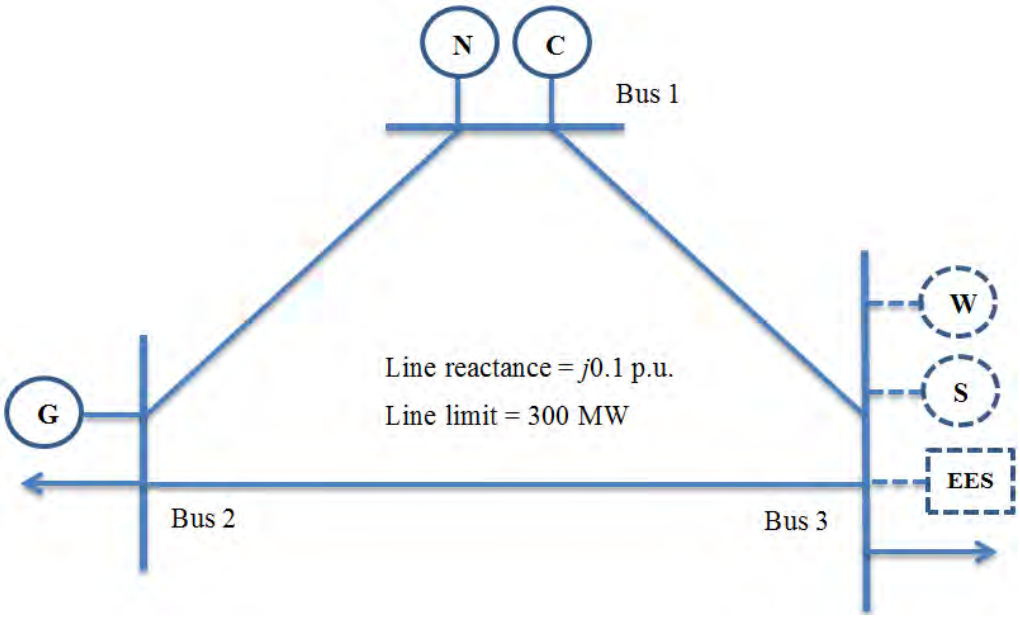

Figure 5.1. Network configuration of 3-bus test system.

Four typical weeks will be used to represent four seasons in a year, with hourly profiles of load and variable renewables (i.e., wind and solar). The load and generation profile is normalized according to the profile provided for the WECC model, as shown in Figure 5.2. Only one wind profile and one solar profile are used for the prospective wind generator and solar generator at bus 3. Those two data profiles are normalized from the profiles of a wind farm and a solar plant in southern California (i.e., bus 2438 in the WECC model). The total peak demand of the simulation year is 600 MW, with total existing generation capacity of 800 MW.

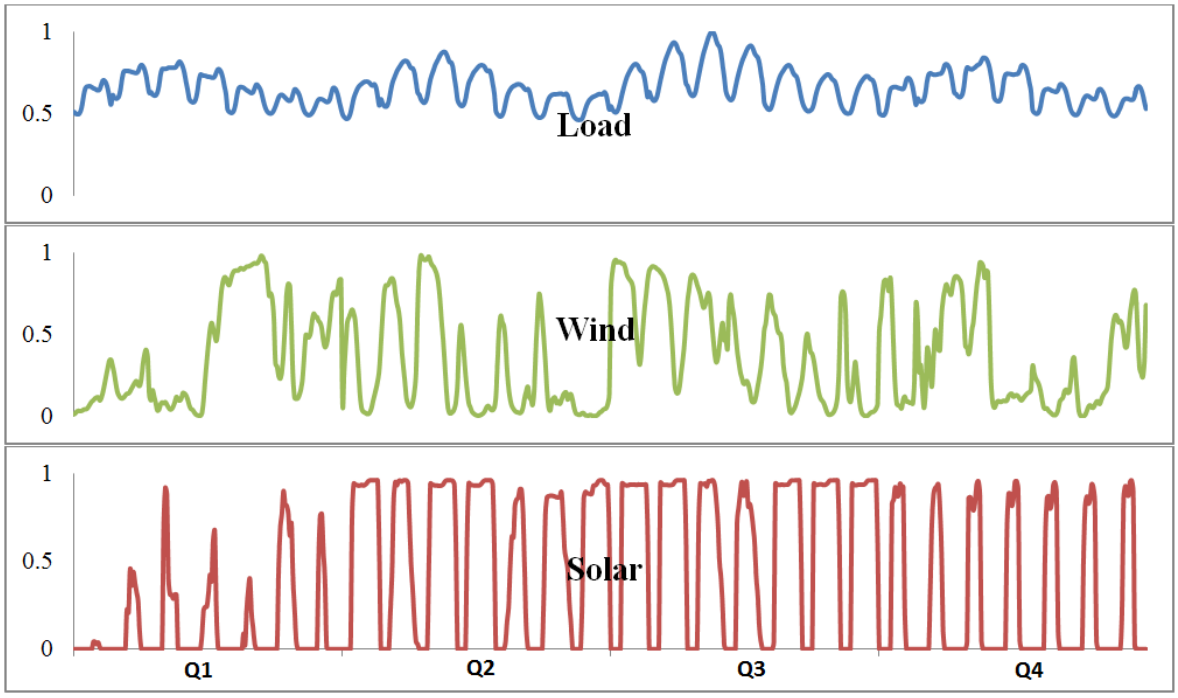

Figure 5.2. Normalized 672-hour profile of load, wind, and solar generation.

The input parameters of the existing generators and the investment targets are listed in Table 5.1. The production cost data approximated from using the forecasted levelized cost of 2015 is shown in Table 4.1. The fixed cost and capital recovery for coal, natural gas, nuclear, wind, and solar generation are taken from Table 4.3 and Table 4.4. Benefited from the advanced combined cycle technology, those new invested natural gas generators are likely to adopt this technology with lower capital and fixed costs, and higher energy conversion efficiency. Thus, an average fuel cost of $40/MWh, the production of natural gas price at $5/MBTU, and average heat rate of a combined cycle [32] at 8 MBTU/MWh are used for the invested natural gas generators (as listed in brackets in Table 5.1). The photovoltaic (PV) cost data is selected for the invested solar generator since it has lower capital, fixed, and production costs, which induce more investment of solar energy in the simulation results. In order to investigate the best scenario for bulk energy storage in the planning study, the cost inputs of energy storage adopt the best case of the CAES technology from Table 4.6.

Table 5.1. Generator Parameters in 3-Bus Test System

Generator Index	1	2	3	4	5	6
Bus Index	1	2	1	3	3	3
Fuel Type	Coal	Gas	Nuclear	Wind (onshore)	Solar (PV)	EES (CAES)
Existing Capacity (MW)	240	400	160	0	0	0
Maximum Investment Allowed (MW)	∞	∞	∞	∞	∞	∞
Maximum Retirement Allowed (MW)	240	400	160	N/A	N/A	N/A
Capacity Factor	0.85	0.87	0.9	0.36	0.40	0.2
Fuel Cost ($/MWh)	18.70	50 (40)	9.92	N/A	N/A	N/A
O&M Cost ($/MWh)	6.54	5.00	12.02	8.08	5.76	3
Annual Fixed Cost ($/MW)	36,780	15,000	93,770	11,980	9,920	0
Annual Capital Recovery ($/MW)	349,780	101,798	566,373	214,206	273,116	19,433/$MW 117/$MWh
Cycle Efficiency	N/A	N/A	N/A	N/A	N/A	0.7

5.1.2 Study Cases

The simulation on the simple 3-bus test system is set up primarily to verify the economic sensitivity of the optimization model with integrated generation planning functions including energy storage. Five study cases with corresponding inputs are set up, as shown in Table 5.2. Cases 1 and 2 test the planning results affected by prospective energy polices such as the CO_2 emissions cap and renewable production tax credit (PTC), respectively. In Case 1, six CO_2 emission prices ranging from $0 to $100/ton by identical steps of 20 are added to the variable cost to simulate the CO_2 emissions regulation under potential policies similar to the Kerry-Lieberman Bill. Case 2 incorporates six renewable incentives ranging from $0 to $50/MWh by identical steps of 10 to simulate the renewable-favorable policies such as the PTC. Case 3 examines the impact to the optimal planning results by a variety of possible natural gas prices covering the EIA recorded lowest and highest annual average from 1997 to 2011 [33]. Case 4 inspects the hourly operational schedule of the CAES in response to wind generation. The planning results with CAES opting out are provided as a comparison in Case 4 to demonstrate the impact

of energy storage. In Case 5, the economic feasibility of the five EES technologies listed in Table 4.6 is investigated in this small test environment.

Table 5.2. Outline of Study Cases

Case Number	CO_2 Price ($/ton)	Wind and Solar Subsidy ($/MWh)	Natural Gas Price ($/MBTU)	EES
1	[0 20 40 60 80 100]	0	5	CAES (best)
2	0	[0 10 20 30 40 50]	5	CAES (best)
3	40	22	[2 4 6 8 10 12]	CAES (best)
4	40	22	8	CAES (best)
5	40	22	8	ALL

5.1.3 Results Analysis

Each study case and corresponding figures are summarized here, and then followed by discussion of the individual study case results explained in more detail with specific references to applicable figures. The generation planning results, the annual CO_2 emissions from burning coal and natural gas, the average energy production costs, and the installed capacity level of wind, solar, and CAES of Case 1, Case 2, and Case 3 are plotted in Figure 5.3 to Figure 5.11. These bar graphs of generation planning results include only the power capacity results of EES. The calculated planning results of both power capacity and energy capacity of each EES are directly specified as numbers at the top of each column, if there is investment in energy storage. The impact of CAES is analyzed in Case 4, with results shown in Figure 5.12 and Figure 5.13. Table 5.3 outlines the planning results simulated in Case 4 to quantify the impact of investing the CAES on total cost, average production cost, renewable investment and energy storage investment. Moreover, the hourly operational results of wind and CAES are demonstrated in Figure 5.14. In Case 5, the potential investment of five bulk storage technologies are simulated with identical emissions cost, renewable subsidy, and natural gas price as in Case 4. The results of Case 5 are summarized in Table 5.4.

Case 1 examines the impact on future planning results by imposing a variety of CO_2 emission costs to the coal and gas generators. As shown in Figure 5.3, neither investment nor retirement is necessary without any CO_2 emission cost. By adding a moderate CO_2 emission cost of $20/ton or $40/ton, the most economical way is replacing or upgrading old combustion turbines (CTs) to a new combined cycle (CC) for natural gas generators. The generator-installed capacity of coal starts to be replaced by wind at a CO_2 emission cost of $60/ton. Beyond the $80/ton CO_2 cost, coal generators are completely retired, while PV and more wind are invested. The amount of technology upgrade of natural gas generators is almost identical to where the CO_2 cost is $60/ton. Under a CO_2 cost of

$100/ton, most CTs are retired with only a small increase in CC. Investment in wind generation is decreased because nuclear generation becomes economically feasible at this time. Although nuclear generation has a much higher capital cost than wind and solar generation, its capacity factor is much higher, leading to a better solution if the production cost of wind and solar is not compensated by any policy. Investment in CAES occurs in this case only when the CO_2 price reaches $100/ton. With a high installed capacity of nuclear (37%), CAES shifts to more nuclear generation (with a production cost of $21.92/MWh) from off-peak to peak hours in order to offset the emission-penalized costly energy from natural gas generators.

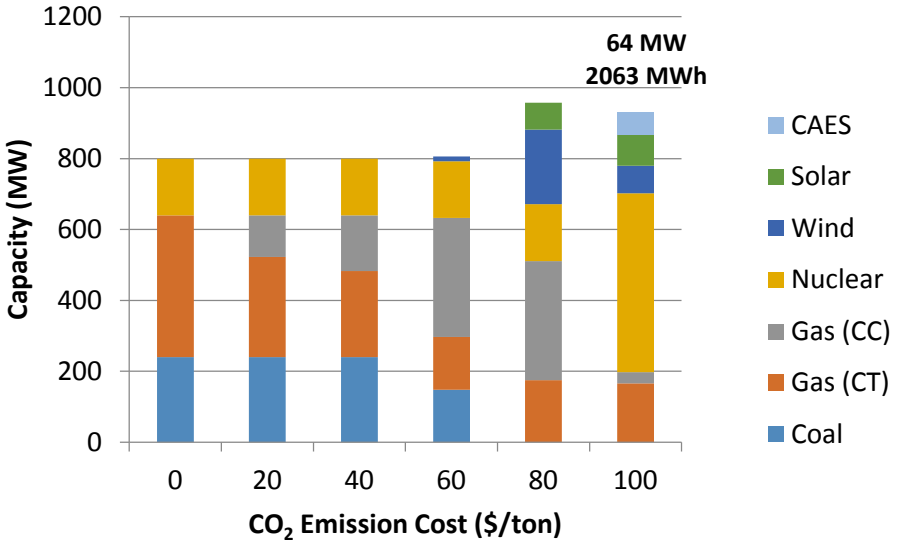

Figure 5.3. Generation planning results of Case 1.

Simulation results of annual CO_2 emission cost and average production cost in Case 1 are plotted in Figure 5.4. It is clear that CO_2 emissions from coal start to decrease with a CO_2 emission cost between $40 and $60/ton. Within a price range of $40 to $80/ton, some energy generation shifts from coal to natural gas before the decline of natural gas consumption. There are a few generation outputs from natural gas generators with a CO_2 cost as high as $100/ton. Since the production cost is defined as the variable cost including fuel cost, O&M cost, emission cost, and subsidy, adding the emission cost raises the production cost until the resource shifts. The highest average production cost is nearly $80/MWh, where only one-third of the coal is retired, and the total capacity of CC and CT are more than the initial state. After that, the average production cost declines with renewable or nuclear investment.

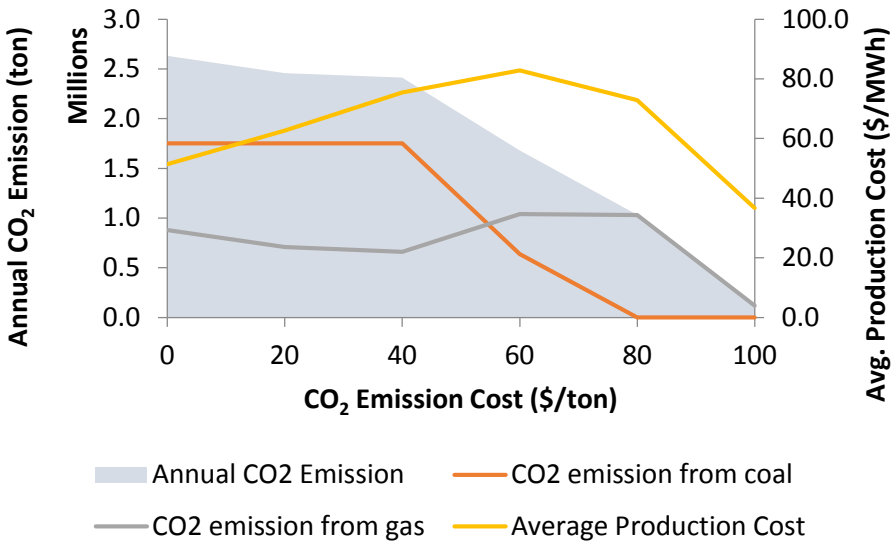

Figure 5.4. Annual CO_2 emissions and average production cost of Case 1

According to the simulated results of Case 1, the bulk CAES operated for energy arbitrage is only economically feasible when the CO_2 price reaches \$100/ton, with an installed capacity level of 18% renewables and 37% nuclear, as shown in Figure 5.5. Although wind and solar generation has a variable output and lower production cost compared to nuclear generation, the storage is not yet an option with 30% renewables alone at the CO_2 price of \$80/ton.

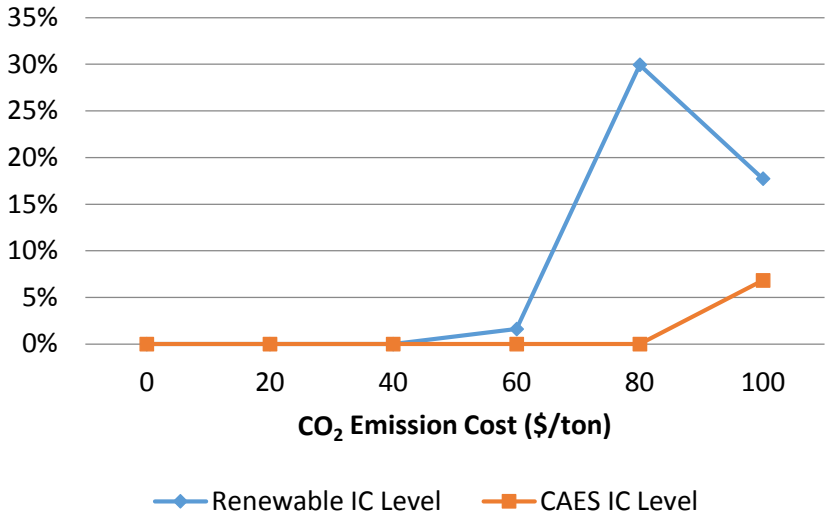

Figure 5.5. Percentage of installed capacity in Case 1

The planning results of Case 2 are shown in Figure 5.6. Without emission penalties, coal and natural gas capacity are not phased out unless there is a high incentive placed on renewable energy. In this small test system, wind and solar generation start to replace

natural gas CT generation under a renewable subsidy between $20 and $30/MWh. Natural gas CT generation is substituted prior to coal and nuclear generation because of its higher production cost (primarily fuel cost). The overall generation capacity increases significantly with the investment in wind and solar energy because of their lower capacity factors (i.e., 36% and 40%, respectively, in this study).

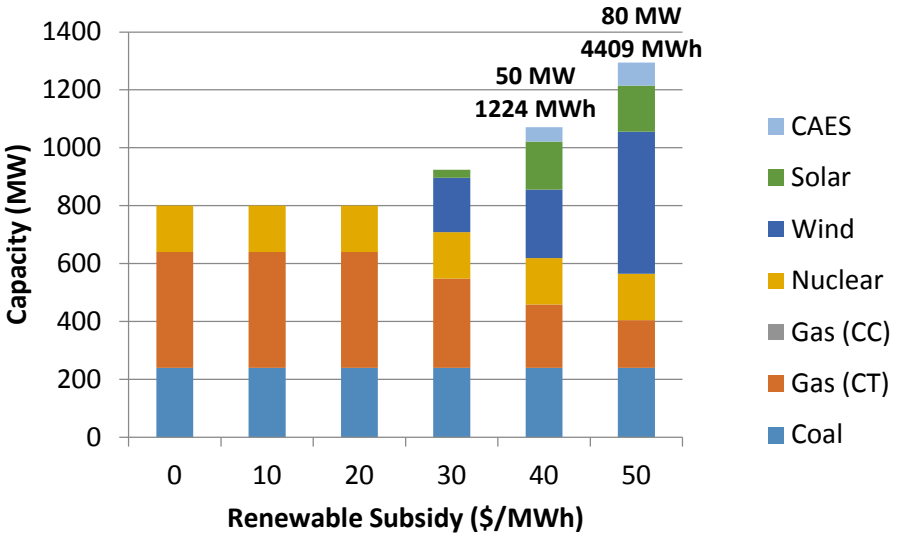

Figure 5.6. Generation planning results of Case 2.

As can be seen in Figure 5.7, building wind and solar generation helps to reduce most CO_2 emissions from the natural gas CT, not from the coal generation, as long as the fuel price of natural gas is higher than that of coal. However, in this case, the average production cost is monotonically declining with the increase of renewable subsidies. From both Figure 5.7 and Figure 5.8, it can be seen as noteworthy that at a high incentive of $50/MWh, the average production cost even drops below zero with 50% installed capacity of wind and solar energy.

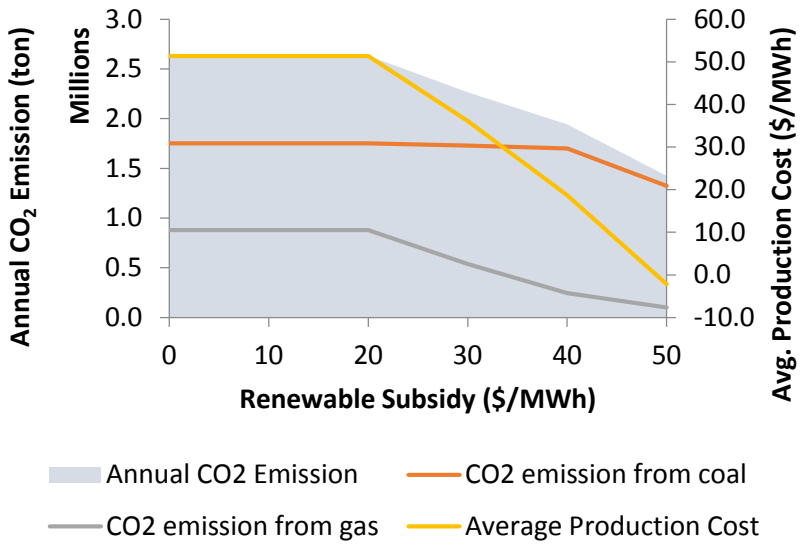

Figure 5.7. Annual CO_2 emissions and average production cost of Case 2.

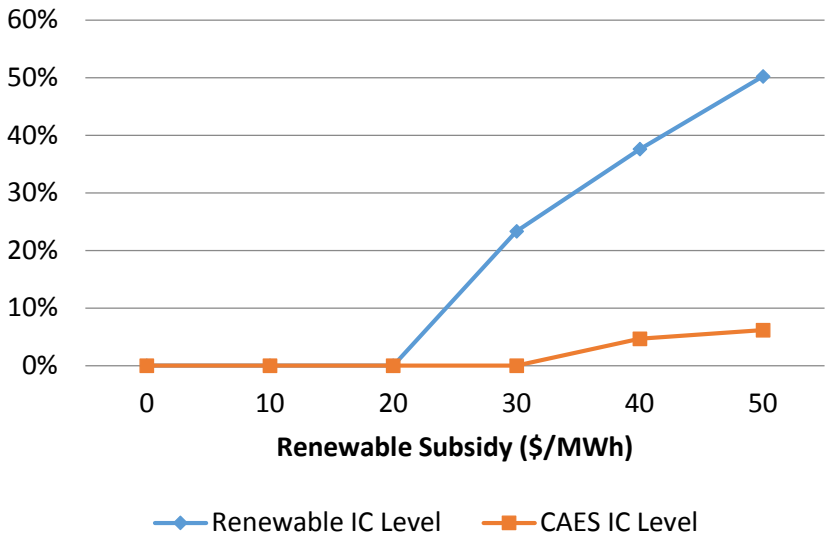

Figure 5.8. Percentage of installed capacity of Case 2.

Figure 5.8 shows the storage investment triggered by the penetration of wind and solar. As stated previously, the size of the bulk energy storage is economically optimized to shift the energy from lower cost hours to higher cost hours. In this test system, installation of 5% of CAES is the best solution when 38% of wind and solar generation is invested at a renewable subsidy of $40/MWh, and installation of 6% of CAES is the best solution when 50% of wind generation is installed at a renewable subsidy of $50/MWh. As described previously, Case 3 simulates the impact of the natural gas price with a designated CO_2 emission cost of $40/ton and renewable incentive of $22/MWh. From the two previous cases, neither imposing a CO_2 cost of $40/ton nor imposing a renewable subsidy is likely to affect the planning results of coal. This study case, shown in Figure

5.9, indicates that at a very low natural gas price of $2/MBTU, coal is completely replaced by the new natural gas combined cycle (NGCC), and no wind or solar generation is invested even with a renewable subsidy in place. With higher natural gas prices, the existing capacity of the CT is gradually replaced by wind and solar energy. Natural gas generation will be phased out when the gas price rises above $12/MBTU. Similar to the previous cases, the investment of energy storage increases along with that of renewables. It can be seen in Figure 5.9 (and later in Figure 5.11) that the increment of renewables and storage slows down when the natural gas price goes beyond $8/MBTU. Instead, the increment of energy capacity of the CAES rises, which is indicated as a better solution than adding more wind and solar generation.

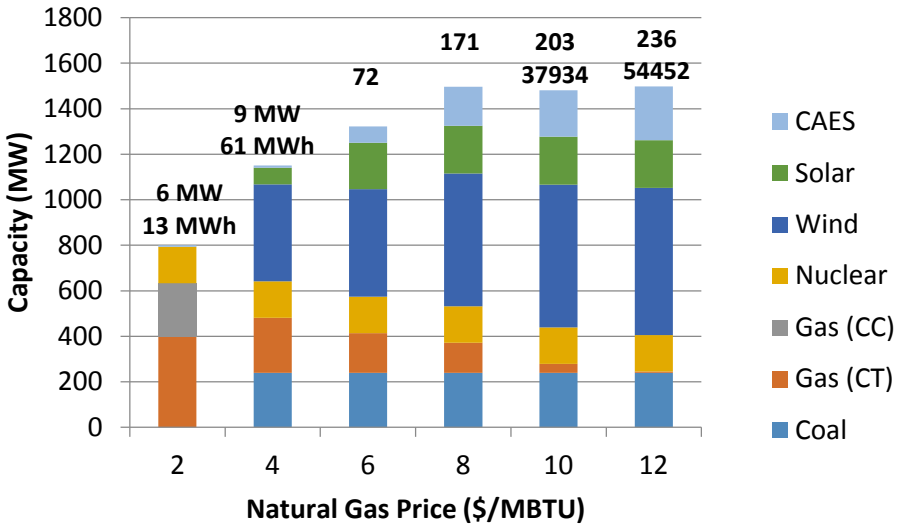

Figure 5.9. Generation planning results in Case 3

From Figure 5.10, it can be seen that the annual CO_2 emissions remains at a relatively constant level in this simulation case. The overall emissions at six simulation points are lower than that of Case 2 because of the $40/ton emission cost. CO_2 emissions from coal and natural gas reverse when the gas price increases from $2 to $4/MBTU. From the coal emission curve, it is clear that coal generation decreases while the gas price increases from $4 to $12/MBTU. Even though coal generation decreases, the installed capacity of coal remains constant to ensure enough capacity to back up wind and solar generation. The average production cost decreases monotonically with the increase in gas price. With both a $40/ton emission cost and a $22/MWh renewable incentive in place, the planning model is highly sensitive to the price of natural gas. At a lower price below $4/MBTU, the new NGCC is more preferable than coal and renewables in this study scenario. When the gas price increases above $4/MBTU, adding renewables is the best solution.

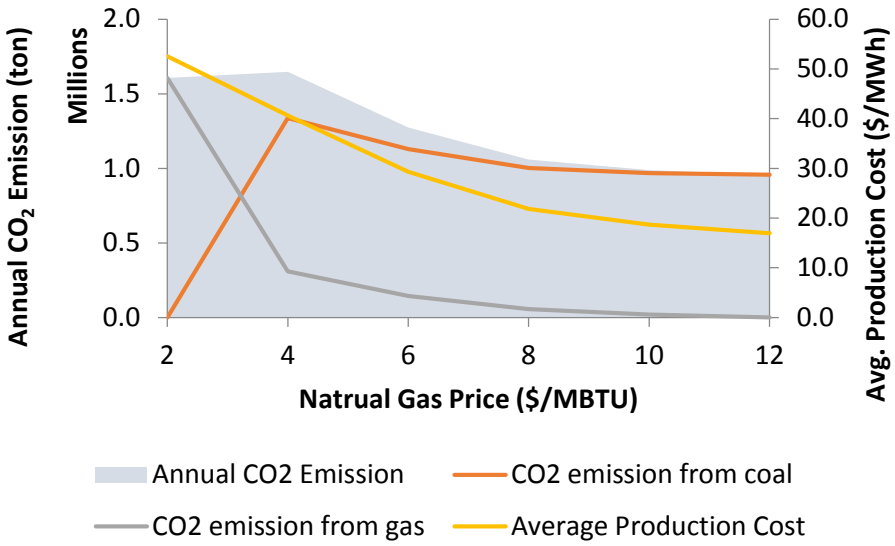

Figure 5.10. Annual CO_2 emissions and average production cost in Case 3.

In Case 3, the IC level of energy storage has a noticeable increase when renewables climb to 50%, as shown in Figure 5.11. After that, the increment of energy storage is higher than that of renewables. The variable output profiles of wind and solar create an economic ceiling that restricts their growth. If the cost of adding energy storage is higher, then the alternative option will be either keeping more of the capacity of natural gas or building new coal or nuclear plants.

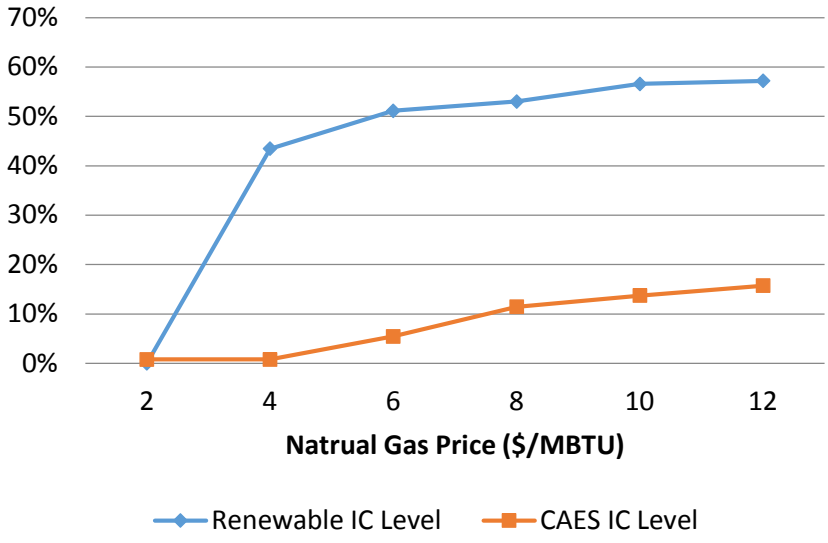

Figure 5.11. Percentage of installed capacity in Case 3.

The simulation shown in Case 4 compares the differences in resource planning, CO_2 emissions, and energy prices between adding and not adding the CAES. As stated previously in Table 5.2, a specific scenario is selected as \$40/ton of CO_2 emission,

$22/MWh of renewable subsidy, and $8/MBTU of natural gas. The price of natural gas is selected at a higher level in order to induce more investment of renewables, which therefore magnifies the impact of adding CAES.

Figure 5.12 illustrates the resource planning results with and without installing CAES. It can be seen that the investment of CAES replaces a portion of capacity from natural gas generator which could be underused in this study case. Meanwhile, it provides more flexibility with more wind capacity. Although the solar profile is less variable and better coordinated with the load profile than wind profile, it has a slightly higher capital cost and lower capacity factor. As long as there is a bulk storage technology with a relatively low unit cost in energy capacity (such as CAES and pumped hydro), wind generation, which benefits from bulk storage, could have a slightly lower cost overall than solar generation.

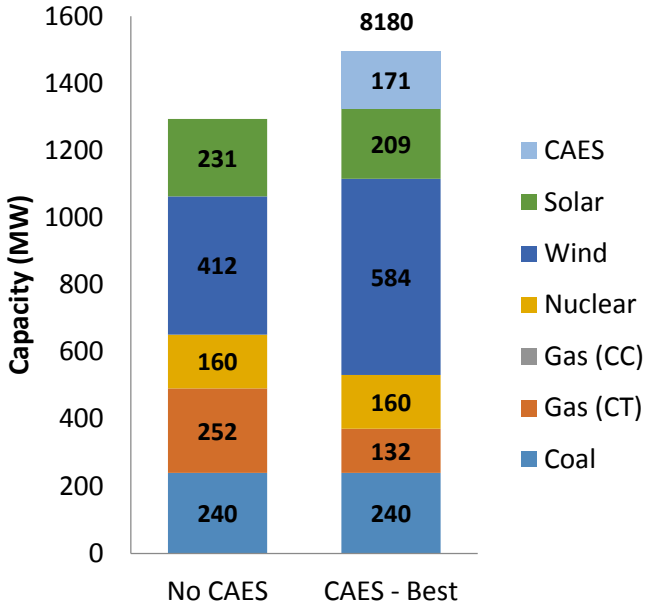

Figure 5.12. Planning results of other resources with and without CAES as an option.

The impact on CO_2 emissions by adding CAES is shown in Figure 5.13. As stated previously, CAES promotes more wind investment in this study scenario. Therefore, it is not surprising to observe that optimal investment of CAES could reduce CO_2 emissions from both coal and natural gas resources. In this case, emissions from natural gas have a larger ratio of reduction because of the higher production cost compared to that of coal.

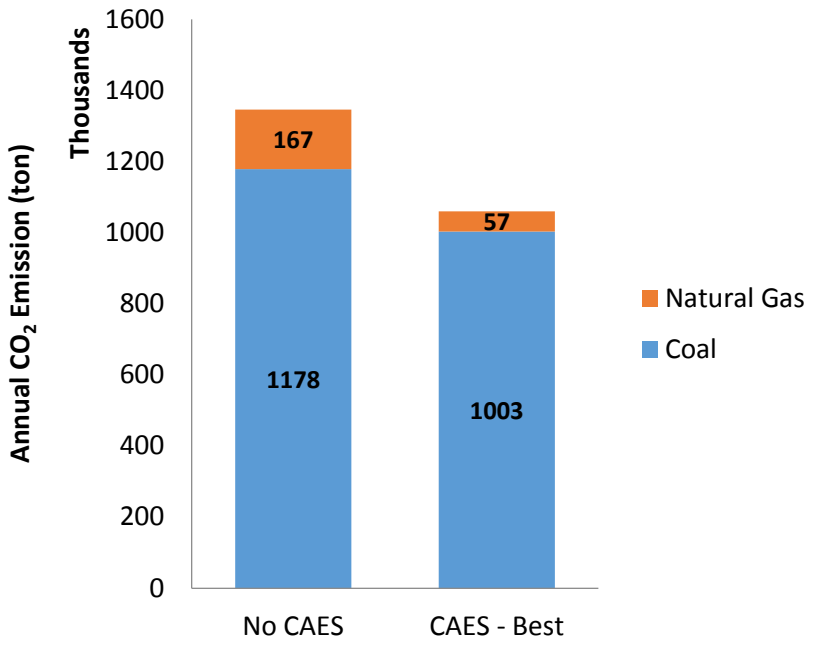

Figure 5.13. Annual CO_2 emissions with and without CAES as an option.

Moreover, comparisons of costs and installed capacity levels are listed in Table 5.3. Although there are capital and O&M costs associated with CAES, the total annual cost is reduced by 1.6%. More generation from wind induces an additional reduction of $11.4/MWh, or 34% of the average production cost.

Table 5.3. Costs and Installed Capacity Levels

Scenarios	**NO CAES**	**CAES - Best**
Total Annual Cost ($ million)	272	267
Average Production Cost ($/MWh)	33.3	21.9
Renewable IC Level (%)	50	53
CAES IC Level (%)	0	11

The hourly operation data of wind generation and CAES are plotted in Figure 5.14. From As can be seen, the wind resource is relatively more sufficient on the second half of Q1 (represented by typical week profile, i.e., from hour 1 to hour 168) and the first half of Q2 and Q3 (i.e., hour 85 to 252, and 337 to 420). As shown, during most of these hours, the CAES is charging with volume increasing. During summer-peaking hours of demand or recession periods of wind (i.e., hour 1 to 80, 250 to 320, 420 to 480, and 550 to 650), CAES releases energy as dispatched by the DC OPF. The remaining energy at the ending period is identical to the initial value, which is set at 20% of maximum capacity. In this study case, CAES operates about 28 cycles within this 672-hour simulation horizon, averaging one cycle per day. According to the size of power and energy capacity, this

CAES is capable of discharging continuously for approximately 40 hours at its rated maximum output. This physical parameter is realistic for up-to-date CAES technology.

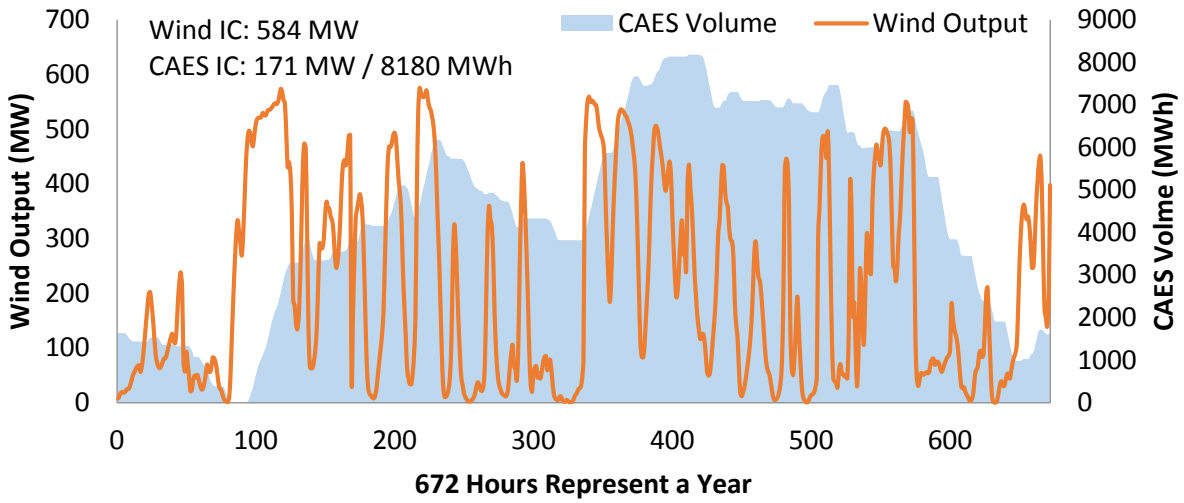

Figure 5.14. Hourly operational results of CAES and wind generator

The simulation scenario in Case 5 is identical to that of Case 4, except that multiple technologies of bulk energy storage are simulated to compare their potential investment in this application. The planning results of each EES technology are listed in Table 5.4. In this energy management scenario, energy storage will be valued through an energy arbitrage operation. Therefore, energy storage with lower capital cost on energy capacity, such as pumped-hydro and CAES, is preferable. Although the PH-Best category has a higher capital cost on power capacity than the other three battery technologies, its remarkably low capital on energy capacity makes it highly desirable with high-level wind and nuclear generation. Other than pumped hydro and CAES, the vanadium redox battery has little possibility in this study case, with 5 MW / 25 MWh installed, capable of providing five hours of continuous discharge.

Table 5.4. Potential of Bulk EES by Technology

Technology	Level	Power Capacity (MW)	Energy Capacity (MWh)
PH	Worst	0.7	16.7
	Best	67.0	2,401.7
CAES	Worst	0	0
	Best	171.1	8,180.0
Na-S	Worst	0	0
	Best	0	0
VR	Worst	0	0
	Best	5.0	24.7
Li-ion	Worst	0	0
	Best	0	0

5.1.4 Discussion

According to the simulation results, this optimal planning model shows moderate sensitivity to regulatory energy policies and the price of natural gas. The results of this 3-bus test system are reasonable for reflecting the prospective trend of each resource including bulk energy storage under realistic energy policies.

There are multiple solutions to reducing CO_2 emissions. Normally without any regulation, coal generators, operating as base-load units, contribute to the major portion of CO_2 emissions. If the average price of natural gas remains under \$4/MBTU, new invested gas generators with CC technology would likely replace some base-load coal units and therefore reduce overall CO_2 emissions. However, the long-term average price of natural gas is about \$4.78/MBTU, as recorded by EIA from 1997 to 2012. It is still a little high to phase out coal units. Imposing a CO_2 emission cost is an effective way to reduce CO_2 emissions, regardless of the price of natural gas. In this 3-bus test system, a CO_2 price between \$40 and \$460/ton effectively reduces CO_2 emissions by 0% to 36%, and a CO_2 price of \$100/ton could reduce CO_2 emissions by 95%.

Providing renewable incentives is an indirect way to reduce CO_2 emissions. If the average price of natural gas is higher than \$4/MBTU, natural gas generation will be replaced by renewables prior to coal generation. In this test system, coal generation would be replaced by wind and solar generation, only when there is a renewable subsidy higher than \$40/MWh.

Although nuclear energy is emission neutral and has the highest capacity factor, its large capital cost reduces the benefits. In this study, the only investment in nuclear generation occurs when the CO_2 price is \$100/ton and no subsidy is provided for wind and solar generation.

The price of natural gas has a large impact on coal generation at a lower price ranging between \$2 and \$4/MBTU. With a renewable subsidy in place, a high natural gas price could stimulate the investment of wind and solar generation. If wind and solar energy are not policy preferable, the investment in nuclear generation is a feasible option under a high natural gas price or high CO_2 price.

In this study, investment in the EES system seems to be economically feasible only under a high penetration level of wind or nuclear generation. With subsidies, the production cost of wind, sometimes even negative, can be extremely lower than that of the traditional resources. Therefore, EES is invested in order to realize more wind capacity at a lower cost, which is an optimal solution. It is reasonable to conclude that bulk energy storage could reduce overall system operation cost by smoothing out the variation of wind output or delivering the surplus nuclear energy from off-peak hours to peak hours.

In general, the cap and trade policy, or carbon emissions tax, is the most effective way to achieve an immediate reduction of CO_2 emissions. Binding with renewable incentive policies, e.g., collecting extra taxes from CO_2 emitting units and distributing them to renewables as subsidies, however, could expedite the energy consumption shift from fossil fuels to renewables instead of nuclear generation. Without any subsidy greater than \$20/MWh and no emissions cap on CO_2, wind and solar technology are not economically competitive with coal, natural gas, hydro, and nuclear energy to generate electricity.

5.2 WECC 240-Bus System

5.2.1 WECC Model Setup for Planning

The 240-bus aggregated WECC model, as described in Chapter 3, is applied to this optimal planning study. Most of the network topologies and parameters remain intact. Some setups in the planning study are different from the operational analysis. In the planning study, the interface flow limit will not be considered. Since the capacity of each transmission line is not publicly available for the full WECC model, this reduced 240-bus WECC model could not obtain accurate data for all transmission lines. Instead, transmission limits are estimated under a best effort according to voltage level, interface flow limit, and other physical parameters of each single transmission line or group of transmission lines. The physical minimal operating output of each generator is ignored in the planning study. In order to consider spinning reserves, the maximal output of each hydro generator is set to be 87% of its installed capacity and that of natural gas generators is set to be 90%. Therefore, 10% of natural gas capacity is not subject to retire, regardless of how high the gas price is.

Energy production from conventional hydro generators is predicted to decline gradually in the future [38]. An annual average capacity factor (i.e., Δ^{hydro}) is applied to all hydro units with a general assumption of 45% for the year 2012, 40% for 2022, and 35% for 2032. Conversely, the electricity demand is predicted to increase for the next two decades. The demand increment is predicted by considering the expansion rate of the population and economics in the pre-divided areas within the WECC footprint, as shown in Table 5.5. The increased rate of electricity demand for 2022 and 2032 are assumed to be identical.

Table 5.5. Demand Expansion Factor for Each Area in WECC

WECC Area	**Demand Expansion Factor**
Southwest	1.296
Mexico (WECC)	1.064
California	1.064
Northwest	1.064
Canada (WECC)	1.066
Idaho	1.137
Rocky Mountain	1.205
North Nevada	1.137

The configurations of generator retirement and investment are similar to the simulation of 3-bus test system. The under-used capacity of coal, natural gas, and nuclear generators is subject to be retired under an optimal decision. Meanwhile, coal, natural gas, nuclear, wind, and solar generators can be invested at any generator bus (i.e., currently any 20 kV-bus with one generator or more attached) in the WECC model. It is less likely to be affected by transmission congestion with more locations allowed to build new generators. Altogether there are 53 generator buses in this 240-bus WECC model. Maximum growth rates are considered for coal, natural gas, and nuclear generation by studying the historical data. Wind and solar generation are assumed to provide, at most, 33% and 20%, respectively, of total demand in 2032 under an average capacity factor of 40%. The two-decade maximum investment of each technology is listed in Table 5.6.

Table 5.6. Investment Limit for Each Technology by 2032

Fuel Type	**Total Addition Limit by 2032 (GW)**
Coal	24
Natural Gas	77
Nuclear	12
Wind	94
Solar	60

In contrast to the operational study, the planning model requires capital cost and fixed O&M cost for each generator and energy storage. The annual capital recovery and annual fixed cost for each type of generator (i.e., coal, natural gas, nuclear, wind, and solar) are described in Chapter 4. The generation profiles for those potentially invested wind and solar generators are normalized from the wind and solar production forecast investigated by Price and Goodin [1]. The future profile of wind and solar generation, however, covers only a small number of locations with short-term projected wind and solar investment. In this planning study, the future profile for a wind or solar generator at a particular bus may be applied to other wind or solar generators to be invested at neighboring buses. The detailed mapping is listed in Table B.4 and Table B.5 in Appendix B, for wind and solar profile, respectively.

In order to keep the problem size acceptable, only six EES units will be deployed in the WECC system, with identical cost data and other parameters. The cost data of CAES-best (data listed in Table 4.6), which was proven to have the highest potential in the 3-bus test system, is selected as the candidate of bulk storage investment in this planning study for the WECC. Through investigating the network topology, the WECC model can be divided into six grand areas: Southwest, Southern California, Northern California, Northwest, Canada, and Rocky Mountain. Each EES is placed at a randomly selected generator bus within each grand area, as listed in Table 5.7.

Table 5.7. Presumed EES Locations

Bus Index	**Bus Name**	**Grand Area**
1131	CORONADO	Southwest
2638	CASTAI4G	Southern California
3432	HELMS PP	Northern California
4035	JOHN DAY	Northwest
5032	CMAIN GM	Canada
7031	COLOEAST	Rocky Mountain

The production costs of each generator by fuel type, except natural gas, are specified in Table 4.1 in Chapter 4. The forecasted data of 2015 is used for the 2012 and 2022 run, and that of 2030 is used for the 2032 run. The heat rate function of each aggregated gas unit is derived as a quadratic curve, approximated from combining the piecewise linear functions of each sub-unit. The future price of natural gas has many uncertainties and is forecasted to have two possible trends by the study report [16], as specified in Table 5.8

Table 5.8. Two Sets of Natural Gas Prices ($/MBtu)

	2012	**2022**	**2032**
High	2.5	7	14
Low	2.5	4.77	5.86

5.2.2 Study Cases

The study cases are designed primarily to assess the planning trend of generator capacity by fuel type under uncertain energy policies and fuel prices in the next two decades. The setup of the study cases is similar to that in the PSERC M-24 report [16]. There is a base case without any policies involved, a cap and trade (C&T) case, and an Environmental Protection Agency (EPA) case with energy policies. Each case has two possible natural gas prices: high gas price (HG) and low gas price (LG). Therefore, six cases are simulated to represent six possible future scenarios, as outlined in Table 5.9.

Table 5.9. Outline of Study Cases

Case No.	**Policy**	**Natural Gas Price**	**CO_2 Emissions Price**	**EPA Regulation**	**Renewable Incentive**
1	Base	HG	×	×	×
2		LG			
3	C&T	HG	✓	×	✓
4		LG			
5	EPA	HG	×	✓	✓
6		LG			

In each case, three representing years (2012, 2022, and 2032) are simulated with each year representing a ten-year investment cycle. The simulation of year 2012 uses present generation capacity without any energy storage involved as a benchmark for comparison. Although a low price of $2.5/MBTU is used to represent the shale gas price in 2012, the investment decision of natural gas generators should rely on a long-term average price of natural gas, which is higher, for the 2022 and 2032 runs that represent the next two

investment cycles. The initial condition of the 2032 run is the planning results of the 2022 run. This ensures that the retired capacity in the 2022 run cannot be used in the 2032 run and that the invested capacity in 2022 cannot be retired in 2032.

In the cap-and-trade case, a CO_2 price is incorporated as a price cap to simulate a cap-and-trade auction, which is similar to the proposed Kerry-Lieberman Bill for CO_2 regulation. According to the report [16], CO_2 prices of $36.94/ton and 60.18/ton are suggested to be used for 2022 and 2032, respectively. The CO_2 prices are not imposed on the EPA case, which represents the new coal regulations [40] proposed by the EPA. The anti-coal regulation prohibits the construction of new coal plants unless it meets the emissions requirement of no more than 1,000 lbs/MWh. The carbon sequestration adds too much cost to the coal plant, which is not economically feasible nowadays. In this study, coal investment is effectively prohibited in the EPA case.

To model the Federal Renewable Electricity Production Tax Credit, $22/MWh, which is equivalent to 2.2 cent/kWh, is directly subtracted from the production cost model of each wind and solar generator. Referred to as a renewable incentive, it is applied to both the C&T case and the EPA case. Because wind and solar are the only renewables to be built in this model, the renewable incentive is not applied to other existing renewables in the WECC model.

5.2.3 Results Analysis

The planning results of 2022 and 2032 are plotted in Figure 5.15 to Figure 5.22 for each type of generator including energy storage. The retirement and investment value of each fuel type is compared across different simulation environment. The installed capacity level of renewables and CAES are illustrated in
Figure 5.23. Finally, the average production cost and annual CO_2 emissions are shown in Figure 5.24 and Figure 5.25, respectively.

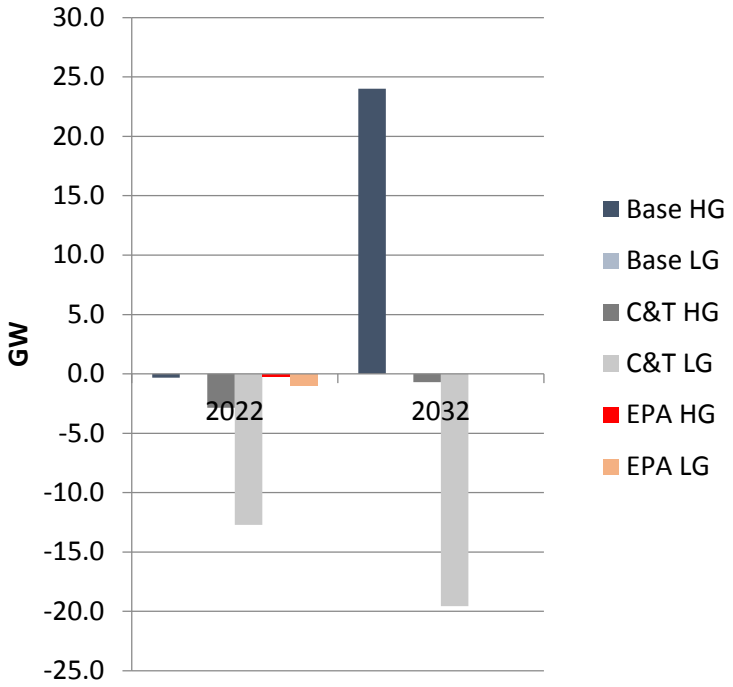

Figure 5.15. Coal retirement and investment in WECC.

There is about 36.8 GW of coal capacity, 18% of the total capacity, existing in the current WECC system. As shown in Figure 5.15, most of the coal capacity will be retired in the C&T LG case, with 8.2 GW retired on 2022 and then 22.9 GW retired on 2032. Most of the coal capacity will be replaced by natural gas, which has a lower production cost including the cost of emissions. In the C&T HG case, coal has less retirement in 2032 because the price of natural gas is extremely high (i.e., $14/MBTU) in this case. In the Base HG case, coal is not competitive when natural gas is $7/MBTU but becomes very economical when the natural gas price reaches $14/MBTU. Coal capacity remains constant in the Base LG case because coal generation stays economically competitive under the normal natural gas price without any regulations. In general, the EPA regulation rule prohibits the investment of new coal plants, while the C&T regulation rule precipitates shutdowns of existing coal generators. Only the soaring natural gas price could slow down the retirement of coal-fired generators.

The installed capacity of natural gas generator occupies 38% in the WECC system, the highest among all types of resources. There is a total of 77.8 GW of natural gas capacity in this WECC model, with most of the generators located in California. From the planning results shown in Figure 5.16, the price of natural gas plays an important role, together with regulation policies. Highest retirement occurs in the Base HG case in 2032 where most of the capacity is replaced by coal. Although new NGCC technology increases overall efficiency of natural gas plants, it is not a feasible solution in EPA cases because the existing coal is still competitive, and wind and solar generation are preferable to being built with a renewable subsidy.

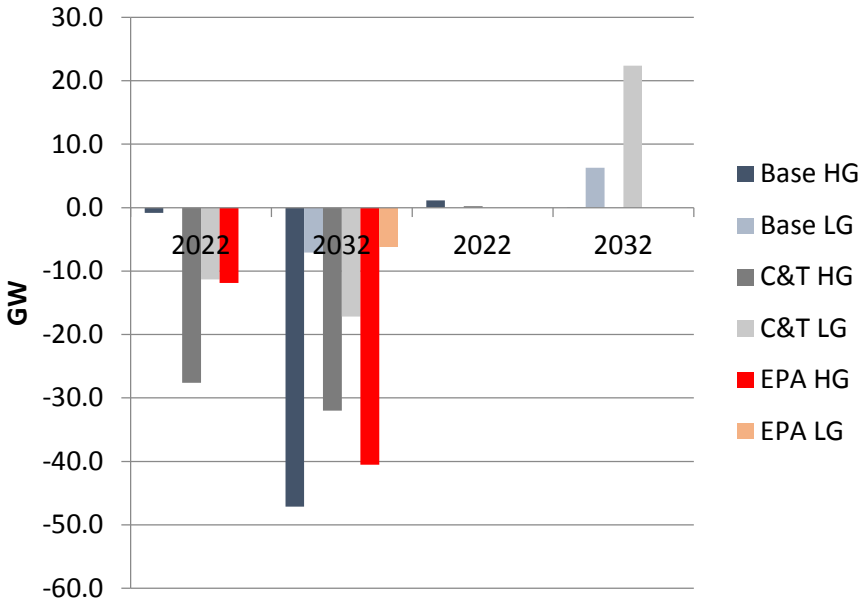

Figure 5.16. Natural gas retirement and investment in WECC.

Nuclear energy is clean, cheap, and stable when generating electricity. However, the large overnight capital cost and high risk of operational reliability compromise its benefits. There are only four nuclear plants on the current WECC footprint, with an install capacity of 9.7 GW. This number is much less compared with the Eastern Interconnection. Most of the nuclear plants were built decades ago, while few have been constructed recently. Without any federal backup, no utility wishes to invest in this long-term, expensive, and unpredictable project. According to an NREL report [34], the overnight capital cost of a nuclear plant falls in the range of $2,500/kW to $4800/kW. From the analyzed data of NREL-SEAC, $3,200/kW is selected in this simulation. Lower capital cost data in the range might be derived with the nuclear loan guaranty program from DOE [39] considered in the model.

The results of nuclear investment are plotted in Figure 5.17. The investment of nuclear generation reaches the maximum additions in the C&T HG case in 2032, when the natural gas price is $14/MBTU and the cost of CO_2 emissions is $60.18/ton. A second high of 9.6 GW of nuclear is invested in the EPA HG case, where there is no emission cost. The Base HG case invests the least amount in nuclear energy, rather investing in coal energy, which is a cheaper solution. No nuclear plant will be built in 2022 because the natural gas price, emission cost, and net demand (i.e., demand increase plus hydro energy decrease) are not extremely high as in 2032. In those cases with low natural gas prices, nuclear generation has no advantage of competing with natural gas, the NGCC technology.

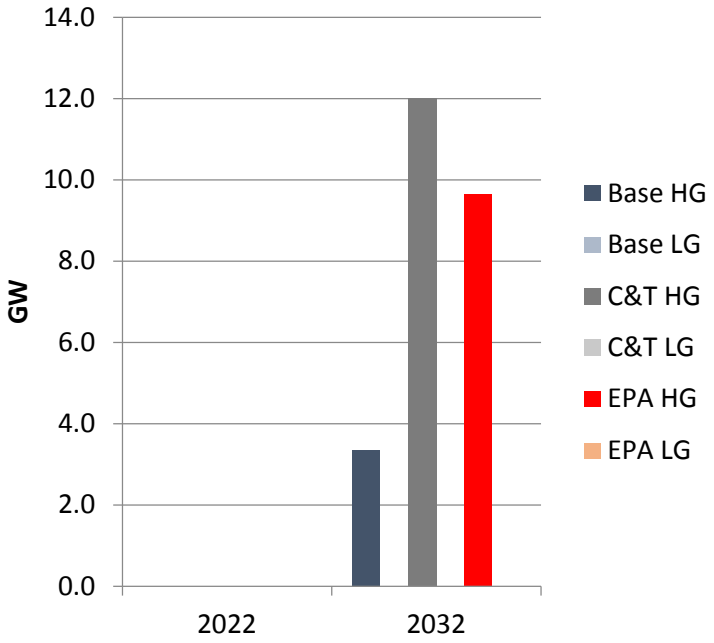

Figure 5.17. Nuclear investment in WECC.

As of year 2012, 6,579 MW of wind capacity is installed in the WECC footprint, only 3% of the total capacity. Future additions of wind generation in 2022 and 2032 are shown in Figure 5.18. If not mandatory, the investment in wind energy in the future has more uncertainties compared to the results shown in the M-24 report, where wind investment reached a maximum in C&T HG, C&T LG, EPA HG, and EPA LG. With the more accurate wind model in this work, i.e., using 672 typical hours representing a year and different capacity factors of different locations, results show less investment in the latter three cases. Wind investment reaches the two-decade limit only in the C&T HG and C&T LG cases. The total two-decade investment of wind in C&T HG, C&T LG, EPA HG, and EPA LG are 94 GW, 94 GW, 88 GW, and 36.1 GW, respectively. There is less wind investment in EPA HG than C&T HG because the existing coal generators are not retired in the EPA cases, and they stay competitive without emission penalties. The relatively lower wind investment in EPA LG indicates that wind generation does not have an evident advantage compared to NGCC technology when the natural gas price stays reasonable. In the C&T cases, wind investment is expedited by emission regulations, whereas in the EPA cases, wind expands slower in the beginning and faster when the gas price and net demand increase. In the base cases, wind is only installed in 2032 in the Base HG case. If current PTC policy ends, the future situation would correspond more to the Base LG, where wind is not an economic solution.

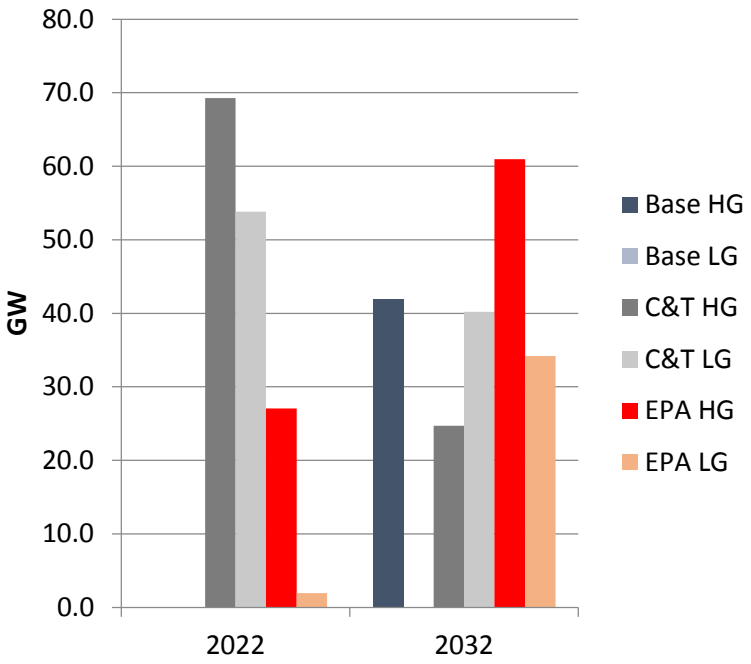

Figure 5.18. Wind investment in WECC.

The investment trend of solar is similar to wind in the WECC system, as shown in Figure 5.19. As stated previously, solar generation is more expensive than wind generation in terms of capital cost, especially solar thermal. For the WECC study here, it is assumed that the additional capacity of solar has 30% solar thermal and 70% PV, which leads to a higher capital cost than the 100% PV assumption used in the 3-bus model study. From the results figures, even with renewable incentives, only solar energy has a similar potential as nuclear energy.

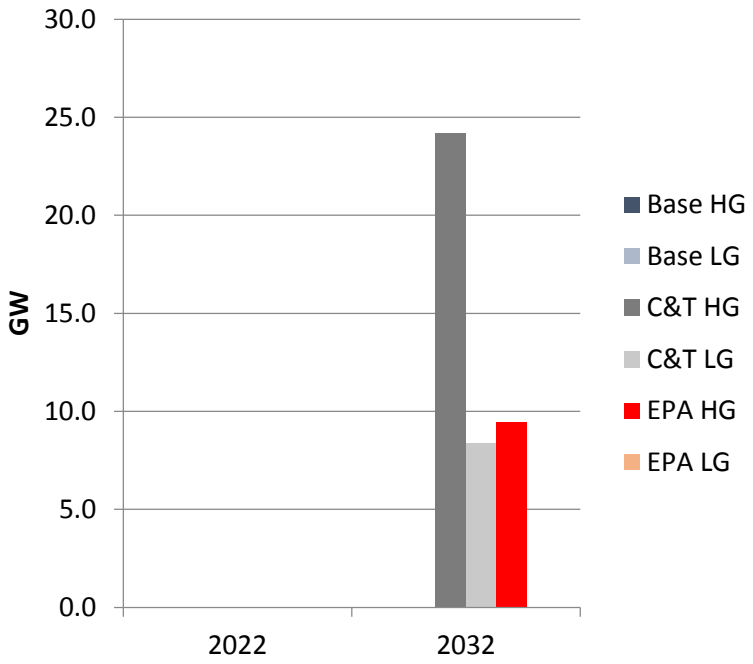

Figure 5.19. Solar investment in WECC.

The results of CAES investment, assuming no energy storage operation in 2012, are plotted in Figure 5.20 and Figure 5.21. The planning results reflect the potential of CAES technology as bulk energy storage. The trend of CAES is correlated with that of wind and nuclear energy. It is interesting to observe that the highest investment of storage occurs in the EPA HG case because this case not only has maximum wind operation in 2032 but also has the most coal generation, which needs to be transported from off-peak to peak when most of the natural gas capacity, 67.3% of 2012, is retired in 2032. Although not included in the simulation, it is necessary to point out that the current bulk storage in the WECC model, all pumped-hydro units, have a total capacity of 3.02 GW and 201.4 GWh. With the increased level of renewables, the EPA HG case requires an additional 675% of power capacity and 498% of energy capacity for CAES in 2032, while the Base LG and EPA LG cases do not need any additions to the existing capacity of pumped-hydro storage.

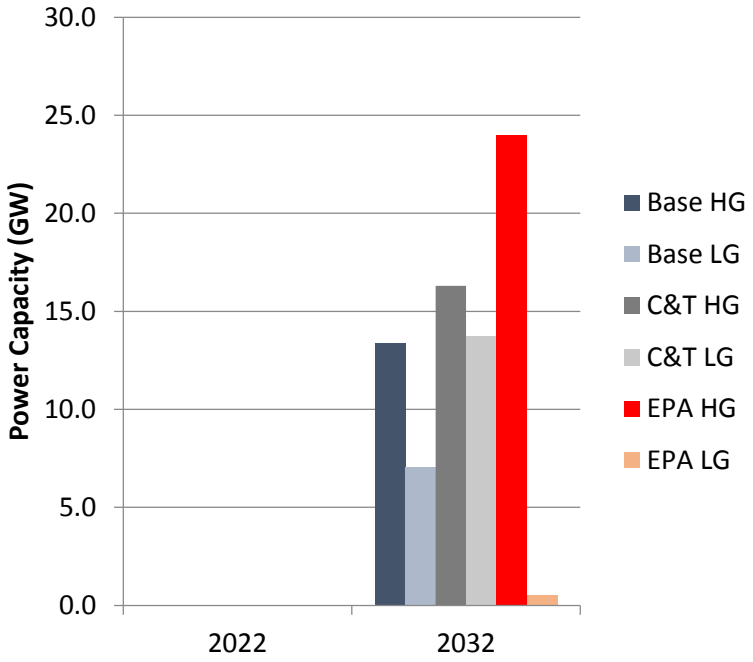

Figure 5.20. Power capacity of EES investment in WECC.

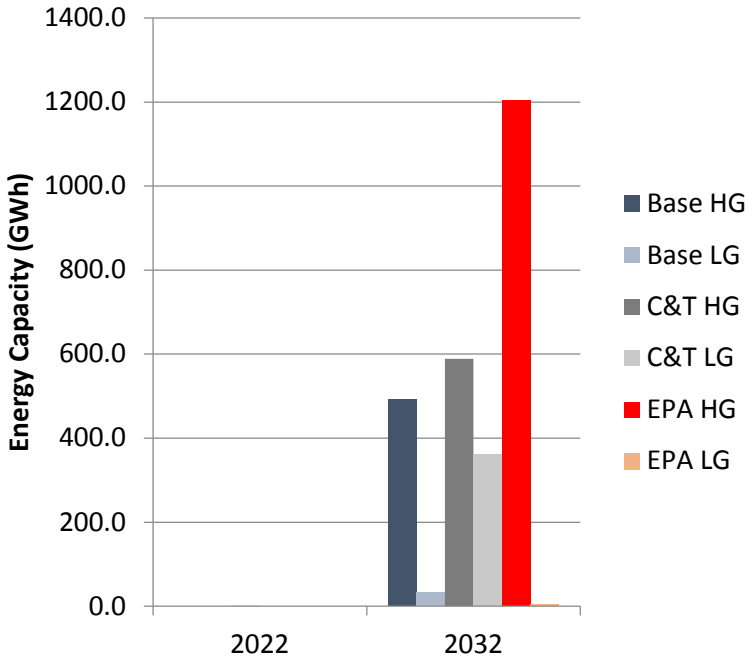

Figure 5.21. Energy capacity of EES investment in WECC.

As an example, with the EPA HG case, the investment of CAES in 2032 at six locations is shown in Figure 5.22. It is surprising to see that the Southwest has the highest potential for building CAES. Currently no bulk energy storage exists in the Southwest area (i.e.,

Arizona, New Mexico, and southern Nevada in the WECC model) including pumped-hydro. Normally, bulk energy storage prefers to be placed at a load pocket or congested import areas, which is California in this WECC model. Thus, 82% of existing pumped-hydro capacity is located in California (42% in southern California and 40% in northern California), and the rest is in the Rocky Mountain area. There are a couple of reasons for the Southwest having the highest potential for bulk energy storage in 2032. First, it has the highest demand expansion factor, i.e., 1.296, for the next two decades, as shown previously in Table 5.5. It gradually shifts from an energy exporter to an energy importer. The second reason is that the capacity factors of both wind and solar generation at locations in the Southwest are relatively high, which leads to more wind and solar investment.

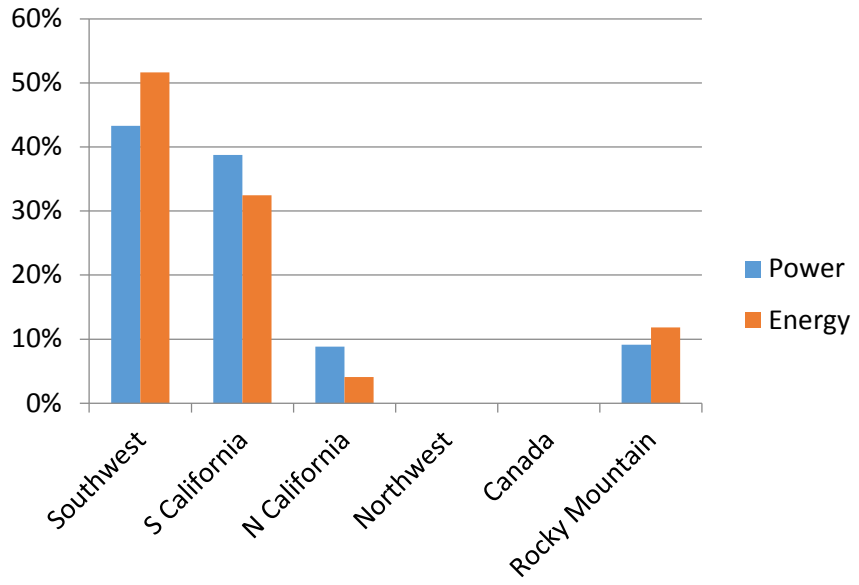

Figure 5.22. CAES investment at each location in 2032 EPA HG case.

Figure 5.23 confirms that the installed capacity of energy storage (i.e., only power capacity of CAES here) could be affected by the investment of wind and solar generation, but not necessarily. A comparison of the installed capacity levels of Base HG and EPA LG shows they have similar IC levels of wind and solar energy but completely different IC levels of CAES. This implies that natural gas generators can provide flexibility with 20% of wind and solar generation in the system, and it is a better solution than CAES at a normal natural gas price.

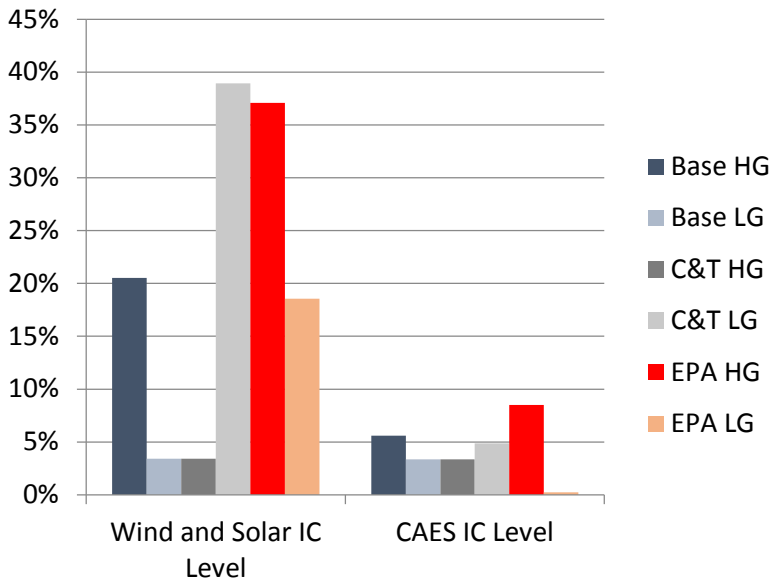

Figure 5.23. 2032 wind, solar, and CAES installed capacity level.

The average production cost in this study is calculated as the total production cost (including EES) divided by the total energy produced. The simulation results are plotted in Figure 5.24. Since the capital cost is not represented, the production cost is lower with more wind, solar, nuclear, or coal generation. In HG cases, the average production costs in 2032 are lower than that in 2022, where the extremely high gas price induces a significant shift from natural gas to coal, nuclear, wind, or solar generation. The results of Base LG represent the linear increase in production cost as the linear increase in electricity demand because there is no renewable investment in this case.

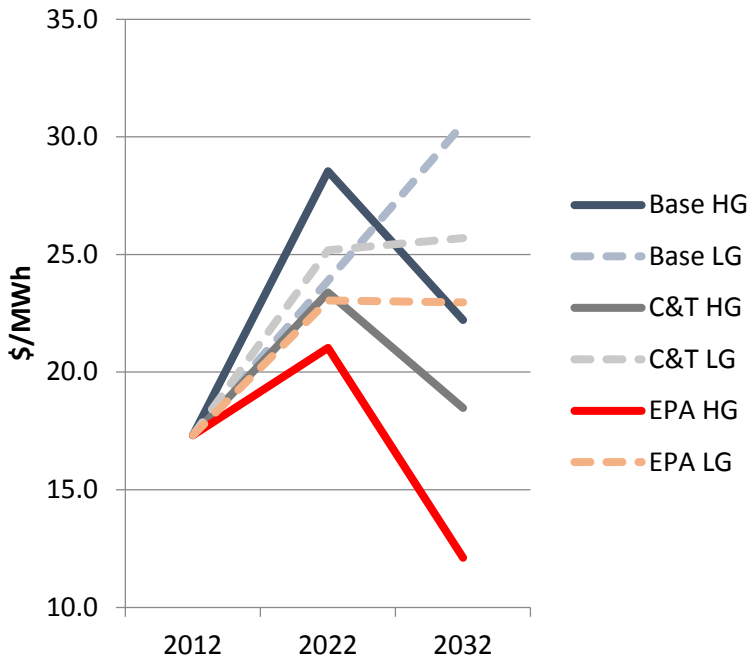

Figure 5.24. Average production cost in WECC.

The results of average annual CO_2 emissions, shown in Figure 5.25, provide important information that indicates the effectiveness of the emission regulatory policies. As expected, only C&T cases effectively regulate the CO_2 emissions with increased demand and decreased hydro electricity generation. The CO_2 emissions in EPA cases are sensitive to the price of natural gas. In EPA LG, renewable incentives even fail to reduce the CO_2 emissions in 2022. In other words, with a continuation of the current low shale gas price, renewable incentives of $22/MWh are not likely to help bring more renewables. If so, either more incentives or CO_2 emission caps, or both, should be added to regulate emissions.

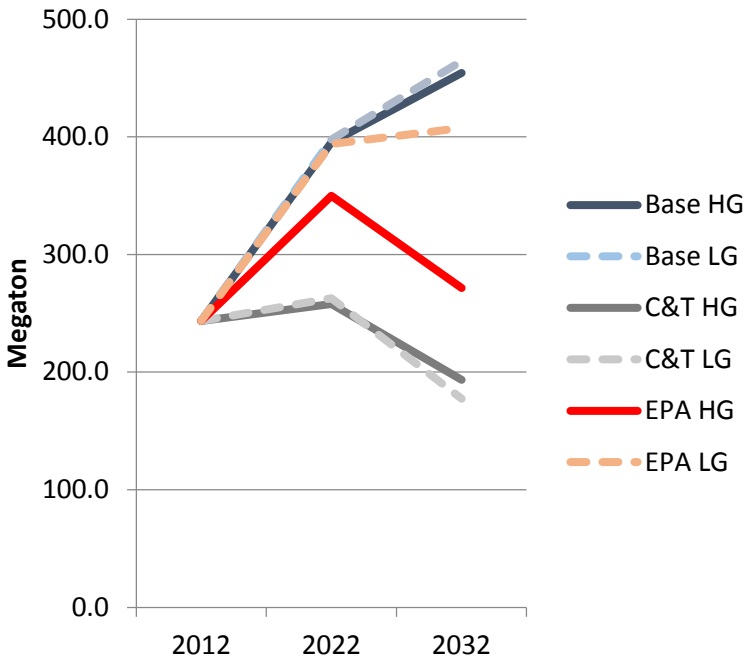

Figure 5.25. Annual CO_2 emissions in WECC.

5.2.4 Discussion

Although the simulation results of the WECC model are different from those shown in the M-24 report, the deviations reflect the modeling differences, such as the modeling of renewable, hydro, EES, and demand response. Some new observations found in this study include the investment uncertainty of wind and solar generation; the higher potential of nuclear and coal generation, and NGCC in certain cases; and the great potential of CAES.

The planning results in this study are critically based on the cost data and the network topology. The cost data of each fuel type are collected from multiple reports with some assumptions through derivation. The transmission interface limits are not used in the planning study because the operation limits are subject to change in the future. The power limit of each transmission line is estimated from the rated voltage, impedance, surge impedance loading (SIL) and thermal rating, and then adjusted to satisfy the power flow limits on each transmission path. These estimations are the major factors that influence the simulation results.

The CAES technology, instead of conventional pumped-hydro storage, is selected as the representative for the investment test of bulk EES. Similar to conventional pumped-hydro storage, CAES has a much lower cost per MWh than its cost per MW. The per unit energy capacity cost of CAES is even lower than pumped hydro. Although the current data report that the average cycle efficiency of CAES is lower than that of pumped hydro, the overall value of CAES is higher than that of pumped hydro. In addition, air is more abundant than water as a media to store energy, and it avoids any future limitations on

water use [41]. In general, CAES technology has the potential to surpass pumped hydro, which has been dominating the bulk storage application for more than a half century.

6. Conclusions and Future Work

6.1 Conclusions

The major accomplishment of this research is the development of an optimization model for generation and energy storage planning research. This model incorporated energy regulatory policies, hourly renewable profiles, and optimal operation-based investment of EES. The work also constructed the 240-bus WECC model in MATPOWER and analyzed the short-term operations under different renewable penetration levels. All optimization problems in this project were solved by utilizing MATPOWER's extensible OPF framework, which provides users with the flexibility of adding extra variables, constraints, and costs by either direct formulation or by using callback functions. In order to test the proposed optimization model, the 3-bus test system and the WECC model were set up and applied to the problem in multiple study scenarios. The key observations and conclusions are summarized as follows:

- The increased penetration level of wind and solar generation challenges both the operation and planning of a power system. The practical models developed in this research will allow for a study of their impacts before connecting them to the grid.
- The generation planning model that includes energy storage developed in this research is needed for researchers, engineers, and policy makers to quantify the potential impacts of the market, costs, and policies on future investment. The cost analysis mechanism, the algorithm of network simplification, and the simulation environments affect simulation results to a great extent.
- The economic value of current CAES and pumped-hydro storage are ahead of other technologies when built as bulk energy storage. Their benefits from energy arbitrage are determined by the LMP deviations at their locations. A higher LMP deviation at a certain bus could be caused by the following: a higher penetration level of a variable renewable, especially wind; a high penetration level of low-production-cost generators, such as nuclear and coal; and one or more congested connected transmission lines.
- Wind and solar generation are limited by resource-dependency, variability, and expensive capital cost. Without emission regulations or renewable incentives, wind and solar investment will slow down in the near future.
- If the natural gas price remains at a lower average of around $3/MBTU, with the shale gas supply, more natural gas generators with advanced combined cycle technology will be installed and operate as base-load units. Coal generators in the WECC system will be phased out automatically because they are located far away from the load center, and their produced energy is not accepted by California.
- If the price of natural gas increases unreasonably, e.g., with the annual average price above $10/ton, the investment in wind, solar, nuclear, and bulk energy storage will be notably increased.
- The size of this optimization problem is larger than the planning model in the M-24 report in terms of having more simulation time points (672 typical hours

annually instead of 12 representative hours), the additional optimal planning model of EES, and optimization of hydro generation. With the DELL Workstation (Intel Xeon 1.60 GHz 8 cores, 54 GB RAM), 64-bit MATLAB, and Gurobi high-performance solver, the average solving time of the proposed planning model for the 3-bus test system is 5 seconds. For the 240-bus WECC model, it takes approximately 3,000 seconds to solve each single year.

6.2 Future Work

According to the observations and conclusions throughout this report, the following future work is recommended:

- Add unit commitment and ramp rates to short-term operation studies to analyze the value of EES.
- Combine the stochastic two-stage solver in SuperOPF with the EES model for short-term operation studies.
- Apply the EES model to the market operation model to verify the practical value of EES in different power markets, or design the market according to a specific application of EES.
- Add a seasonal or even monthly capacity factor for each hydro generator if the data are available in long-term planning studies.
- Reduce the simulation time points (typical hours) to shrink the problem size without losing too much accuracy in long-term planning studies.
- Add a transmission planning model to the generation planning model.
- Add demand response to either the operation model or the planning model.

References

[1] Zhouxing Hu, *Optimal generation expansion planning with integration of variable renewables and bulk energy storage systems*. PhD dissertation, Wichita State University, 2013. soar.wichita.edu:8080/handle/10057/6724

[2] J. E. Price and J. Goodin, "Reduced Network Modeling of WECC as a Market Design Prototype," IEEE General Meeting, Detroit, MI, Jul. 2011.

[3] M. Shao, "The Effects of Greenhouse Gas Limits on Electric Power System Dispatch and Operations," Ph.D. dissertation, Wichita State University, Wichita, KS, 2008.

[4] L. T. Anstine and R. J. Ringlee, "Susquenhanna River Short-Range Hydrothermal Coordination," *AIEE Trans*., vol. 82, part III, pp. 185–191, Apr. 1963.

[5] A. J. Wood and B. F. Wollenberg, *Power Generation Operation and Control*, Second Edition, John Wiley & Sons, Inc., 1996.

[6] T. Y. Lee and N. Chen, "The Effect of Pumped Storage and Battery Energy Storage Systems on Hydrothermal Generation Coordination," *IEEE Trans., EC-7*, vol. 4, pp. 631–637, 1992.

[7] K. Aoki, T. Satoh, and M. Itoh, "Unit Commitment in a Large-Scale Power System Including Fuel Constrained Thermal and Pumped-Storage Hydro," *IEEE Trans. PWRS-2*, vol. 4, pp. 1077–1084, 1987.

[8] R. Walawalkar and J. Apt, "Market Analysis of Emerging Electric Energy Storage Systems," Final Report, DOE/NETL-2008/1330, Jul. 2008.

[9] H. Liu, L. Tesfatsion, and A. A. Chowdhury, "Derivation of Locational Marginal Prices for Restructured Wholesale Power Markets," California Independent System Operator.

[10] Z. Hu and W. T. Jewell, "Optimal Power Flow Analysis of Energy Storage for Congestion Relief, Emissions Reduction, and Cost Savings," IEEE Power Systems Conference and Exposition, Phoenix, AZ, Mar. 2011.

[11] H. Oh, "Optimal Planning to Include Storage Devices in Power Systems," *IEEE Trans. Power Syst*., vol. 26, no. 3, pp. 1118–1128, Aug. 2011.

[12] A. J. Lamadrid, T. D. Mount, and R. J. Thomas, "Scheduling of Energy Storage Systems with Geographically Distributed Renewables," Ninth IEEE International Symposium on ISPAW, Busan, South Korea, May 2011.

[13] D. J. Swider, "Compressed Air Energy Storage in an Electricity System With Significant Wind Power Generation," *IEEE Trans. Power Syst*., vol. 22, no. 1, pp. 95–102, Mar. 2007.

[14] A. Tuohy and M. O'Malley, "Impact of Pumped Storage on Power Systems with Increasing Wind Penetration," IEEE PES GM, Alberta, Canada, Jul. 2009.

[15] H. Daneshi, A. K. Srivastava, and A. Daneshi, "Generation Scheduling with Integration of Wind Power and Compressed Air Energy Storage," IEEE PES TDCE, New Orleans, LA, Apr. 2010.

[16] W. Schulze, W. Jewell, D. Tylavsky, J. Taber, J. Yan, D. Shi, N. Li, Y. Qi, T. Hardy, and Z. Hu, "Interactions of Multiple Market-Based Energy and Environmental Policies in a Transmission-Constrained Competitive National Electricity Market," Final Project Report of PSERC Project M-24, Sept. 2012.

[17] R. D. Zimmerman and C. E. Murrillo-Sanchez, *SuperOPF 1.0 User's Manual*, Jun. 2011.

[18] R. D. Zimmerman, C. E. Murrillo-Sanchez, and R. J. Thomas, "MATPOWER's Extensible Optimal Power Flow Architecture," IEEE PES GM, Alberta, Canada, Jul. 2009.
[19] P. Poonpun, "Effects of Low Carbon Emission Generation and Energy Storage on Greenhouse Gas Emissions in Electric Power Systems," Ph.D. dissertation, Wichita State University, Wichita, KS, 2009.
[20] PowerWorld Corporation, *PowerWorld Simulator Version 14 User's Guide*.
[21] H. Wang, C. E. Murillo-Sanchez, R. D. Zimmerman, and R. J. Thomas, "On Computational Issues of Market-Based Optimal Power Flow," *IEEE Trans. Power Syst.*, vol. 22, no. 3, pp. 1185–193, Aug. 2007.
[22] MINOPF. [Online]. URL: http://www.pserc.cornell.edu/minopf/ [cited Nov. 10, 2012].
[23] TSPOPF. [Online]. URL: http://www.pserc.cornell.edu/tspopf/ [cited Nov. 10, 2012].
[24] BPMPD. [Online]. URL: http://www.pserc.cornell.edu/bpmpd/ [cited Nov. 10, 2012].
[25] MOSEK. [Online]. URL: http://www.mosek.com/ [cited Nov. 10, 2012].
[26] CPLEX, IBM ILOG CPLEX Optimizer. [Online].
URL: http://www-01.ibm.com/software/integration/optimization/cplex-optimizer/ [cited Nov. 10, 2012].
[27] GUROBI, Gurobi Optimization. [Online]. URL: http://www.gurobi.com/ [cited Nov. 10, 2012].
[28] N. P. Yu, C. C. Liu, and J. Price, "Evaluation of Market Rules Using a Multi-Agent System Method," *IEEE Trans. Power Syst.*, vol. 25, no. 1, pp. 470–479, Jan. 2010.
[29] J. Jung, C. C. Liu, S. Tanimoto, and V. Vital, "Adaptation in Load Shedding under Vulnerable Operating Conditions," *IEEE Trans. Power Syst.*, vol. 17, no. 4, pp. 1199–1205, Nov. 2002.
[30] Description of the PTI Load Flow Data Format, URL: http://www.ee.washington.edu/research/pstca/formats/pti.txt [cited Nov. 10, 2012].
[31] C. Grigg, etc., " The IEEE Reliability Test System – 1996, A Report Prepared by the Reliability Test System Task Force of the Application of Probability Methods Subcommittee," *IEEE Trans. Power Systems*, vol. 14, no. 3, pp. 1010–1020, Aug. 1999.
[32] EIA, Average Operating Heat Rate for Selected Energy Sources, 2001 through 2010. URL: http://www.eia.gov/electricity/annual/pdf/table5.3.pdf [cited Feb. 2012].
[33] EIA, Henry Hub Gulf Coast Natural Gas Spot Price, URL: http://www.eia.gov/dnav/ng/hist/rngwhhdA.htm [cited: Nov. 2012].
[34] R. Tidball, J. Bluestein, N. Rodriguez, and S. Knoke, "Cost and Performance Assumptions for Modeling Electricity Generation Technologies," Subcontract Report, NREL/SR-6A20-48595, Nov. 2010.
[35] P. Poonpun and W. Jewell, "Analysis of the Cost per Kilowatt Hour to Store Electricity," *IEEE Trans. Power Systems*, vol. 23, no. 2, Jun. 2008.
[36] M. Kintner-Meyer, P. Balducci, W. Colella, M. Elizondo, C. Jin, T. Nguyen, V. Viswanathan and Y. Zhang, "National Assessment of Energy Storage for Grid Balancing and Arbitrage: Phase 1, WECC," PNNL-21388, Jun. 2012.

[37] S. Schoenung, "Energy Storage Systems Cost Update, A Study for the DOE Energy Storage Systems Program," SANDIA Report, SAND2011-2730, Apr. 2011.
[38] S. Phinney, R. McCann, M. Cubed, G. Franco and M. Fagundes, "Potential Changes in Hydropower Production From Global Climate Change in California and the Western United States," prepared in support of 2005 Integrated Energy Policy Report Proceeding (Docket # 04-IEPR-01G), Jun. 2005.
[39] Loan Programs of Office, U. S. Department of Energy, URL: https://lpo.energy.gov/?page_id=31 [cited: Dec. 2012].
[40] EPA, Carbon Pollution Standard for New Power Plants, URL: http://epa.gov/carbonpollutionstandard/index.html [cited Feb. 25 2013].
[41] W. Jewell, J. Twomey, M. Overcash, J. Cardell, and L. Anderson, "Future Grid: The Environment," *Future Grid Initiative White Paper*, PSERC Publication 12-04, May 2012.

Appendix A: Input Data Format

The input data format of the constructed m-files that support the planning model proposed in this work are listed in Table A.1, Table A.2, and Table A.3.These data are specified as matrices in the case struct file.

Table A.1. EES Data (*Mpc.Storage2*)

Name	**Column**	**Description**
BUS	1	Bus number (EES location)
PS_MIN	2	Minimum investment of power capacity
PS_MAX	3	Maximum investment of power capacity
ES_MIN	4	Minimum investment of energy capacity
ES_MAX	5	Minimum investment of energy capacity
PS_CC	6	ACR of power capacity
ES_CC	7	ACR of energy capacity
OM_CC	8	O&M cost
INI_RATE	9	Initial rate of energy storage (0~1)
EFF_C	10	Efficiency of charging cycle
EFF_D	11	Efficiency of discharging cycle
PS†	12	Power capacity invested
ES†	13	Energy capacity invested

†Only included in OPF output, i.e., *results.storage2*

Table A.2. Generator Retirement Data (*Mpc.Retire*)

Name	**Column**	**Description**
GEN_IDX	1	Sequence number of generator that can be retired in *mpc.gen*
R_MIN	2	Requirement of minimum retirement
R_MAX	3	Allowance of maximum retirement
CR_R	4	Annual total fixed cost ($/MW)
CF_R	5	Capacity factor
R†	6	Retirement result

†Only included in the OPF output, i.e. *results.retire*

Table A.3. Generator Investment Data (*Mpc.Invest*)

Name	**Column**	**Description**
BUS	1	Bus number that new generator can be placed
TYPE	2	Fuel type – 1_coal, 2_natural gas, 3_ nuclear, 4_wind, 5_solar
I_MIN	3	Requirement of minimum investment
I_MAX	4	Allowance of maximum investment
CI	5	Annual capital recovery ($/MW)
CR_I	6	Annual total fixed cost ($/MW)
CF	7	Production cost including emission cost and renewable subsidy ($/MWh)
R_IDX	8	Column index of the associated renewable profile (particularly for wind and solar)
CF_I	9	Capacity factor
I†	10	Investment result

†Only included in the OPF output, i.e., *results.invest*

Appendix B: Renewable Profile Approximated from Available Data

Table B.4. Wind Profile Mapping at Each Generator Bus

Bus Index	Name	Wind Profile Index	Capacity Factor (%)
1032	FCNGN4CC	CORONADO {1131 W future}	35.18
1034	SJUAN G4		
1131	CORONADO		
1232	NAVAJO 2		
1331	HOOVER		
1333	H ALLEN		
1431	PALOVRD2		
2030	MEXICO	MESA CAL {2438 SW future}	37.03
2130	IMPERIAL		
2233	MISSION		
2332	IMPRLVLY		
2438	MESA CAL		
2533	S.ONOFRE		
2630	HAYNES3G		
2631	OLIVE		
2634	INTERM1G		
2637	OWENS G		
2638	CASTAI4G		
3133	SANMATEO	PITSBURG {3234 NW future}	15.82
3135	POTRERO		
3234	PITSBURG		
3333	METCALF		
3432	HELMS PP		
3433	MC CALL		
3531	FULTON		
3631	HUMBOLDT		
3731	SUMMIT		
3831	DIABLO1	TESLA {3933 NW future}	16.26
3835	MIDWAY		
3836	MORROBAY		

Bus Index	Name	Wind Profile Index	Capacity Factor (%)
3931	ROUND MT		
3932	MOSSLAND		
3933	TESLA		
4031	MALIN	MALIN {4031 W future}	22.45
4035	JOHN DAY	JOHN DAY {4035 W future}	23.87
4039	DALLES21	DALLES21 {4039 W future}	21.49
4131	COULEE	COULEE {4131 W future}	25.86
4132	HANFORD	HANFORD {4132 W future}	19.80
4231	NORTH G3	WCASCADE {4232 W future}	16.37
4232	WCASCADE		
5031	CANAD G1	CMAIN GM {5032 W future}	42.48
5032	CMAIN GM		
6132	MIDPOINT	MIDPOINT {6132 W future}	20.35
6231	COLSTRP	MONTA G1 {6235 W future}	32.69
6235	MONTA G1		
6333	BRIDGER	BRIDGER {6333 W future}	41.41
6335	NAUGHT		
6433	VALMY	VALMY {6433 W future}	25.83
6533	EMERY		
7031	COLOEAST	COLOEAST {7031 W future}	36.72
7032	CRAIG		
8033	COTWDWAP	TESLA {3933 NW future}	16.26
8034	RNCHSECO		

Table B.5. Solar Profile Mapping at Each Generator Bus

Bus Index	Name	Solar Profile Index	Capacity Factor (%)
1032	FCNGN4CC	H ALLEN {1333 S future}	36.03
1034	SJUAN G4		
1131	CORONADO		
1232	NAVAJO 2		
1331	HOOVER		
1333	H ALLEN		
1431	PALOVRD2	PALOVRD2 {1431 S future}	36.53
2030	MEXICO	IMPERIAL {2130 S future}	41.73
2130	IMPERIAL		
2233	MISSION		
2332	IMPRLVLY		
2438	MESA CAL	MESA CAL {2438 SS Future}	41.73
2533	S.ONOFRE		
2630	HAYNES3G		
2631	OLIVE		
2634	INTERM1G		
2637	OWENS G		
2638	CASTAI4G		
3133	SANMATEO	PALOVRD2 {1431 S future}	36.53
3135	POTRERO		
3234	PITSBURG		
3333	METCALF		
3432	HELMS PP		
3433	MC CALL		
3531	FULTON		
3631	HUMBOLDT		
3731	SUMMIT		
3831	DIABLO1		
3835	MIDWAY		
3836	MORROBAY		
3931	ROUND MT		
3932	MOSSLAND		
3933	TESLA		

Bus Index	Name	Solar Profile Index	Capacity Factor (%)
4031	MALIN	EMERY {6533 S future}	32.40
4035	JOHN DAY		
4039	DALLES21		
4131	COULEE		
4132	HANFORD		
4231	NORTH G3		
4232	WCASCADE		
5031	CANAD G1		
5032	CMAIN GM		
6132	MIDPOINT		
6231	COLSTRP		
6235	MONTA G1		
6333	BRIDGER		
6335	NAUGHT		
6433	VALMY		
6533	EMERY		
7031	COLOEAST		
7032	CRAIG		
8033	COTWDWAP	PALOVRD2 {1431 S future}	36.53
8034	RNCHSECO		

Intentionally Blank

Part II

The Cost and Benefit of Bulk Energy Storage in the Arizona Power Transmission System

Gerald T. Heydt, Faculty
John R. Ruggiero, Graduate Research Assistant

Arizona State University

For information about Part II, contact

Gerald T. Heydt
Regents' Professor
School of Electrical, Computer and Energy Engineering
Arizona State University
PO Box 875706
Tempe, AZ 85287-5706
Telephone: 480 965 8307
Fax: 480 965 0745
Email: heydt@asu.edu

Power Systems Engineering Research Center

The Power Systems Engineering Research Center (PSERC) is a multi-university Center conducting research on challenges facing the electric power industry and educating the next generation of power engineers. More information about PSERC can be found at the Center's website: http://www.pserc.org.

For additional information, contact:

Power Systems Engineering Research Center
Arizona State University
527 Engineering Research Center
PO Box 875706
Tempe, AZ 85287-5706
Phone: 480-965-1643
Fax: 480-965-0745

Notice Concerning Copyright Material

Table of Contents

List of Figures

List of Tables

Nomenclature

a	The quadratic coefficient of the approximation for the cost of generation
A	Coefficient matrix (m x n) of inequality constraints
A_{eq}	Coefficient matrix (k x n) of equality constraints
ACE	Area control error
AGC	Automatic generation control
b	The linear coefficient of the approximation for the cost of generation
b	Vector (m x 1) of inequality right-hand side constraints
B	Frequency bias (MW/mHz); part of supplementary control
b_{eq}	Vector (k x 1) of equality right-hand side constraints
B_k	Susceptance of transmission element k
c	The coefficients of the cost function of generator g
c	The no load coefficient of the approximation for the cost of generation
CA	Combined cycle steam part
CAES	Compressed air energy storage
C_g	The linear coefficient, b, of the cost function of generator g
CSP	Concentrated solar power
CT	Combined cycle combustion turbine part
D	Frequency independent component of the load in AGC
DP	Dynamic programming
ED	Economic dispatch
E/P	The ratio of maximum energy stored in a pumped hydro facility to the maximum power (i.e., rated power). E is usually in MWh and P in MW.

EPAct	Energy policy act
E_s	The energy stored in storage unit *s* in MWh
$E_{s,max}$	Maximum energy capacity of storage unit *s* in MWh
E_T	Total energy supplied in MWh
F_C	Generator fuel cost in $/MBTU
FES	Flywheel energy storage
Governor	Measures speeds and adjusts steam valves to change generation
GT	Gas turbine
i	Interval number
K/s	Gain of the AGC integral controller; part of supplementary control
k(. ,n)	Set of transmission assets with *n* as the 'FROM' node
k(n, .)	Set of transmission assets with *n* as the 'TO' node
l	Vector of lower bound variables
LMP	Locational marginal price
Load	Represents the transfer function of a specified load. Parameter *M* is the frequency dependent component and *D* is the frequency independent component
LP	Linear programming
M	Frequency dependent component of the load in AGC
m,n	Bus number (nodes)
MIPs	Mixed integer programming
P_g	The real power output of generator *g* in MW
$P_{g,max}$	Maximum power capacity of generator *g* in MW

$P_{g,min}$	Minimum power capacity of generator g in MW
PHES	Pumped hydro energy storage
P_k	The power flow of transmission line k in MW
$P_{k,max}$	Maximum line flow rating of transmission element k in MW (generally $P_{k,max=} - P_{k,max}$)
P_l	The active power of load l in MW
PM	Prime mover; provides torque necessary to turn the shaft of a generator
P_{peak}	Peak power demand in MW
P_s	The real power output of storage unit s in MW
$P_{s,max}$	Maximum power capacity of storage unit s in MW
$P_{s,min}$	Minimum power capacity of storage unit s in MW
PSO	Particle swarm optimization
PV	Photovoltaic
Q_g	The quadratic coefficient, a, of the cost function of generator g
QP	Quadratic programming
1/R	Speed droop characteristic of the generator (included in the governor system)
R_g	Ramp rate limit of generator g in $\frac{MW}{hr}$
RPS	Renewable portfolio standard
s	Laplace transform variable
SCES	Supercapacitor energy storage
SLP	Successive linear programming
SMES	Superconductor magnetic energy storage
SRP	Salt River Project

ST	Steam turbine
T	Time period in hours
T/s	Tie line constant
TES	Thermal energy storage
u	Vector of upper bound variables
V_{OM}	Generator variable operation and maintenance costs in $/MWh
WECC	Western Electricity Coordinating Council
x	The vector generated system variable outputs
x_j	Variables that must be integers
δ_k	Bus voltage angle at node *k*
ΔP_{Tie}	Tie line power flow between areas one and two
Δt	Length of the time interval *i* in hours
$\Delta\omega$	Change in area frequency, r/s

1. Objectives relating to bulk energy storage in power transmission systems

1.1 Description of this research: bulk energy storage

Motivation

High penetrations of renewables are inevitable as higher renewable portfolio standards are implemented. There are a variety of proposed methods to address the variability issues associated with many renewable resources. It is possible to rely on conventional generators to provide ancillary services and backup generation; however, this may reduce the value of renewable resource investments. Demand response and demand side management can transition the system from 'supply following load' to at least a partial 'load following supply' structure. Energy storage provides a third and potentially attractive resource for matching supply to load. Bulk storage has the potential to become a competitive solution in the mix of approaches to achieve high levels of variable renewable resources. The central question relating to bulk storage use is an economic question. When do bulk energy storage and its concomitant transmission deferral possibilities, reserve margin alleviation, generation expansion deferral, and other enhancements offset the potentially high cost of storage?

Bulk energy storage

The project examines the economic case for various types of bulk energy storage. One primary objective is the evaluation of the cost to benefit ratio of bulk energy storage with variable renewable resources and to understand how the cost to benefit ratio changes for penetration levels from 2% to 50%. The researchers will provide a thorough examination of the economic benefits for energy storage and compare bulk energy storage to conventional generation.

Energy storage can provide a long list of benefits. The integration of renewable resources with their variability in supply motivates the use of bulk energy storage. Storage can also dramatically improve system load factor, thereby maximizing the utilization of generation and transmission assets. Additionally, storage can help defer both generation and transmission expansion. However, the cost and novelty of bulk energy storage is still a detractor today. The following subsections discuss the various benefits of bulk energy storage given high levels of variable renewable resources, with these subsections defining the focal points of this research.

1.2 An introduction to bulk energy storage

This research addresses the economic case for bulk energy storage optimized for multiple objectives including cost, congestion, and peak shaving for increasing levels of renewable resource penetration. The test bed used is the Arizona electric transmission system.

Arizona, like most states, has put forth a road map plan for the incorporation of renewable energy resources [1]. This type of plan is generally known as a Renewable Portfolio Standard (RPS). High penetration of solar and wind resources is inevitable as the RPS is implemented. There are a variety of proposal methods to address the variability issues associated with wind and solar renewable sources. It is possible to rely on conventional generators to provide ancillary services and backup generation; however this may reduce the value of renewable resource investment. Energy storage provides a potentially attractive resource for matching supply to load.

The central question relating bulk storage use is an economic question: when do bulk energy storage and its concomitant transmission deferral possibilities, reserve margin alleviation, and other enhancements offset the potentially high cost of storage. This is the main subject of this research.

This research focuses on how energy storage can be used to potentially reduce conventional generator operating costs. The possible cost reduction will be shown through an economic dispatch model comparing the cost of generation before and after the inclusion of energy storage in the system. The focus is on Arizona, and therefore the test bed used is the 2010 summer peak Arizona system. The analysis investigates peak shaving in order to lower the generating costs during periods of high demand. Also, the alleviation of congestion in the transmission system shall be studied for its benefits. Finally, this research will examine how bulk energy storage might be used to maximize the use of renewables.

Bulk energy storage at the transmission level will be evaluated based on benefits of:

- alleviation of uncertainty in the energy supply
- reduction of peak loading
- potential deferral of transmission expansion
- improvement in system efficiency
- incorporation of required RPS renewable generation
- maintaining system frequency by maintaining load-generation balance
- reduction of transmission congestion
- maintaining required reserve margins
- improvement of system reliability.

The objectives listed above will be applied to the state of Arizona using data provided by a statewide utility, Salt River Project (SRP), of the electric power grid. The results gathered from this test bed will be used to evaluate the practicality of bulk energy storage in Arizona.

1.3 Bulk energy storage applications

In this section, the main bulk energy storage applications in large electric power systems are discussed.

Peak shaving/ load leveling

Load leveling or peak shaving refers to the use of electric energy stored during times of low demand to supply the peak electric demand. Peak shaving reduces the need to draw on generation resources from peaking power plants or increasing the grid structure [2]. For most load profiles, the system demand is low during the early morning hours and high in the midday through the evening hours [3]. With peak shaving, during the early morning hours, the generation can be raised while storing energy. The stored energy can then be discharged during peak load hours so that the load peak is reduced. With load shaving however, the same process

occurs except the goal is to flatten the load profile. Figure 1.1 shows pictorially the process of peak shaving.

Frequency and area control error regulation

In a large interconnected power system, nominally the demand plus system losses are balanced by the generation. If there is a short term unbalance in this basic operating condition, the difference (power) comes from the rotating mass of the generating units,

$$\Delta P = \frac{dW}{dt}$$

where the difference in the power balance is ΔP and W is the system inertial energy. If energy is recovered from the rotating mass, the system frequency will change. For example, forced outage of generators can result in power unbalance. To restore the power balance, and to restore the operating frequency, power generation may be increased (or decreased). There is a limitation of how fast the power balance can be restored, and this suggests the potential use of high speed sources of power as might be available from electronically switched batteries.

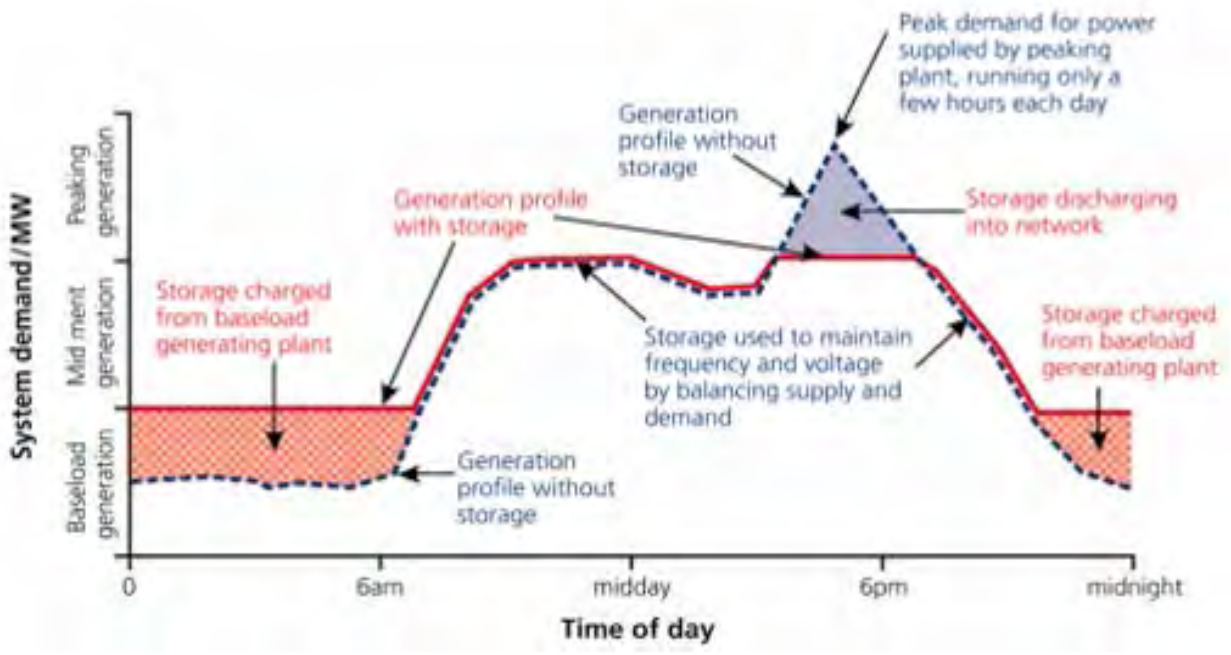

Figure 1.1 A diagram of showing peak shaving with energy storage (taken directly from [4])

The basic mechanism of frequency and system load control is accomplished using Automatic Generation Control (AGC), and Figure 1.2 shows a simplified two-area system under AGC [5]. Table 1.1 defines the nomenclature used in Figure 1.2. Analysis of a system under AGC indicates that as generation increases or load decreases, the frequency will increase (and energy storage can be used to store energy thus making the effective load higher). Similarly, energy storage may be used if generation decreases or load increases.

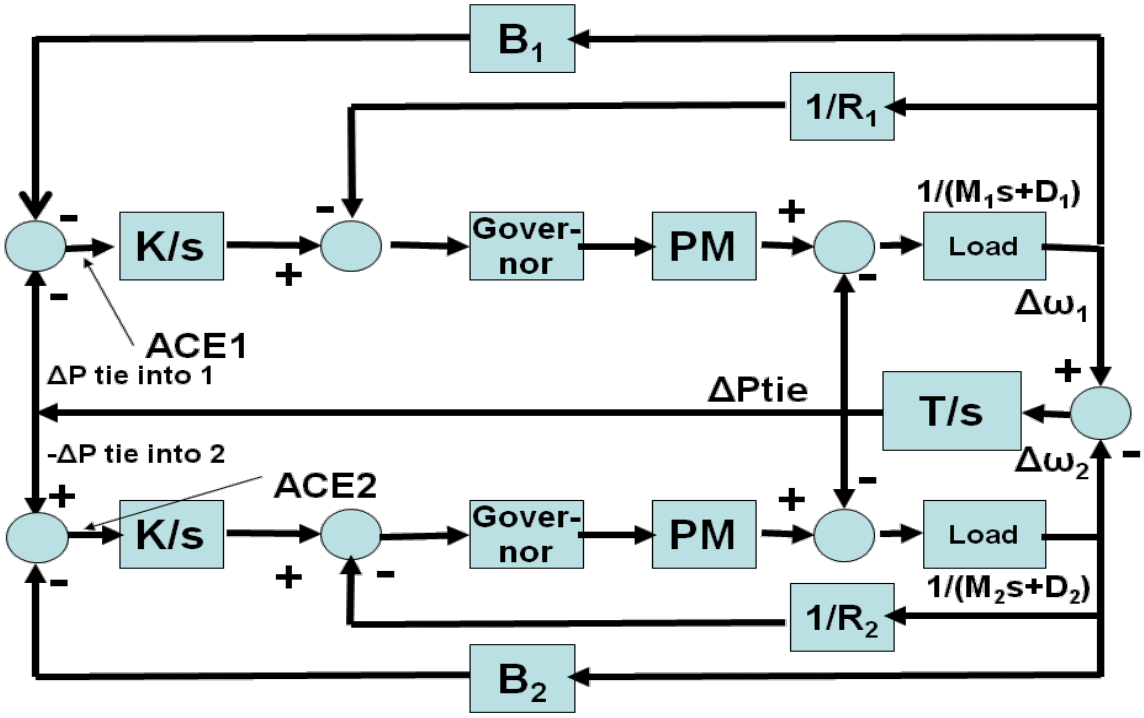

Figure 1.2 Automatic generation control of two control areas

Energy storage devices such as batteries have the capabilities of absorbing energy when the AGC Area Control Error (ACE) is high, and discharge the energy back into the grid when the ACE is low. Battery energy storage has a very fast response time and offers an alternative to the traditional strategy of maintaining adequate spinning reserve margins [6, 7]. Battery storage is electronically switched and can supply needed power rapidly. Energy storage can also help reduce or eliminate supplementary power from combustion turbines. With a large increase in wind generators in certain areas, there could be serious frequency problems in the electrical system because of the intermittent behavior of wind generation [8]. Again, energy storage can be used to reduce the generation uncertainty.

Transmission line expansion deferral

Transmission upgrades and new construction investments are necessary when line congestion limits the power that can be sent through an existing circuit [9]. Congestion can be avoided by using bulk energy storage on the 'receiving' end of a circuit to reduce transmission line loading. There is the potential, therefore, to reduce the need for transmission expansion and upgrades through the use of energy storage [10-13].

Other reasons for transmission line upgrades or expansion include:

- demand increase in existing networks
- demand increase due to new developments
- interconnection of renewable energy (i.e., wind or solar)
- existing lines reaching critical values of ampacity or sag
- enhancing system stability.

Table 1.1 Nomenclature for an AGC system

Symbol	Meaning	Symbol	Meaning
Area control error (ACE)	Instantaneous difference between a Balancing Authority's net actual and scheduled interchange	$1/R$	Speed droop characteristic of the generator (included in the governor system).
K/s	Gain of the AGC integral controller. Part of supplementary control.	Load $(\frac{1}{Ms+D})$	Represents the load at the specified area. Parameter *M* is the frequency dependent component and *D* is the frequency independent component.
B	Frequency bias (MW/MHz). Part of supplementary control.	*T/s*	Tie line constant
Governor	Measures speeds and adjusts steam valves to change generation.	$\Delta\omega$	Change in area frequency
Prime mover (PM)	Provides turning force necessary to turn the shaft of the generator.	ΔP_{tie}	Tie line power flow between areas one and two

Integration of renewables

There is a lot of interest in the area of renewable generation in North America [10]. Renewable energy has even become popular enough that various books have been written on the subject [15-18].A large amount of wind and solar generation are likely to be added over the next 30 years in order to follow the CO2 emission reduction policies [19]. EPRI's Prism Analysis estimates about 1350 MW of new renewable generation will be added to the US grid by 2030, thus representing 15% of the generation mix. One of the major drawbacks of renewable energy is that it is time of day and weather dependent. These resources are generally undispatchable and uncontrollable. Weather data from many resources are available to predict of solar and wind levels. These predictions can be used to forecast the energy outputs, but these are only predictions and there will exist a level of uncertainty. With energy storage integrated with renewable generation, two problems may be solved [20]. First, storage can stabilize the intermittent power output of the generators and improve the capacity factor of the system. Wind generation capacity factor is currently less than 40%. Secondly, energy storage can take the energy from wind that is usually higher at night and integrate the energy into periods of higher demand [9]. With larger MW scale solar photovoltaic (PV) installations, energy storage is useful to levelize output even under conditions of cloudiness [21].

Transmission line congestion

Transmission congestion occurs when the physical limitations of a transmission infrastructure prevent electricity transactions from occurring [22]. When this occurs, Locational Marginal Prices (LMPs) increase because the system would need to be redispatched to accommodate the transmission constraints. Transmission congestion charges are fees that are charged during periods of peak electricity usage because of the increased cost of providing power under high congestion [23]. Part of this charge is eventually passed onto the customer because of their use

during peak demand times. Energy storage can alleviate response to system contingencies if the storage elements are located properly [22]. Energy storage can be sited near congestion such that it could shift the delivery of generation from off peak to on peak. When reducing congestion in transmission lines relatively smaller energy storage systems, such as batteries, can be used during peak hours [24]. Other types of storage such as PHES and CAES are possible solutions but are very location dependent [25, 26]. Battery storage also has the advantage of having a fast response time, meaning it could respond quickly to transmission lines becoming congested.

Reserve margins

In power systems, scheduling reserve margins are kept in order to maintain security of the system if an unpredicted event occurs [27]. This security is maintained by the redispatch of the generators in the system. The expected load must be predicted (short term load forecasting) and sufficient generation must be planned. Reserve generation must also be scheduled in order to account for load forecast uncertainties and possible outages of a generation plant. According to Antonio [28], a reserve margin is defined as the amount of capacity, usually on standby, to be activated only under exceptional situations, typically during peak conditions. This approach disaggregates the generation into two categories, the main generation devoted to meet the demand in "normal conditions" and the reserve devoted to face "exceptional" system conditions. For the Southwest region, reserve margin estimates for the summer of 2012 were around 14-22% [29]. This means that an electric system must have excess capacity of 14-22% of the expected peak demand. Instead of having a high amount of generation only being used for "exceptional" conditions, energy storage can be used. The output from reserve generators may possibly vary from several hours to a few minutes but can respond instantaneously with some storage technologies. The amount of excessive generation to meet peak loads can also be reduced with storage since generated energy can be stored during off peak hours.

1.4 Principal energy storage technologies

The four main forms of energy storage that have the capability of performing some or all of the applications listed in Section 1.2 include:

Pumped Hydro Energy Storage (PHES)

PHES consists of two large reservoirs located at different elevations and a number of pump/turbine units [30]. During off peak electrical demand, water is pumped from the lower reservoir to the higher reservoir where it is stored. Once required during peak demands, the water in the upper reservoir is released through the turbines and electricity is produced from the connected generators. PHES is thus very similar to a conventional hydroelectric system. The storage capacity is very dependent on the head and the volume of the reservoirs. In order to create the highest storage capacity, pumped hydro is usually designed with the greatest hydraulic head possible. PHES has the capability of generating between 100-4000 MW of electrical power at efficiency 70-80%. PHES can be used for peak shaving and as spinning reserve. Also, with variable speed machines it can now be used for frequency regulation in pumping and generation.

Compressed Air Energy Storage (CAES)

In conventional gas turbines, 66% of the gas is used to compress the air at the time of generation. CAES pre-compresses the air using off peak electrical power, which is taken from the grid or

renewable generators, to drive a motor and compress air into a large storage reservoir [30]. When the gas turbine is producing electricity during peak hours, the compressed air is released and used in the conventional gas turbine cycle. Instead of using expensive gas to compress air, cheaper off peak power is used to pre-compress it in advance. CAES has the capability of producing 50-300 MW with proposed facilities capable of up to 2700 MW and an efficiency of 68-75%. It also provides a longer lifetime than a standard gas turbine. CAES has a fast reaction time with the capability of full power from 0% in less than 10 minutes. It is ideal for acting as a large sink for bulk energy supply and demand and can undertake frequent startups and shutdowns. CAES can be used for frequency regulation, load following, and voltage control.

Battery energy storage (lead acid)

Lead-acid batteries are made up of two electrodes that are constructed using lead plates immersed in a mixture of water and sulfuric acid [30]. The battery has alternating lead and lead oxide plates. Current flows from the lead oxide cathode to the lead anode. Electrons are passed to the lead acid plate and both plates are converted to lead sulfate. When voltage is applied to the battery, which is greater than the batteries volt-age, current will flow through the battery in the reverse direction of when it is supplying current and will charge the battery. The rate of charge depends on the voltage difference. When the battery is switched to a load, the current will flow towards that load and the battery voltage will begin to drop due a decrease in the internal resistance. Lead acid batteries use these operating characteristics to store energy and release the power when it is required. They have a long lifespan, fast response, and low self-discharge rate. Batteries also have very fast ramp rates and can respond within milliseconds at full power. It has been shown that they can have capacities up to 50 MW and can store up to 200 MWh of energy at an efficiency of 75-85%. Batteries can be used for peak shaving, backup energy, load leveling, power quality, and frequency fluctuations [31-33].

Solar Thermal Energy Storage (TES)

Concentrated Solar Power (CSP) technology uses heat collected from solar thermal troughs. The heat is focused on oil (e.g., *thermoil*) in tubing [30]. The oil flows from a low temperature storage tank and uses the high concentration of the sun from solar troughs to heat the oil and raise it to high temperatures, e.g., 150–350 °C. The oil is then heat exchanged with molten salt (e.g., calcium sulfate) and stored in a high temperature storage tank. When it desired to recover the stored energy, the molten salt is released into another heat exchanger with water. The steam produced is then used in the conventional Rankine cycle power plant [34, 35]. CSP has the capability to store energy captured from the sun during off peak hours and use it during peak demand when less energy from the sun is available. Depending on the material and the size of the tank, CSP has the capability to store heat up to 24 hours. To give an idea of the capabilities of CSP, note that a large CSP plant has the ability of storing up to 400 MWh of energy at an efficiency of 85-95% with an overall plant efficiency of about 30-60%. CSP can be used for peak shaving and as spinning reserve.

Other smaller scale energy storage methods that were not considered for this project include:

Supercapacitor Energy Storage (SCES)

Supercapacitors store energy in the chemical valence states or in the so called “Helmholtz” double layer that exists around the carbon fibers in the alkaline solution [36]. The main attraction

of SCES is its fast charge and discharge, combined with its extremely long life of approximately 1 x10^6cycles [30]. SCES is primarily used where pulsed power is needed in the millisecond to second time range, with discharge times up to one minute. However, SCES has a very low energy storage density leading to high capital costs for larger scale applications.

Flywheel Energy Storage (FES)

Flywheels store energy by accelerating the rotor/flywheel to a very high speed and maintaining the energy in the system as kinetic energy [30]. They release energy by reversing the charging process so that the motor is then used as a generator. Flywheels have an extremely fast dynamic response, a long life, and require little maintenance. They are used for power quality enhancements like capturing waste energy and dampening frequency variations. However, they are optimal for power or storage capacities, but the need of one application can often make the design poorly suited for the other. Also, they are kept in vacuum so it is difficult to transfer heat out of the system, thus a cooling system is usually needed.

Fuel cells

A fuel cell is an apparatus that produces power through an electrochemical reaction rather than combustion [37]. It allows the continuous supply of fuel and electricity. Fuel cells run off hydrogen 'fuel' and produce energy and waste products, mostly water vapor. They can achieve high efficiencies in energy conversion terms and have a high power density which allows them to be a relatively compact source of electric power [38, 39]. However, they have very high costs compared to other energy system technologies.

A few applications of fuel cells at the distribution level include [40-42]:

- grid reinforcement
- deferring or eliminating the need for system upgrades
- improving system integrity, reliability, and efficiency
- generating heat for residential, commercial, or industrial applications.

Superconducting Magnetic Energy Storage (SMES)

A SMES is a device made up of a superconducting coil, a power conditioning system, a refrigerator, and a vacuum to keep the coil at a low temperature [30]. Energy is stored in the magnetic field created by the flow of direct current in the SMES. Due to the high power capacity, and its instantaneous discharge rates, it is used for protection of industrial equipment from rapid momentary voltage sags and to stabilize fluctuations within the entire network. However, due to high energy consumption of the refrigerator system, SMES is unsuitable for daily cycling applications such as peak reduction, renewable applications, and generation and transmission deferral [35].

1.5 Organization of this report

This report is organized into five chapters and three appendices.

- Chapter 2 defines the economic dispatch problem and gives different methods to solve it. Also, a method is selected to formulate the problem used throughout the report.
- Chapter 3 uses the algorithm from Chapter 2 to introduce energy storage in the state of Arizona, which is the chosen test bed.
- Chapter 4 uses the same test bed as Chapter 3 but analyzes an "extreme" amount of energy storage to the system.
- Chapter 5 analyzes how relaxing selected constraints in the system affects the results.
- Chapter 6 presents conclusions and suggests future work related to bulk energy storage in energy systems.

There are also three appendices: Appendix A which provides the MATLAB code used for this research and Appendix B, which describes the quadratic programming algorithm and observation made related to the algorithm. Appendix C contains brief comments on the environmental impacts of pumped hydro energy storage. This subject is beyond the scope of this report, but site specific references are cited to partially document the subject of environmental impact.

2. The optimization tools needed to address the engineering of bulk energy storage

2.1 Economic dispatch

The goal of power Economic Dispatch (ED) is the constrained minimization of the generator operating cost [43]. This is accomplished by determining the power output of all generating units under the constraint conditions of the system topology and the system load demand. That is, this is a constrained minimization problem in which the operating cost is minimized subject to the constraint that the load is satisfied and the electric circuit laws are satisfied. Additional constraints include operation within the ratings of the circuit assets, contractual limits, and environmental limits. Figure 2.1 shows the basic concept pictorially. The figure shows the input data, the principal constraints, and the dispatch schedule that minimize the operating cost. According to EPAct, economic dispatch is defined as "the operating of generation facilities to produce energy at the lowest cost to reliably serve consumers, recognizing any operating limits of generation and transmission facilities" [44].

For thermal units, the input-output characteristic mentioned earlier is the generating unit fuel consumption function, or the operating cost function [43]. Generator fuel consumption is measured in BTU/h or its multiple 106 BTU/h = 1 MBTU/h. The fuel cost multiplied by the generating fuel consumption function is the operating cost expressed in$/ h, and is denoted as F. The function F for a given generator is often expressed as an approximately quadratic function of the power output (MW) of the unit. The output of the generating unit is designed by PG, the megawatt net power output. In addition to the fuel consumption cost, the operating cost includes labor cost, maintenance cost, and fuel transportation cost. It is difficult to express these costs as a function, so they are included as a fixed portion, or a no load cost. Figure 2.2 shows an example of the cost curve of a representative thermal generating unit.

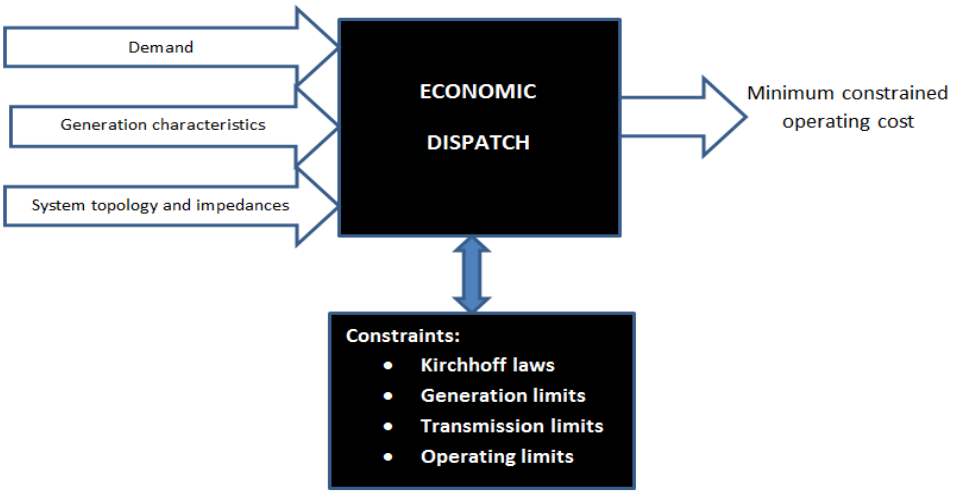

Figure 2.1A pictorial of the economic dispatch problem

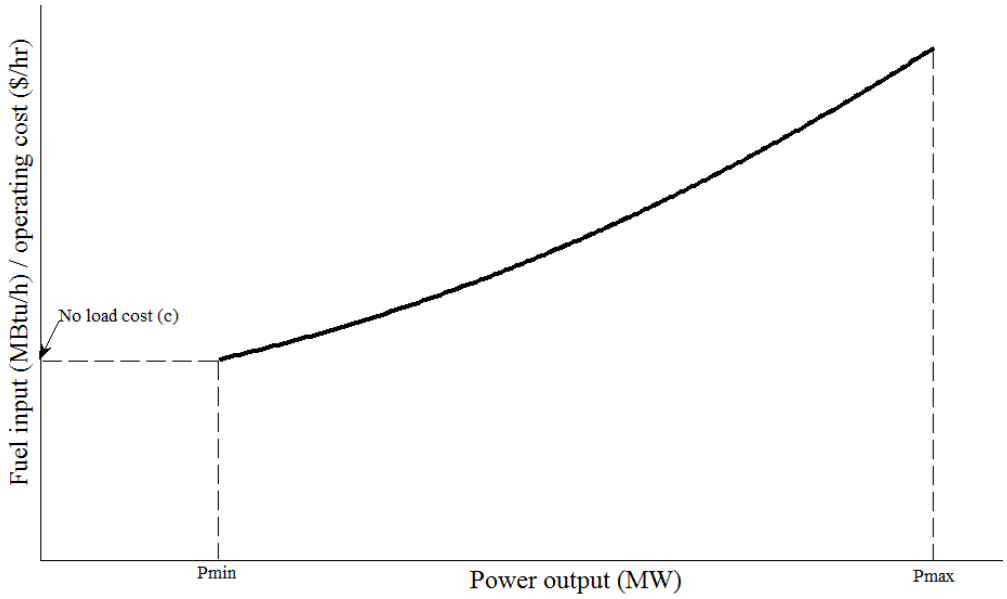

Figure 2.2 Operating cost curve of a thermal generating unit

For a given steam generating unit, the minimal power output, P_{Gmin}, is determined by technical conditions or other factors of the boiler or turbine. The incremental cost, \$/MWh, or the slope of the operating cost curve, is the derivative of an assumed quadratic function and this is linear with respect to the generator power output. The economic dispatch problem is formulated as a Lagrange multiplier problem with the Lagrangian $L(P_i, P_D)$ as [45, 46],

$$L(P_i, P_D) = F(P_i) - \lambda(\sum_{i=1}^{n} P_i - P_D) \tag{2.1}$$

where λ is a Lagrange multiplier, P_i is the power at bus i, and P_D is the total power demand. There are n generators in this formulation. The economical generation levels occur when the derivative of L in (2.1) with respect to the control variables (i.e., the individual generation levels) is zero,

$$\frac{\partial L}{\partial P_i} = 0 \quad \Rightarrow \quad \frac{\partial F(P_i)}{\partial P_i} = \lambda, \;\; i = 1, \dots, n \tag{2.2}$$

$$\frac{\partial L}{\partial \lambda} = 0 \Rightarrow \sum_{i=1}^{n} P_i - P_D = 0. \tag{2.3}$$

The result is that the incremental costs of all available generators are equal,

$$\frac{dF_1}{dP_{G1}} = \frac{dF_2}{dP_{G2}} = \cdots \frac{dF_i}{dP_{Gi}} = \lambda \tag{2.4}$$

where $\frac{dF_i}{dP_{Gi}}$ is the incremental cost of generator i. Eq. (2.4) holds for only the generators that have not yet reached their maximum (rated) output power. Eq. (2.4) is known as the *equal incremental cost rule*. The equal incremental cost rule simply says that at the minimum cost operating point of the system, the incremental cost for all operating (cycling) generators will be equal. When the load increases or decreases, the generator with the lowest incremental cost will deliver, or withdraw, the next MW. When the MW output level of a generator reaches its upper limit, the generator is fixed at that upper limit even when a load increase occurs. Subsequently that generator is dropped out of the equal incremental cost rule. Other units which have not reached their limit will share the load increase based on the equal incremental cost rule.

Some conventional methods for solving the economic dispatch problem such as Lagrange multiplier method, lambda iteration need to compute the economic dispatch every time the load changes.

2.2 Economic dispatch methodologies

There are numerous methods that exist that can be used to solve the economic dispatch of a system. These techniques include conventional optimization methods such as lambda- iteration and the equal incremental cost rule, Linear Programming (LP), Dynamic Programming (DP), Quadratic Programming (QP), and Mixed Integer Programming (MIP) [5]. The lambda iteration method discussed below is used in several commercial economic dispatch programs because of its simplicity; however, other techniques such as MIPs are becoming more popular. Also, intelligent methods for solving the economic dispatch problem have been proposed but are largely unused: these ideas use Artificial Intelligence (AI) concepts which may or may not be suited for the economic dispatch problem [47]. An example of an AI approach is Particle Swarm Optimization (PSO), and this is discussed below.

The key to finding the most economical solution to the economic dispatch problem is solving for the system lambda, or the incremental operating cost. The system lambda method is suitable for the conventional techniques listed above when the cost function is linear or quadratic. These methods are discussed below.

Lambda-iteration method

In the lambda iteration method, the variable lambda in (2.4) is used to solve the optimization problem and λ is the Lagrange multiplier. The equations are solved using the iterative method described in steps 1-4 [5]:

Step 1- Assume a reasonable value of λ

Step 2- Calculate the individual generations, P_i for $i=1,\ldots,n$

Step 3- Calculate the equality, ε, using the equation $\varepsilon = P_{load} - \sum_{i=1}^{N} P_i$. If this is the first iteration, the first estimate will be incorrect. The λ value must be set to a better estimated value and the above steps must be repeated

Step 4- Check the epsilon value calculated in step 3. If ε is less than the user defined tolerance, the solution converges and the schedule is printed. If not, the projected λ is sent back to Step 2 and the above steps are rerun until the system converges.

The lambda iteration method is illustrated in Figure 2.3.

Linear programming method

Linear programming is a widely used optimization technique [5]. Linear programming seeks to find x^* to optimize a linear objective function $f(x)$ while meeting a set of linear equality and inequality constraints,

$$\min_x f(x) = \min_x \sum_g c^T x \tag{2.5}$$

subject to

$$Ax \leq b \tag{2.6}$$

$$A_{eq}x = b_{eq}. \tag{2.7}$$

where

c	The coefficients of the cost function of generator g
x	The vector generated power levels
A	Coefficient matrix (m x n) of inequality constraints
A_{eq}	Coefficient matrix (k x n) of equality constraints
b	Vector (m x 1) of inequality right-hand side constraints
b_{eq}	Vector (k x 1) of equality right-hand side constraints.

There can also be specified upper and lower limits, that is,

$$x_i^{min} \leq x_i \leq x_i^{max} \tag{2.8}$$

Eqs. (2.5)- (2.8) are then used in an iterative technique to obtain the optimal solution, thus it is called the Successive Linear Programming (SLP) method [43]. The solution procedures of SLP for economic dispatch are summarized in steps 1-7:

Step 1- Select the set of initial control variables.

Step 2- Solve the power flow problem to obtain a feasible solution that satisfies the power balance equality constraint.

Step 3- Linearize the objective function and inequality constraints around the power flow solution and formulate the LP problem.

Step 4- Solve the LP problem and obtain the optimal incremental control variables $\Delta P_{Gi.}$

Step 5- Update the control variables $P_{Gi}^{(k+1)} = P_{Gi}^k + P_{Gi}$.

Step 6- Obtain the power flow solutions with updated control variables.

Step 7- Step 7- Check the convergence. If ΔP_{Gi}, in step 4, are below the user defined tolerance, the solution converges. Otherwise go back to step 3.

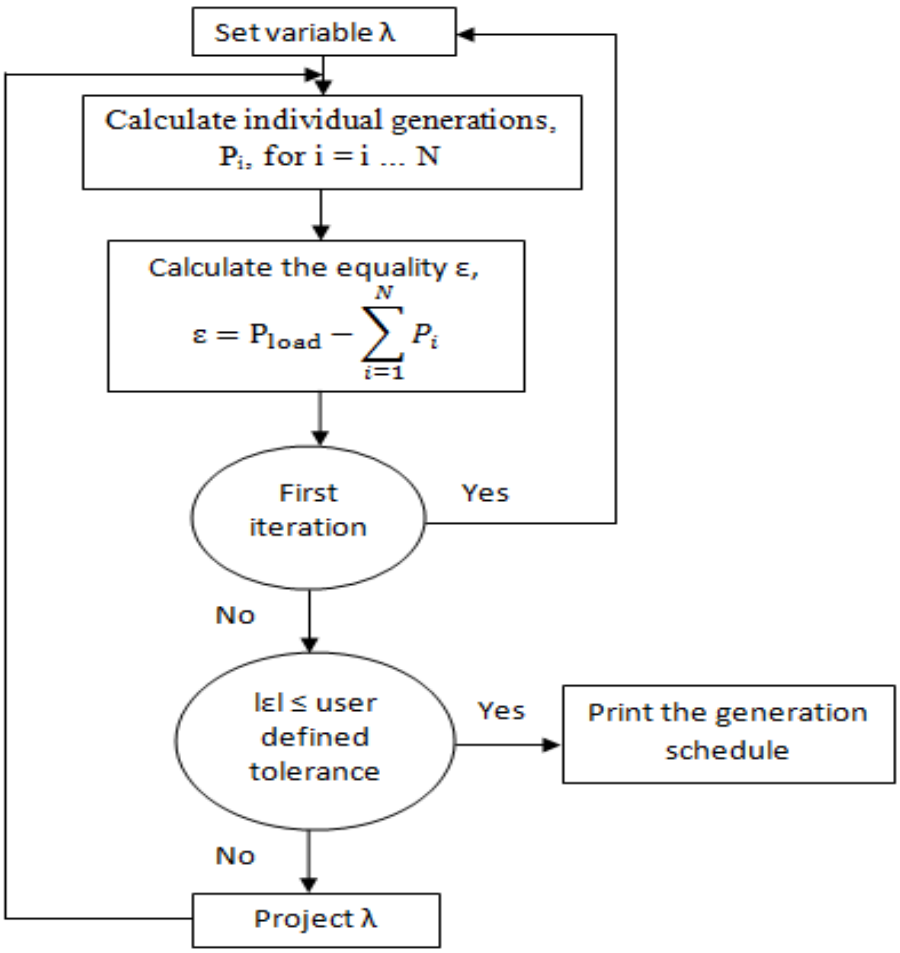

Figure 2.3 Pictorial of the lambda-iteration method

Dynamic programming method

From Bellman [48], the basic idea of the theory of dynamic programming is that of viewing an optimal policy as a policy determining the decision required at each time in terms of the present states of the system. Bellman defines the *principle of optimality* as the optimal policy having the property that whatever the initial state and initial decisions are, the remaining decisions must constitute an optimal policy with regard to the state resulting from the first decisions. The theory was designed to help solve mathematical problems arising from the study of various multi-stage decision processes. Dynamic programming is used to determine the decision in a system at a certain state that will result in the best outcome in later states. The previous outcomes are used to guide the choice of future decisions, with the objective of extremizing a given function.

One could set up a dynamic programming algorithm to run backward in time starting from the final hour to be studied back to the initial hour [5]. Conversely, the algorithm could also be set to run forward in time from the initial hour to the final hour. One of the reasons for using the

forward method is initial conditions are easily specified and the computations can go forward in time.

Mixed integer programming

A mixed integer program is a special case of a linear program in which some of the decision variables are constrained to take only integer values [49]. Given matrices A_{eq}, A, and vectors c^T, b_{eq}, and b, the general form of a MIP problem is:

$$\min_x f(x) = c^T x \tag{2.9}$$

subject to

$$Ax \leq b \tag{2.10}$$

$$A_{eq}x = b_{eq} \tag{2.11}$$

$$l \leq x \leq u \tag{2.12}$$

$$x_j \, integer \tag{2.13}$$

where

c	The coefficients of the cost function of generator g
x	The vector generated power levels
A	Coefficient matrix (m x n) of inequality constraints
A_{eq}	Coefficient matrix (k x n) of equality constraints
b	Vector (m x 1) of inequality right-hand side constraints
b_{eq}	Vector (k x 1) of equality right-hand side constraints
l	Vector of lower bound variables
u	Vector of upper bound variables
x_j	Variables that must be integers.

The problem is inherently non-convex. It also is in the class of a *NP-complete* problem [50, 51]. This means that there is no algorithm that can guarantee solving any MIP problem in a time that is a polynomial function of the problem size, i.e., the number of decision variables and constraints (n, k, m shown above). However, with good software and modeling, many useful MIP problems can be solved quickly enough to be of practical use, even though the worst case guaranteed solution time is far longer.The branch-and-bond algorithm is the most popular choice

for solving MIP problems [52]. The great advantage of the branch-and-bound method is that, when it terminates, the solution is known to be globally optimal. This is the great benefit of the MIP approach: it can achieve globally optimal solutions for non-convex problems. The branch-and-bound algorithm begins by solving a relaxed form of the problem, replacing integrality constraints with simple bounds, and then "branching" on a chosen variable. The variable is fixed at various integer settings, each generating a new relaxed sub-problem and a better bound on the optimal solution. This procedure continues searching a "tree" with different integer settings for each branch. If the result of a relaxed sub-problem satisfies the integrality constraints, that branch does not need to be searched any further, and its solution is a feasible solution to the original MIP. If the solution to a relaxed sub-problem is not integral, but has a cost worse than the best MIP solution found already, that branch can be terminated as further branching will only increase the cost. The search ends when all branches have been terminated. A small example of the branch and bound method is shown in Figure 2.4.

The branch and bound method example shown above shows a case where the original set A is branched off into four subsets: A1, A2, A3, and A4. These subsets are all different integer relaxations of A. The subsets blacked out, A2 and A3, do not contain a feasible solution, and thus the branch is terminated. SubsetsA1 and A4 contain a feasible solution and are branched off into additional subsets. The method continues until all branches are terminated.

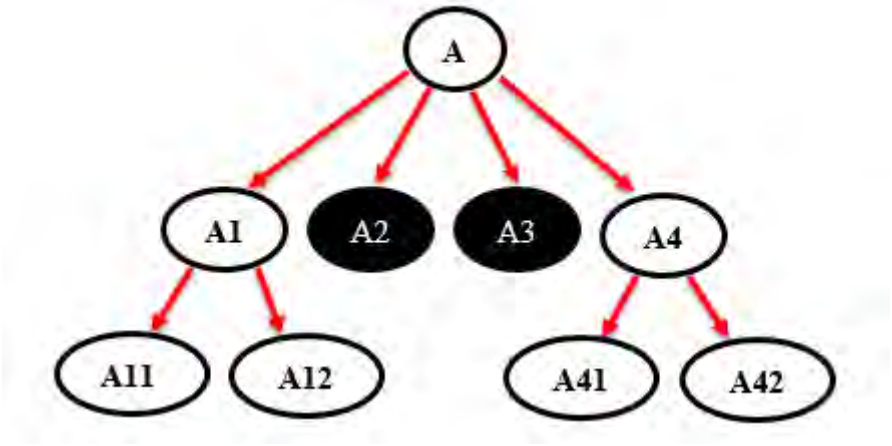

Figure 2.4 Example of the branch and bound method

Quadratic programming method

A quadratic programming method contains a quadratic objective rather than the linear objective function as seen in the linear programming formulation [43]. However, both QP and LP have linear constraints. This method is usually ideal for power system optimization because the generator cost function is often modeled in a quadratic form. A description of how quadratic programming is implemented appears in Appendix B. Quadratic programming is shown in Section 2.3 where it is used in the formulation of the optimization of the bulk energy storage problem.

This report uses the quadratic programming method in order to solve the economic dispatch problem. The objective function is assumed quadratic, and thus, the quadratic method is the

determined as the best option. The formulation of the problem that will be used throughout this report is explained in the Section 2.4.

2.3 AI based optimization methods

A number of AI approaches to the economic dispatch problem have been proposed. These methods often use little mathematical information from the problem, but patterns and intelligent observations are used to obtain a solution. These methods have an advantage that the objective function *f(x)* might be very nonlinear. Only one example is shown from the plethora of papers on these AI based methods (e.g., [53]-[59]).

Particle swarm optimization

Particle swarm optimization is a technique used to explore the search space of a given problem to find the settings or parameters required to maximize a particular objective function [60]. This technique, described by Kennedy and Eberhart in 1995 [61, 62], originates from two separate concepts: the idea of swarm intelligence based on the observation of swarming habits of certain kinds of animals, and the field of evolutionary computation.

The PSO algorithm works by retaining many possible solutions in a specified search space. During every iteration of the algorithm, each solution is assessed by the objective function, determining the "fitness" of the solution [60]. Each possible solution can be thought of as a particle searching through the fitness landscape finding the maximum or minimum of the objective function. The PSO algorithm uses the objective function to the possible solutions, and operates upon the subsequent fitness values.

The PSO algorithm consists of three steps, which are repeated until some stopping condition is met [63]:

1. Evaluate the fitness of each particle
2. Update individual and global best fitness and positions
3. Update velocity and position of each particle.

This method uses very little mathematical information to solve a given problem and relies more on patterns and observations. It is useful in the fact that the PSO algorithm can solve very non-linear functions. However, the economic dispatch problem usually assumes a quadratic objective function and other methods with a better mathematical approach may serve as a better option.

2.4 Formulation of the bulk energy storage problem

In order to perform an accurate economic dispatch of the system being modeled, a simple linear program cannot be used. Generally, the input-output characteristic (cost curve) of a generating unit is non-linear. The cost curve of a generator is often expressed as a quadratic function,

$$F(P_i) = (A + BP_i + C * {P_i}^2)F_C + V_{OM}{P_i}^2 \quad (2.14)$$

where *A, B,* and *C* are the coefficients of the input-output characteristic of generator operating at a power level of P_i [64]. The variable F_C is the fuel cost in *$/MBTU* and V_{OM} represents the variable operation and maintenance costs in *$/MWh*. The coefficients depend on the type of generator and the constant *A* is equivalent to the fuel consumption of the generating unit operation at $P_i = 0$, or the no-load cost. Table 2.1 displays the cost coefficients for the different types of generators [64].

In Table 2.1, the following notation for the different generators is used:

GT	Gas Turbine
ST	Steam Turbine
CT	Combined Cycle Combustion Turbine Part
CA	Combined Cycle Steam Part

The values from Table 2.1 can be simplified to a more commonly used quadratic formula, that is,

$$F(P_i) = aP_i^2 + bP_i + c \tag{2.15}$$

where the constants *a*, *b*, and *c* include the constants F_C and V_{OM} shown in Table 2.1. Table 2.2 presents the cost coefficients for the different types of generators using the simplified cost curve shown in (2.15).

Table 2.1 Cost coefficients for different types of generators [64]

Generator Type	*A*	*B*	*C*	Fuel Cost ($/MBTU)	VO&M ($/MWh)
Coal Fired	0	20.000	0.01	0.761	0.22
Nuclear	0	20.000	0.01	0.72	1.28
NG (GT)	0	12.170	0.01	1.078	0.419
NG (ST)	0	11.270	0.01	1.15	0.225
NG (CT/CA)	0	12.193	0.01	1.091	0.149
Hydro	0	10.000	0	1.77	2.28

Table 2.2 Simplified cost curve coefficients by generator type

Gen. Type	Linear Cost \$/MWh	Quadratic Cost \$/(MW)^{2}h
Coal	15.44	0.00761
Nuclear	15.68	0.0072
NG(GT)	13.54	0.01078
NG(ST)	13.19	0.0115
NG(CT/CA)	13.45	0.01091
Hydro	19.98	0

For purposes of this work, MATLAB is used to run an economic dispatch of the system being modeled. To implement the non-linear cost curve of the generators, the function *QUADPROg* is used. *QUADPROG* is an in-line MATLAB function that works similar to linear programming but allows for the minimization of a quadratic objective function rather than a linear function. The method used in *QUADPROG* is basically the Kuhn-Tucker-Karush method [5]. The method is gradient based, and involves the numerical solution of an expression that is the derivative of a lagrangian equal to zero. The primal of the function *QUADPROG* is in the form,

$$\min_X f(X) = \min_X \sum_g C_g^T X + \frac{1}{2} X^T Q_g X \tag{2.16}$$

subject to

$$AX \leq b \tag{2.17}$$

$$A_{eq} X = b_{eq}. \tag{2.18}$$

The matrix A_{eq} and vector b_{eq} model the *equalities,*

$$\sum_{\forall k(n,.)} P_k - \sum_{\forall k(.\ ,n)} P_k + \sum_{\forall g} P_{g,n} + \sum_{\forall s} P_{s,n} = \sum_{\forall l} P_{l,n} \ \forall n\,, \tag{2.19}$$

$$P_k - B_k(\delta_n - \delta_m) = 0 \quad \forall k, \tag{2.20}$$

$$\sum_{\forall i} P_{s,i} = 0 \quad \forall s. \tag{2.21}$$

The matrix A and vector b model the *inequalities,*

$$-P_{k,max} \leq P_k \leq P_{k,max} \quad \forall k, \tag{2.22}$$

$$P_{g,min} \leq P_g \leq P_{g,max}; \quad \forall g, \tag{2.23}$$

$$P_{s,min} \leq P_s \leq P_{s,max} \quad \forall s, \tag{2.24}$$

$$0 \leq E_s \leq E_{s,max} \quad \forall s, \tag{2.25}$$

$$-R_g \leq \frac{P_{g,i} - P_{g,i-1}}{\Delta T} \leq R_g \qquad \forall g; \ \forall i \tag{2.26}$$

where the following notation is used:

B_k	Susceptance of transmission element *k*
C_g	The linear coefficient, *b*, of the cost function of generator *g*
E_s	The energy stored in storage unit *s* in MWh
$E_{s,max}$	Maximum energy capacity of storage unit *s* in MWh
f	The objective function, operating cost
i	Interval number
k(. ,n)	Set of transmission assets with *n* as the 'FROM' node
k(n, .)	Set of transmission assets with *n* as the 'TO' node
m,n	Bus number (nodes)
P_g	The real power output of generator *g* in MW
$P_{g,max}$	Maximum power capacity of generator *g* in MW
$P_{g,min}$	Minimum power capacity of generator *g* in MW
P_k	The power flow of transmission line *k* in MW
$P_{k,max}$	Maximum line flow rating of transmission element *k* in MW

P_l The active power of load l in MW

P_s The real power output of storage unit s in MW

$P_{s,max}$ Maximum power capacity of storage unit s in MW

$P_{s,min}$ Minimum power capacity of storage unit s in MW

Q_g The quadratic coefficient, a, of the cost function of generator g

R_g Ramp rate limit of generator g in $\frac{MW}{hr}$

δ_k Bus voltage phase angle at node n or m

Δt Length of interval i in hrs.

The vector X includes the bus voltage phase angles (δ), line flows (P_k), generator outputs (P_g), and storage outputs (P_s) for each interval i. Note that most studies entail multiple time intervals (e.g., $i = 1, 2, \ldots, 24$ for a one day study with each interval having a time span of Δt). Most of the quantities listed above need to be specified for each individual time interval, and therefore the notation indicated might also be written with an additional subscript, namely i. The equality constraints in matrix A_{eq} and vector b_{eq} include the conservation of power at each bus (2.19), the power flow across each line (2.20), and the charge/discharge of the storage elements (2.21). The inequality constraints in matrix A and vector b include the line flow limits (2.22), generator output limits (2.23), charging power storage limits (2.24), charging energy storage limits (2.25), and the generator ramp rate limits (2.26).

Solving (2.19)-(2.26) gives the optimal $X = X^*$, and also the optimal system wide operating cost $f(X) = f^*$.The operating cost then can be compared using two different models: one including storage and another without storage to evaluate the effectiveness of storage in operating cost reduction. The program is used with a model of the Arizona power grid to demonstrate the benefits of storage.

3. Example using the state of Arizona as a test bed

3.1 Description of the test bed: State of Arizona

This chapter focuses on the presence of bulk energy storage and minimization of operating cost, subject to constraints, of a large test bed system. The test bed selected is essentially the state of Arizona. In this chapter, the effect of energy storage on the minimization of the objective function described in Section 2.3 is studied using the state of Arizona as a test bed. The Arizona electrical power system is part of the Western Electricity Coordinating Council (WECC). Using the present topology, generation and transmission limits, and the 2010 heavy summer load case, energy storage is added to appropriate buses in the system and operating results are evaluated. The test bed used for this purpose is an *equivalent* system, including 115 kV transmission and higher transmission voltages.

Using the system briefly described above, the objective function, or system wide operating cost*($/day*), is minimized while the constraints and formulation of the problem is the same as described in Chapter 2. Figure 3.1 is a pictorial of the basic concept.

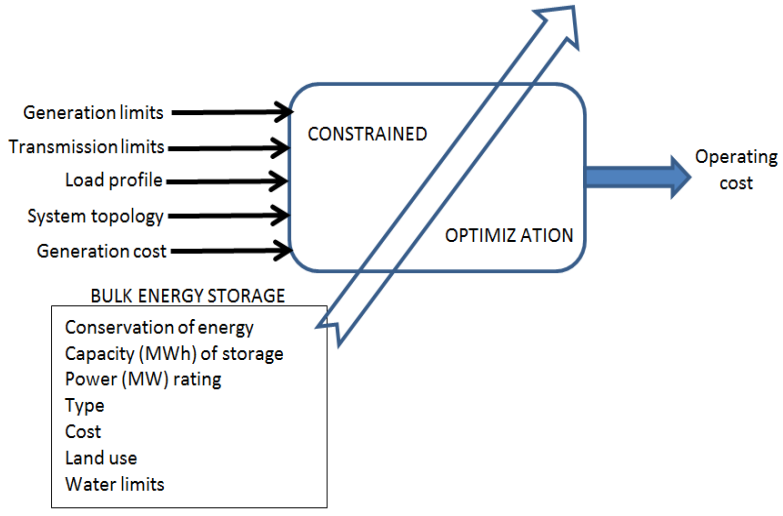

Figure 3.1 Pictorial of the concept of bulk energy storage

The quadratic programming algorithm explained in Section 2.3 is used to optimize generation while meeting the load demand at each interval and to schedule energy storage appropriately. The generation, line flow, and energy storage (charge/discharge) schedule are control variables along with the bus voltage angles. These values are calculated and the generation outputs are used to determine the system wide operating costs.

The system load is the 2010 summer peak, heavy load case. To approximate the time variation of the load in a day, the system wide load of 13,627 MW is multiplied by the function $0.45cos\left(\frac{\pi t}{12}+0.5\pi\right)+0.55$ using eight intervals of three hours each to replicate the common load profile in a 24 hour day, where *t* is the time at the beginning of each interval (e.g., *t = 0, 3, 6, ..., 21*). This can be seen in Figure 3.2. The objective of the modeled system is to

economically dispatch the available generation while optimally charging/ discharging the energy storage.

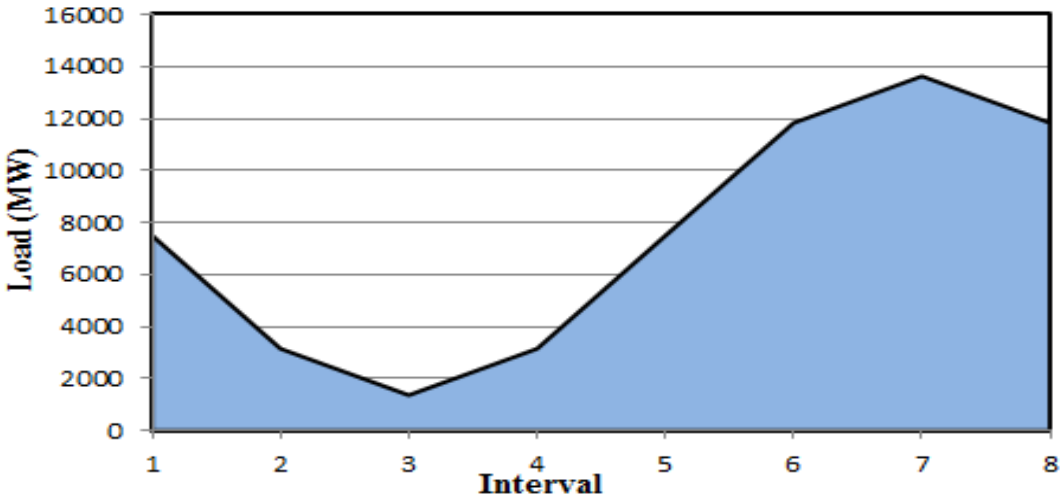

Figure 3.2 Arizona 2010 summer peak load modeled over a day (typical, assumed values shown)

The following assumptions are made for the described test bed:

- Transmission line losses are not included in the system
- Reactive power flows are neglected
- Bus voltages are all assumed 1 per unit (p.u.)
- The DC load flow study approximation is used, namely the linearization of the sine function near the assumed operating point, e.g., $\sin(\theta) \approx \theta$ [5].

The Arizona system under study has the profile shown in Table 3.1.

Table 3.1 State of Arizona system profile*

Number of buses	Number of transmission lines	Number of generators	Number of time intervals, *i*	Duration of time interval, hours
206	277	26	8	3

*This is an equivalent of the Arizona transmission system

The quadratic programming algorithm determines the total constrained optimum operating cost of the system. The cost is then multiplied by 365 to show the yearly system wide operating cost assuming the load modeled is the average over the year.

3.2 Description of test cases

The Arizona transmission system described in Section 3.1 is tested using three different cases. The first case tested is without any energy storage added to the system. This case is analyzed to

determine a system wide operating cost that can be used for comparisons with the second two cases when bulk energy storage is added to the test bed.

The two cases that include bulk energy storage look at locations in Arizona where pumped hydro energy storage can be added. PHES is chosen as the technology to be simulated because it is currently the most mature form of bulk energy storage and the most feasible for very high levels of energy capacity. The locations chosen to place PHES are near existing hydroelectric dams in Arizona including: Hoover (Boulder) Dam, Glen Canyon Dam, and Horse Mesa Dam. These locations do not currently exist and are used purely for simulation purposes. PHES is placed near existing dams because of the high amount of water in the area and the large elevation differences. Figure 3.3 shows the locations of the simulated pumped hydro energy storage added to the system.

Various information about the three PHES locations is shown in Tables 3.2 and 3.3. Some of the numbers, including the lower and upper reservoir volume and area, is approximated using actual Arizona PHES locations issued to FERC for approval. These locations are discussed in Chapter 4.

Figure 3.3 Locations of simulated pumped hydro energy storage

Table 3.2 Simulated PHES location information and operating entity

	Location	County	Nearby bus	Year of development	Water source	Operating Entity	*Power limit (MW)
★	Lake Mead	Mohave	Mead N/S	N/A	Lake Mead	WAPA[$]	2080
■	Glen Canyon	Coconino	Glen Canyon N/S	N/A	Colorado River	WAPA[$]	1296
●	Horse Mesa	Maricopa	Horse Mesa	N/A	Salt River	SRP[+]	130

[$]Western Area Power Administration, [+]Salt River Project

Table 3.3 Simulated PHES reservoir numbers

	*Lower reservoir volume (acre-ft.)	*Lower reservoir surface area (acres)	*Lower reservoir average depth (ft.)	*Upper reservoir volume (acre-ft.)	*Upper reservoir surface area (acres)	*Upper reservoir average depth (ft.)
★	25,323	265	95.6	24,624	289	85.2
■	15,778	165	95.6	15,343	180	85.2
●	1,583	17	93.1	1,539	18	85.5

*Approximations based on actual Arizona PHES locations issued to FERC

3.3 Base case for the state of Arizona

The original topology described in Section 3.1 is studied first without energy storage and is considered the base case. The economic dispatch of the generators is determined by solving the quadratic programming algorithm in MATLAB. Again, in order for the constraints listed earlier to comply, active power losses and reactive power are neglected. These constraints include:

- Generation output and ramp rate limits
- Transmission line power flow limits
- Storage power and energy charging limits.

The cost of economic dispatch of generation per day is calculated to be $3.544 million and $1.294 billion per year. As expected, the total generation output matches the total system load at each interval shown in Figure 3.2. The yearly system wide operating cost from the base case will be used for comparison with tests that include bulk energy storage.

3.4 Pumped hydro energy storage added to various buses

The system described in Section 3.1 is used again however four different cases are studied implementing possible locations in Arizona for pumped hydro energy storage. For each case included in this study, pumped storage is added to Horse Mesa Dam (bus 83) at a maximum storage of 130 MW, similar to the capacity of the existing dam. This bus is chosen to be used in combination with one of each of the four largest scale pumped hydro locations as it gives the best results (i.e., minimum system wide operating costs) when used in a two bus example.

Case 3.1: Pumped hydro energy storage added to Lake Mead S. bus

One possible location for a large scale pumped hydro energy storage is near Hoover (Boulder) Dam located in the Black Canyon of the Colorado River, on the border between the US states of Arizona and Nevada. Hoover Dam has a nameplate capacity of 2080 MW, so this is assumed the maximum value of the pumped hydro placed at this location. There are two buses located near Hoover Dam, one on both the north and south end of the river. This case will test the scenario where pumped hydro is added to the south bus. Again, pumped hydro is also placed at Horse Mesa Dam with a capacity of 130 MW.

Using the program created in MATLAB shown in Appendix A, storage is added to the Lake Mead S. Bus (Bus 149) and studied. The pumped storage is set to have three different values of energy / power (E/P) ratios: 2, 5, and 10. The ratio describes the size of the upper reservoir, or how much water can be stored. For a higher ratio, the reservoir can store more water thus it has a higher energy (MWh) rating. The E/P ratio determines how long the pumped hydro energy storage can provide rated power (assuming the water is already stored in the upper reservoir). Table 3.4 provides some existing PHES in the United States and their E/P ratios [65.]. A range of 4-12 hours at rated power is shown in Table 3.4 with an average of around 8 hours. Table 3.5 shows the three different cases that are studied at the Lake Mead S. bus.

Each E/P scenario shown in Table 3.5 is studied at different levels of storage ranging from a power level of 600-2080 MW. This test shows how increasing the storage power limit effects the system wide operating cost as well as how various system limits are effected such as generation or line limits. The results are plotted together along with the base case yearly value of $1.294 billion. The results can be seen in Figure 3.4.

Table 3.4 Power and energy ratings of selected PHES in the U.S.

Pumped hydro storage name	Power (MW)	Energy (MWh)	E/P ratio	Location
Bath County	3003	30030	10	Virginia
Ludington	1872	14976	8	Michigan
Olivenhain-Hodges	40	320	8	California
Castaic	1427	14270	10	California
Mount Elbert	200	2400	12	Colorado
Bear Swamp	600	3600	6	Massachusetts
Yards Creek	400	2400	6	New Jersey
Taum Sauk	440	3520	8	Missouri
Cabin Creek	324	1296	4	Colorado

Table 3.5 Lake Mead S. bus pumped storage scenarios

Scenario	E/P ratio	Lake Mead S. bus charging power limit (MW)	Lake Mead S. bus charging energy limit (MWh)
1	2	2080	4160
2	5	2080	10400
3	10	2080	20800

From Figure 3.4, it can be seen that with energy storage added to Lake Mead S. bus, the system wide operating cost is lower than the base case cost for an E/P ratio of 5 or 10. The plot of the E/P = 2 scenario however is actually higher than the base case cost up until about 800 MW. This is because the small amount of storage available causes the system to hit more generation and line limits. Once the 800 MW of storage is reached, there is enough storage in the system and the operating cost decreases below the base case value. It can be seen from Figure 3.4 that as the E/P ratio increases, the operating cost decreases. Also, when the energy storage power limit increases in each case, the operating cost decreases as expected. This occurs because the pumped hydro storage can "shave" more of the peak demand. An example of peak shaving from the simulations is shown in Figure 3.5 using an E/P ratio of 10 and storage charging power of 2080 MW, where the minimum operating cost occurs of $1.216 billion per year.

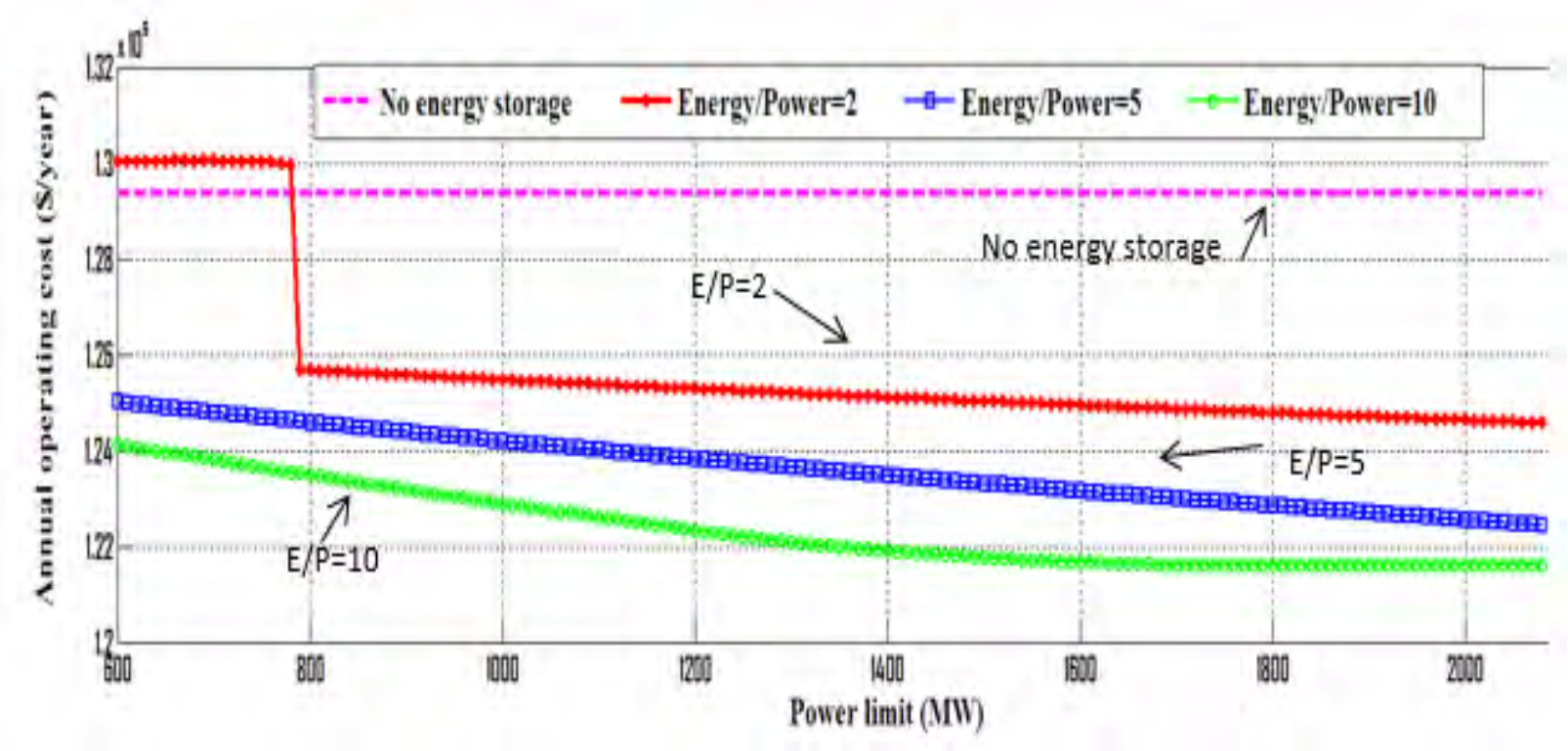

Figure 3.4 Case 3.1 system wide annual operating cost with storage at Lake Mead S. bus

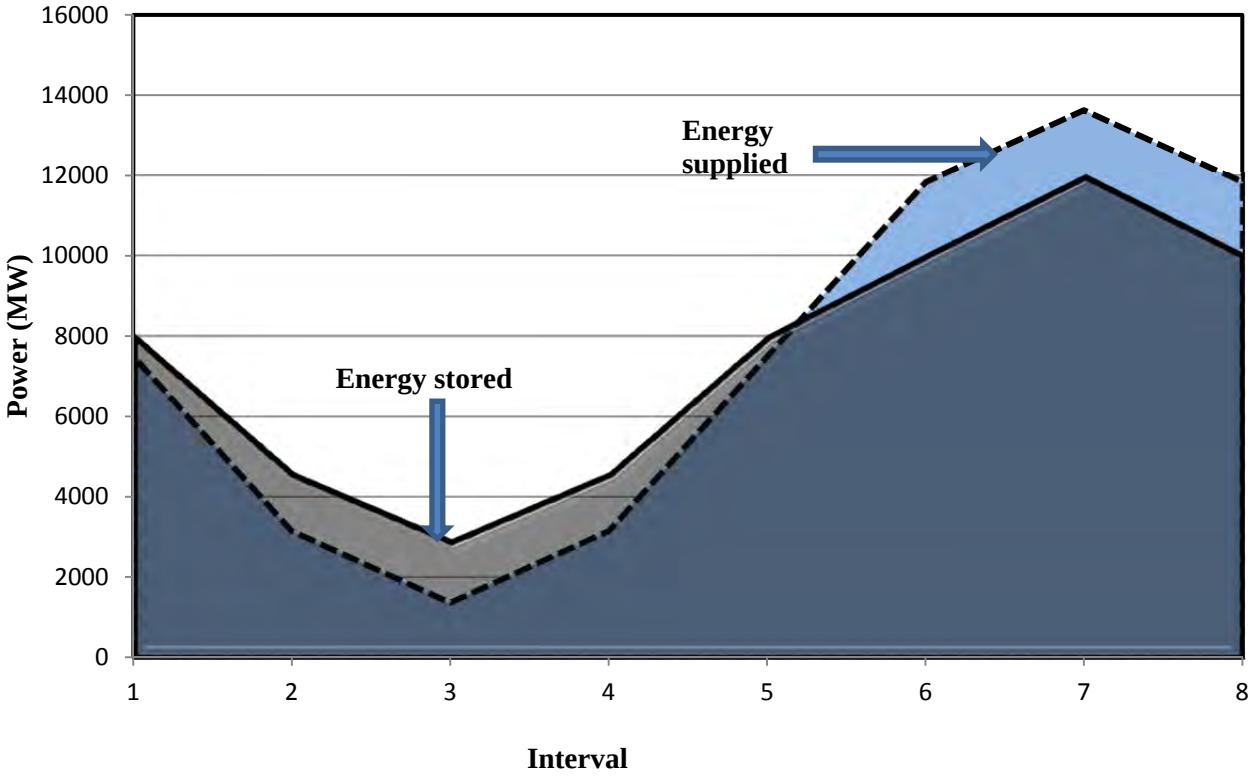

Figure 3.5 Example of peak shaving at Lake Mead S. bus

Another important calculation that can be made to determine the value of the energy storage is the payback period. The payback period compares the investment cost of the energy storage with the annual savings. The time period calculated illustrates how long it would take to recover the investment. Using the yearly operating cost savings and an estimate of the capital costs of pumped hydro storage, a payback period can be calculated using,

$$C = OC_{saved} Y \tag{3.1}$$

where C is the overall capital cost in dollars, OC_{saved} is the yearly operating cost savings in dollars, and Y is the payback period in years. To estimate the payback period for the storage used in at Lake Mead S. bus, two costs are used based on the nameplate power and energy ratings. The power related costs, in $/kW, include the various pumps and turbines while the energy related costs, in $/kWh, contain the reservoir costs. Table 3.6 shows a range of typical power and energy related costs for pumped hydro storage.

Table 3.6 Assumed pumped hydro storage power and energy related costs [18, 20]

	Minimum	*Maximum*
Power related costs ($/ kW)	500	2000
Energy related costs ($/kWh)	7	20

Using the values from Tables 3.5 and 3.6 and the operating costs shown in Figure 3.3, (3.1) is used to determine the payback period. The payback period for the three scenarios at each power level is shown in Figure 3.6.

Figure 3.6 shows that with added storage the payback period increases. This is due to the fact that a decrease in operating cost is less than the cost to add that amount of storage. However, with a higher E/P ratio, the capital costs increase but the annual operating cost decrease is greater allowing a lower payback period. The plot of E/P = 2 starts at about 800 MW because the operating cost is higher than the base case before that point, thus $OC_{saved} = 0$. In the range shown in Figure 3.5, a reasonable payback period is shown for the Lake Mead S. bus with a minimum value of 7.95 years when an E/P ratio of 10 is used and a maximum value of 23.69 years when an E/P ratio of 2 is used. With a typical lifetime of pumped hydro storage being 40 years, the range would give a practical length of time where the investment is already covered and the system is saving a significant amount of money.

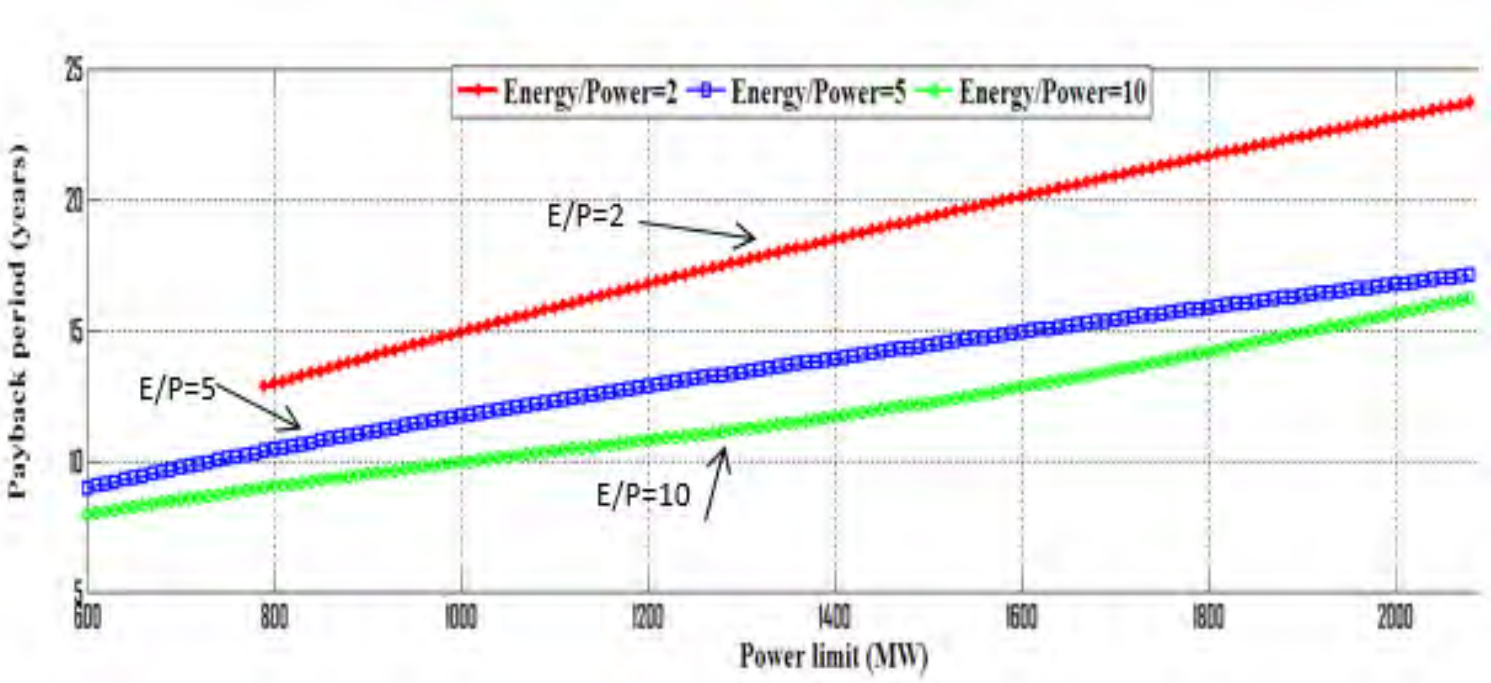

Figure 3.6 Case 3.1 payback periods for Lake Mead S. bus

Case 3.2: Pumped hydro energy storage added to Lake Mead N. bus

Similar to Case 3.1, pumped hydro energy storage is added near Hoover Dam but on the Lake Mead N. bus (bus 150). Comparable results are expected because of its close vicinity to the south bus. Once again, the pumped storage is set to have three different values of an E/P ratio: 2, 5, and 10. The three scenarios being tested are the same as what is shown in Table 3.5.

The three scenarios are again studied at different levels of storage ranging from a power level of 600-2080 MW. The variation in power allows the possibility to analyze the effect of more storage on operating cost, various system limits, and the payback discussed earlier. The results are again plotted together along with the base case yearly value of $1.294 billion. The plots for storage at Lake Mead N. bus can be seen in Figure 3.7.

The operating costs shown in Figure 3.7 display that energy storage added to Lake Mead N. bus also help decrease the system wide operating cost between power levels of 600 and 2080 MW for an E/P ratio of 5 and 10. Similar to Case 3.1 however, when the E/P ratio is 2, the operating cost is higher than the base case value up until around 800 MW. This is once again due to the small amount of storage available that causes more generation and line limits to be reached. Again, once around 800 MW of storage is added, there is enough storage in the system and the operating cost decreases below the base value. Figure 3.6 shows that both as the E/P ratio and the storage power limit increases at the Lake Mead N. bus, the operating cost decreases. This is again demonstrating how added storage is “shaving” more of the peak demand, as shown in Figure 3.5. The minimum operating cost for all three scenarios occurs between 1150 and 2080 MW where the system wide operating cost levels off at $1.2317 billion.

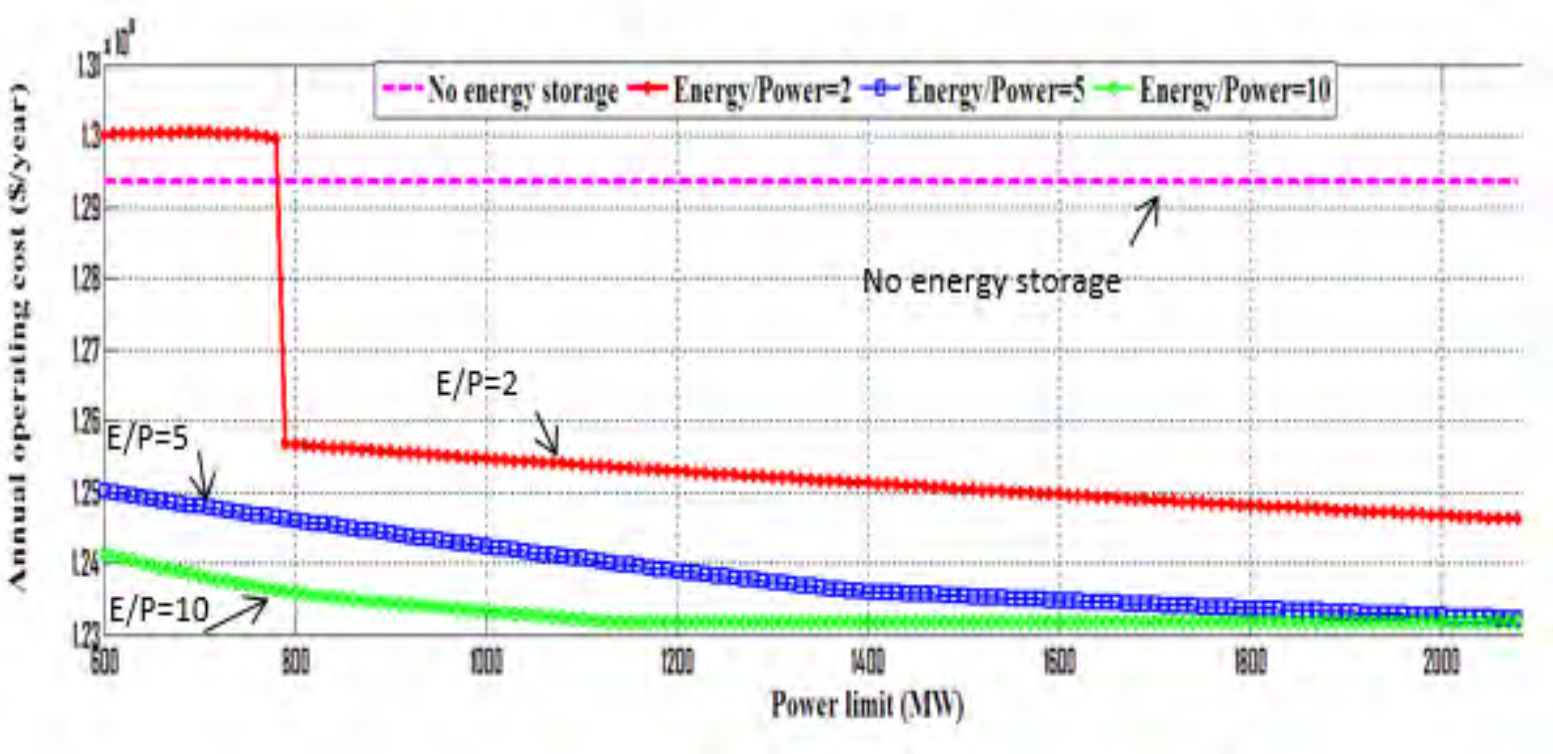

Figure 3.7 Case 3.2 system wide annual operating cost with storage at Lake Mead N. bus

The payback period is calculated for the Lake Mead N. bus using the operating costs from Figure 3.7 and the capital costs found from the numbers in Tables 3.5 and 3.6. These values along with (3.1) are used to determine the payback period for the three scenarios at each power level. The results are shown in Figure 3.8.

In Figure 3.8, the various payback periods show similar results as in Case 3.1. All three scenarios show a positive slope as the energy storage power limit is increased at the bus. This is again due to the decrease in operating cost being less than the cost to increase the power limit. However, in this case increasing the E/P ratio only decreases the payback period up until a certain power level once the ratio gets higher. As seen in Figure 3.8, the plots for E/P = 5, 10 intersect around 1600 MW and the plot of E/P=10 continues above the plot of E/P = 5. The plot of E/P=2 again starts around 800 MW because the operating cost is higher than the base case before that point, thus $OC_{saved} = 0$. The minimum payback period occurs at 600 MW when the E/P ratio is 10 at a value of 7.97 years, slightly above the minimum from Case 3.1. The longest payback period occurs at an E/P ratio of 2 when the power limit is raised to 2080 MW at a length of 23.92 years. This is once again a reasonable range compared to the typical 40 year lifetime of a pumped hydro energy storage plant.

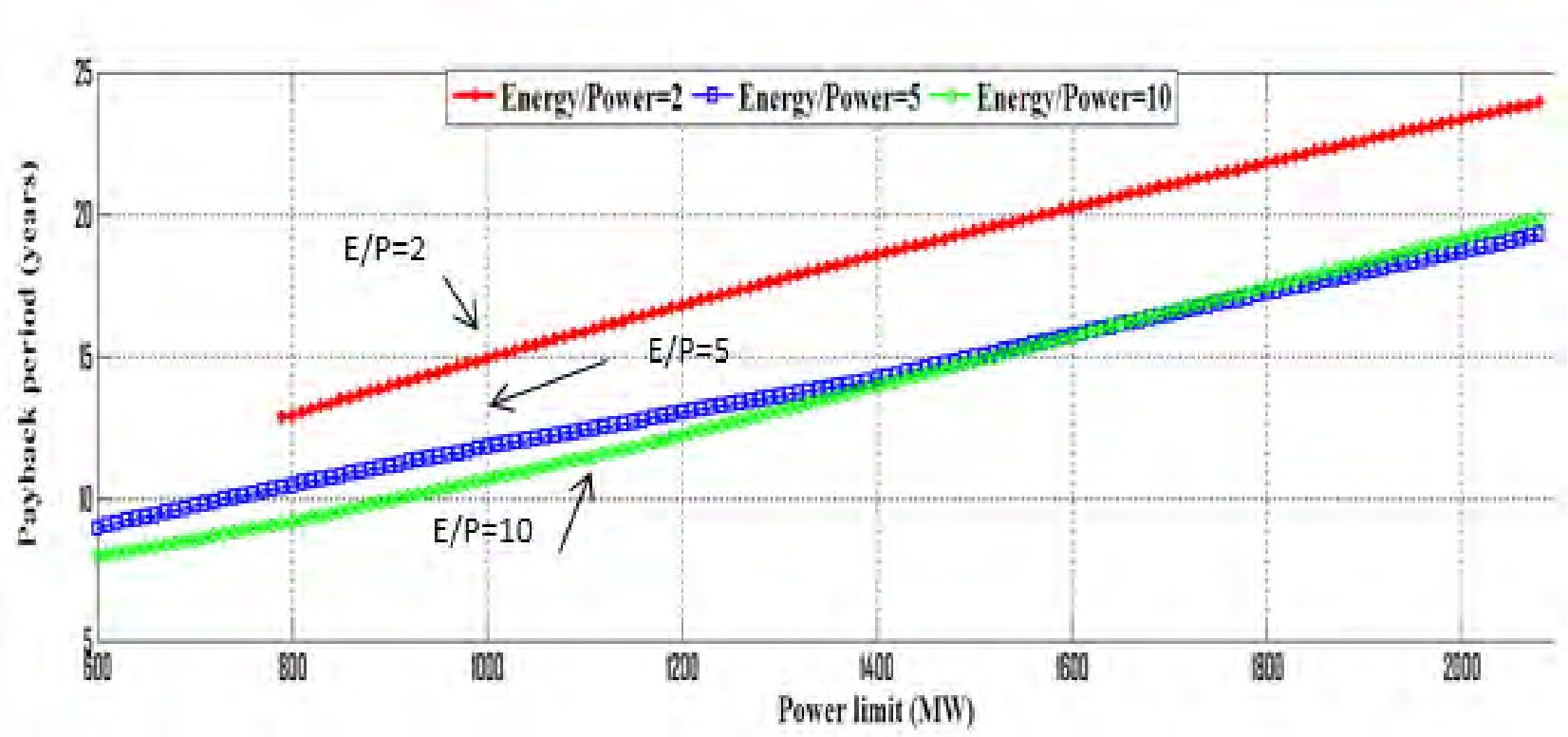

Figure 3.8 Case 3.2 payback periods for Lake Mead N. bus

Case 3.3: Pumped hydro energy storage added to Glen Canyon S. bus

Another possible location for a large scale pumped hydro energy storage plant is near Glen Canyon Dam, which is on the Colorado River near the town of Page, AZ, on the border of Arizona and Utah. Glen Canyon Dam has a nameplate capacity of 1296 MW, thus this is assumed the maximum value of the pumped hydro plant place at this location. There are two buses located near Glen Canyon Dam, one on both the north and south end of the river. Both buses will be tested but this case will test the scenario where pumped hydro is added to the south bus. Once again, pumped hydro is placed at Horse Mesa Dam with a capacity of 130 MW in both cases.

The program shown in Appendix A is used again but storage is this time added to the Glen Canyon S. bus (bus 187) and studied. The pumped storage is set to have three different values of E/P ratios: 2, 5 and 8. It was found this time that at an E/P ratio of 8 or greater, the operating cost remains constant over all power levels, or an increase in the ratio has no effect on the solution. Thus, a value of E/P = 8 is chose as the maximum E/P ratio. Table 3.7 shows the three different cases that are studied at the Glen Canyon S. bus.

Table 3.7 Glen Canyon S. bus pumped storage scenarios

Scenario	E/P ratio	Glen Canyon S. bus charging power limit (MW)	Glen Canyon S. bus charging energy limit (MWh)
1	2	1296	2592
2	5	1296	6480
3	8	1296	10368

Each E/P ratio scenario shown in Table 3.7 is studied over the energy storage power rating range of 500-1296 MW. The results are plotted together along with the base case yearly value of $1.294 billion. The results plotted together can be seen in Figure 3.9.

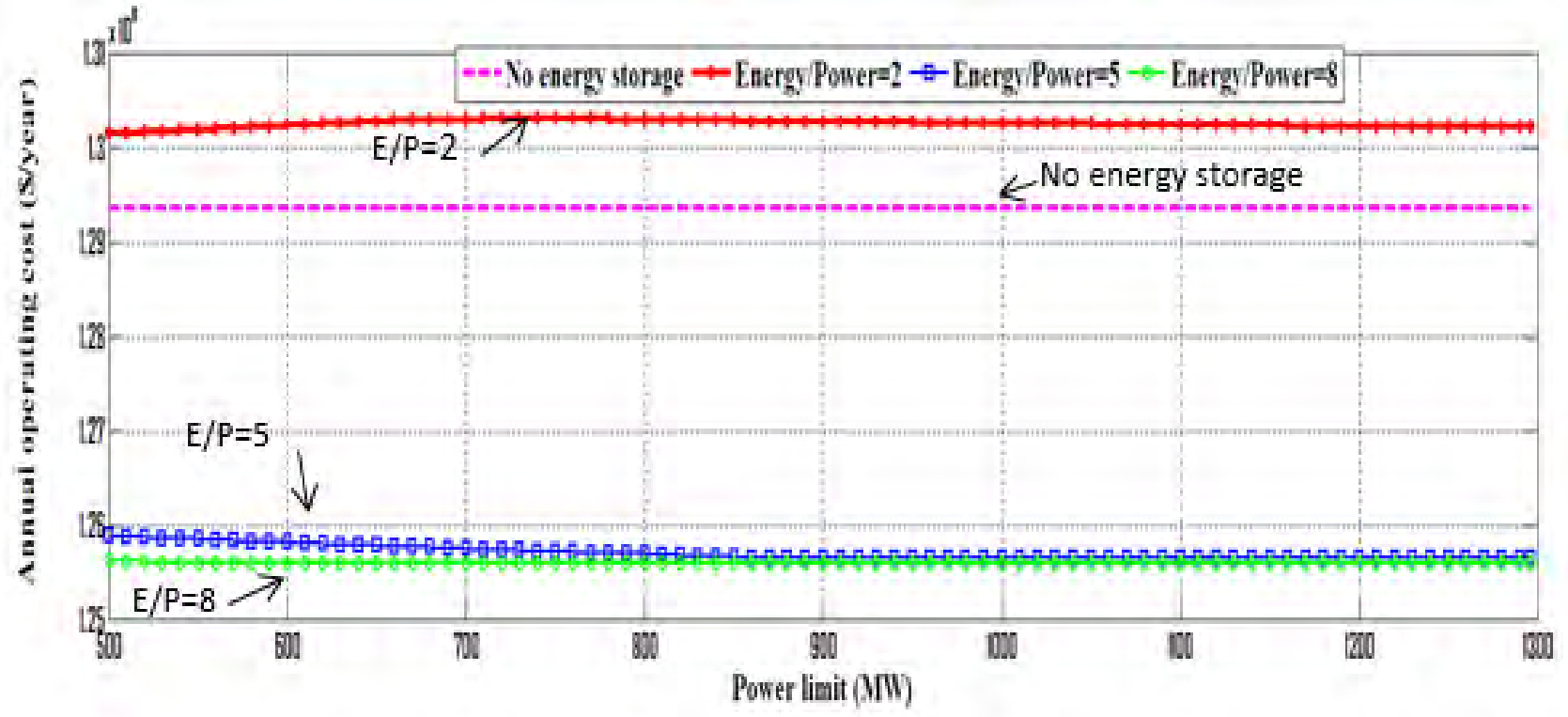

Figure 3.9 Case 3.3 system wide annual operating cost with storage at Glen Canyon S. bus

In Figure 3.9, for an E/P ratio of 5 and 8, the operating cost is lower than the base case. However, it seems that increasing the E/P ratio from 5 to 8 has little effect on the cost as the two plots begin to converge around 900 MW. It is evident that there is a limit on how much the E/P ratio can be increased before there is little to no effect on the system wide operating cost. In the case of the plot of E/P = 2, the limit on how much energy can be stored being so small causes the operating cost to always be higher than the base case. It seems there is never a sufficient amount of energy storage available and more generation and line limits are hit. It is apparent that at the Glen Canyon S. bus, the increase of the energy storage power limit or the E/P ratio has little effect on the operating cost after a certain point. The minimum operating cost for this case is $1.2559 billion which occurs for a ratio of E/P = 8 over the range of 550-1296 MW.

The payback periods are calculated for the Glen Canyon S. bus using the operating costs from Figure 3.8 and the capital costs using Tables 3.6 and 3.7. The values are inserted into (3.1) and the payback periods are calculated. The results can be seen in Figure 3.10. The payback periods for E/P = 5 and 8 are shown above in Figure 3.10. There is no plot for E/P = 2 because the operating cost is always greater than the base case, thus $OC_{saved} = 0$. The plots for E/P = 5 and 8 both display a positive slope, meaning the annual system wide operating cost savings is less than the added cost to increase the energy storage power limit. Also, the plot of E/P = 8 crosses and eventually increases above the plot of E/P = 5 around 700 MW. Around this point, the added cost of energy for E/P = 8 exceeds the operating cost savings and causes the payback period to increase above the E/P = 5 plot. This can be observed in Figure 3.10 where the plots converge.

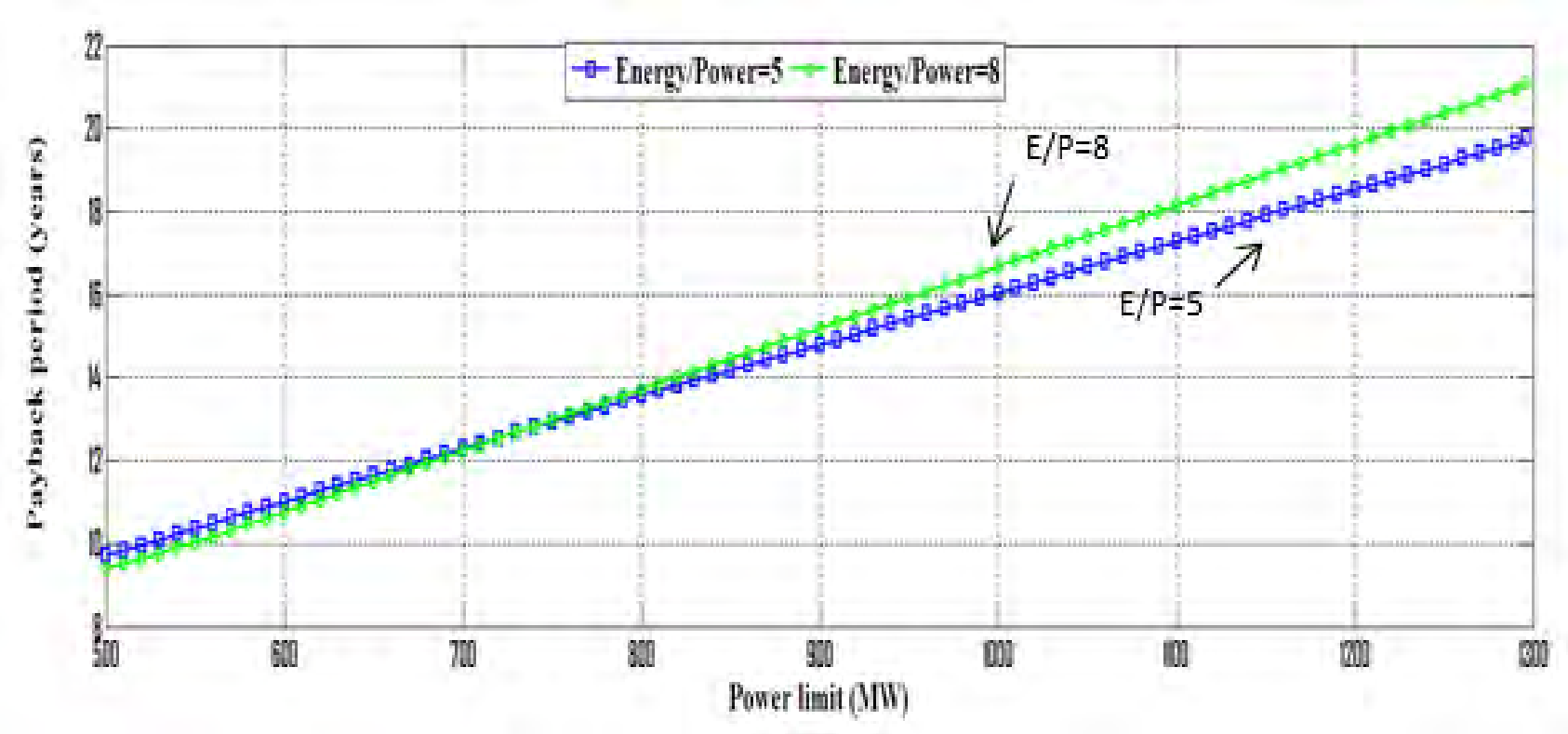

Figure 3.10 Case 3.3 payback periods for Glen Canyon S. bus

The operating costs for the two plots in Fig. 3.10 are roughly equal; however, the energy storage plant with E/P = 8 would cost more due to the higher energy rating. The minimum payback occurs at 500 MW at an E/P ratio of 8 for a length of 9.39 years, higher than the minimum values for both Cases 3.1 and 3.2. The longest payback period occurs for the same E/P ratio when the power limit reaches 1296 MW at a length of 21.09 years. This range is also reasonable when compared to the average lifetime of a pumped hydro energy storage plant.

Case 3.4: Pumped hydro energy storage added to Glen Canyon N. bus

Pumped hydro energy storage is also added to the north bus located near the Glen Canyon Dam to compare the results with Case 3.3. In this case, the energy storage is set to have three different E/P ratios: 2, 5, and 10. The Glen Canyon N. (bus 186) bus does not have a limit at an E/P of 8 or 10, thus 10 is used as the maximum value. The three scenarios being tested are shown in Table 3.8.

Table 3.8 Glen Canyon N. bus pumped storage scenarios

Scenario	E/P ratio	Glen Canyon N. bus charging power limit (MW)	Glen Canyon N. bus charging energy limit (MWh)
1	2	1296	2592
2	5	1296	6480
3	10	1296	12960

The three scenarios shown in Table 3.8 are again studied at different levels of energy storage power ratings ranging from 500-1296 MW. The results are then plotted together with the annual base case value of $1.2945 billion calculated earlier. The results for storage at the Glen Canyon N. bus can be seen in Figure 3.11.

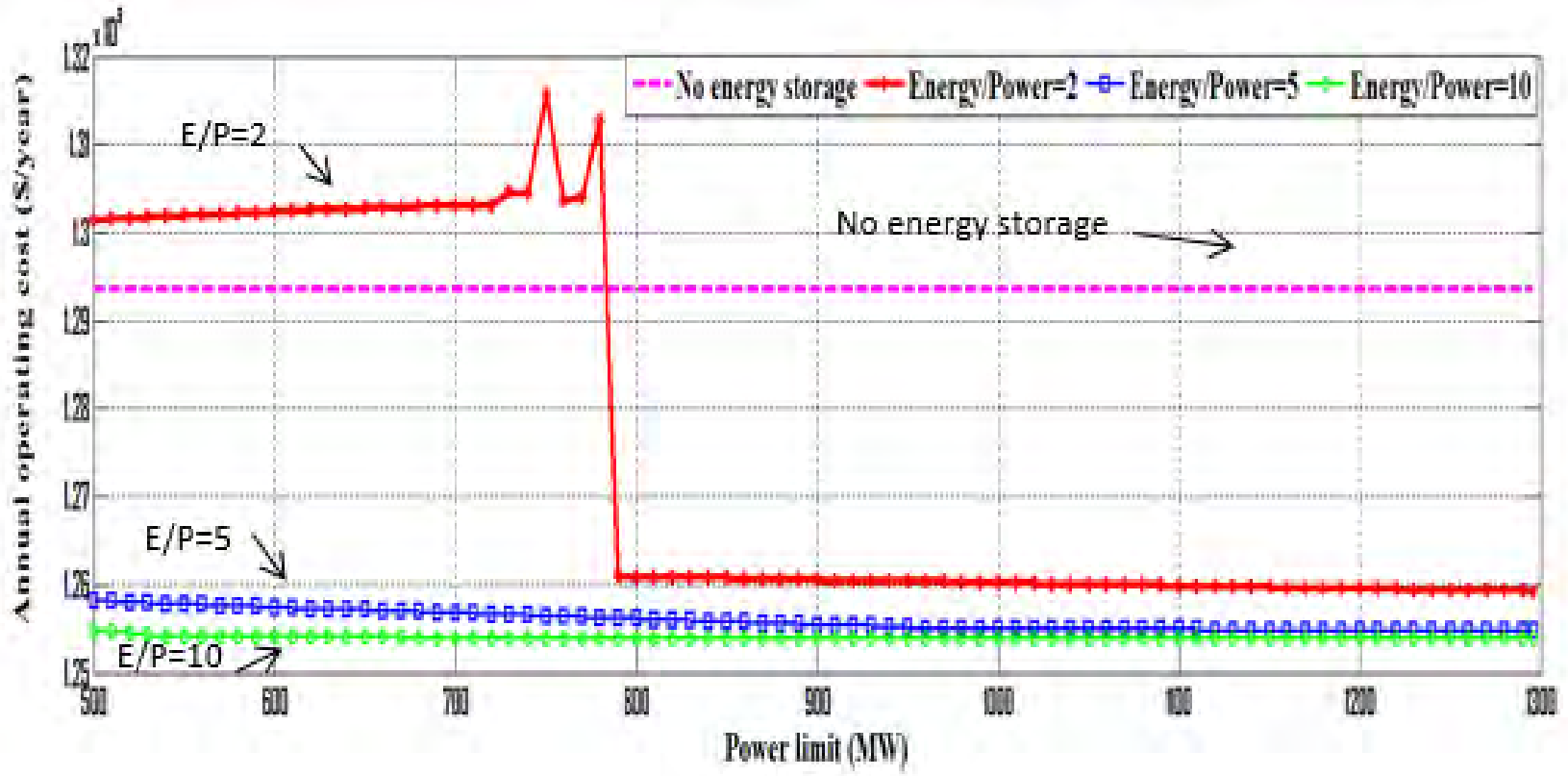

Figure 3.11 Case 3.4 system wide annual operating cost with storage at Glen Canyon N. bus

The operating costs shown in Figure 3.11 demonstrate a similar trend as previous cases. Other than the plot of E/P = 2, adding energy storage cause a decrease in system wide operating cost at all power levels. For the plot of E/P = 2, the results show a similar trend as in Cases 3.1 and 3.2 where the operating cost is higher than the base case value up until 790 MW. After this point, there is enough storage at the bus and the operating cost drops below the base case value. For this case, the operating cost seems to level out around one number for all three E/P ratios and the plots for E/P = 5 and 10 start to converge at higher power limits. It is also apparent that an increase in the E/P ratio to higher values has little effect on the operating cost as there is very little difference between the E/P = 5 and 10 plots even at lower power levels.

The payback periods are calculated for the Glen Canyon N. bus from Figure 3.10 and the capital costs using Tables 3.6 and 3.8. The values are inserted into (3.1) and the payback periods are calculated. The results can be seen in Figure 3.12.

The payback periods shown in Figure 3.12 all have a positive slope, meaning the operating cost savings is less than the cost to add the same amount of storage. For each E/P ratio, the slope is roughly the same which is about 0.0178 $\frac{yrs}{MW}$. For this case, the higher E/P ratio of 10 eventually intersects and increases above the payback period of E/P = 5. This occurs once again because the operating costs for both ratios eventually converge towards each other. With the added cost for an E/P ratio, the payback period is eventually higher around 750 MW.

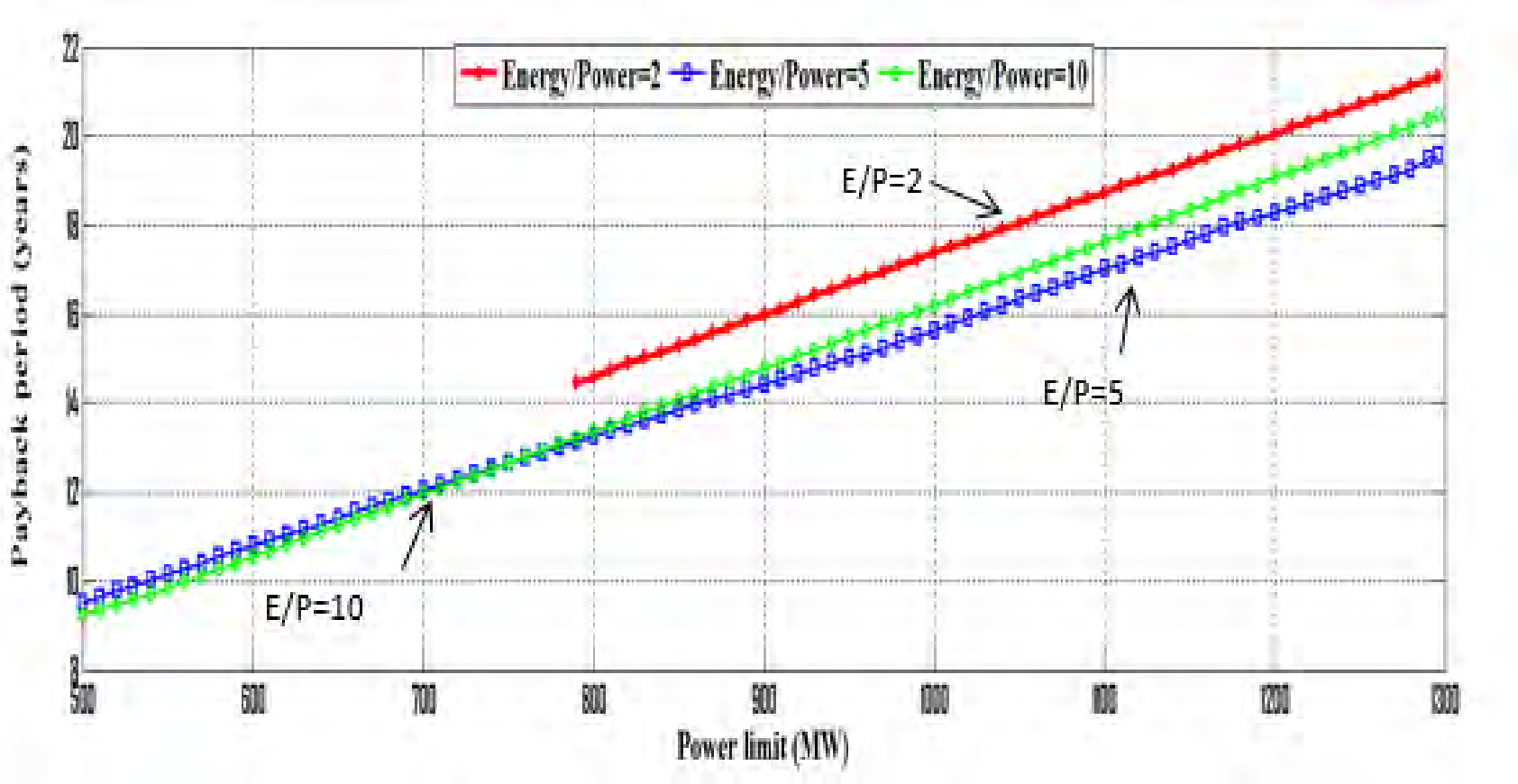

Figure 3.12 Case 3.4 payback periods for Glen Canyon N. bus

The lowest payback period for the Glen Canyon N. bus is 9.25 years, which is at an E/P ratio of 10 at 500 MW, slightly lower than Glen Canyon S. bus. The maximum payback period length occurs at the same E/P ratio at 1296 MW for a length of 20.5 years. This range is a reasonable length compared to the average 40 year lifetime of a pumped hydro energy storage plant.

3.5 Summary of results

The previous section showed through four cases that the use of bulk energy storage can lower the system wide generator operating cost. This is accomplished by the peak shaving application discussed in Chapter 1. A payback period calculation was also specified and used to calculate a range of payback periods for each case. Table 3.9 summarizes the results from the base case and cases 3.1-3.4 including the operating cost and payback period ranges. The table will show the ranges for the E/P ratio in each case with the best results.

Table 3.9 Summary of Arizona test bed case results with bulk energy storage

Case	Best E/P ratio	Minimum annual operating cost (billion-$/yr)	% decrease	Maximum annual operating cost (billion-$/yr)	% decrease	Minimum payback period (years)	Maximum payback period (years)
Base	0	1.294	N/A	1.294	N/A	N/A	N/A
3.1	10	1.216	6.03	1.2413	4.07	7.95	16.22
3.2	10	1.2317	4.81	1.2444	3.83	7.97	19.85
3.3	8	1.2559	2.94	1.2563	2.91	9.39	21.09
3.4	10	1.2538	3.11	1.2548	3.03	9.25	20.5

Table 3.9 shows that the best E/P ratio in all four cases is the maximum ratio tested, or between 8-10 hours at rated power. This length matches well when compared with the E/P ratios displayed in Table 3.4 of existing PHES in the United States. Also, a range of 3-6% annual operating cost savings was found when using high levels of energy storage in the Arizona test bed. This percentage of annual savings equates to between $37.8-78 million each year, depending on the location and size of the PHES. Note that the operating cost savings only includes the difference in the generator operating cost of the specified case and the base case. The operating cost savings does not include any capital costs including the power and energy costs specified earlier. Using the range of operating cost savings and (3.1), the payback period was found to be between 8-21 years. When compared to average lifetime of PHES, the payback period range seems feasible.

A common occurrence in all four cases is as both the E/P ratio and the power limit of the PHES increases, the operating cost decreases. However, there were a few scenarios where increasing either one had no effect on the operating cost. This could be caused by different limits in the system and is looked into with more detail in Chapter 5. Another observation related to the payback period is that in every case, the slope of the payback period versus the power limit is

positive. A positive slope in this case means that the additional operating cost savings from increasing the PHES power limit is less than the added capital cost. However, in most cases the payback period did decrease as the E/P ratio increased.

4. Chapter 4: Bulk energy storage at very high levels of pumped hydro implementation

4.1 Description of high level test cases

The focus of this chapter is to analyze the effect of adding very high levels of bulk energy storage to the Arizona test bed described in Section 3.1. With a load ranging between 1.36-13.6 GW, the best case scenario for "shaving" the peak would be to completely flatten the load profile, which is known as load leveling. For 100 % load factor, it would be necessary to add bulk storage with a total simultaneous power limit of at least 6 GW.

Three cases are studied using bulk energy storage between power ratings of 5-6 GW. The locations chose to add PHES include the different combinations of the three simulated locations used in Chapter 3 as well as three additional PHES waiting approval from FERC. These locations include:

- Longview Pumped Storage located in Big Chino Valley, southeast of Seligman, AZ which would tie into the El-Dorado – Moenkopi 500 kV line [66].
- Table Mountain Pumped Storage located near the towns of Peach Springs and Kingman, AZ that would tie into the Mead – Phoenix 500 kV line [67].
- Eagle Mountain Pumped Storage located northeast of Palm Springs, CA which would tie into the Devers – Palo Verde 500 kV line [68].

Figure 4.1 shows the locations of the proposed pumped hydro energy storage added that will be analyzed using the Arizona test bed. Appendix C has a very brief discussion of environmental issues related to large scale pumped hydro at the sites listed.

Figure 4.1 Locations of pumped hydro energy storage proposed to FERC

Tables 4.1 and 4.2 provide information on the three proposed locations [66-68]. Some of this information includes reservoir volume and area as well as power limits and operating entities.

Table 4.1 Proposed PHES location information and operating entity

	Location	County	Nearby bus	Year of development	Water source	Operating entity	Power limit (MW)
▲	Longview	Yavapai AZ	Moenkopi	2012	Local ground water	Energy Storage Systems	2000
■	Table Mountain	Mohave AZ	Mead	2011	Colorado River	Table Mountain Hydro, Arizona	400
●	Eagle Mountain	Riverside CA	Palo Verde	2009	Chuckwalla ground water	Eagle Crest Energy	1300

Table 4.2 Proposed PHES location reservoir numbers

	Lower reservoir volume (acre-ft.)	Lower reservoir surface area (acres)	Lower reservoir average depth (ft.)	Upper reservoir volume (acre-ft.)	Upper reservoir surface area (acres)	Upper reservoir average depth (ft.)
▲	17,400	175	99.4	17,400	209	83.3
■	5,683	68	83.6	5,280	66	80
●	17,700	163	108.6	17,700	191	92.7

4.2 Case 4.1: Longview and Table Mountain pumped storage

The first case tested for very high levels of energy storage includes five locations in Arizona. The locations tested using the Arizona test bed described in Section 3.1 includes: Longview Pumped Storage, Horse Mesa Pumped Storage, Boulder Pumped Storage, Table Mountain Pumped Storage, and Glen Canyon Pumped Storage. Table 4.3 shows the locations, system bus numbers, and the power limit of each PHES.

Table 4.3 Case 4.1 PHES locations and power limit

Location of PHES	Bus number	Power capacity (MW)
Longview	3	2000
Horse Mesa	83	130
Boulder	149	2080
Table Mountain	153	400
Glen Canyon	186	1296
	Total	5906

Case 4.1 has a total power limit of 5.91 GW, which is very close to the maximum power limit of 6 GW to perform load leveling. This case is tested over a range of energy / power ratios to see the effect on operating cost, payback period, peak shaving, and the load factor. The program created in MATLAB shown in Appendix A is again used with the PHES in Table 4.2 added to their specified bus.

Case 4.1 operating cost and payback period evaluation

The first test run on Case 4.1 is to see how varying the E/P ratio between 1-10 hours for each PHES location and seeing its effect on the output. This test gives a good understanding as to how large the upper reservoir should be in order to get the lowest operating cost and payback period. The payback period is calculated using the operating cost savings found using the $1.294 billion value from the base case in Section 3.3, the capital cost calculated for each location using the values in Table 3.6, and (3.1). The results are shown in Table 4.4 and plotted in Figures 4.2 and 4.3.

Table 4.4 Case 4.1 annual operating cost and payback period as E/P ratio increases

E/P ratio	Annual operating cost (billion $/ year)	Payback period (year)
1	1.2423	58.4
2	1.2247	44.1
3	1.2103	36.9
4	1.1994	33.1
5	1.1924	31.2
6	1.1886	30.5
7	1.1869	30.4
8	1.1861	30.6
9	1.1858	30.9
10	1.1858	31.2

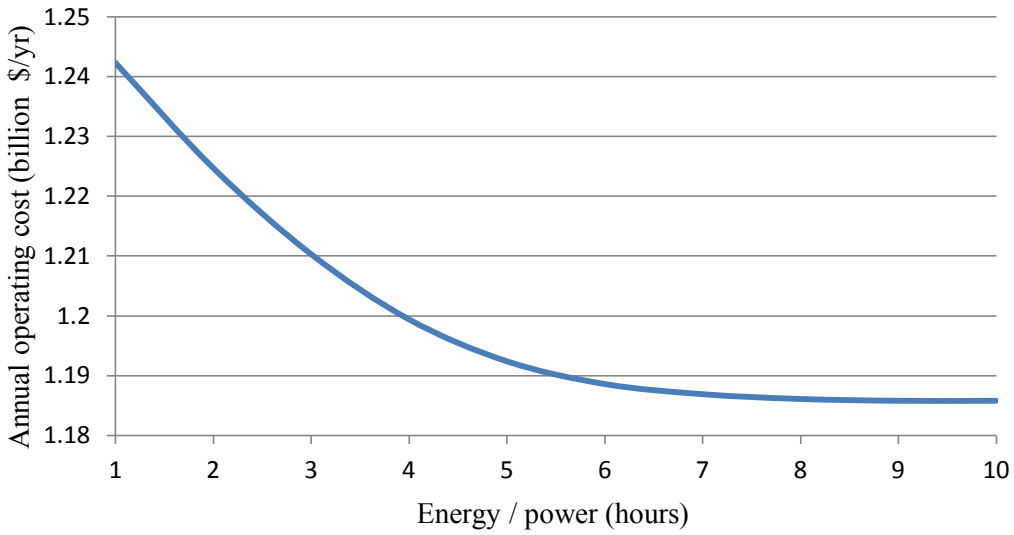

Figure 4.2 Case 4.1 annual operating cost as E/P ratio varies

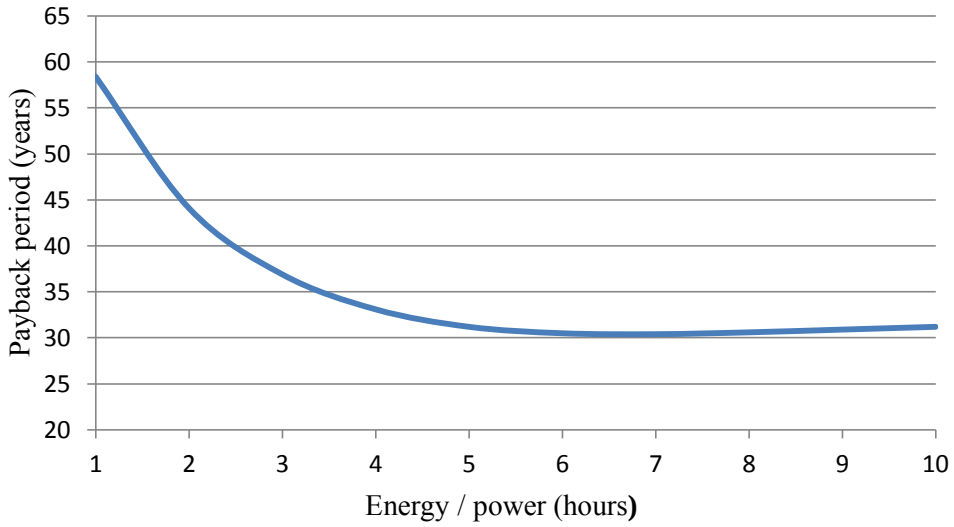

Figure 4.3 Case 4.1 payback period as the E/P ratio varies

Figures 4.2 and 4.3 show that as the E/P ratio increases, the operating cost and payback period both decrease and eventually level off to a constant value. However, if the E/P ratio was to continue to past 10 hours, the payback period would continue to slowly increase because the operating cost savings would remain constant but the power related capital costs would increase. For Case 4.1, the minimum operating cost was found to be $1.1858 billion at E/P ratios of 9 and 10 hours, or an annual operating cost savings of 8.4%. This percentage savings equates to roughly $108 million of annual generator operating cost savings. The minimum payback period occurs at an E/P ratio of 7 hours at a length of 30.4 years. The payback period begins to increase above 30.4 years because the operating cost savings to capital cost ratio begins to decrease.

Case 4.1 peak shaving evaluation

The next test used on Case 4.1 is how much energy is stored and recovered to "shave" the peak as the E/P ratio increases for each location. Based on the results from Section 4.2, the amount of the peak "shaved" should increase as the E/P ratio increases because the operating cost is decreasing. Figures 4.4-4.6 show plots of the generation level plotted with the load profile to show how the amount of energy stored / recovered change as the E/P ratio increases. This is done using E/P ratios of 2, 5 and 10.

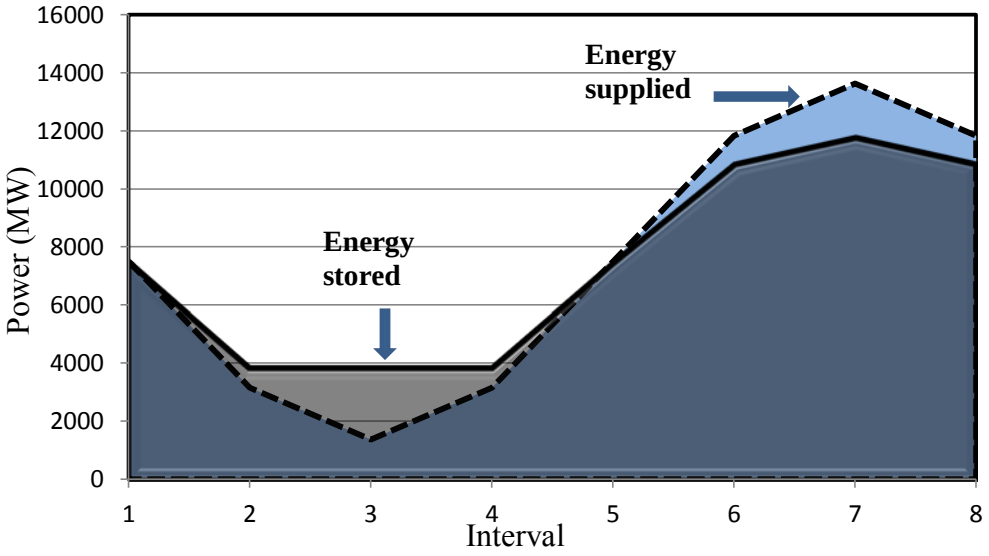

Figure 4.4 Case 4.1 daily generation output and load profile: E/P = 2

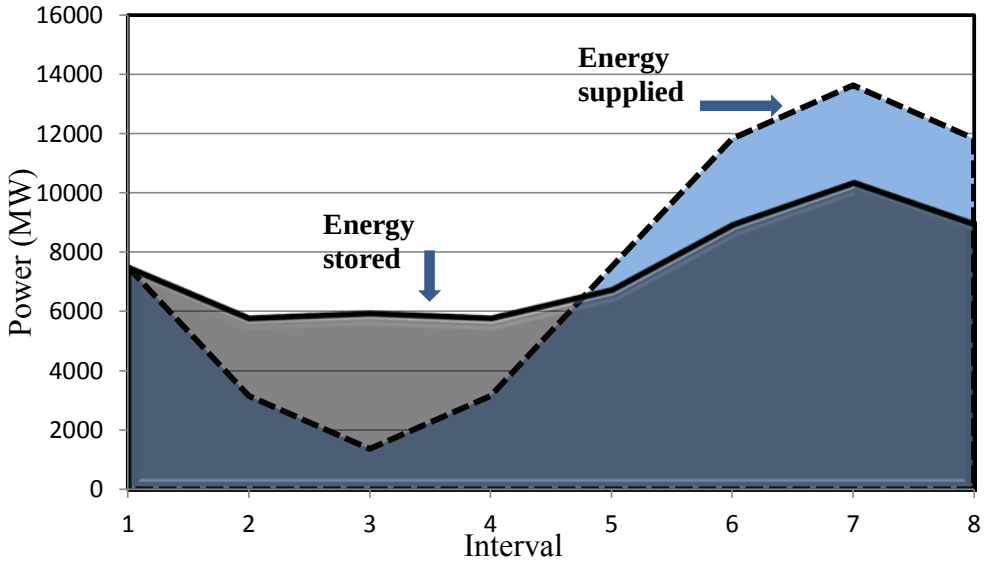

Figure 4.5 Case 4.1 daily generation output and load profile: E/P = 5

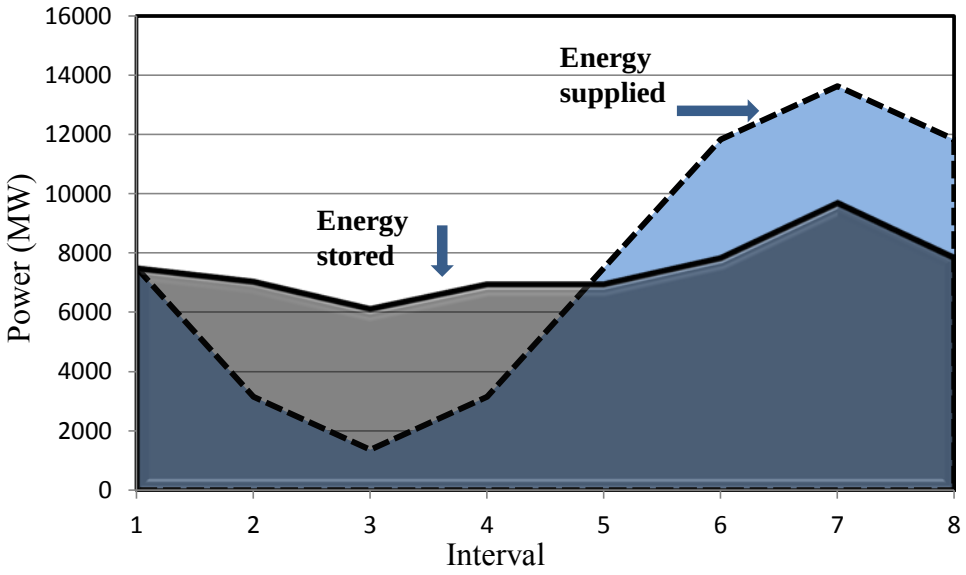

Figure 4.6 Case 4.1 daily generation output and load profile: E/P = 10

Figures 4.4 – 4.6 demonstrate that as the E/P ratio increases, more energy can be stored during off peak hours and recovered when the demand increases towards a peak. The figures display that with very high amounts of energy storage available close to the average of the load, the generation output begins to flatten out to a constant value. However, the output never completely flattens out meaning there is some limit preventing this from occurring. Chapter 5 will look into how the system limits affect the amount of energy storage and its energy rating. Table 4.5 quantifies the amount of energy shaved from the peak demand period for each E/P ratio and Figure 4.7 plots the results.

Figure 4.7 shows that as the E/P ratio increases, more energy is stored/ recovered during periods of peak demand. This result is expected because as the ratio increases, the PHES has a larger upper reservoir and can store more water / energy (MWh). However, as the E/P ratio increases to around 9 hours, it begins to flatten out to a constant value of around 36.6 GWh. Chapter 5 will investigate why there is a limit on the amount of energy stored and used to "shave" the peak demand.

Table 4.5 Case 4.1 daily energy recovered as E/P ratio varies

Energy / power (hours)	Daily energy recovered* (MWh)
1	5905.9757
2	11730.757
3	17249.767
4	22988.487
5	28403.799
6	31792.531
7	33880.329
8	35528.326
9	36550.404
10	36577.106

*"Energy recovered" refers to the energy stored during off peak, and this is identical to the energy recovered and used during on-peak

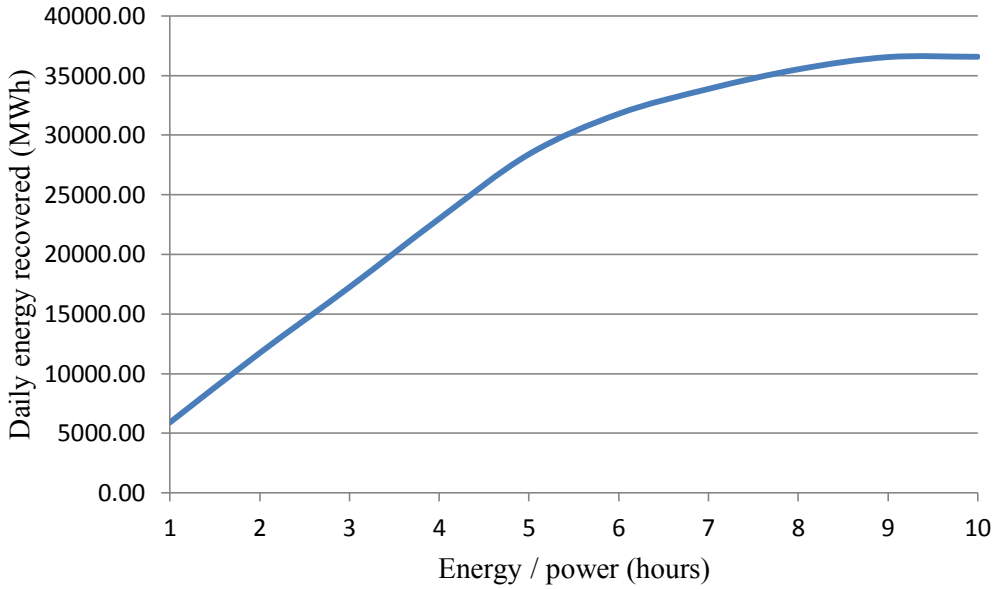

Figure 4.7 Case 4.1 daily energy recovered during peak demand as E/P ratio varies

Case 4.1 load factor evaluation

The final test used on Case 4.1 is to analyze the effect of the E/P ratio on the load factor. The load factor is defined as the "ratio of the average load over a designated period to the peak load occurring in that period [69]." The load factor is a measure of the utilization rate, or efficiency of electrical energy usage. The higher the load factor, the better the system is utilizing its generation resources. The load factor is formulated as,

$$LF = \frac{E_T}{P_{peak}T} \tag{4.1}$$

where

E_T Total energy supplied in MWh

P_{peak} Peak power demand in MW

T Time period in hours (e.g., T = 8760 h for annual LF)

Using (4.1), the load factor is calculated for each E/P ratio including the base case to see how energy storage and the size of the upper reservoir can improve the load factor of the Arizona test bed. The results can be seen in Table 4.6 and Figure 4.8 plots the results.

Table 4.6 Case 4.1 annual load factor as E/P ratio varies

E/P Ratio	Annual load factor (%)
0	54.98
1	61.60
2	63.78
3	66.10
4	69.03
5	72.51
6	74.45
7	75.73
8	76.64
9	77.00
10	77.31

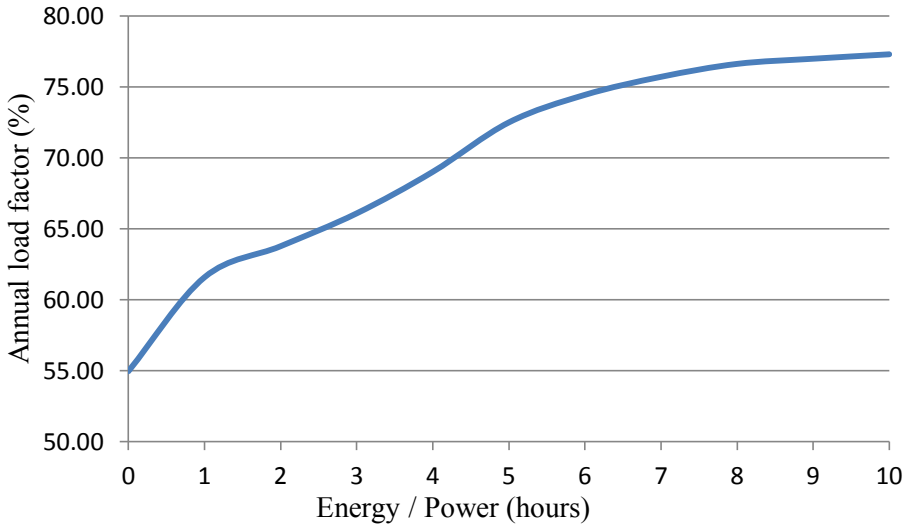

Figure 4.8 Case 4.1 annual load factor percentage as the E/P ratio increases

Figure 4.8 shows that as the E/P ratio increases to around 9 hours, the load factor also increases. After 9 hours, the load factor remains constant at around 77% which is expected because the energy recovered during periods of peak demand shown in Table 4.5 also remains constant. By adding very high amounts of energy storage to the test bed and increasing the E/P ratio close to the typical values seen in existing PHES locations, the load factor was able to improve by about 22%. This load factor increase shows that for Case 4.1, energy storage can help improve the utilization of the generators significantly.

4.3 Case 4.2: Eagle Mountain and Table Mountain pumped storage

The second case tested for very high levels of energy storage includes five locations again, with four in Arizona and one location in California close to the California Arizona border. The locations include: Eagle Mountain Pumped Storage, Horse Mesa Pumped Storage, Boulder Pumped Storage, Table Mountain Pumped Storage, and Glen Canyon Pumped Storage. Eagle Mountain Pumped Storage is a location pending approval from FERC and is located in California close to the border with Arizona. Table 4.7 provides the locations, system bus numbers, and the power limit of each PHES location added to the system in Case 4.2.

Case 4.2 has a total power limit of 5.21 GW, which is closer to the 5 GW minimum needed to perform load leveling to the system. With a lower amount of energy storage available, it is expected that the amount of energy "shaved" from the peak will be less than what occurred in Case 4.1. Again, the MATLAB program in Appendix A is used to test the effect of the E/P ratio on the operating cost, payback period, peak shaving, and the load factor.

Table 4.7 Case 4.2 PHES locations and power limit

Pumped storage location	Bus number	Power capacity (MW)
Eagle Mountain (CA)	66	1300
Horse Mesa	83	130
Boulder	149	2080
Table Mountain	153	400
Glen Canyon	186	1296
	Total	5206

Case 4.2 operating cost and payback period evaluation

Similar to Case 4.1, the E/P ratio is varied between 1-10 hours of rated power output for each location and the operating cost and payback period are analyzed. The base case operating cost of $1.294 billion is compared with the operating cost savings and the capital costs of the five PHES locations to determine a payback period for each E/P ratio using (3.1). The results are shown in Table 4.8 and plotted in Figures 4.9 and 4.10.

Figures 4.9 and 4.10 show similar results to Figures 4.2 and 4.3 in Case 4.1. As the E/P ratio increases, the operating cost decreases and levels out to an operating cost of $1.983 billion between $8 \leq E/P \leq 10$. Compared to Case 4.1, the minimum system wide operating cost is slightly higher because there is 700 MW less of storage available. However, the minimum payback period is slightly less in this case resulting from a lower total capital cost than Case 4.1 but only a $12.5 million difference is operating cost savings. The minimum operating cost savings is around $95.7 million or around 7.4%. The payback period decreases to a minimum length of 29.9 years at E/P = 6 and starts to increase as the E/P ratio increases past 6. Again, the payback period approaches a minimum and increases because the operating savings to capital cost ratio begins to decrease.

Table 4.8 Case 4.2 annual operating cost and payback period as E/P ratio increases

E/P ratio	Annual operating Cost (billion $ / year)	Payback period (year)
1	1.2452	54.5
2	1.2297	41.9
3	1.2167	35.3
4	1.2068	31.7
5	1.2016	30.3
6	1.1992	29.9
7	1.1984	30.0
8	1.1983	30.4
9	1.1983	30.8
10	1.1983	31.1

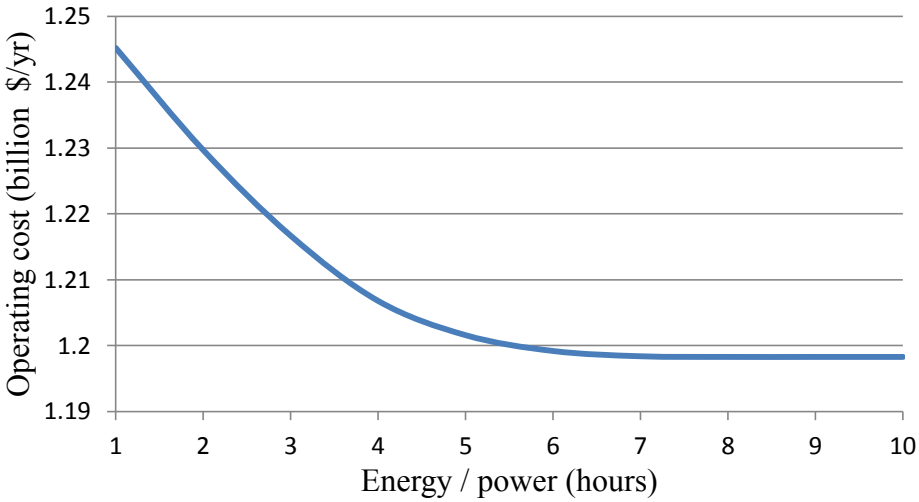

Figure 4.9 Case 4.2 annual operating cost as E/P ratio varies

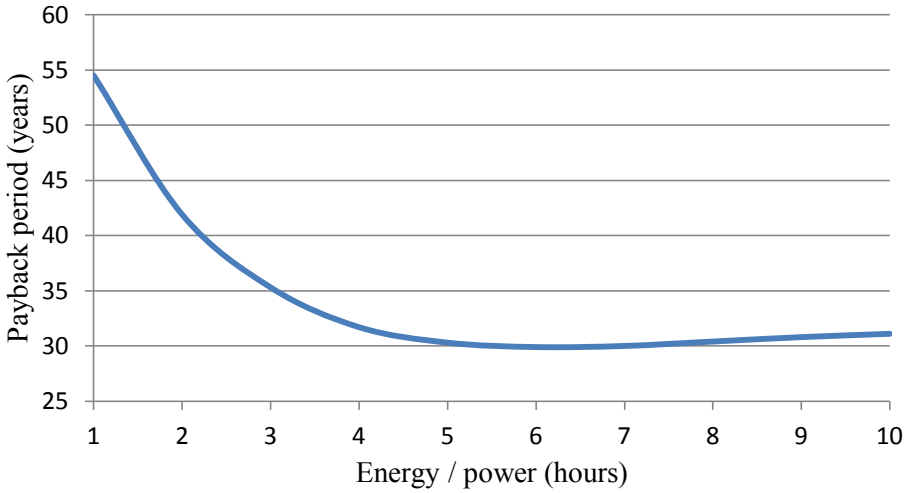

Figure 4.10 Case 4.2 payback period as the E/P ratio varies

Case 4.2 peak shaving evaluation

Case 4.2 is tested for how much energy is stored and recovered to "shave" the peak as the E/P ratio increases. Again, the results are expected to be very similar to Case 4.1 in that the amount of energy recovered during the peak demand should increase because the operating cost decreases up until E/P = 8. After that point, the amount of energy recovered should remain constant because the system wide operating cost does not change. Figures 4.11-4.13 show plots of the generation output and load profile for E/P ratios of 2, 5, and 10 to show how much energy is stored / recovered as the ratio is varied.

Again, Figures 4.11-4.13 are very similar to Figures 4.4-4.6 in Case 4.1. As the E/P ratio increases, more energy is recovered during peak demand hours. However, as the ratio increases from 5 to 10 hours, there is very little change in the energy recovered. This small change in the peak "shaved" is quantified by the small change in the system wide operating cost. Similar to

Case 4.1, the generation output never completely flattens out due to a limit preventing the maximum amount of energy being stored. Table 4.9 shows the amount of energy recovered during the period of peak demand for each E/P ratio and Figure 4.14 plots the results.

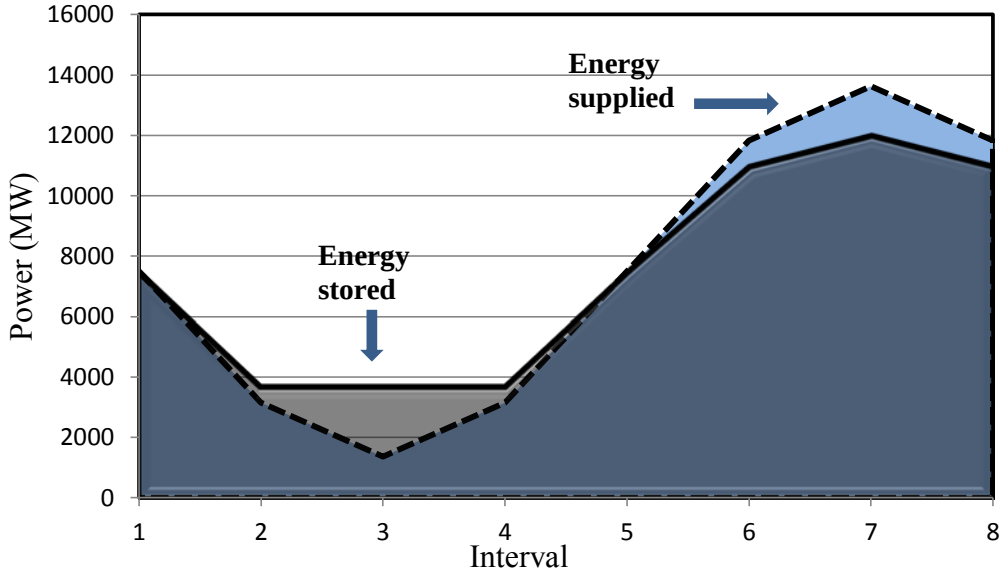

Figure 4.11 Case 4.2 daily generation output and load profile: E/P = 2

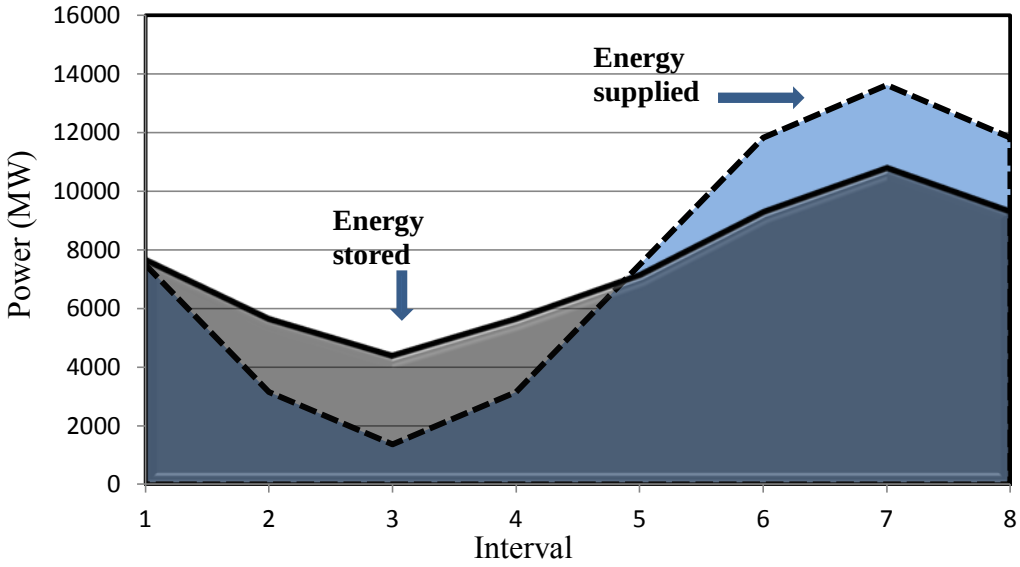

Figure 4.12 Case 4.2 daily generation output and load profile: E/P = 5

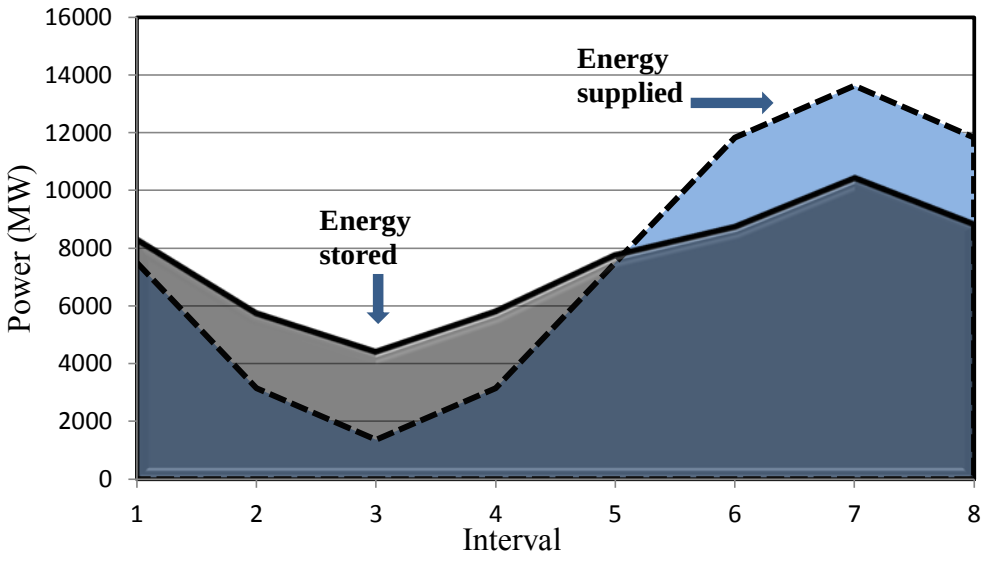

Figure 4.13 Case 4.2 daily generation output and load profile: E/P = 10

Table 4.9 Case 4.2 energy recovered as E/P ratio varies

E/P Ratio	Daily energy recovered (MWh)
1	5205.96
2	10348.19
3	15145.21
4	20181.07
5	23971.18
6	25654.34
7	26301.00
8	26425.89
9	26520.13
10	26514.12

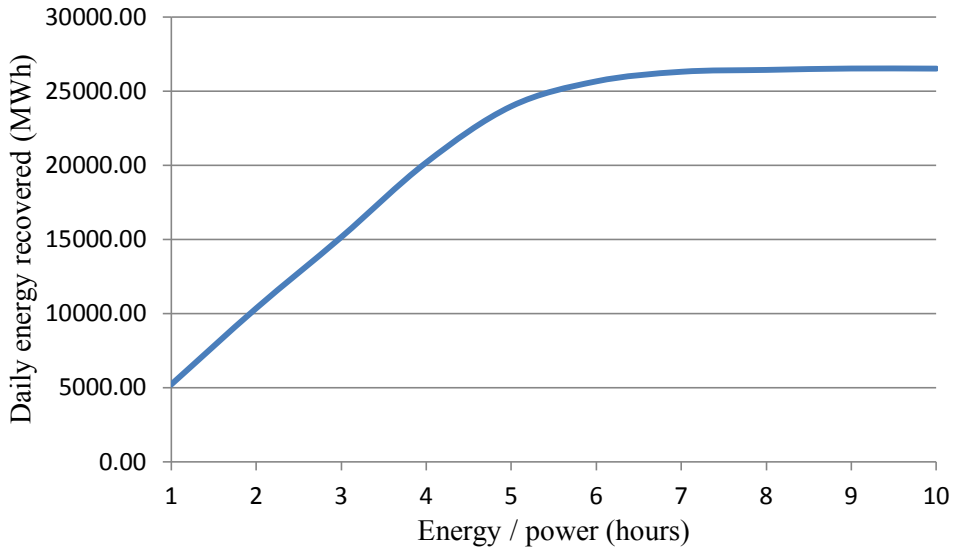

Figure 4.14 Case 4.2 daily energy recovered as E/P ratio increases

Similar to Case 4.1, as the E/P ratio increases, more energy is stored/ recovered when the load profile as a higher demand. However, in this case the amount of energy "shaved" from the peak actually starts to flatten out earlier around 7 hours rather than 9 hours. Also, the maximum amount of energy recovered is around 26.5 GWh which is about 10 GWh less than the first case. This decrease is partially the result of having 700 MW less energy storage available.

Case 4.2 load factor evaluation

Case 4.2 is analyzed using the load profile test discussed in Case 4.1. Using (4.1), the load factor is calculated at each E/P ratio and compared with the base case load factor to understand how the PHES locations in Case 4.2 can improve the load factor for the Arizona test bed. The results are also compared with Case 4.1. Table 4.10 shows the resulting load factor percentages and Figure 4.15 graphs the results versus the E/P ratio.

Table 4.10 Case 4.2 annual load factor as E/P ratio varies

E/P Ratio	Annual load factor (%)
0	54.98
1	60.93
2	62.62
3	64.46
4	66.68
5	69.45
6	71.01
7	71.69
8	72.00
9	72.00
10	71.99

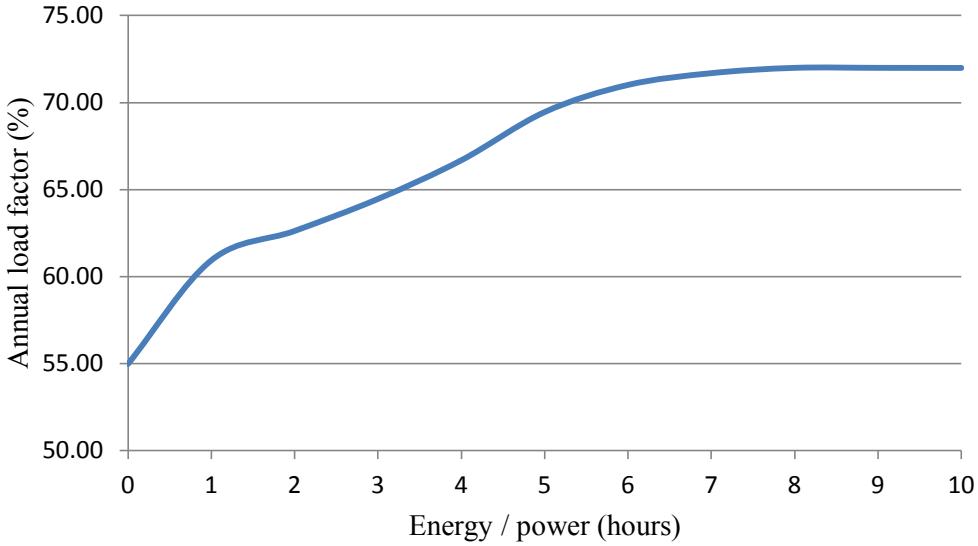

Figure 4.15 Case 4.2 annual load factor as the E/P ratio increases

Figure 4.15 shows that the load factor increases to a minimum of 60.9% from 55% using the locations in Case 4.2 with the minimum E/P ratio of 1. As the ratio increases to 7 hours, the load factor increases up to 72% and remains constant. The results when testing the load factor change show that by adding the PHES shown in Table 4.7, the load factor can improve by as much as 17%. However, this load factor increase is 5% less than in Case 4.1.

4.4 Case 4.3: Longview, Eagle Mountain, and Table Mountain pumped storage

Case 4.3 uses five of the six locations shown in Section 4.1 to try to accomplish load leveling in the Arizona test bed. The locations include: Longview Pumped Storage, Eagle Mountain Pumped Storage, Horse Mesa Pumped Storage, Boulder Pumped Storage, and Table Mountain Pumped Storage. Again, one PHES location in California, Eagle Mountain Pumped Storage, is chose because of its high energy capacity. Table 4.11 gives the PHES locations, test bed bus numbers, and the power limit of each location in Case 4.3.

Table 4.11 Case 4.3 PHES locations and power limits

Pumped storage location	Bus number	Power capacity (MW)
Longview	3	2000
Eagle Mountain (CA)	66	1300
Horse Mesa	83	130
Boulder	149	2080
Table Mountain	153	400
	Total	5910

Case 4.3 has a total power limit of 5.91 GW, the maximum level of storage of all three cases and closest to the 6 GW needed to completely level the load. With a slightly higher level of storage available, the minimum operating cost should be the lowest of all three cases, and thus the

energy recovered should be the maximum of the three. Again, the E/P ratio is varied to study its effect on operating cost, payback period, peak shaving, and the change in load factor.

Case 4.3 operating cost and payback period evaluation

Using the PHES locations shown in Table 4.11, the E/P ratio is varied again between 1 and 10 hours of rated power output to determine how this affects the operating cost and payback period. The total capital costs of all five PHES locations are first determined to be used in (3.1). The operating cost savings found from the difference of the base case cost of $1.294 billion are then with the total capital cost to find the payback period at each E/P ratio. The results are shown in Table 4.12 and plotted in Figures 4.16 and 4.17.

Similar results to the previous two cases are found when observing Figures 4.16 and 4.17. Figure 4.16 shows that increasing the E/P ratio decreases the operating cost before it levels off to $1.1863 billion at E/P = 9 and 10. Even with a slightly higher total power rating, the minimum operating cost is barely higher than the minimum found in Case 4.1. The annual operating cost savings for Case 4.3 is calculated at $107.7 million for an annual savings percentage of 8.32%. Figure 4.13 shows that the minimum payback period occurs for E/P = 5 and 6 at a length of 30.1 years. The payback period increase above the minimum after E/P = 6 because of the operating cost to capital cost ratio decreasing.

Table 4.12 Case 4.3 annual operating cost and payback period as E/P ratio increases

E/P ratio	Annual operating cost (billion $ / year)	Payback period (year)
1	1.2398	55.7
2	1.2203	41.4
3	1.2048	34.8
4	1.1934	31.1
5	1.1884	30.1
6	1.1871	30.1
7	1.1866	30.3
8	1.1864	30.7
9	1.1863	31.0
10	1.1863	31.4

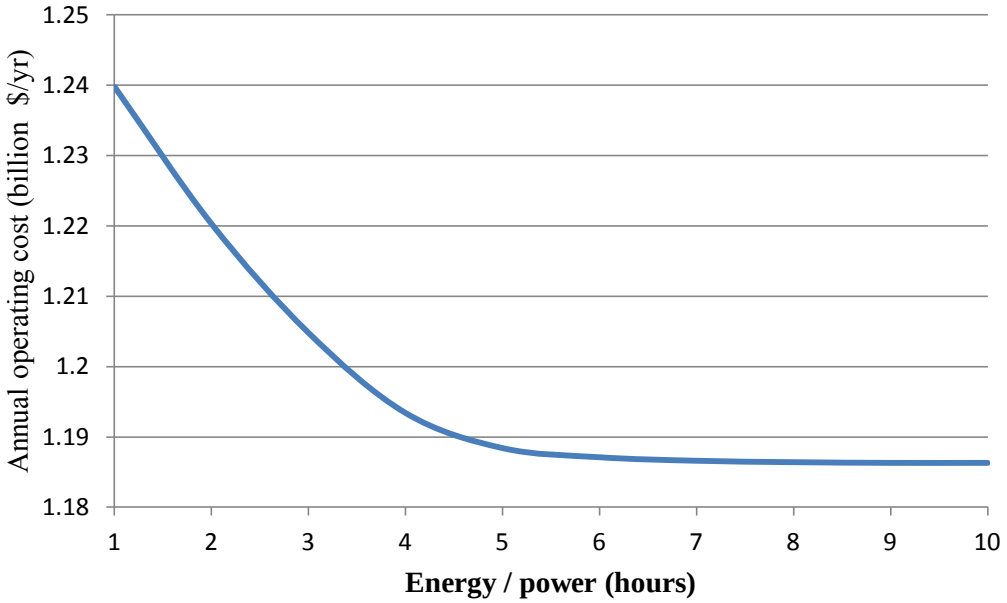

Figure 4.16 Case 4.3 annual operating cost as E/P ratio varies

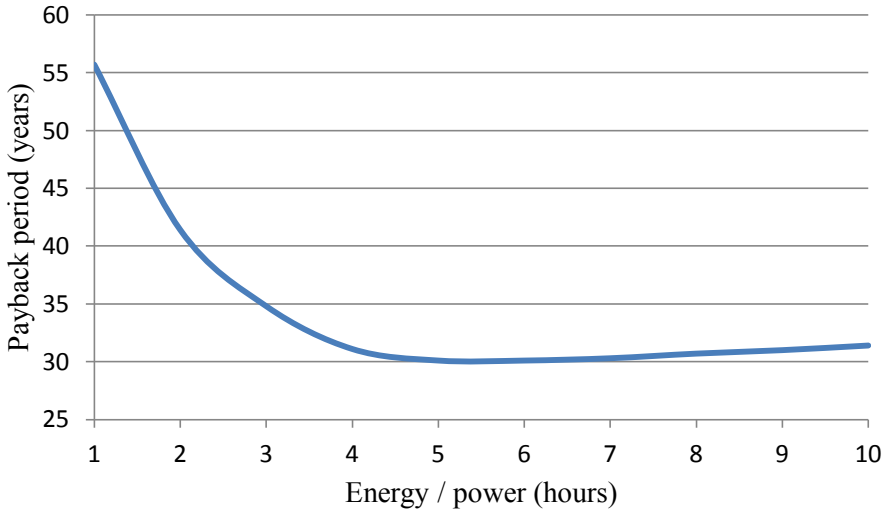

Figure 4.17 Case 4.3 payback period as the E/P ratio varies

Case #3 peak shaving evaluation

The E/P ratio of the locations in Case 4.3 are varied to analyze how this affects the energy recovered during the period of peak demand. The amount of the peak "shaved" as the E/P ratio increases is expected to increase because, similar to Cases 4.1 and 4.2, the operating cost decreases up until E/P = 9 and 10. The energy recovered for these two ratios should remain constant and there should be no change in the plots. Figures 4.18-4.20 display the generation output plotted with the load profile for E/P ratios 2, 5, and 10 to analyze the effect on peak shaving.

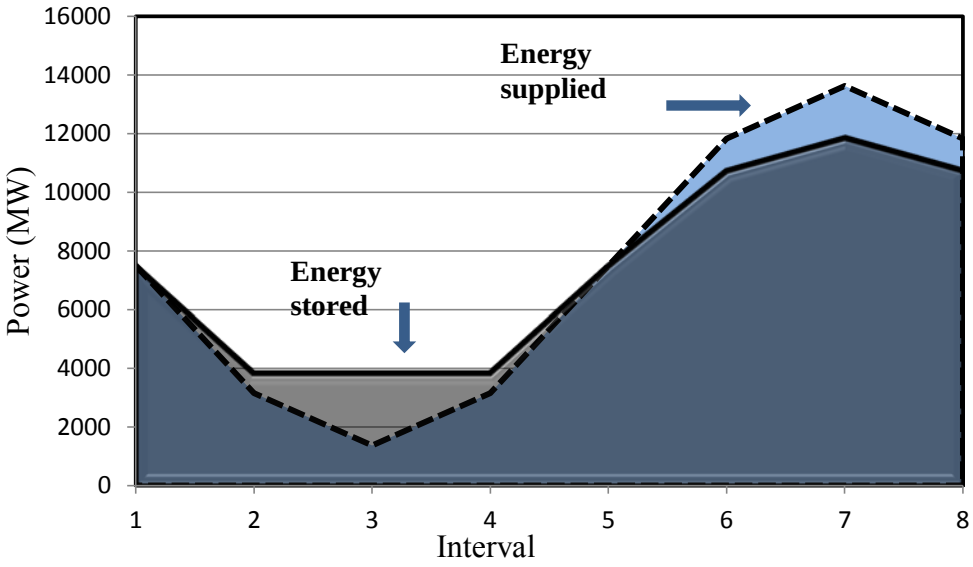

Figure 4.18 Case 4.3 daily generation output and load profile: E/P = 2

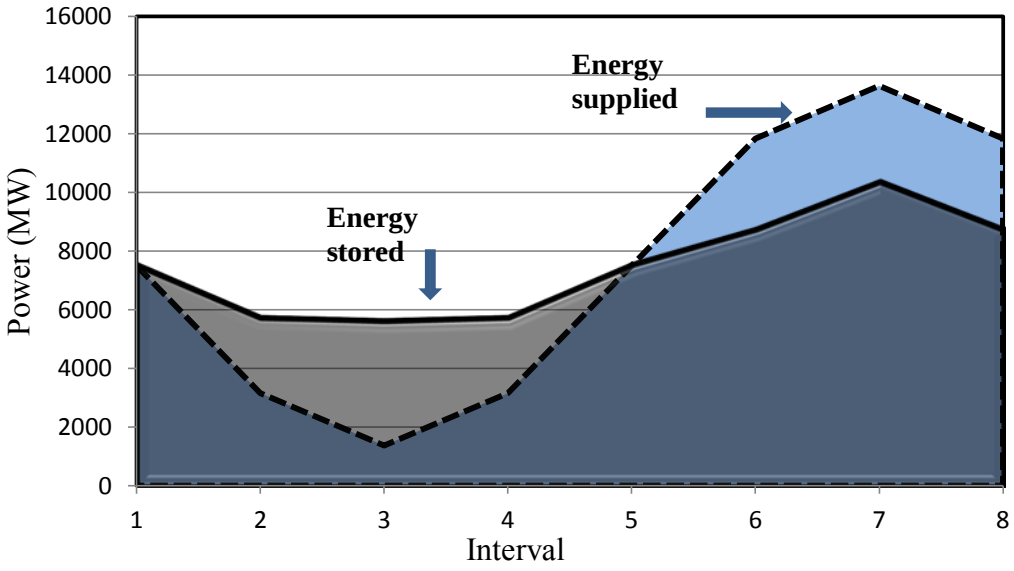

Figure 4.19 Case 4.3 daily generation output and load profile: E/P = 5

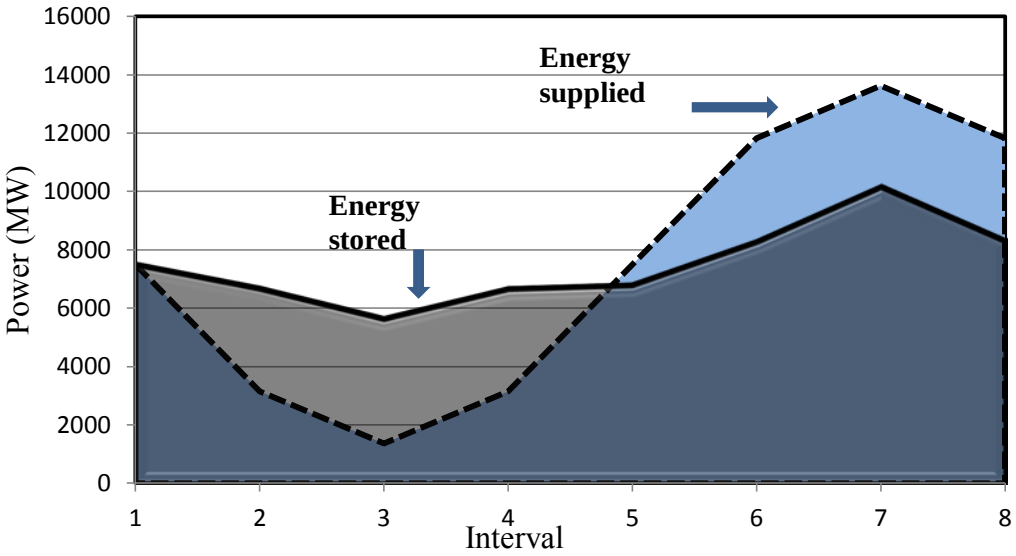

Figure 4.20 Case 4.3 daily generation output and load profile: E/P = 10

Figures 4.18-4.20 demonstrate that as the E/P ratio increases, the energy recovered during the intervals of peak demand also increase. As the E/P ratio approaches 10 hours, the generation output begins to level out with a small peak occurring around interval 7. Similar to Cases 4.1 and 4.2 however, some limit(s) in the system are preventing the maximum amount of energy from being stored. This problem is again analyzed in Chapter 5 to determine the limiting constraint. Table 4.13 shows the amount of energy recovered at each E/P ratio and Figure 4.21 plots the results.

As shown in Cases 4.1 and 4.2, the energy stored / recovered increase as the E/P ratio increases. Again, this result is expected because as the ratio increases, the size of the upper reservoir also increases and can store more water as potential energy. In Case 4.3, the energy recovered remains constant around 8 hours at rated power, which is between the lengths of Cases 4.1 and 4.2. The maximum amount of energy recovered during periods of peak demand is around 32.8 GWh, which is also in between the amount of Cases 4.1 and 4.2.

Table 4.13 Case 4.3 daily energy recovered as E/P ratio varies

E/P Ratio	Daily energy recovered (MWh)
1	5909.97
2	11819.10
3	17729.61
4	23639.25
5	28386.53
6	30418.58
7	31817.35
8	32472.11
9	32819.92
10	32834.19

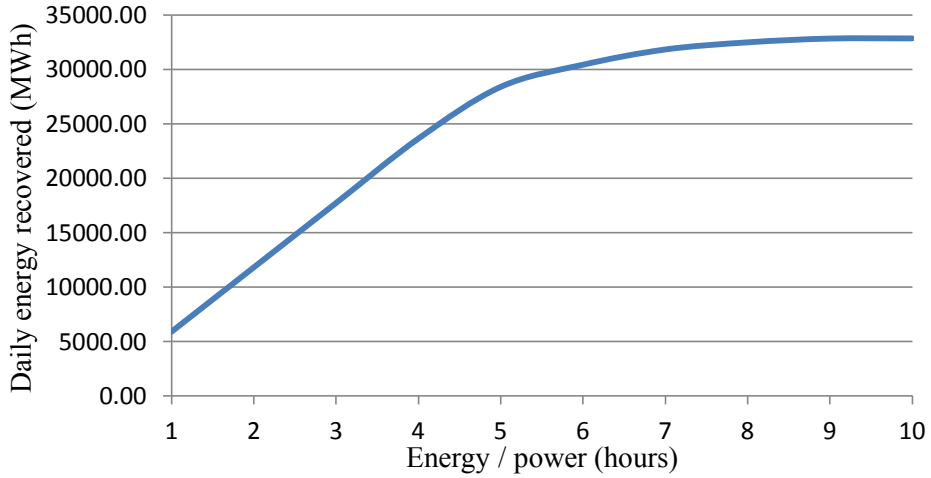

Figure 4.21 Case 4.3 daily energy recovered as the E/P ratio increases

Case 4.3 load factor evaluation

The final test used to analyze the PHES locations added to the Arizona test bed in Case 4.3 is the load factor test discussed in Case 4.1. The E/P ratio is varied and using the generation output, the load factor is calculated using (4.1). The load factor is then compared with the base case and Cases 4.1 and 4.2. Table 4.14 shows the load factor percentages at each E/P ratio and Figure 4.22 graphs the results from the table.

Table 4.14 Case 4.3 annual load factor percentage as the E/P ratio varies

E/P Ratio	Annual load factor (%)
0	54.98
1	60.40
2	63.15
3	65.77
4	68.80
5	72.36
6	73.35
7	73.57
8	73.60
9	73.84
10	73.86

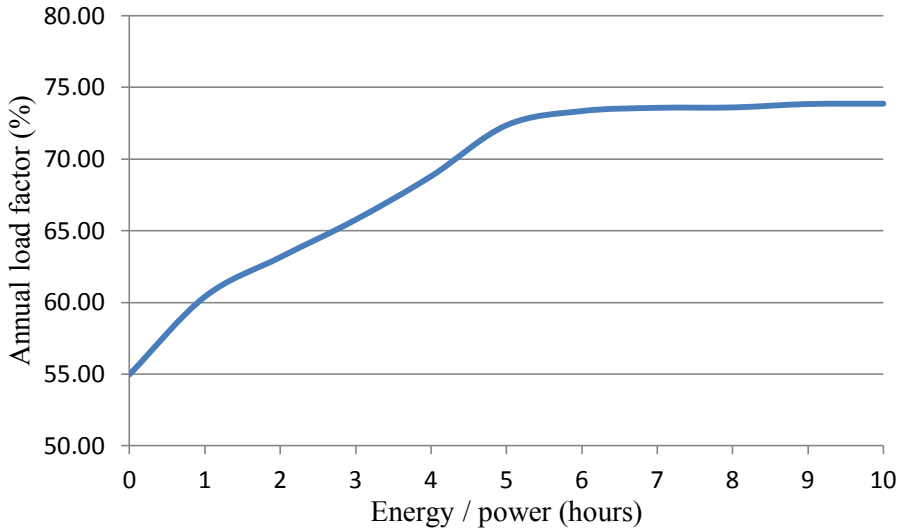

Figure 4.22 Case 4.3 annual load factor as the E/P ratio increases

Figure 4.22 displays the results of the load factor test for Case 4.3. By adding the PHES locations shown in Table 4.11 to the Arizona test bed, the load factor was able to improve from 55% to between 66.9% and 73.9%. The load factor begins to level out around an E/P ratio of 5 hours at rated power. When compared to Cases 4.1 and 4.2, Case 4.3 has a load factor around 3% less than Case 4.1 and 2% greater than Case 4.2. The load factor increase for Case 4.3 when compared to the base case is about $\Delta LF = 19\%$.

4.5 Summary of results for very high levels of storage

In all three cases using very high levels of pumped hydro energy storage, the operating cost was reduced from the base case value of $1.294 billion. This operating cost savings was achieved using the method of peak shaving and in some cases, the load was almost completely leveled.

The payback period, energy recovered, and the load factor were also calculated in all three cases to compare with the base case. Table 4.15 summarizes the results of the three cases. The table displays the minimum operating cost and payback period as well as the maximum energy recovered and load factor in each case.

Table 4.15 Summary of best case results for Cases 4.1-4.3

Case	Minimum annual operating cost (billion $ / yr.)	Annual operating cost savings (million $ / yr.)	Operating cost savings (%)	Minimum payback period (years)	Maximum daily Energy recovered (MWh)	Maximum annual load factor (%)
4.1	1.1858	108.2	8.36	30.40	36.58	77.31
4.2	1.1983	95.7	7.40	29.90	26.51	72.00
4.3	1.1863	107.7	8.32	30.10	32.83	73.86

Table 4.15 shows a maximum operating cost savings in the range of $95.7 – 108.2 million per year when using the three cases of very high levels of PHES. This savings equates to between 7.4-8.4% of savings each year, which is higher than the results from Chapter 3. The minimum payback period was calculated to be between 29.9 – 30.4 years. For high levels of energy storage, the payback period is significantly higher because of the large increase in energy storage capital costs that exceed the additional operating cost savings. When looking at the magnitude of the peak "shaved" from adding large amounts of energy storage, the energy stored/ recovered is between 26.5 – 26.6 GWh, which helped increase the 55% load factor of the base case to between 72-77.3%. This equates to a 17-22% increase which is a significant improvement in utilizing the system generation. This chapter showed that adding very high levels of energy storage to the Arizona test bed had a notable impact on various aspects. It is evident that the PHES locations in Case 4.1 produced the best results for all four test analyzed on the system. Case 4.1 was able to decrease the operating cost by almost $110 million annually and improved the load factor 22%. However, it was observed in all three cases that even with high amounts of storage as well as high E/P ratios that some system constraint(s) were preventing load leveling from occurring. This result was apparent from the operating cost, energy recovered, and load factor all eventually approaching a limit after the E/P ratio increased to a certain point. Chapter 5 will examine the relaxation of selected constraints and how the previously stated advantages and observations change.

5. Relaxation of selected constraints

5.1 Description of relaxed constraint cases

The results from Chapters 3 and 4 make it apparent that some system constraint(s) are *active constraints* that impact load leveling, attaining maximum operating cost savings, and attaining the maximum amount of energy storage. These observations come from the various system tests approaching limits as the E/P ratio is increased. The most evident indicator of the foregoing is that the load factor does not increase above 80% even with enough energy storage available to completely levelize the load. In order to analyze the system constraint(s) effect on the various tests, several relaxation scenarios are tested: e.g., the system line limits, the storage energy limits; and the storage power limits. Figure 5.1 displays the eight selected relaxation scenarios studied.

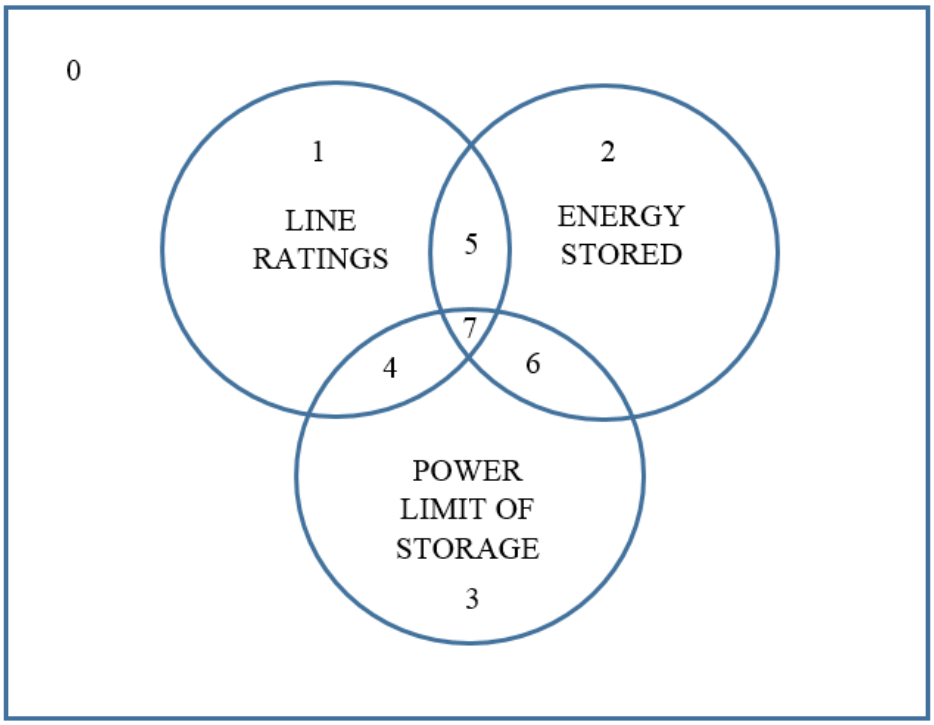

Figure 5.1 System constraint relaxation tests

Figure 5.1 displays the eight tests that are used with the Case 4.1 PHES test bed from Chapter 4. Inspection of Figure 5.1 shows a base case denominated by the numeral '0'; a test in which line rating limits are relaxed denominated by the numeral '1'; and so forth to a test in which the line ratings and storage power limits are relaxed (denominated by '4' in the figure); and so forth to the case in which all limits are relaxed. The latter is denominated by the numeral '7' in Figure 5.1.

The first test, Case 5.0, involves relaxing none of the constraints and uses the results from Chapter 4 to compare with Cases 5.1 – 5.7 which are described in this chapter. The following numbering system is used to distinguish the eight cases studied. Cases 5.*k*, *k* = 0, 1, 2, 7, refer to

case *k* shown in Figure 5.1. In order to relax any of the constraints, the corresponding limit is increased to 10^9 to remove the constraint from the system.

5.2 Case 5.0, no constraint relaxations

Case 5.0 is defined as the base case and thus has no constraints that are relaxed. The PHES locations from Case 4.1 in Chapter 4 are chosen as the test case for all seven constraint relaxation tests. The results from this case are thus the exact same seen in Case 4.1. The operating cost, operating cost savings, load factor, and the total energy stored from Case 4.1 will be used for comparisons with Cases 5.1- 5.7 to see how the various constraints affect the listed tests.

5.3 Case 5.1, relaxation of system line limits

The first test is the relaxation of the system transmission line limits. The relaxation of the line limits analyzes the outcome when the system transmission lines have no maximum operating limit. By removing the line limits, the system wide operating cost should be minimized as there would nothing preventing the maximum amount of energy from being stored as well as the cheaper generators being utilized at their maximum power output levels. The E/P ratio is varied between 1 and 10 and the results are compared with Case 4.1. Tables 5.1 and 5.2 displays the results from Cases 4.1 and 5.1 with the line limits relaxed. Figures 5.1-5.4 plot the results from Table 5.1 together to show how the relaxation of the line limits improve the various tests from Chapter 4.

Table 5.1 Case 4.1 test results as the E/P ratio varies

E/P ratio	Annual operating cost (billion $/year)	Payback period (years)	Daily energy recovered (GWh)	Annual load factor (%)
1	1.2423	58.4	5.91	61.6
2	1.2247	44.1	11.73	63.8
3	1.2103	36.9	17.25	66.1
4	1.1994	33.1	22.99	69.0
5	1.1924	31.2	28.40	72.5
6	1.1886	30.5	31.79	74.5
7	1.1869	30.4	33.88	75.7
8	1.1861	30.6	35.53	76.6
9	1.1858	30.9	36.55	77.0
10	1.1858	31.2	36.58	77.3

Table 5.2 Case 5.1 test results as the E/P ratio varies

E/P ratio	Annual operating cost (billion $/year)	Payback period (years)	Daily energy recovered (GWh)	Annual load factor (%)
1	1.2329	26.15	5.90	63.5
2	1.2149	22.91	11.81	67.4
3	1.2001	20.89	17.72	71.6
4	1.1885	19.63	23.62	76.4
5	1.1802	18.90	29.53	81.9
6	1.1754	18.61	35.42	88.2
7	1.1733	18.62	41.33	95.6
8	1.1731	18.84	43.74	97.0
9	1.1731	19.08	43.75	97.0
10	1.1730	19.30	43.76	97.0

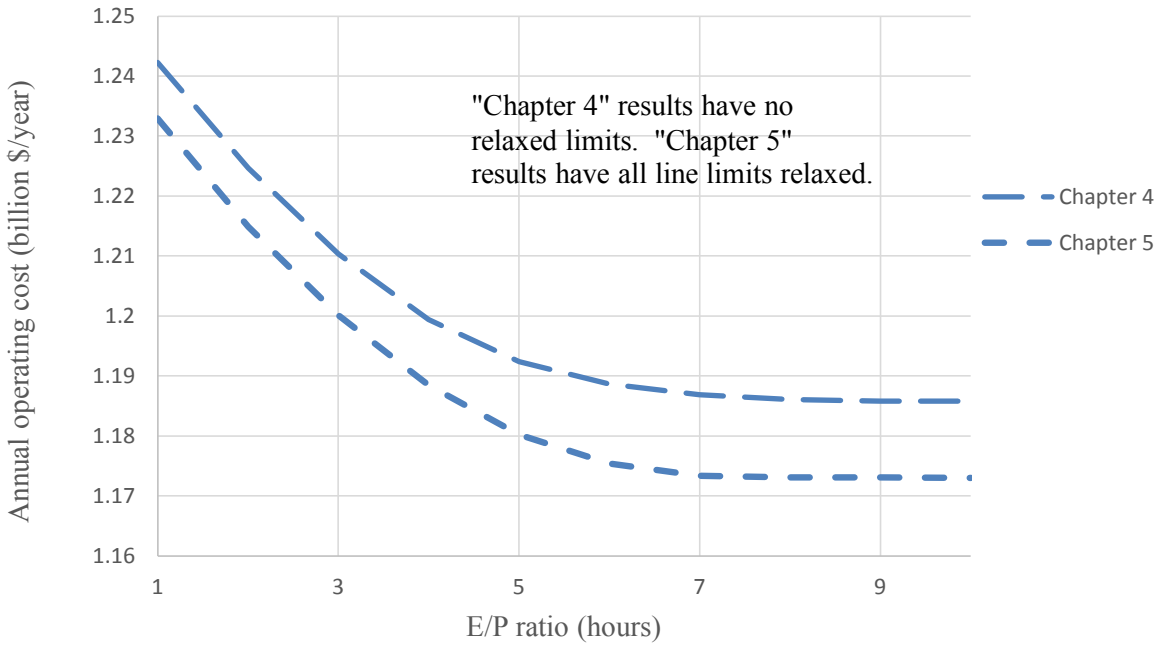

Figure 5.2 Cases 4.1 and 5.1 annual operating cost as the E/P ratio varies

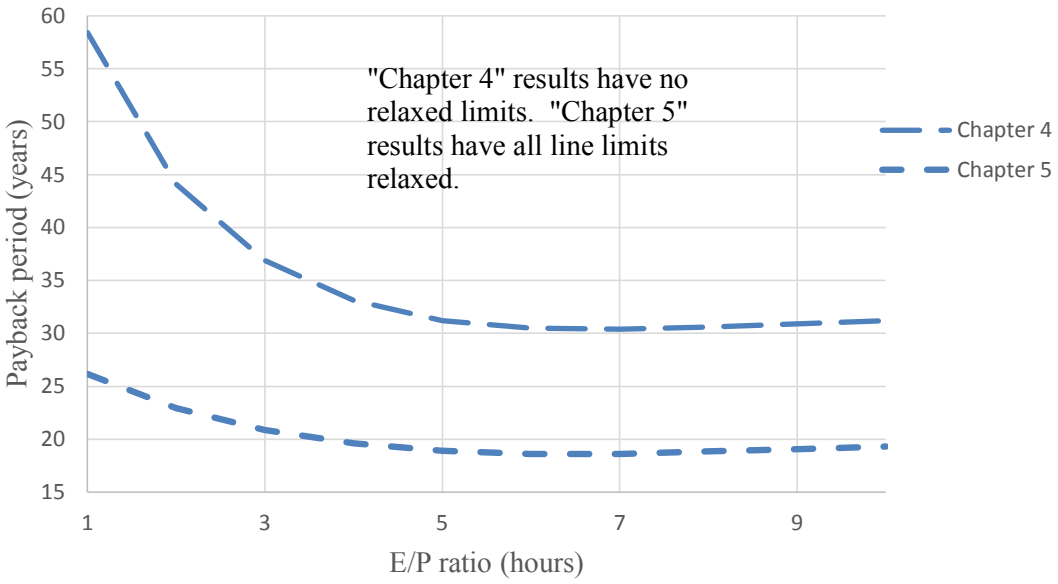

Figure 5.3 Cases 4.1 and 5.1 payback period as the E/P ratio varies

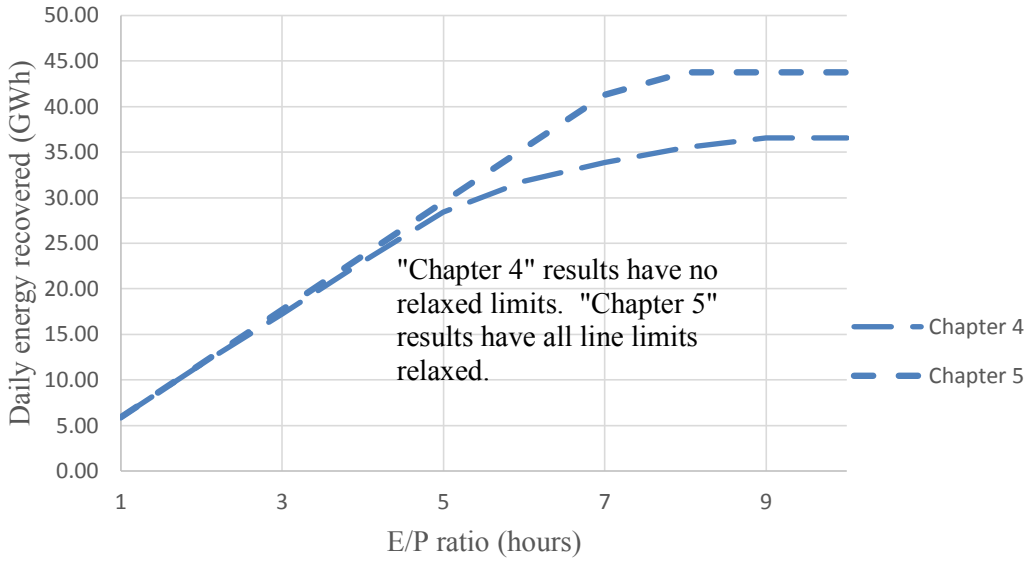

Figure 5.4 Cases 4.1 and 5.1 daily energy stored / recovered as the E/P ratio varies

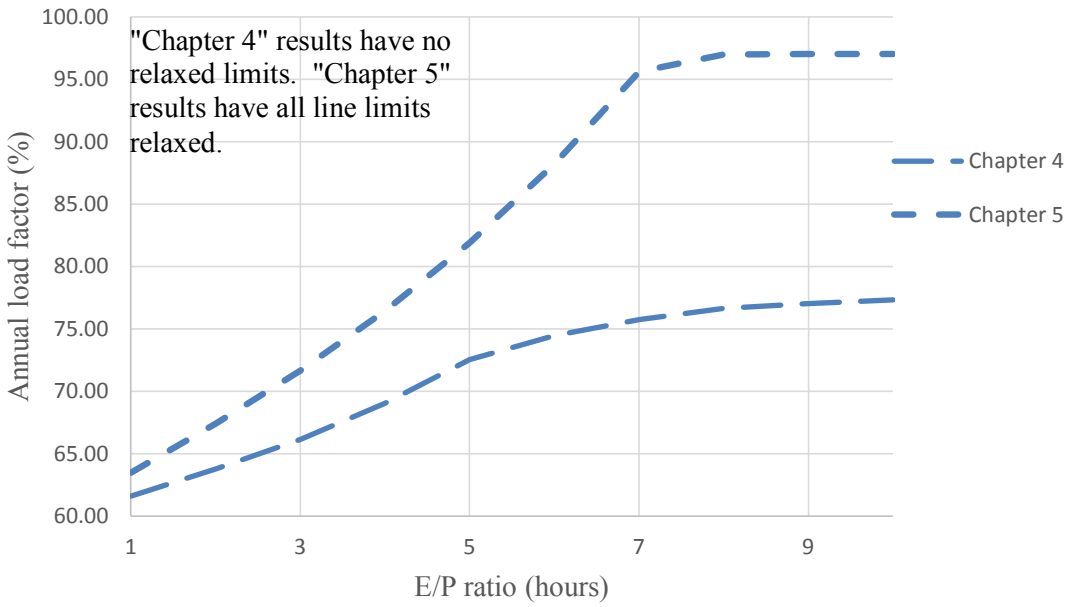

Figure 5.5 Cases 4.1 and 5.1 annual load factor percentage as the E/P ratio varies

As expected, all four test results improved with the line limits relaxed. Figure 5.2 shows that at all E/P ratios, the operating cost decreases for Case 5.1. The minimum operating decreases by as much as 1.09%, or $12.8 million for a minimum of $1.173 billion. The payback periods in Figure 5.3 show a significant decrease for Case 5.1 compared to Case 4.1 with as much as a 38.8% decrease. This equates to an 11.8 year decrease for a minimum of 18.61 years at E/P = 6. Note that the payback period does not include the added cost to increase the transmission line limits and only calculates the PHES payback period. Figure 5.4 displays that for higher E/P ratios, the energy stored / recovered increases up to 16.4%, or 7.18 GWh with a maximum value of 43.8 GWh. Finally, Figure 5.5 shows a very large increase at higher E/P ratios by as much as 19.7% and a load factor as high as 97%. These results show that the existing line limits have a significant impact on the various tests run on Case 4.1. The line limits are preventing the load factor from increasing to nearly 100% and are increasing the payback period by a considerable amount.

5.4 Case 5.2, relaxation of storage energy limits

Case 4.2 studies the effect of relaxing the pumped hydro energy limits. By relaxing the energy limits of the storage, the PHES upper reservoir is modeled to have an infinite volume. An infinite reservoir is unrealistic; however, the relaxation analyzes the limitations the storage energy limit is having on the four test results from Case 4.1. Using the PHES locations form Case 4.1, the results of Case 5.2 can be seen in Table 5.3. Table 5.3 includes the system wide operating cost when there is no energy storage present in the system. The generation output plotted and the load profile can be seen in Figure 5.6 to model peak shaving.

Table 5.3 5.3 Case 5.2 test results

Annual operating cost (billion $/year)	Annual operating cost savings (%)	Annual operating cost savings (million $/year)	Daily energy recovered (GWh)	Annual load factor (%)	No energy storage annual operating cost (billion $/year)
1.1858	8.33	107.8	36.60	77.4	1.2936

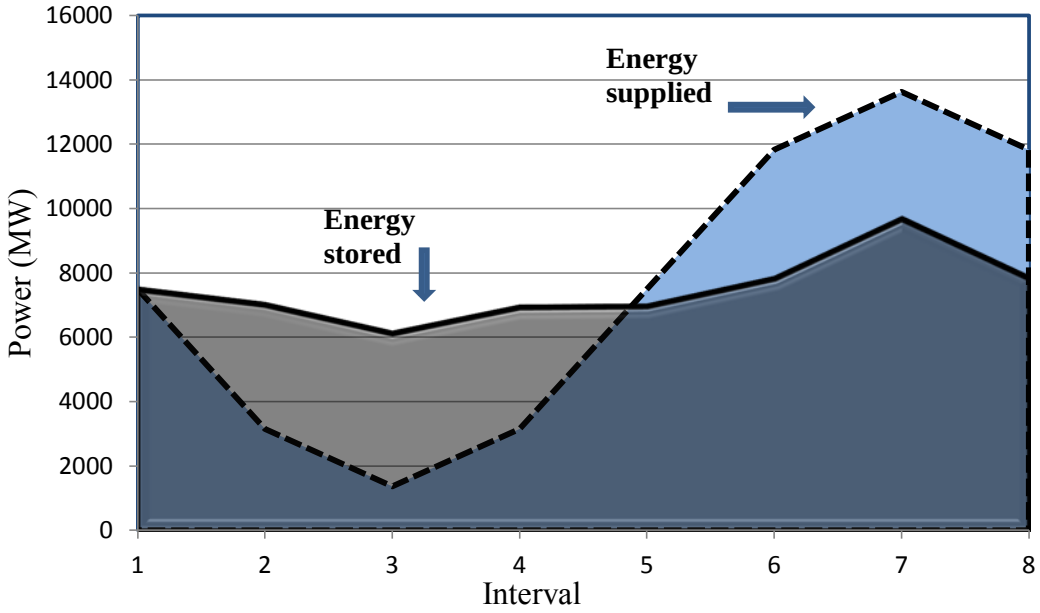

Figure 5.6 Case 5.2 daily generation output and load profile

When comparing the results from Table 5.3 and Figure 5.6 with the results from Case 4.1 at its maximum E/P ratio of 10, there is little to no change. The operating cost remains at $1.1858 billion with an annual savings of $107.8 million, which is an 8.33% reduction when compared to the no storage case. The load factor also remains constant at 77.4% which is why the generation output in Figure 5.6 looks the same as in Figure 4.6 seen in Case 4.1. From these results compared with Case 4.1, it is evident that relaxing the pumped hydro energy limits has no effect on the output. All items tested seem to remain constant as the energy ratio increases to unrealistic numbers.

5.5 Case 5.3, relaxation of storage power limits

The results when the PHES power limits are relaxed are analyzed in Case 5.3. A relaxation of all of the storage power limits indicates replacing the turbine and generator of all existing PHES locations with ones that have impractically high power ratings. The storage power rating relaxations is only to evaluate the constraints effect on the tests run in Case 4.1 and do not represent a realistic upgrade that could be made to the PHES. For this case, the energy ratings of

each PHES remain at the same values as they were with an E/P ratio of 10 before the power limits are relaxed. The results of Case 5.3 can be seen in Table 5.4 and the generator output and load profile are plotted in Figure 5.7.

Table 5.4 Case 5.3 test results

Annual operating cost (billion $/year)	Annual operating cost savings (%)	Annual operating cost savings (million $/year)	Daily energy recovered (GWh)	Annual load factor (%)	No energy storage annual operating cost (billion $/year)
1.1852	8.38	108.40	38.06	78.3	1.2936

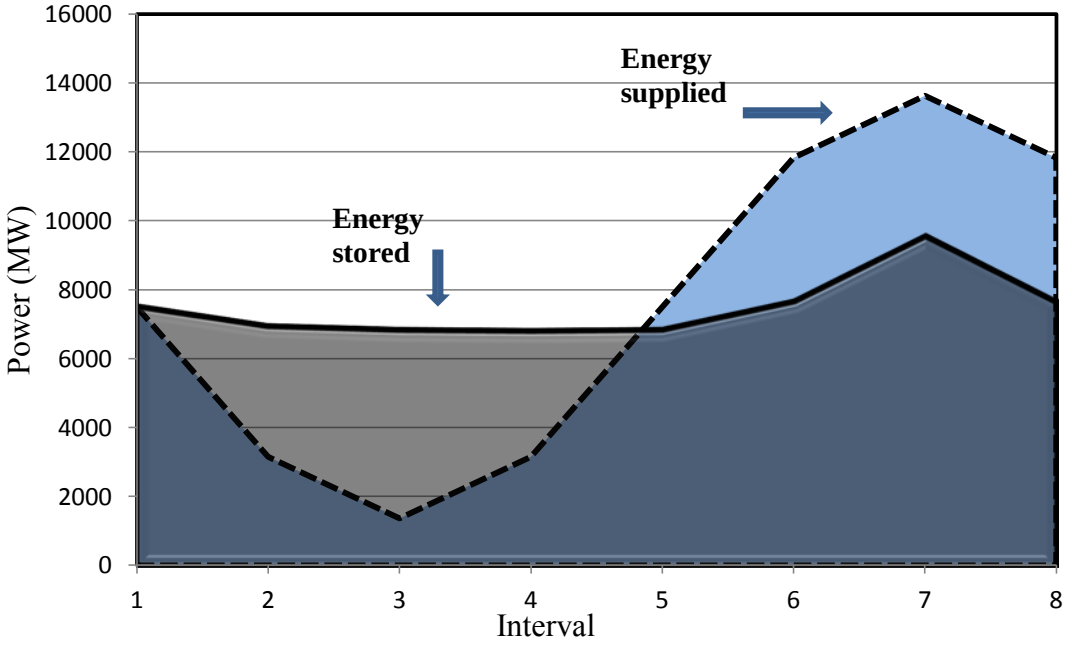

Figure 5.7 Case 5.3 daily generation output and load profile

Table 5.4 shows that by relaxing only the storage power limits, the system wide operating cost decreases by only a small amount when compared with Case 4.1 at an E/P = 10. The operating cost decreases by .05%, or $0.6 million to a value of $1.1852 when compared with Case 4.1 When compared with the base case, or no energy storage, the operating cost improves by $108.4 million, or 8.38%. The load factor increases to 78.3%, or a 1% improvement from the highest load factor in Case 4.1. By relaxing the storage power limits, only a small improvement can be made to the items tested including operating cost and load factor. The small additional operating cost savings may not enough to make up for the high added capital costs that would occur for a significant turbine / generator power limit increase.

5.6 Case 5.4, relaxation of line / storage power limits

The fourth case is the relaxation of both the line and storage power limits in the Arizona test bed. These two relaxations are equivalent to having an infinite bus with all generators, loads, and storage elements connected to it and the PHES turbines having an infinite power rating. Both cases are unrealistic, similar to previous cases, and are purely to analyze the two constraints effect on the test results. Table 5.5 shows the outcome of the various tests when both the line and storage power limits are relaxed. Figure 5.8 displays the generator output and load profile for a 24 hour day.

Table 5.5 Case 5.4 test results

Annual operating cost (billion $/year)	Annual operating cost savings (%)	Annual operating cost savings (million $/year)	Daily energy recovered (GWh)	Annual load factor (%)	No energy storage annual operating cost (billion $/year)
1.1730	12.94	174.41	44.44	100.0	1.3474

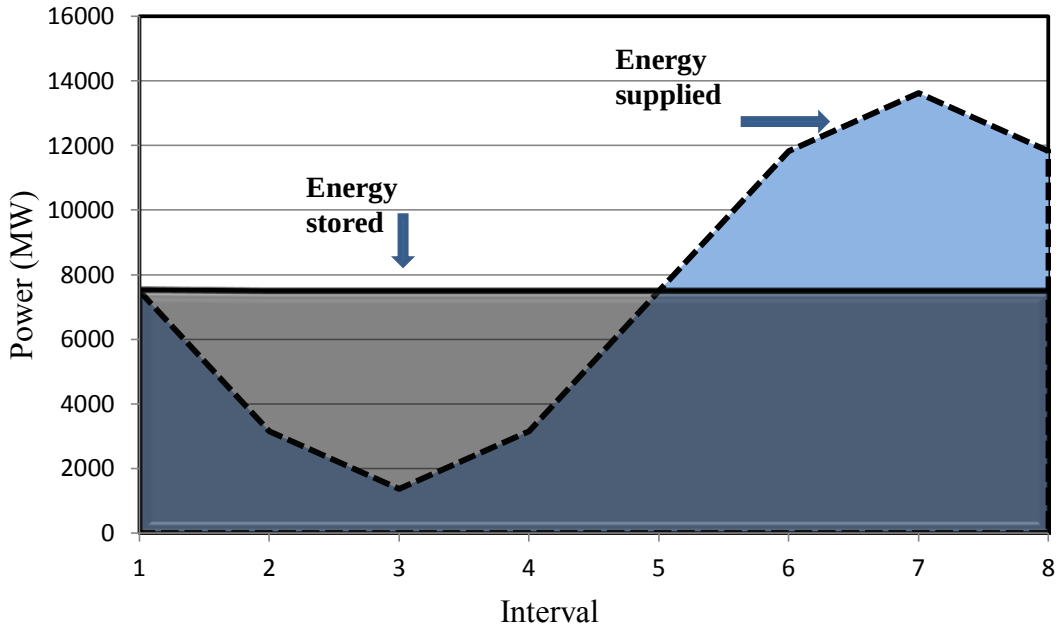

Figure 5.8 Case 5.4 daily generation output and load profile

The results in Table 5.5 and Figure 5.8 show that when relaxing both the line and storage power limits, a 100% load factor can be achieved. A complete load shave results in the minimum operating cost of $1.173 billion. This equates to an operating cost savings of 12.94% or $174.41 million when compared to the case with no storage. Compared to Case 5.1 with only a relaxation of the line limits, the operating cost is about the same but the load factor increased by 3% to 100%. A combination of relaxing the line and storage power limits allows enough energy to be stored to completely shave the peak and minimize operating costs. However, the additional

energy shaved during peak hours from the power limit increasing decreases the operating cost by only a small amount.

5.7 Case 5.5, relaxation of line / storage energy limits

Case 5.5 involves relaxing both the line limits and the storage energy limits. This test analyzes the effect of removing all transmission lines and replacing them with an infinite bus. Also, the reservoirs of all PHES locations would be unrealistically large in volume and can store very large amounts of water. Again, these two relaxations are purely to see how the two constraints affect the various tests on the test bed. Table 5.6 shows the results of case 5.5 and Figure 5.9 plots the generation output with the load profile.

Table 5.6 Case 5.5 test results

Annual operating cost (billion $/year)	Annual operating cost savings (%)	Annual operating cost savings (million $/year)	Daily energy recovered (GWh)	Annual load factor (%)	No energy storage annual operating cost (billion $/year)
1.1730	12.94	174.40	43.74	97.0	1.3474

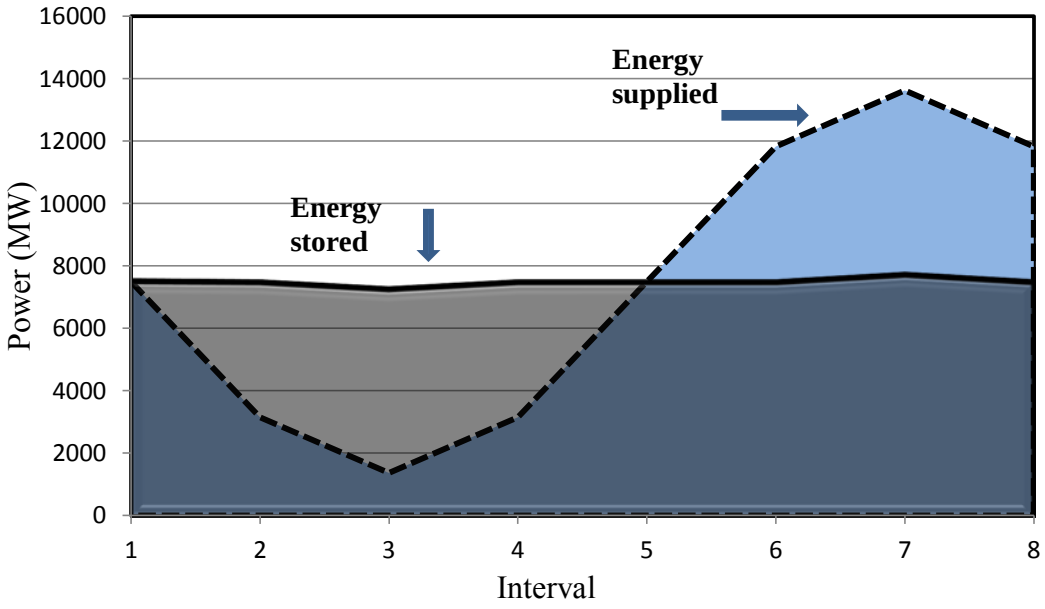

Figure 5.9 Case 5.5 daily generator output and load profile

The results in Table 5.6 are very similar to the higher E/P ratio results in Case 5.1 with only the line limits relaxed. The annual operating cost is the same at $1.173 billion and an operating cost savings of $174.4 million. This equates to a 12.94% annual operating cost savings. The generation output in Figure 5.9 is very similar to the output in Case 5.1 with the load factor the same at 97%. From these results, it can be concluded that relaxing the storage energy limits has

no effect on the generation output when the line limits are already relaxed. The results from Case 5.1 where only the line limits are relaxed remain exactly the same when the storage energy limits are relaxed.

5.8 Case 5.6, relaxation of storage energy and power limits

The sixth case involves relaxing a combination of both the PHES energy and power ratings. By relaxing both limits of the pumped hydro locations in Case 4.1, the reservoirs are assumed unrealistically large and the turbines and generators are replaced with ones that have unconventionally high power limits. Again, these two relaxations do not represent real world applications and are merely to analyze the effect of the storage energy and power limits on the previous tests. The results of Case 5.6 can be seen in Table 5.7 and Figure 5.10 displays the generation output and load profile for the purpose of demonstrating peak shaving.

Table 5.7 Case 5.6 test results

Annual operating cost (billion $/year)	Annual operating cost savings (%)	Annual operating cost savings (million $/year)	Daily energy recovered (GWh)	Annual load factor (%)	No energy storage annual operating cost (billion $/year)
1.1852	8.38	108.40	38.12	78.2	1.2936

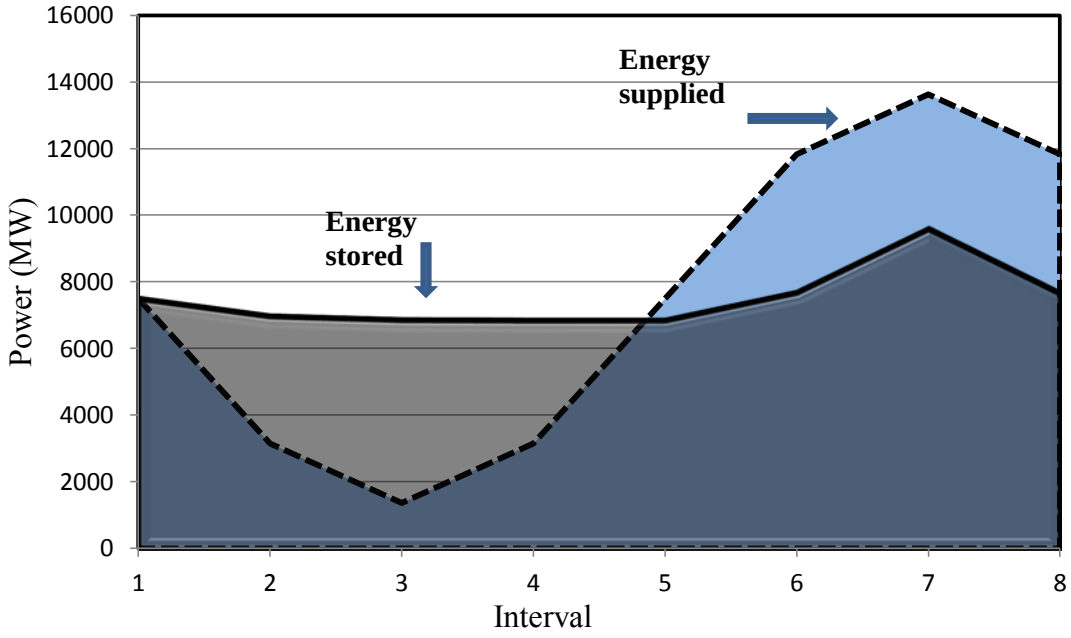

Figure 5.10 Case 5.6 daily generation outputs and load profile

It is found that by relaxing both the storage energy and power limits, the results do not change when compared with relaxing only the storage power limits. The results in Table 5.7 and the generation output in Figure 5.10 remain exactly the same as Table 5.1 and Figure 5.7 in Case 5.3.

From these results, it is further evident that the storage energy rating has no effect on the system operating costs after an E/P ratio of around 10. Increasing the reservoir volume would only increase capital costs and would have no effect on the system operating costs.

5.9 Case 5.7, relaxation of line / storage energy and power limits

The last case is the relaxation of all three constraints tested in this chapter. Case 5.7 involves replacing all transmission lines with an infinite bus, increasing the volume of all PHES locations to an extremely high value, and replacing all PHES turbines with ones with unrealistically high power ratings. Similar to all previous relaxation cases, all three relaxations are just to see how relaxing all three constraints effects the system results. The results of Case 5.7 can be seen in Table 5.8 and Figure 5.11 plots the generation outputs with the load profile.

Table 5.8 Case 5.7 test results

Annual operating cost (billion $/year)	Annual operating cost savings (%)	Annual operating cost savings (million $/year)	Daily energy recovered (GWh)	Annual load factor (%)	No energy storage annual operating cost (billion $/year)
1.1730	12.95	174.5	44.44	100.0	1.3474

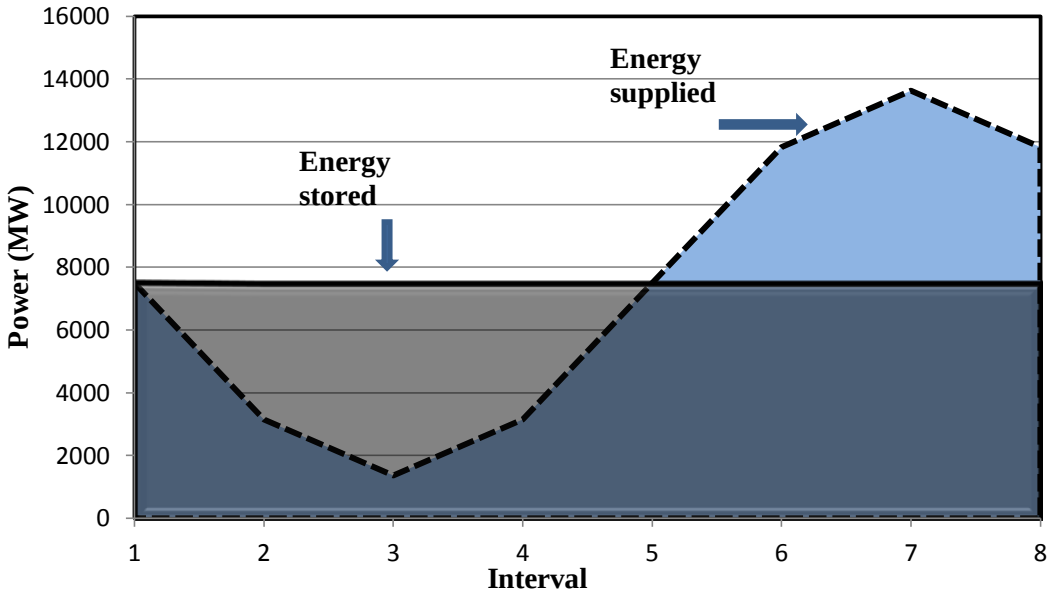

Figure 5.11 Case 5.7 daily generator output and load profile

The results for Case 5.7 shown in Table 5.8 are almost exactly the same as in Case 5.4 with the line and storage power limit relaxed. The annual operating cost is $1.173 billion for a $174.5 million per year savings. This savings is 12.95% less when compared to the same case with no energy storage. Also, the load factor is calculated to be 100% meaning the peak is completely shaved. Again, the results of Case 5.7 are very close to Case 5.4 meaning that relaxing the

storage energy limits has little to no effect on the output when the line and storage power limits are also relaxed. Similar to Case 5.4, the relaxation of the storage power limits improves the load factor by 3% and decreases the operating cost by a very small amount.

5.10 Summary of results

This chapter focused on relaxing various constraints to see the effect on the results obtained in Chapter 4. The results from the previous chapter showed that some constraint(s) were limiting load leveling, and attainment of the minimal operating cost. Seven relaxed cases using combinations of the line limits, storage energy limits, and the storage power limits were analyzed and the results were compared with Case 4.1 from Chapter 4. Table 5.9 displays the results of Case 4.1 and the seven relaxation cases studies.

Table 5.9 Chapter 5 relaxed constraint case results

Case	Annual operating cost (billion $/year)	Annual operating cost savings (%)	Annual operating cost savings (million $/year)	Daily energy recovered (GWh)	Annual load factor (%)	No energy storage annual operating cost (billion $/year)
5.0*	1.1858	8.33	107.8	33.66	77.3	1.2936
5.1*	1.1730	12.94	174.4	43.76	97.0	1.3474
5.2	1.1858	8.33	107.8	36.60	77.4	1.2936
5.3	1.1852	8.38	108.4	38.06	78.3	1.2936
5.4	1.1730	12.94	174.4	44.44	100.0	1.3474
5.5	1.1730	12.94	174.4	43.74	97.0	1.3474
5.6	1.1852	8.38	108.4	38.12	78.2	1.2936
5.7	1.1730	12.94	174.4	44.44	100.0	1.3474

* Includes the minimum value for each test

When comparing the cases in Table 5.9 with the base case (Case 5.0), it is evident that the cases that relax the line limits have the best improvements for all tests. The cases that relax line power ratings are Cases 5.1, 5.4, 5.5, and 5.7. This is clear when Case 5.1, which relaxes only the line limits, is compared with the other three cases (5.4, 5.5, 5.7) that also relax the line limits. In Cases 5.4, 5.5, and 5.7, the system wide operating cost does not change from what was found in Case 5.1. However, in Cases 5.4 and 5.7 where the storage power limits are also relaxed, the load factor does improve to 100% as more energy is stored / recovered. Also, when the storage power limit is relaxed in Cases 5.2 and 5.6 but not the line limits, the operating cost does improve slightly.

The cases that relax the storage energy limit (Cases 5.2, 5.5, and 5.7) have no change in performance indicators (i.e., load factor or annual operating cost measures) compared to those that do not. This result apparently means that the energy stored / recovered during every time interval is not approaching or hitting the energy limit of each PHES. Thus relaxation of the energy storage limits has no effect. By increasing the line limits in the system, high levels of

PHES would realize improvement of load factor and annual operating cost. In a realistic analysis, upgrading line ratings should be done so that the desired system operating metrics are improved in an optimal way. The foregoing study employed wholesale upgrading of transmission circuits system-wide; a realistic study would need to identify those circuits which have the greatest impact on the system performance metrics as well as cost / benefit effectiveness. The latter is relegated to 'future work'. For example, this approach is applied by Tokombayev in [70] to identify transmission circuits for upgrade by high temperature, low sag construction.

6. Conclusions and future work

6.1 Conclusions

In this report, a test bed utilizing the Arizona transmission system with a 2010 summer peak load, was used to demonstrate several topics related to bulk energy storage. The following conclusions can be made based on the research and results discovered:

- *Literature review:* the literature review offered in Chapter 2 explained important applications that bulk energy storage can provide including:
    - peak shaving
    - frequency and area control regulation
    - transmission line expansion deferral
    - integration of renewables
    - lowering transmission line congestion
    - Improving regional reserve margins.
- *The economic dispatch problem:* the second chapter gave a review of the economic dispatch problem and provided various methodologies to solve that problem. Quadratic programming was chosen as the method to solve the economic dispatch problem and simulate energy storage and its effect on the Arizona test bed.
- *Addition of modest levels of energy storage:* the third chapter illustrates the calculation of the minimum annual operating cost of the system with no energy storage. This is denominated as the base case. The annual operating cost for a stated load scenario was found to be $1.294 billion with a 55% load factor. By adding energy storage to different locations in the system, a maximum annual savings of 6% or $78 million was determined. The maximum saving was then utilized to show that the corresponding minimum payback period for the locations tested was about 8 years.
- *Addition of high levels of energy storage:* Chapter 4 illustrates the result of adding very high amounts (e.g., ~6 GW) of pumped hydro storage to the Arizona test bed. This is done to model load leveling in the system. The goal was to add enough storage such that the energy stored during off peak intervals would be enough to completely "shave" the peak during the peak demand intervals. From the results in the three cases, an annual operating cost savings of up to $108.8 million or 8.4% was found. The load factor for the corresponding case was found to be 77.3%. Note that this is an improvement from the case without storage in which the load factor was 55%.
- *Relaxation of line, storage-energy, and storage-power limits:* the final chapter looked into relaxing various system constraints and analyzing the change in the operating cost and load factor. The results showed that relaxing the line limits had the greatest change with a minimum operating cost of $1.173 billion. This stated operating cost represents a decrease of about $174 million annually. The operating cost savings represents about 12.94% annually compared to the base case. In order to have a 100% load factor, the line

and storage power limits had to be relaxed. Also, the relaxation of the storage energy limits showed that there was no effect on the results.

- *Load factor:* it was shown that large scale energy storage can decrease generation operating costs in the system by storing off peak energy and recovering this energy during peak demand periods. By doing so, the load factor of the system increases. However, a 100% load factor is not necessarily the desired operational goal.

6.2 Future work

In the research and tests performed for this report, the economic dispatch was studied using the Arizona test bed with various simplifying assumptions, mainly omission of: modeling reactive power flows, transmission losses, energy storage losses, and system voltages and their limits. The research discussed could be extended in the following ways:

- modeling the losses related to the transmission and energy storage devices
- performing an ACOPF on the Arizona test bed to examine system stability related to both the system bus voltages and a *N*-1 analysis
- including reactive power in the system analysis and quantifying its effects
- modeling correct bus voltages in the system
- identifying the transmission circuits that have the greatest impact on the system performance metrics as well as a cost / benefit effectiveness
- extending the analysis out to the entire WECC and determining PHES locations in this larger milieu
- modeling large scale non-hydro energy storage and showing the resulting operating cost and load factor changes
- demonstrating examples of lowering the transmission line congestion in the system with correct placement of energy storage
- creating a program to make pumped storage (or other energy storage) “off the shelf” technology.

In addition, it is recommended that investigation of alternative software tools be used to assess the value of pumped hydro in large scale power systems. These should include Gurobi and AMPL both of which have capabilities that go beyond those of MATLAB used in the present work.

References

[1] S. Olea, "Renewable energy standard and tariff," available at: http://www.azcc.gov/divisions /utilities/electric/environmental.asp.

[2] S. Vazquez, S. M. Lukić, E. Galvan, L. G. Franquelo, J. M. Carrasco, "Energy storage systems for transport and grid applications," *IEEE Transactions on Industrial Electronics*, Dec. 2010, vol. 57, no. 12, pp. 3881-3895.

[3] R. J. Kerestes, G. F. Reed, A. R Sparacino, "Economic analysis of grid level energy storage for the application of load leveling," *IEEE Power and Energy Society General Meeting*, 22-26 July 2012, pp. 1-9.

[4] J. Mankansi, J. Abboud, "Energy storage- the missing link in the electricity value chain," available at: http://www.energystoragecouncil.org/ESC%20White%20Paper%20.pdf.

[5] B. Wollenberg, A. Wood, *Power generation operation and control*, J Wiley and Sons, New York, Second edition, 1996.

[6] EPRI-DOE Handbook, "Energy storage for transmission and distribution applications," Dec. 2003.

[7] M. T. Holmberg, M. Lahtinen, J. McDowall, T. Larsson, "SVC light with energy storage for frequency regulation," *IEEE Conference on Innovative Technologies for an Efficient and Reliable Electricity Supply (CITRES)*, 27-29 Sept. 2010, pp. 317-324.

[8] L. Liang, J. Zhong, Z. Jiao, "Frequency regulation for a power system with wind power and battery energy storage," *IEEE International Conference on Power System Technology,* Oct. 30 -Nov. 2 2012, pp. 1-6.

[9] D. Rastler, "Electric energy storage technology options," available at: http://www.electricitystorage.org/images/uploads/static_content/technology/resources/ESA_TR_5_11_EPRIStorageReport_Rastler.pdf.

[10] J. A. Jardini, D. Missali, M. G. Jardini, R. L. Vasquez-Arnez, M. Masuda, "On the analysis and evaluation of a transmission line upgrading assisted by line arresters," *IEEE Power & Energy Society General Meeting,* 26-30 July 2009, pp. 1-7.

[11] I. Zamora, A. J. Mazon, P. Eguia, R. Criado, C. Alonso, J. Iglesias, J. R. Saenz, "High-temperature conductors: a solution in the uprating of overhead transmission lines," *IEEE Porto Power Tech Proceedings*, 10-13 September 2001, vol. 4, pp. 1-6.

[12] D. P. Manjure, M. D. McMullen, D. O. Subakti, D. Tewari, "Managing wind energy: from interconnection planning to real time operations, an integrated approach to ensure energy and transmission capacity," *IEEE Power & Energy Society General Meeting*, 26-30 July 2009, pp. 1-8.

[13] D. M. Larruskain, *et al.*, "Power transmission capacity upgrade of overhead lines," University of the Basque Country, San Sebastián, Spain, 2006.

[14] A. Oudalov, T. Buehler, D. Chartouni, "Utility scale applications of energy storage," *IEEE Energy 2030 Conference*, 17-18 Nov. 2008, pp. 1-7.

[15] R. Ayyanar, V. Vittal, *Grid integration and dynamic impact of wind energy (power electronics and power systems)*, Springer, New York, 2012.

[16] M. Patel, *Wind and solar power systems: design, analysis, and operation*, CRC Press, Florida, Second edition, 1996.

[17] P. Gevorkian, *Large-scale solar power system design*, McGraw-Hill Professional, New York, 2011.

[18] G. Boyle, *Renewable energy: power for a sustainable future*, Oxford University Press, England, Third edition, 2012.

[19] S. C. Smith, P. K. Sen, B. Kroposki, "Advancement of energy storage devices and applications in electrical power systems," *IEEE Power and Energy Society General Meeting – Conversion and Delivery of Electrical Energy in the 21st Century*, 20-24 July 2008, pp. 1-8.

[20] S. Yeleti, F. Yong, "Impacts of energy storage on the future power system," *North American Power Symposium*, 26-28 Sept. 2010, pp. 1-7.

[21] J. Kleissl, M. Lave, M. Jamaly, J. Bosch, "Aggregate solar variability," *IEEE Power and Energy Society General Meeting*, 22-26 July 2012, pp. 1-3.

[22] N. Ming, Z. Zheng, D. Osborn, "Economic and operation benefits of energy storage — a case study at MISO," *IEEE Power and Energy Society General Meeting,* 22-26 July 2012, pp. 1-7.

[23] S. O. Geurin, A. K. Barnes, J. C. Balda, "Smart grid applications of selected energy storage technologies," *IEEE PES Innovative Smart Grid Technologies,* 16-20 Jan. 2012, pp. 1-8.

[24] W. Jewell, H. Zhouxing, "The role of energy storage in transmission and distribution efficiency," *IEEE PES Transmission and Distribution Conference and Exposition*, 7-10 May 2012, pp. 1-4.

[25] K. Furusawa, H. Sugihara, K. Tsuji, Y. Mitani, "A new operation framework of demand-side energy storage system cooperated with power system," *International Conference on Power System Technology*, 21-24 Nov. 2004, vol. 1, pp. 385-390.

[26] H. Zhouxing, W. T. Jewell, "Optimal power flow analysis of energy storage for congestion relief, emissions reduction, and cost savings," *IEEE/PES Power Systems Conference and Exposition*, 20-23 March 2011, pp. 1-8.

[27] M. S. Habibi, "Model for impact of storage on spinning reserve requirements and distributed generation," *Proceedings of the 33rd Southeastern Symposium on System Theory*, Mar. 2001, pp. 161-165.

[28] A. L. de Sebastian, "Investment requirements in generation capacity and reserve margin," *IEEE Power Engineering Society General Meeting,* June 2004, pp. 1023-1025.

[29] US Energy Information Administration, "Reserve electric generating capacity helps keep the lights on," available at: http://www.eia.gov/todayinenergy/detail.cfm?id=6510.

[30] D. Connolly," A review of energy storage technologies," available at: http://www.dconnolly.net/files/David%20Connolly,%20UL,%20Energy%20Storage%20Techniques,%20V3.pdf.

[31] Q. Hao, Z. Jianhui, L. Jih-Sheng, "A grid-tie battery energy storage system," *IEEE 12th Workshop on Control and Modeling for Power Electronics*, 28-30 June 2010, pp. 1-5.

[32] S. Kalyani, S. Nagalakshmi, R. Marisha, "Load frequency control using battery energy storage system in interconnected power system," *Third International Conference on Computing Communication & Networking Technologies*, 26-28 July 2012, pp. 1-6.

[33] M. C. Such, C. Hill, "Battery energy storage and wind energy integrated into the Smart Grid," *IEEE PES Innovative Smart Grid Technologies*, 16-20 Jan. 2012, pp. 1-4.

[34] K. Y. Cheung, S. T. Cheung, R. G. Navin De Silva, M. P. Juvonen, R. Singh, "Large-scale energy storage systems," Imperial College, London, England, 2003.

[35] A. Gonzalez, B. Ó'Gallachóir, E. McKeogh, K. Lynch, "Study of electricity storage technologies and their potential to address wind energy intermittency in Ireland," Sustainable Energy Ireland, 2004.

[36] R. E. Horn," Supercapacitor energy storage," available at: http://www.macrovu.com /image/PVT/NASA/RPC/uc%3DSupercapacitors.v3.pdf.

[37] E. Harkins, M. Prado, D. Sodel," Electrical energy storage using fuel cell technology," available at: http://www.esru.strath.ac.uk/EandE/Web_sites/0001/fuel_cells/Fuel%20cell%20advantages.htm.

[38] The University of Strathclyde in Glasgow, "Fuel cell advantages," available at: http://www.esru.strath.ac.uk/EandE/Web_sites/0001/fuel_cells/Fuel%20cell%20advantages.htm.

[39] FERC, "Economic dispatch: concepts, practices and issues," available at: http://www.ferc.gov/eventcalendar/Files/20051110172953-FERC%20Staff%20Presentation.pdf.

[40] W. Caisheng, M. H. Nehrir, "Distributed generation applications of fuel cells," *Power Systems Conference: Advanced Metering, Protection, Control, Communication, and Distributed Resources*, 14-17 March 2006, pp. 244-248.

[41] X. Yu, M. R. Starke, L. M. Tolbert, B. Ozpineci, "Fuel cell power conditioning for electric power applications: a summary," *IET Electric Power Applications*, Sept. 2007, vol. 1, no. 5, pp. 643-656.

[42] S. Srinivasan, *Fuel cells: from fundamentals to applications*, Springer, New York, 2006.

[43] J. Zhu, *Optimization of power system operation,* J Wiley and Sons, New Jersey, First edition, 2009.

[44] W. Ongsakul, V. N. Dieu, *Artificial intelligence in power system optimization*, CRC Press, Florida, 2013.

[45] N. M. Pindoriya, S.N. Singh, K.Y. Lee, "A comprehensive survey on multi-objective evolutionary optimization in power system applications," *IEEE Power and Energy Society General Meeting*, 25-29 July 2010, pp. 1-8.

[46] H. H. Happ, "Optimal power dispatch-a comprehensive survey," *IEEE Transactions on Power Apparatus and Systems*, May-June 1977, vol. 96, pp. 841-854.

[47] F. Gao, G. Sheblé, "Economic dispatch algorithms for thermal unit system involving combined cycle units," *15th Power Systems Computation Conference*, 22-26 August 2005.

[48] R. Bellman, "The theory of dynamic programming," RAND Corporation, Proc. National Academy of Sciences, 1952, pp. 503-715.

[49] A. Richards, J. How, "Mixed-integer programming for control," *American Control Conference*, 8-10 June 2005, vol. 4, pp. 2676-2683.

[50] D. Bertsimas, J. N. Tsitsiklis, *Introduction to Linear Optimization*, Athena Scientific, Belmont, MA, 1997.

[51] C. A. Floudas, *Nonlinear and Mixed-Integer Programming – Fundamentals and Applications,* Oxford University Press, 1995.

[52] J. Linderoth, M. Savelsbergh, "A computational study of branch and bound search strategies for mixed integer programming," *INFORMS Journal on Computing,* Nov. 1999, pp. 173–187.

[53] G. Pengfui, W. Xuezhi, H. Yingshi, "The enhanced genetic algorithm for the optimization design," *3rd International Conference on Biomedical Engineering and Informatics*, 16-18 Oct. 2010, vol. 7, pp. 2990-2994.

[54] M. R. Nayak, K. R. Krishnanand, P. K. Rout, "Modified differential evolution optimization algorithm for multi-constant optimization power flow," *International Conference on Energy, Automation, and Signal*, 28-30 Dec. 2011, pp. 1-7.

[55] Y. Xiaohi, Z. Yunlong, Z Wenping, "A hybrid artificial bee colony algorithm for numerical function optimization," *11th International Conference on Hybrid Intelligent Systems*, 5-8 Dec. 2011, pp. 127-132.

[56] D. Simon, "Biogeography based optimization," *IEEE Transactions on Evolutionary Computation*, Dec. 2008, vol. 12, no. 6, pp. 702-713.

[57] M. Dorigo, M. Biratteri, T. Stutzle, "Ant colony optimization," *IEEE Computational Intelligence Magazine*, Nov. 2006, vol. 1, no. 4, pp. 28-39.

[58] M. Hai, W. Yanjiang, "An artificial fish swarm algorithm based on chaos search," *Fifth International Conference on Natural Computation*, 14-16 Aug. 2009, vol. 4, pp. 118-121.

[59] S. Yichuan, C. Hanning, "Cooperative bacterial foraging optimization," *International Conference on Future Biomedical Information Engineering*, 13-14 Dec. 2009, pp. 486-488.

[60] J. Blondin, "Particle swarm optimization: a tutorial," available at: http://cs.armstrong.edu/saad/csci8100/pso_tutorial.pdf.

[61] J. Kennedy, R. Eberhart, "Particle swarm optimization," *Proceedings of the IEEE International Conference on Neural Networks*, 1995, volume IV, pp. 1942–1948.

[62] J. Kennedy, R. Eberhart, Y. Shi, *Swarm Intelligence,* Morgan Kaufmann Publishers, San Francisco, 2001.

[63] Frans van den Bergh, "An analysis of particle swarm optimizers," PhD thesis, University of Pretoria, South Africa, 2001.

[64] S. Eftekharnejad, "The Impact of increased penetration of photovoltaic generation on smart grids," PhD. dissertation, Arizona State University, Tempe AZ, December 2012, p. 48.

[65] "DOE international energy storage database: open loop pumped hydro storage," available at:

http://www.energystorageexchange.org/projects?utf8=%E2%9C%93&technology_type_sort_eq=Open+Loop++Pumped+Hydro+Storage&country_sort_eq=&state_sort_eq=&kW=&kWh=&benefit_stream_inf=&ownership_model_eq=&status_eq=&siting_eq=&show_unapproved=%7B%7D&order_by=&sort_order=&search_page=1&size_kw_ll=&size_kw_ul=&size_kwh_ll=&size_kwh_ul=.

[66] K. F. Kumli, "Application for preliminary permit for the Longview Pumped Storage project," available at: http://longviewee.com/admins/wp-content/uploads/2012/02/Application%20for%20Preliminary%20Permit.pdf.

[67] Table Mountain LLC, "Table Mountain Pumped Storage project: notice of preliminary permit," available at: http://www.gpo.gov/fdsys/pkg/FR-2011-11-14/pdf/2011-29248.pdf.

[68] G. Gillen *et. al*., "Eagle Mountain Pumped Storage project draft environmental impact report volume I," GEI Consultants, Inc., Rancho Cordova, CA, Report No. 2009011010, July 2010, vol. 1.

[69] V. M. Montsinger, "Effect of load factor on operation of power transformers by temperature," *Transactions of the American Institute of Electrical Engineers*, Nov. 1940, vol. 59, no. 11, pp. 632-636.

[70] A. Tokombayev, G. T. Heydt, "HTLS upgrades for the economic operation improvement of power systems," paper submitted October 2013 to the IEEE Power and Energy Society, *Transactions on Power Delivery*.

[71] MATLAB, ”Interior-point-convex quadprog algorithm,” available at:

http://www.mathworks.com/help/optim/ug/quadratic-programming-algorithms.html#bsqspm.

[72] J. Ruggiero, G. Heydt, “Making the economic case for bulk energy storage in electric power systems,” *North American Power Symposium,* 22-24 Sept. 2013, pp. 1 – 8.

[73] United States Congress, “The Endangered Species Act of 1973,” 7 U.S.C. § 136, 16 U.S.C. § 1531 and subsequent acts, Washington DC, 1973.

APPENDIX A MATLAB code

A.1 MATLAB code used in this project

```
clear;
clc;

%Changes specific options in the quadprog algorithm including a change to
%the interior-point-convex.
options= optimset('MaxIter',50,'LargeScale','off', 'Display', 'off',...
'Diagnostics','off', 'MaxFunEvals',100,'TolFun',.0001,...
'TolX',.0001,'Algorithm','interior-point-convex');

%Reads xlsx file with network data
 A=xlsread('Large System Casev2.xlsx','System data');
%Determines number of each category
 b=A(1,1);                                                    % b=# of buses
 l=A(1,2);                                                    % l=# of lines
 g=A(1,3);                                                 % g=# of generators
 s=A(1,4);                                              % s=# of storage units
int=A(1,5);                                          % int=# of load intervals
dT=A(1,6);                                % dT= delta t or hours per interval
 d=A(1,7);                                                  % d=number of days
  B=xlsread('Large System Casev2.xlsx','Bus data');         %Extracts bus data
 L=xlsread('Large System Casev2.xlsx','Line data');        %Extracts line data
 G=xlsread('Large System Casev2.xlsx','Generator data'); %Extracts generator
data
 S=xlsread('Large System Casev2.xlsx','Storage data');   %Extracts storage
data

 X=(3*b+l-1)*int;                                  %Creates size of 'x' matrix

%GENERATION OF THE Q MATRIX (QUADRATIC COSTS)
%Extracts generator quadratic cost terms and inputs into a matrix
 c=1;
 j=1;
 a=zeros(b,b);
for k=1:1:g

a(G(c,1),G(c,1))=G(c,5)*2;
    c=c+1;
    j=j+1;
end
%Matrix of generator quadratic costs at each hour
c=1;
j=1;
for k=1:1:int

    Q1(c:c+b-1,j:j+b-1)=a;
    c=c+b;
    j=j+b;
end
%Overall Q matrix with Q1 in the correct location
Q=zeros(X,X);
```

```
Q((b+l-1)*int+1:(2*b+l-1)*int,(b+l-1)*int+1:(2*b+l-1)*int)=Q1;
Q=sparse(Q);

%GENERATION OF THE C MATRIX (LINEAR COSTS)
%Extracts generator linear cost terms and inputs them into a matrix
c=1;
j=1;
C1=zeros(1,b);
for k=1:1:g

C1(1,G(c,1))=G(c,4);
    c=c+1;
    j=j+1;
end
%Repeats the linear costs over the amount of hours
j=1;
for k=1:1:int

CT(1,j:j+b-1)=C1;
    j=j+b;
end
%Inputs the total linear costs into the overall C matrix
C=zeros(1,X);
C(1,(b+l-1)*int+1:(2*b+l-1)*int)=CT;
C=sparse(C);

%GENERATION OF THE B MATRIX (INEQUALITY LIMITS)
%Generates vector of line limits
c=1;
j=1;
b1=zeros(2*l*int,1);
for k=1:1:l

        b1(c:2*j*int,1)=L(j,6);
        c=c+2*int;
        j=j+1;
end
%Generates vector of generator limits
i=1;
j=1;
b2=zeros(2*b*int,1);
b2i=zeros(2*int,1);
for k=1:1:g
for u=1:1:int
b2i(i,1)=G(j,3);
b2i(i+1,1)=-G(j,2);
        i=i+2;
end
b2(2*G(j,1)*int-(2*int-1):2*G(j,1)*int,1)=b2i;
    j=j+1;
    i=1;
    b2i=zeros(2*int,1);
end
%Generates vector of storage charging power limits
i=1;
j=1;
```

```
b3=zeros(2*b*int,1);
b3i=zeros(2*int,1);
for k=1:1:s
for u=1:1:int
b3i(i:i+1,1)=S(j,2);
        i=i+2;
end
b3(2*S(j,1)*int-(2*int-1):2*S(j,1)*int,1)=b3i;
    j=j+1;
    i=1;
    b3i=zeros(2*int,1);
end
%Generates vector of generator ramp rate limits
i=1;
j=1;
b4=ones(2*b*(int-1),1)*10000;
b4i=zeros(2*(int-1),1);
for k=1:1:g
for u=1:1:(int-1)
b4i(i:i+1,1)=G(j,6);
        i=i+2;
end
b4(2*G(j,1)*(int-1)-(2*(int-1)-1):2*G(j,1)*(int-1),1)=b4i;
    j=j+1;
    i=1;
    b4i=zeros(2*(int-1),1);
end
%Generates vector of storage charging energy limits
i=1;
j=1;
b5=zeros(2*b*int,1);
b5i=zeros(2*int,1);
for k=1:1:s
for u=1:1:int
b5i(i,1)=S(j,3);
b5i(i+1,1)=0;
        i=i+2;
end
b5(2*S(j,1)*int-(2*int-1):2*S(j,1)*int,1)=b5i;
    j=j+1;
    i=1;
    b5i=zeros(2*int,1);
end
%Inputs 5 vectors (b1,b2,b3,b4 and b5) into overall b vector
bT=zeros(2*int*(l+2*b)+2*b*(int-1)+2*b*int,1);
bT(1:2*l*int,1)=b1;
bT(2*l*int+1:2*int*(l+b),1)=b2;
bT(2*int*(l+b)+1:2*int*(l+2*b),1)=b3;
bT(2*int*(l+2*b)+1:2*int*(l+2*b)+2*b*(int-1),1)=b4;
bT(2*int*(l+2*b)+2*b*(int-1)+1:2*int*(l+2*b)+2*b*(int-1)+2*b*int,1)=b5;
bT=sparse(bT);

%GENERATION OF THE beq MATRIX (EQUALITY LIMITS)

%Generates beq1 vector which contains the load value at each bus and each
%interval
```

```
c=1;
j=1;
m=1;
beqa=zeros(int,1);
beq1=zeros(b*int,1);
for k=1:1:b
        p=5;
for u=1:1:int
beqa(c,1)=B(j,p);
        c=c+1;
        p=p+1;
end
        c=1;
beq1(m:int*j,1)=beqa;
    m=m+int;
    j=j+1;
end
%Inputs load values into the overall beq vector with zeros at every other
%point
beq=zeros((b+l)*int+b,1);
beq(l*int+1:(l+b)*int,1)=beq1;
beq=sparse(beq);

%GENERATION OF THE A MATRIX (INEQUALITIES)
%Generates the A1 matrix(line inequalities)
t=1;
i=1;
j=1;
m=1;
A1=zeros(2*l*int,l*int);                          %Sets up size of A1 matrix
A1i=zeros(2*int,l*int);                       %Sets up size of inner A1i matrix
for k=1:1:l
for u=1:1:int
A1i(i,j)=1;
A1i(i+1,j)=-1;
        i=i+2;
        j=j+l;
end
A1(m:2*t*int,1:l*int)=A1i;                        %Inputs inner matrix of each
    m=m+2*int;                                  %line into the larger A1 matrix
    t=t+1;
    i=1;
    j=t;
    A1i=zeros(2*int,l*int);
end;
%Generates the A2 matrix(generator inequalities)
t=1;
i=1;
j=1;
m=1;
A2=zeros(2*b*int,b*int);                          %Sets up size of A2 matrix
A2i=zeros(2*int,b*int);                       %Sets up size of inner A2i matrix
for k=1:1:b
for u=1:1:int
A2i(i,j)=1;
A2i(i+1,j)=-1;
            i=i+2;
```

```
            j=j+b;
end
A2(m:2*t*int,1:b*int)=A2i;
   m=m+2*int;
   t=t+1;
   i=1;
   j=t;
   A2i=zeros(2*int,b*int);
end
%Generates A3 matrix (storage inequalities)
t=1;
i=1;
j=1;
m=1;
A3=zeros(2*b*int,b*int);                          %Sets up size of A3 matrix
A3i=zeros(2*int,b*int);                       %Sets up size of inner A3i matrix
for k=1:1:b
for u=1:1:int
A3i(i,j)=1;
A3i(i+1,j)=-1;
        i=i+2;
        j=j+b;
end
A3(m:2*t*int,1:b*int)=A3i;                          %Inputs inner matrix of each
    m=m+2*int;                                 %storage into the larger A3 matrix
    t=t+1;
    i=1;
    j=t;
    A3i=zeros(2*int,b*int);
end;
%Generates the A4 matrix(generator ramp rate inequalities)
i=1;
j=1;
m=1;
t=1;
A4=zeros(2*b*(int-1),b*int);
A4i=zeros(2*(int-1),b*int);
for k=1:1:b
for u=1:1:(int-1)
A4i(i,j)=1/dT;
A4i(i,j+b)=-1/dT;
A4i(i+1,j)=-1/dT;
A4i(i+1,j+b)=1/dT;
        i=i+2;
        j=j+b;
end
A4(m:2*t*(int-1),1:b*int)=A4i;
    m=m+2*(int-1);
    t=t+1;
    i=1;
    j=t;
    A4i=zeros(2*(int-1),b*int);
end
%Generates the A5 matrix (bulk energy storage limit on energy storage)
i=1;
j=1;
t=0;
```

```
z=1;
f=1;
y=int;
A5=zeros(2*b*int,b*int);
A5i=zeros(2*int,b*int);
for k=1:1:b
for m=1:1:int
for u=1:1:y
A5i(i+2*t,j)=dT;
A5i(i+2*t+1,j)=-dT;
            i=i+2;
end
        i=1;
        y=y-1;
        t=t+1;
        j=j+b;
end
A5(f:2*z*int,1:b*int)=A5i;
    y=int;
    f=f+2*int;
    z=z+1;
    j=z;
    t=0;
    A5i=zeros(2*int,b*int);
end
%Stores each of the smaller matrices (A1,A2,A3,A4, and A5) into the A matrix
A=zeros(2*int*(l+2*b)+2*b*(int-1)+2*b*int,X);
A(1:2*l*int,(b-1)*int+1:(b+l-1)*int)=A1;
A(2*l*int+1:2*int*(l+b),(b+l-1)*int+1:(2*b+l-1)*int)=A2;
A(2*int*(l+b)+1:2*int*(l+2*b),(2*b+l-1)*int+1:X)=A3;
A(2*int*(l+2*b)+1:2*int*(l+2*b)+2*b*(int-1),(b+l-1)*int+1:(2*b+l-1)*int)=A4;
A(2*int*(l+2*b)+2*b*(int-1)+1:2*int*(l+2*b)+2*b*(int-1)+2*b*int,(2*b+l-
1)*int+1:X)=A5;
%A=sparse(A);

%GENERATION OF THE AEQ MATRIX (EQUALITIES)
Aeq=zeros((b+l)*int+s,X);                  %Sets up the size of the Aeq matrix
%GENERATION OF AEQ1A MATRIX(LINE DELTA VALUES)
p=1;
t=1;
i=1;
j=0;
m=1;
Aeq1a=zeros(l*int,b*int);                %Sets up the size for the Aeq1a matrix
Aeq1ai=zeros(int,b*int);                %Sets up the size for the Aeq1ai matrix
for k=1:1:l
    kV2=B(L(p,2),4)*B(L(p,3),4);
for u=1:1:int
if (L(p,2)< L(p,3))
Aeq1ai(i,L(p,2)+j)=-kV2/L(p,5);
Aeq1ai(i,L(p,3)+j)=kV2/L(p,5);
            i=i+1;
            j=j+b;
elseif (L(p,2) > L(p,3))
Aeq1ai(i,L(p,2)+j)=kV2/L(p,5);
Aeq1ai(i,L(p,3)+j)=-kV2/L(p,5);
            i=i+1;
```

```
            j=j+b;
end
end
Aeq1a(m:t*int,1:b*int)=Aeq1ai;
    m=m+int;
    t=t+1;
    Aeq1ai=zeros(int, b*int);
    i=1;
    p=p+1;
    j=0;
end
%Deletes the swing bus because it has an angle of zero
i=1;
j=0;
for k=1:1:b
if B(i,2)==3
for u=1:1:int
Aeq1a(:,B(i,1)+j)=[];
            j=j+b-1;
end
end
     i=i+1;
end
Aeq(1:l*int,1:(b-1)*int)=Aeq1a; %Stores the line delta values in the Aeq
matrix
%GENERATION OF AEQ1B MATRIX (LINE POWER FLOW VALUES)
m=1;
i=1;
j=1;
t=1;
Aeq1b=zeros(l*int,l*int);              %Sets up the size for the Aeq1b matrix
Aeq1bi=zeros(int,l*int);              %Sets up the size for the Aeq1bi matrix
for k=1:1:l
for u=1:1:int
Aeq1bi(i,j)=1;
        i=i+1;
        j=j+l;
end
Aeq1b(m:t*int,1:l*int)=Aeq1bi;
    m=m+int;
    t=t+1;
    j=t;
    i=1;
    Aeq1bi=zeros(int,l*int);
end
Aeq(1:l*int,(b-1)*int+1:(b+l-1)*int)=Aeq1b; %Stores the Aeq1b matrix into Aeq
%GENERATION OF THE AEQ2A MATRIX(BUS POWER FLOW VALUES)
i=1;
j=0;
t=1;
e=1;
m=1;
Aeq2a=zeros(b*int,l*int);                      %Sets up the Aeq2a matrix size
Aeq2ai=zeros(int,l*int);
for k=1:1:b
for u=1:1:l
```

```
if ((L(i,2)== t) || (L(i,3) == t))  %Tests to see if a line contains a bus
number
%Determines which way power is flowing based on order of buses
for v=1:1:int
if L(i,2)==t
Aeq2ai(e,L(i,1)+j)=-1;
elseif L(i,3)==t
Aeq2ai(e,L(i,1)+j)=1;
end
                e=e+1;
                j=j+l;
end
            j=0;
            e=1;
end
        i=i+1;
end
Aeq2a(m:t*int,1:l*int)=Aeq2ai;
        m=m+int;
        t=t+1;
        i=1;
        j=0;
        e=1;
        Aeq2ai=zeros(int,l*int);
end
Aeq(l*int+1:(l+b)*int,(b-1)*int+1:(b+l-1)*int)=Aeq2a;   %Stores Aeq2a into
Aeq
%GENERATION OF THE AEQ2B MATRIX (BUS GENERATION VALUES)
i=1;
j=1;
t=1;
m=1;
Aeq2b=zeros(b*int,b*int);               %Sets up the size of the Aeq2b matrix
Aeq2bi=zeros(int,b*int);
for k=1:1:b
for u=1:1:int
Aeq2bi(i,j)=1;
            j=j+b;
            i=i+1;
end
Aeq2b(m:t*int,1:b*int)=Aeq2bi;
    m=m+int;
    t=t+1;
    i=1;
    j=t;

    Aeq2bi=zeros(int,b*int);
end
Aeq(l*int+1:(l+b)*int,(b+l-1)*int+1:(2*b+l-1)*int)=Aeq2b; %Stores it in the
Aeq matrix
%GENERATION OF THE AEQ2C MATRIX(BUS STORAGE VALUES)
i=1;
j=1;
t=1;
Aeq2c=zeros(b*int,b*int);               %Sets up the size of the Aeq2c matrix
%Aeqxi=zeros(int,b*int);
for k=1:1:b
```

```
for u=1:1:int
Aeq2c(i,j)=-1;
        i=i+1;
        j=j+b;
end
    t=t+1;
    j=t;
end
Aeq(l*int+1:(l+b)*int,(2*b+l-1)*int+1:(3*b+l-1)*int)=Aeq2c;   %Stores the
Aeq2c matrix into Aeq
%GENERATION OF THE AEQ3 MATRIX(STORAGE VALUES AT EACH HOUR)
i=1;
j=1;
Aeq3=zeros(b,b*int);
for k=1:1:b
for u=1:1:int
Aeq3(i,j)=1;
        j=j+b;
end
    i=i+1;
    j=i;
end
Aeq((l+b)*int+1:(l+b)*int+b,(2*b+l-1)*int+1:(3*b+l-1)*int)=Aeq3; %Stores the
Aeq3 matrix into the Aeq matrix
Aeq=sparse(Aeq);
[x,fval,exitflag]=quadprog(Q,C,A,bT,Aeq,beq,[],[],[],options); %Determines
the x values and the final generation cost
formatlong
Cost=fval*dT*d
%Extracts line flows at each interval
x1=x(int*(b-1)+1:int*(b-1)+l);
x2=x(int*(b-1)+l+1:int*(b-1)+2*l);
x3=x(int*(b-1)+2*l+1:int*(b-1)+3*l);
x4=x(int*(b-1)+3*l+1:int*(b-1)+4*l);
x5=x(int*(b-1)+4*l+1:int*(b-1)+5*l);
x6=x(int*(b-1)+5*l+1:int*(b-1)+6*l);
x7=x(int*(b-1)+6*l+1:int*(b-1)+7*l);
x8=x(int*(b-1)+7*l+1:int*(b-1)+8*l);
%Extracts generator output at each interval
y1=x(int*(l+b-1)+1:int*(l+b-1)+b);
y2=x(int*(l+b-1)+b+1:int*(l+b-1)+2*b);
y3=x(int*(l+b-1)+2*b+1:int*(l+b-1)+3*b);
y4=x(int*(l+b-1)+3*b+1:int*(l+b-1)+4*b);
y5=x(int*(l+b-1)+4*b+1:int*(l+b-1)+5*b);
y6=x(int*(l+b-1)+5*b+1:int*(l+b-1)+6*b);
y7=x(int*(l+b-1)+6*b+1:int*(l+b-1)+7*b);
y8=x(int*(l+b-1)+7*b+1:int*(l+b-1)+8*b);
%Extracts storage output at each interval
z1=x(int*(l+2*b-1)+1:int*(l+2*b-1)+b);
z2=x(int*(l+2*b-1)+b+1:int*(l+2*b-1)+2*b);
z3=x(int*(l+2*b-1)+2*b+1:int*(l+2*b-1)+3*b);
z4=x(int*(l+2*b-1)+3*b+1:int*(l+2*b-1)+4*b);
z5=x(int*(l+2*b-1)+4*b+1:int*(l+2*b-1)+5*b);
z6=x(int*(l+2*b-1)+5*b+1:int*(l+2*b-1)+6*b);
z7=x(int*(l+2*b-1)+6*b+1:int*(l+2*b-1)+7*b);
z8=x(int*(l+2*b-1)+7*b+1:int*(l+2*b-1)+8*b);
%Writes line flows at each interval to excel file
```

```
xlswrite('Output.xlsx',x1,'Test output','C2:C278');
xlswrite('Output.xlsx',x2,'Test output','D2:D278');
xlswrite('Output.xlsx',x3,'Test output','E2:E278');
xlswrite('Output.xlsx',x4,'Test output','F2:F278');
xlswrite('Output.xlsx',x5,'Test output','G2:G278');
xlswrite('Output.xlsx',x6,'Test output','H2:H278');
xlswrite('Output.xlsx',x7,'Test output','I2:I278');
xlswrite('Output.xlsx',x8,'Test output','J2:J278');
%Writes generation output at each interval to excel file
xlswrite('Output.xlsx',y1,'Test output','N2:N207');
xlswrite('Output.xlsx',y2,'Test output','O2:O207');
xlswrite('Output.xlsx',y3,'Test output','P2:P207');
xlswrite('Output.xlsx',y4,'Test output','Q2:Q207');
xlswrite('Output.xlsx',y5,'Test output','R2:R207');
xlswrite('Output.xlsx',y6,'Test output','S2:S207');
xlswrite('Output.xlsx',y7,'Test output','T2:T207');
xlswrite('Output.xlsx',y8,'Test output','U2:U207');
%Writes storage output at each interval to excel file
xlswrite('Output.xlsx',z1,'Test output','Y2:Y207');
xlswrite('Output.xlsx',z2,'Test output','Z2:Z207');
xlswrite('Output.xlsx',z3,'Test output','AA2:AA207');
xlswrite('Output.xlsx',z4,'Test output','AB2:AB207');
xlswrite('Output.xlsx',z5,'Test output','AC2:AC207');
xlswrite('Output.xlsx',z6,'Test output','AD2:AD207');
xlswrite('Output.xlsx',z7,'Test output','AE2:AE207');
xlswrite('Output.xlsx',z8,'Test output','AF2:AF207');
%Equality limit testing
Eql=Aeq*x-beq;
%Inequality limit testing
Ineql=A*x-bT;
Llmt=Ineql(1:2*l*int,1);
Glmt=Ineql(2*l*int+1:2*int*(l+b));
CPlmt=Ineql(2*int*(l+b)+1:2*int*(l+2*b));
Rlmt=Ineql(2*int*(l+2*b)+1:2*int*(l+2*b)+2*b*(int-1));
CElmt=Ineql(2*int*(l+2*b)+2*b*(int-1)+1:2*int*(l+2*b)+2*b*(int-1)+2*b*int);
i=1;
LlmtO=zeros(length(Llmt),1);
for k=1:1:length(Llmt)
ifLlmt(i,1) >= 0
LlmtO(i,1)=1;
else
LlmtO(i,1)=0;
end
    i=i+1;
end
LLreached=sum(LlmtO);
i=1;
LlmtA=zeros(length(Llmt),1);
for k=1:1:length(Llmt)
ifLlmt(i,1)/b1(i,1) >= -.05 &Llmt(i,1)/b1(i,1) < 0
LlmtA(i,1)=1;
else
LlmtA(i,1)=0;
end
    i=i+1;
end
LL95=sum(LlmtA);
```

```
i=1;
GlmtO=zeros(length(Glmt),1);
for k=1:1:length(Glmt)/2
ifGlmt(i,1)>=0 & b2(i,1) ~= 0
GlmtO(i,1)=1;
else
GlmtO(i,1)=0;
end
    i=i+2;
end
i=2;
for k=1:1:length(Glmt)/2
ifGlmt(i,1)>=0 & b2(i-1,1) ~= 0
GlmtO(i,1)=1;
else
GlmtO(i,1)=0;
end
    i=i+2;
end
GLreached=sum(GlmtO);
i=1;
GlmtA=zeros(length(Glmt),1);
for k=1:1:length(Glmt)
ifGlmt(i,1)/b2(i,1)>=-.05 & b2(i,1) ~= 0 &Glmt(i,1)/b2(i,1)<0
GlmtA(i,1)=1;
else
GlmtA(i,1)=0;
end
    i=i+1;
end
GL95=sum(GlmtA);
i=1;
CPlmtO=zeros(length(CPlmt),1);
for k=1:1:length(CPlmt)
ifCPlmt(i,1)>=0 & b3(i,1) ~= 0
CPlmtO(i,1)=1;
else
CPlmtO(i,1)=0;
end
    i=i+1;
end
CPLreached=sum(CPlmtO);
i=1;
CPlmtA=zeros(length(CPlmt),1);
for k=1:1:length(CPlmt)
ifCPlmt(i,1)/b3(i,1) >= -.05 &CPlmt(i,1)/b3(i,1) < 0
CPlmtA(i,1)=1;
else
CPlmtA(i,1)=0;
end
    i=i+1;
end
CPL95=sum(CPlmtA);
i=1;
RlmtO=zeros(length(Rlmt),1);
for k=1:1:length(Rlmt)
ifRlmt(i,1) < 0
```

```
RlmtO(i,1)=0;
else
RlmtO(i,1)=1;
end
    i=i+1;
end
RLreached=sum(RlmtO);
i=1;
RlmtA=zeros(length(Rlmt),1);
for k=1:1:length(Rlmt)
ifRlmt(i,1)/b4(i,1) >=-.05 &Rlmt(i,1)/b4(i,1) < 0
RlmtA(i,1)=1;
else
RlmtA(i,1)=0;
end
    i=i+1;
end
RL95=sum(RlmtA);
i=1;
CElmtO=zeros(length(CElmt),1);
for k=1:1:length(CElmt)/2
ifCElmt(i,1)>=0 & b5(i,1) ~= 0
CElmtO(i,1)=1;
else
CElmtO(i,1)=0;
end
    i=i+2;
end
i=2;
for k=1:1:length(CElmt)/2
ifCElmt(i,1)>=0 & b5(i-1,1) ~= 0
CElmtO(i,1)=1;
else
CElmtO(i,1)=0;
end
    i=i+2;
end
CELreached=sum(CElmtO);
i=1;
CElmtA=zeros(length(CElmt),1);
for k=1:1:length(CElmt)
ifCElmt(i,1)/b5(i,1) >= -.05 & b5(i,1) ~= 0 &CElmt(i,1)/b5(i,1) < 0
CElmtA(i,1)=1;
else
CElmtA(i,1)=0;
end
    i=i+1;
end
CEL95=sum(CElmtA);
Limits=[LLreached, LL95, GLreached, GL95, CPLreached, CPL95, RLreached, RL95,
CELreached, CEL95]
xlswrite('Output.xlsx',Eql,'Limit testing','B3:B4072');
xlswrite('Output.xlsx',Ineql,'Limit testing','H3:H17204');
xlswrite('Output.xlsx',x,'Limit testing','N3:N7154');
%Prints out line limits into the output spreadsheet for comparison
Linelim=L(:,6);
xlswrite('Output.xlsx',Linelim,'Test output','B2:B278');
```

```
%Prints out generator limits into the output spreadsheet for comparison
Genlim=zeros(206,1);
i=1;
for k=1:1:g
Genlim(G(i,1),1)=G(i,3);
    i=i+1;
end
xlswrite('Output.xlsx',Genlim,'Test output','M2:M207');
%Prints out storage power limits into the output spreadsheet for comparison
Storlim=zeros(206,1);
i=1;
for k=1:1:s
Storlim(S(i,1),1)=S(i,2);
    i=i+1;
end
xlswrite('Output.xlsx',Storlim,'Test output','X2:X207');
%Prints out generator ramp rate limits into the output spreadsheet for
comparison
Ramplim=zeros(206,1);
i=1;
for k=1:1:g
Ramplim(G(i,1),1)=G(i,6);
    i=i+1;
end
xlswrite('Output.xlsx',Ramplim,'Ramp rates','B3:B208');
```

APPENDIX B The quadratic programming method

B.1 Quadratic programming

Quadratic programming is used in this thesis for optimization of a nonlinear (quadratic) performance index constrained by linear constraints. The method used was directly from the MATLAB toolbox. The following description of quadratic programming largely comes directly from [71].

Interior-point-convex QUADPROG algorithm

Quadratic programming is a technique to find a vector x that minimizes a quadratic objective function, subject to linear constraints,

$$\min_X f(x) = \min_X \frac{1}{2} x^T H x + c^T x$$

$$Ax \leq b$$

$$A_{eq} x = b_{eq}$$

$$l \leq x \leq u$$

where

c Vector(n x 1) of linear terms of the quadratic objective function

H Symmetric matrix ($n \times n$) describing the coefficients of the quadratic terms

A Coefficient matrix (m x n) of inequality constraints

b Vector (m x 1) of inequality right-hand side constraints

A_{eq} Coefficient matrix (k x n) of equality constraints

b_{eq} Vector (k x 1) of equality right-hand side constraints.

l Vector of lower bound variables

u Vector of upper bound variables

The quadratic programming in MATLAB uses the interior-point-convex algorithm which has the following steps:

1. Presolve / postsolve
2. Generate initial point
3. Predictor- corrector
4. Multiple corrections.

Each of these steps are described in [71] in more detail and are summarized below.

Presolve / postsolve
The interior-point-algorithm starts by trying to remove redundancies and constraints that simplify the problem. The presolve portion of the algorithm attempts to perform the following operations in order to simplify the problem can be seen in [71].

In the presolve step the algorithm searches for an infeasible or unbounded problem. If one is found, the program is terminated and displays the appropriate exit message. If an infeasible or unbounded problem is not detected, the algorithm continues on to the other steps. The algorithm then restructures the original problem removing any of the transformations performed during the presolve section. Finally, the postsolve is the last step performed.

Generate initial point
The initial point x_0 for the algorithm is:

1. Initialize x_0 to ones(n,1), where n is the number of rows in H.
2. For components that have both an upper bound u_b and a lower bound l_b, the component is set to $(u_b + l_b)/2$ if a component of x_0 in not inside these bounds.
3. For components that have only one bound, the component is modified to lie strictly inside the bound.

Predictor- corrector
The interior-point-convex algorithm tries to find a point where the Karush-Kuhn-Tucker (KKT) conditions hold. For the quadratic programming problem described, these conditions can be seen in [71].

Multiple corrections
The multiple corrections step is used after the Newton phase in the predictor/ corrector section and prepares the solution for better succeeding steps. The corrections are used to possibly improve the algorithm performance and robustness.

B.2 Observations in the use of MATLAB quadprog

The forgoing was a quick description of the in line function quadprog in MATLAB where the full description can be seen in [71]. The following observations are made by the author in the use of this software:

- Unlike linear programming, increasing the limit of various constraints in the system when the output variable is not at that limit can actually improve the results. This outcome does not happen in linear programming where a relaxation of a limit that the variable is not hitting has no effect on the optimization results. When a line in the Arizona test be was approaching the line limit, relaxing that limit showed that it is possible to improve the system wide operating cost.
- Utilization of different algorithms can improve simulation times in MATLAB. The interior-point-convex algorithm seemed to have the fastest simulation times compared to the other algorithms.
- Decreasing the program tolerance levels improved the optimization results and actually lowered the system operating cost in both the base case and the cases with energy storage.
- The portion of the simulation time that took the longest was reading and writing to / from the program Excel.

APPENDIX C A brief discussion of environmental issues related to the sites selected for energy storage

C.1 Environmental issues

In this appendix, a few citations and comments are provided for the three bulk energy sites discussed in this thesis. This thesis focuses on the electric power engineering issues of bulk energy storage. The reader is directed to the citations listed below for a discussion of environmental issues.

C.2 Eagle Mountain Pumped Storage

The following comments apply to the Eagle Mountain Pumped Storage facility between Desert Center and Chiriaco Summit, California (a few miles north of Interstate 10):

- The project will have no impact on local surface waters as there are none in the area affected by the project [68]. There are no perennial streams in the area, therefore no in stream or out stream flows will be affected by the operation of the pumped hydro energy storage. A closed loop system will be used where the reservoir water is re-used and resupplied when needed due to evaporation. However, the water quality in the new reservoirs can be degraded through evaporation resulting in salts and pit material resulting in elevated metal concentrations.
- Section 7 of the Endangered Species Act (ESA) [73] requires that the building of this PHES does not affect the existence of endangered or threatened species or destroy local habits of these species. In this location, Coachella Valley, the species of concern are the milkvetch and the desert tortoise. In this location, there is a critical habitat for the desert tortoise that must be protected during construction and operation.

C.3 Table Mountain Pumped Storage

The following comments apply to the Table Mountain Pumped Storage facility between Peach Springs and Kingman Arizona:

- An environmental impact study has not been performed for this PHES location yet. Only a preliminary permit has been filed for the project [67]. The proposed location will be a closed loop orientation and the circulated reservoir will be reused. Its effect on the local steams has not been studied yet. Also, an analysis has yet to be performed on local endangered species and the local habitat that these species occupy.

C.4 Longview Pumped Storage

The following comments apply to the Longview Pumped Storage facility near Chino Valley (north of Prescott and south of Seligman), Arizona:

- The project reservoirs will be closed loop, meaning that water in the reservoirs will be reusable [66]. However, the source of water will be the locally available ground water that will come from the Big Chino aquifer. This aquifer is used downstream by residents

in Prescott, Prescott Valley, and Chino Valley. There is some concern that the use of this water by the PHES will affect the water available for these residents as well as the water quality.

- Big Chino aquifer also supplies 80% of the backflow of the Upper Verde River, which is branded as one of the countries most endangered rivers because it is home to many endangered species. There is concern that these species could be affected if the PHES uses a significant amount of water from the aquifer.

Part III

Economic Assessment of Energy Storage in Systems with High Levels of Renewable Resources

Nan Li
Kory W. Hedman

Arizona State University

For information about this project, contact

Kory W. Hedman
Arizona State University
Department of Electrical Engineering
P.O. BOX 875706
Tempe, AZ 85287-5706
Phone: 480 965-1276
Fax: 480 965-0745
Email: kory.hedman@asu.edu

Power Systems Engineering Research Center

The Power Systems Engineering Research Center (PSERC) is a multi-university Center conducting research on challenges facing the electric power industry and educating the next generation of power engineers. More information about PSERC can be found at the Center's website: http://www.pserc.org.

For additional information, contact:

Power Systems Engineering Research Center
Arizona State University
527 Engineering Research Center
Tempe, Arizona 85287-5706
Phone: 480-965-1643
Fax: 480-965-0745

Notice Concerning Copyright Material

Table of Contents

List of Figures

List of Tables

Nomenclature

c_g	Marginal cost for generator *g*
c_g^{NL}	No load cost for generator *g*
c_g^R	Ramping cost for generator *g*
c_g^{SU}	Startup cost for generator *g*
C_{gkt}^{Total}	Total costs for generator *g* in scenario *k* and period *t*
d_{nkt}	Real power demand at node *n* in scenario *k* and period *t*
DT_g, UT_g	Minimum down time and up time for unit *g*
E_{gkt}	Energy generated by generator *g* in scenario *k* and period *t*
g	Index of generators
$Indx_{min}$	Variable used to determine the minimum forecast error ε_w^{min}
$Indx_{max}$	Variable used to determine the maximum forecast error ε_w^{max}
k	Index of scenarios
K	Number of scenarios
l	Index of line segments for the piecewise linear function
L	Number of line segments for the piecewise linear approximation
L_g^{In}, U_g^{In}	Minimum and maximum power absorbed by energy storage unit *g*
L_g^{Out}, U_g^{Out}	Minimum and maximum power output for energy storage unit *g*
m	Index of transmission lines
n	Index of buses
N_g^{On}	Number of units dispatched in the system
P_w	Wind generation with forecast error
P_{aw}	Wind farm output obtained from NREL Wind Datasets

P_{gkt}	Power output for generator *g* at bus *n* in scenario *k* and period *t*
P_{mkt}	Real power flow on transmission line *m* in scenario *k* and period *t*
P_{gkt}^{In}	Power absorbed by energy storage unit *g* at bus *n* in scenario *k* and period *t*
P_{m}^{Max}	Maximum MVA rating for transmission line *m*
P_{g}^{Max}	Maximum real power output for generator *g*
P_{g}^{Min}	Minimum real power output for generator *g*
P_{gkt}^{Out}	Power generated by energy storage unit *g* at bus *n* in scenario *k* and period *t*
P_{wkt}^{Wind}	Power output for wind generator *w* at bus *n* in scenario *k* and period *t*
R_{g}^{10+}	Maximum 10-minute ramp up rate for generator *g*
R_{g}^{+}	Maximum hourly ramp up rate for generator *g*
R_{g}^{10-}	Maximum 10-minute ramp down rate for generator *g*
R_{g}^{-}	Maximum hourly ramp down rate for generator *g*
R_{g}^{SD}	Maximum shut down ramp rate for generator *g*
R_{g}^{SU}	Maximum start up ramp rate for generator *g*
R_{g}^{NS}	Maximum non-spinning reserve ramp rate for generator *g*
s_{gkt}	Reservoir inventory of the energy storage unit *g* in scenario *k* at the end of period *t*
s_{g}^{begin}	Initial reservoir inventory of energy storage unit *g*
s_{g}^{end}	Target reservoir inventory of energy storage unit *g*
s_{g}^{Min}, s_{g}^{Max}	Minimum and maximum capacity of the reservoir
t	Index of time periods
t_{gkt}^{on}	Variable indicates if generator g is online in scenario *k* and period *t*
T	Number of time periods

$U_{\%}$	Utilization rate for conventional generators
w	Index of wind generators
α	Ramping cost coefficient associated with generators during ramping process
ε_w	Wind forecast error generated from Monte-Carlo simulation
ε_w^{max}	Minimum wind forecast error
ε_w^{min}	Maximum wind forecast error
π_k	Probability of transition to scenario *k*
β_g	Conversion factor that converts energy to power in the reserve constraints for energy storage units
η_g^{In}	Efficiency of the absorbing cycle of energy storage unit *g*
η_g^{Out}	Efficiency of the generating cycle of energy storage unit *g*
$\delta_m^+(n)$	For any transmission line *m* with "to" bus *n*
$\delta_m^-(n)$	For any transmission line *m* with "from" bus *n*
σ	Standard deviation for Gaussian distribution
$\phi(\cdot)$	Probability density function for standard Gaussian distribution
$\Phi(\cdot)$	Cumulative distribution function for standard Gaussian distribution
Ω_G	Set of generators
Ω_{Gs}	Set of slow generators
Ω_{Gf}	Set of fast generators
Ω_P	Set of pumped storage units
Ω_C	Set of compressed air energy storage units
$\forall g(n)$	For any generator *g* at bus *n*

1. Introduction

1.1 Background

For the past decades, power systems have been relying on fossil fuels, such as coal, oil and natural gas, to produce electric power. With the growing concern regarding climate change and environmental issues, renewable energy is playing an increasingly important role in power systems. By the end of 2012, the worldwide installed wind capacity has reached 282.5 GW [1], [2], while the solar installed capacity reached 100GW [3]. In the U.S, both the government policies and the concerns regarding environmental problems have sped up the integration of renewable energy. As of January 2012, thirty states have enforced Renewable Portfolio Standards (RPS) or other mandated renewable capacities policies. In California, the RPS requires that electric utilities should have 33% of their retail sales derived from eligible renewable energy resources by 2020 [4]. On the other hand, the tightened standards on CO2 and NO2 emissions have also stimulated the needs for renewable energy. As a result, 60 GW of wind power capacity has been installed by 2012 in the U.S., while the total installed capacity for solar power is 7.2 GW [5]. The fast-growing integration of renewable energy has significantly increased the complexities with balancing generation and demand in power systems. Greater flexibilities in generation resources are needed to maintain the reliable supply of power under high renewables penetration levels. Under such circumstances, new interests have been raised in energy storage (ES).

The use of energy storage in power system has a long history. Back in 1880s, lead-acid batteries have been used in the private New York City area as the original nighttime load solution [6]. Starting in late 19th century, with the rapid development in storage technologies, energy storage has been used in a variety of power system applications, such as peak shaving, load leveling, and frequency and area control error regulation. With the fast growth of integration of renewable resources in recent years, the energy-shifting and fast-ramping capability of energy storage provides a potential attractive resource to balance the uncertainty and variability in renewable generation. By absorbing excess clean energy and shifting it to hours when scheduled generation cannot meet demand, energy storage can effectively balance the variability in renewable generation. Meanwhile, because of its fast ramping capability, energy storage has a great potential to provide large quantities of fast ancillary services. Yet the primary question associated with energy storage is when the use of energy storage becomes economical.

To address the economic case for energy storage, it is important to evaluate and identify the benefits of energy storage. As renewable penetration level increases, the traditional solution is to utilize conventional generators to balance the intermittency and variability in renewable generation. However, the effectiveness and efficiencies for conventional generators may decrease as they will be primarily used to provide backup generation and ancillary services. Under such conditions, the incentive to invest and utilize conventional generators may also be reduced. Therefore, the attractiveness of conventional generator and energy storage under high levels of renewable penetration level should be evaluated and compared to assess the economic case for energy storage. In this report, studies will be conducted from the viewpoint of the day-ahead generation scheduling problem as well as

real-time operations to analyze the economic value for energy storage under high renewable penetration levels.

1.2 Summary of Chapters

This report is structured as follows. In chapter 2, existing and emerging bulk energy storage technologies are introduced. Operating characteristics, power system applications, and capital costs are discussed for different energy storage technologies.

Chapter 3 reviews previous studies on different power system applications of energy storage technologies, such as peak shaving, load leveling, price-arbitrage opportunity, integration of renewable resources, transmission congestion mitigation, and transmission expansion deferral.

Chapter 4 reviews the concept of unit commitment and its formulation. Two different formulations of unit commitment are discussed, namely deterministic unit commitment and stochastic unit commitment.

In chapter 5, a traditional day-ahead generation scheduling problem is formulated to compare the short-term profitability of conventional generators and energy storage under increasing renewable penetration levels.

In chapter 6, the benefit of using energy storage in real-time operation is evaluated and identified.

In chapter 7, the conclusions to this report are presented.

2. Energy Storage Technologies

In this chapter, available and emerging bulk energy storage technologies are introduced. Operating characteristics, technology maturity and commercial availability of these energy storage technologies are presented. A summary of power system applications for different energy storage technologies and their costs are discussed.

2.1 Introduction to Bulk Energy Storage Technologies

Contemporarily, many energy storage technologies already exist, such as pumped hydro storage (PHS), compressed air energy storage (CAES) and battery energy storage, while some emerging technologies are anticipated to be available within the coming years. Among all types of energy storage technologies, pumped hydro storage has the largest installed capacity of 127,000 MW. Following pumped storage is compressed air energy storage with 440-MW installed capacity. Sodium-sulfur (NaS) batteries have a total installed capacity of 316 MW, which is the third largest existing storage technology. At the same time, another 606 MW of sodium-sulfur batteries have been planned or announced. Worldwide installed capacities for different energy storage technologies are summarized in Figure 2.1 [8]. In the U.S., the mix of energy storage technologies is similar. As shown in Figure 2.2 [9], pumped hydro storage also has the largest capacity, which consists of 95% of the total energy storage capacity. Thermal storage has the second largest capacity, followed by compressed air, batteries, and then flywheel energy storage.

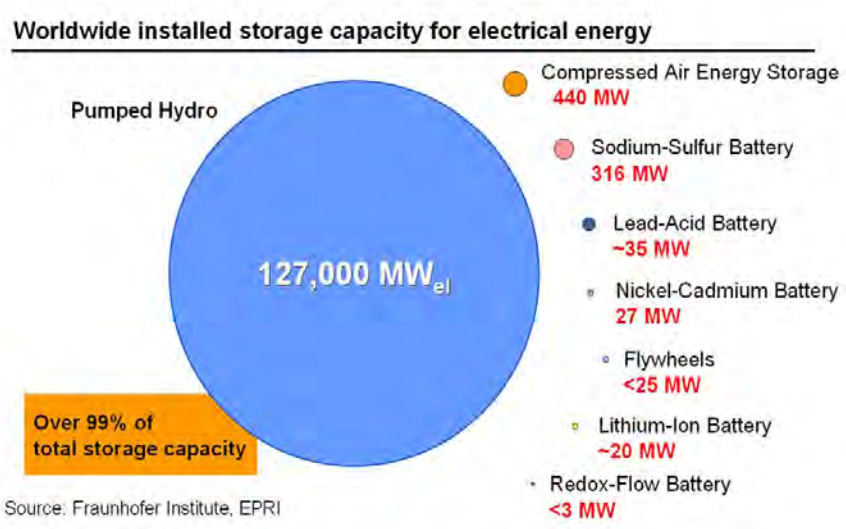

Figure 2.1 Worldwide Installed Capacity for Different Energy Storage Technologies

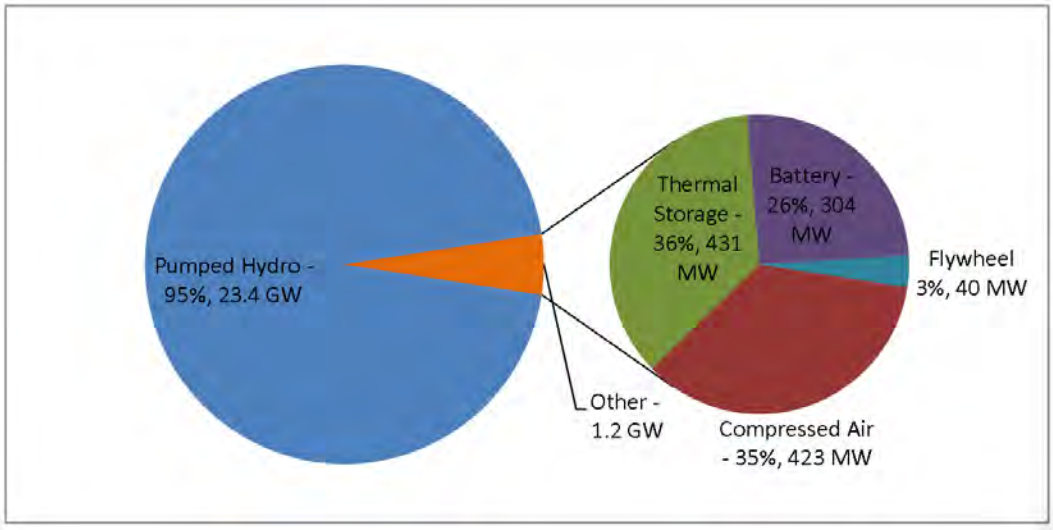

Figure 2.2 Summary of Grid Storage Projects in the U.S. (Including Announced Projects)

2.2 Pumped Hydro Energy Storage

The first of use of pumped hydroelectric energy storage can be traced back to 1890 in Italy and Switzerland. After a hundred years, more than two hundred pumped hydro storage facilities are now in operation or under planning worldwide. A pumped hydro storage facility utilizes large reservoirs to store water at different elevations. During off-peak periods or when excessive renewable resources are available, pumped hydro storage absorbs energy from grid to pump water from its lower reservoir to its higher reservoir. During on-peak hours or when renewable resources are not available, pumped hydro storage supplies energy back to grid by running water to drive a water turbine. A pumped hydro storage facility can have more than 3000 MW of power capacity and store 30,000 MWh of energy. The round-trip efficiency for pumped hydro storage is typically from 75% to 85%. The life-cycle is long for pumped hydro storage, which ranges from 50 to 60 years. Pumped hydro storage also has a fast ramping capability. It can be started and ramped up to full capacity within several minutes and transition between pumping and generation mode in less than ten minutes. The main drawbacks with pump hydro storage are its negative impact on the environments, the large land use requirement, the specific siting requirements, and the cost. For a pumped hydro storage facility to hold enough water to generate 10,000 MWh, the upper reservoir has to be one kilometer in diameter, twenty-five meters deep and having an average head of 200 meters.

As the most widely used bulk energy storage technology, pumped hydro storage technologies have been advanced significantly since its first introduction. The advances in pumped hydro storage technology include the use of reversible pump-turbines, integration of power electronic devices, and improvement in energy-conversion efficiencies. Since the 1990s, a newer pumped hydro storage technology, named adjustable pumped hydro storage (ASH), has been developed and used in commercial operation. Different from traditional single-speed pump turbine whose input power is fixed during the pumping process, ASH units are able to adjust the power consumed during pumping mode. This novel feature enables ASH units to provide large quantities of frequency regulation services in both

pumping and generation modes and gain higher round-trip efficiencies [10]. Globally, there are around 270 pumped hydro storage stations currently either in operation or under construction, where 36 of them are equipped with adjustable-speed machines. In the U.S., although several projects in the design or planning stages are evaluating the use of adjustable-speed technologies, none of the existing pumped hydro storage stations are equipped with adjustable-speed units. All the existing adjustable-speed pumped hydro storage projects are located in Europe, China, Japan, and India.

2.3 Compressed Air Energy Storage

A compressed air energy storage facility works in a similar way as pumped hydro storage. During off-peak hours, a compressed air energy storage facility absorbs power to compress air into an underground cavern. During peak hours, air is withdrawn from the cavern and heated with natural gas in a chamber, where the expansion in volume is used to drive a combustion turbine. A compressed air energy storage plant burns two-thirds the natural gas of a conventional combustion turbine during generation process, which results in a lower fuel cost compared to a conventional gas-fired combustion turbine plant [11]. Currently several technologies are available for compressed air energy storage. The aforementioned is referred to as the first-generation compressed air energy storage system. For a more advanced compressed air energy storage system, no natural gas is needed during the generation process. Instead, the compressed air is heated using the heat recovered from the compression process. However, the second-generation compressed air energy storage system is still under test and has not been used for utility-scale applications.

Compressed air energy storage systems can be designed with either aboveground storage or underground storage. Aboveground compressed air energy storage systems have relative small power and energy capacities, which are typically in the range of 3 to 50 MW and 6 to 300 MWh. For underground compressed air energy storage systems, power capacity can be sized up to 400 MW, while the energy durations generally range from 8 to 26 hours. Compressed air energy storage has fast ramping capability. It can be started up and ramp up to full load within ten minutes. However, the transition process between generation and compression mode is relative slow, which will take more than ten minutes. One drawback with compressed air energy storage is that the first-generation system requires the use of natural gas during generation process. If natural gas price increases, the economic potential for compressed air energy storage may be reduced. Another drawback is that compressed air energy storage has strict siting requirements. It requires specific locations to build the cavern to store compressed air.

Currently, there are only three utility-scale compressed air energy storage plants in operation: one 290 MW plant built in 1979 in Huntorf, Germany; one 110 MW plant built in 1991 in Alabama, USA, and one 2 MW plant built in 2012 in Texas, USA [12].

2.4 Battery Energy Storage

Battery storage is a developing and promising energy storage technology. Compared to pumped hydro storage and compressed air energy storage, batteries have smaller capacities but require much less land use. However, the battery life cycle is much shorter and may

degrade as a result of its charge and discharge processes. Factors like temperature, rate of discharge, and depth of discharge (DOD) may all have an impact on the life cycle of batteries. Contemporarily several battery storage technologies are available, such as lead-acid batteries, sodium-sulfur (NaS) batteries, lithium-ion (Li-ion) batteries and nickel-cadmium batteries.

Lead-acid batteries are the oldest and most commercially mature battery technology. It has been used in a wide range of areas, such as automotive, marine, and uninterruptable power supply (UPS) systems. Generally, lead-acid batteries are designed either for power application or energy application. Therefore, a lead-acid battery may have either a large power capacity or a large energy capacity, but not both. For a lead-acid battery manufactured by Xtreme Power [13], its cycle life is about 500,000 cycles at 1% DOD and 1,000 cycles at 100% DOD. Several concerns about lead-acid exist. One is the environmental and safety hazards related to lead. Since lead is one kind of toxic metal, the disposal of lead-acid batteries should be handled carefully and requires a number of government policies and regulations. Other concerns with lead-acid battery technology are its limited cycle-life, low power density and self-discharge issues.

Lithium-ion batteries are a newer technology compared to lead-acid battery technology. Currently, Li-ion batteries are being recognized as the leading technology for applications in electric vehicles (EV). Li-ion battery systems have the merits of high power densities and a low weight, which make them competitive in spatial-constrained applications. Li-ion batteries also have long life cycles and high round-trip efficiencies, up to 85% to 90%. Compared to other battery technologies, Li-ion batteries pose less negative environmental impact as they do not contain toxic metals such as lead or cadmium. However, Li-ion batteries are sensitive to over temperature and over discharge, as the life cycle and performance of Li-ion may be degraded as a result of these two issues.

Sodium-sulfur (NaS) batteries are a more mature technology compared to Li-ion batteries. The round-trip efficiencies for sodium-sulfur batteries are approximately 80%. Sodium-sulfur batteries have long rated-power discharge durations as high as six hours, which is a great potential for power grid applications. The power densities for sodium-sulfur batteries are high. The estimated life cycle for a sodium-sulfur battery is approximately 4500 cycles at 90% depth of discharge. However, since sodium-sulfur batteries contain metallic sodium, which is combustible if exposed to water, more safety features are required during the construction and operation of sodium-sulfur batteries. Meanwhile, sodium-sulfur batteries also require high-temperature operating conditions, which is in the range of 300℃ to 350℃.

With the development in battery technologies and the increasing need for flexible generation resources, battery energy storage is gaining its popularity in power system applications. In Alaska, a 1 MW/1.5 MWh lead-acid battery has been operating for 12 years to provide load-leveling services to the area of Metlakatla [14]. In 2003, a 27 MW/6.75 MWh nickel-cadmium battery was installed in Fairbanks, Alaska, which is used to provide backup power during outages. In 2011, a 32 MW/8 MWh Li-ion battery that operates along with a wind farm was installed in Laurel Mountain, West Virginia. This battery is by far the largest Li-ion battery and its main application is to provide clean and flexible reserves and moderate wind farm outputs at Laurel Mountain.

2.5 Flywheel Energy Storage

Flywheel energy storage is a short energy duration technology. Flywheels store energy in a spinning rotor in the form of kinetic energy and convert kinetic energy to electric power through power conversion systems. Flywheels have fast response times and high efficiencies. The response times for flywheels can be as short as four milliseconds and the efficiencies can be as high as 93%. High peak power can be provided by flywheels in short time intervals without over heating concerns. Life cycles are long for flywheels, which can exceed 100,000 cycles at 100% depth of discharge. Flywheels have power densities five to ten times that of batteries and pose much less adverse environmental impact than batteries. However, a flywheel facility should be built with more safety features to prevent damage and injuries in case flywheels crack and break off during rotation. Another drawback with flywheels is their limited energy capacities, which constrains their power system applications primarily to frequency regulation and power quality services. Currently, a 20 MW/5 MWh flywheel facility is in operation in Stephentown, New York.

2.6 Other Bulk Energy Storage Technologies

In recent years, there have been many emerging energy storage technologies, in spite of the fact that most of which are still under development or undergoing testing. One of the emerging storage technologies is thermal energy storage. For a thermal energy storage facility, solar energy is first stored as thermal energy and it is then converted to power when needed. In 2011, the world's first commercial-scale solar thermal plant, the Gemasolar solar thermal plant, using central tower receiver and molten salt heat storage technology, was built and commissioned in Seville, Spain. The solar thermal plant is rated at 19.9 MW and can provide power up to 15 hours without solar feed. The plant is equipped with more than 2600 heliostats and has a surface area of 185 hectares [15]. When solar is available, the heliostats reflect and concentrate the solar radiation to a receiver located at the top of a tower. Molten salts flow in the tower and are heated in the receiver. Then the heated salts flow through a chamber at the bottom of the tower where steam is generated to power a steam turbine. Excessive heat is stored in a hot tank located under the tower [16]. The panoramic view of the Gemasolar solar thermal plant is shown in Figure 2.3. In 2013, another thermal plant project was completed in Ivanpah, California [17]. The Ivanpah solar thermal plant also uses a tower solar thermal system and has a power capacity of 377 MW.

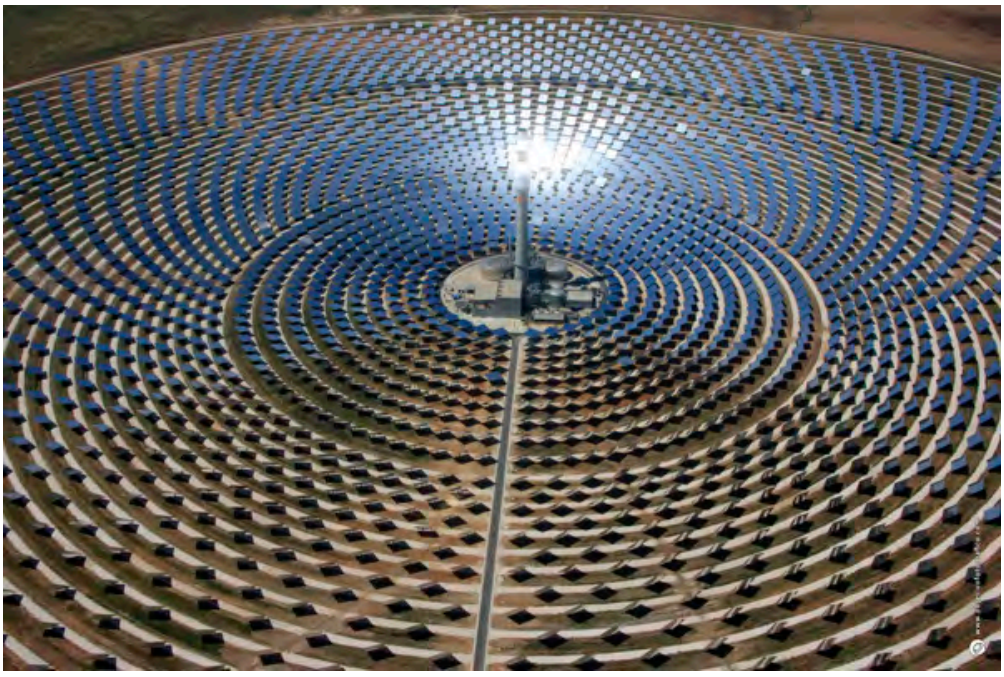

Figure 2.3 The Gemasolar Solar Thermal Plant

Flow batteries are another emerging battery technology. A flow battery utilizes two electrolytes that circulate through an electrochemical cell. Chemical energy is converted to electricity when the two electrolytes flow through the electrochemical cell. Flow batteries have the advantage of long life cycles. However, the downsides are that they have relative low power densities and require additional equipment, such as a pump in order to operate a flow battery facility. Flow batteries are still in development and none of them have been used for utility-scale applications.

Cryogenic energy storage utilizes low temperature liquids, such as liquid air or liquid nitrogen, to store energy. During off-peak hours, electricity is used to liquefy air and store the liquid air in an insulated tank at low pressure. During on-peak hours, liquid air is pumped at high temperature to a heat exchanger. In the heat exchanger, heat is applied to turn liquid air back to gas. The increase in pressure and volume during the phase change of air is used to drive a turbine [18], [19]. Currently, a 300 kW/ 2.5MWh pilot cryogenic energy storage system is in operation in United Kingdom [20].

2.7 Power System Applications of Bulk Energy Storage Technologies

Depending on the power capacity, energy capacity, and response time, bulk energy storage can be used in a wide range of applications in power systems. A figure illustrating the applications of energy storage technologies with different power ratings and energy capacities (or expressed in discharge time at rated power) is shown in Figure 2.4 [11]. As shown in Figure 2.4, pumped hydro storage and compressed air energy storage have the largest power and energy capacities. These two types of energy storage can be used for energy arbitrage opportunities, peak shaving, load leveling, and providing ancillary services such as spinning reserve and frequency regulations. Traditional single-speed

pumped hydro storage can only provide frequency regulations during generation mode, since it has to be operated at constant speed and consume constant power during pumping mode [21]. However, adjustable-speed pumped hydro storage can provide frequency regulation services in both generating and pumping mode, which increases its competitiveness as renewable penetration level increases.

Batteries have the medium power ratings and energy capacities. Contemporarily most of the utility-scale batteries are used to provide operating reserves and frequency regulation services. Some batteries are installed at wind farm locations to moderate the intermittent wind generation outputs. Other batteries have also been used to provide short-term power and stabilize power grid during occurrence of contingencies. Such projects include the 27 MW nickel-cadmium batteries deployed by Golden Valley Electric Association in Alaska and the 20 MW lithium-ion batteries operated by Sistema Interconnectado del Norte Grande (SING) in Northern Chilean grid [22]. Flywheels have small to medium power ratings and small energy capacities. As a result of their limited energy capacities, flywheels are primarily used to provide frequency regulation and power quality services.

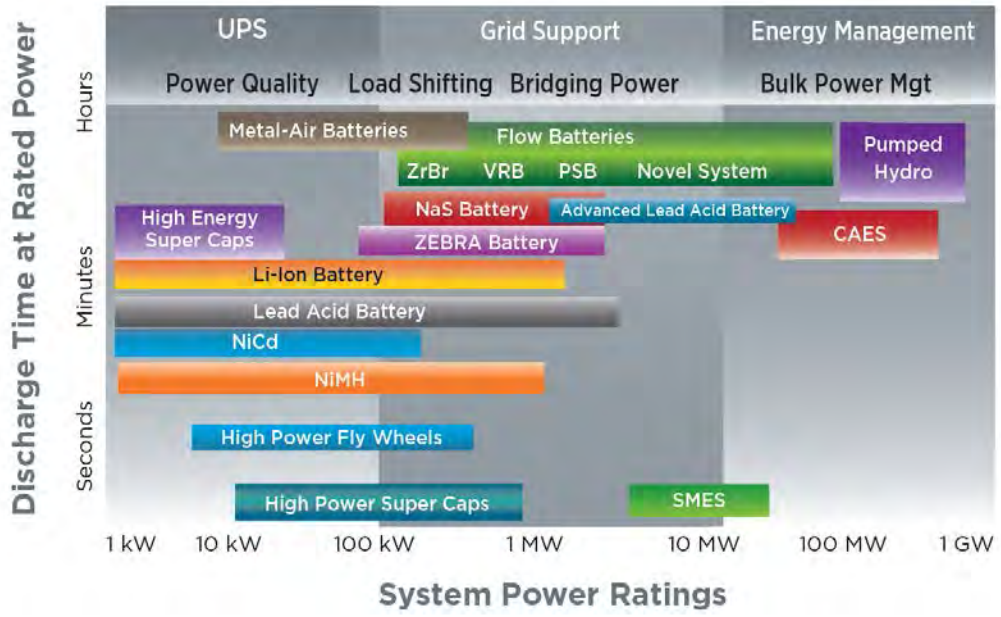

Figure 2.4 Applications of Energy Storage Technologies with Different Power Rating and Energy Capacities

2.8 Costs of Bulk Energy Storage Systems

A summary of the costs of energy storage technologies is shown in Table 2.1. The power ratings and energy capacities for different energy storage technologies are presented, along with the corresponding costs. From Table 2.1, it can be found that compressed air energy storage has the lowest power and energy subsystem costs, which are 1250 $/kW and 60 $/kWh respectively. Pumped hydro storage has the second lowest costs, which are 1500 $/kW to 2700 $/kW for power subsystem and 250 $/kWh to 270 $/kWh for energy storage subsystem. The costs for battery technologies are much higher than pumped hydro and

compressed air energy storage. Li-ion battery has the highest energy subsystem costs among all battery technologies, which is also a reason for its short energy-duration design. Flywheel has the highest energy subsystem costs among all the energy storage technologies, which is 7800 $/kWh to 8800 $/kWh.

Table 2.1 Costs for Energy Storage Technologies in Power System Applications

Technology	**Power Capacity (MW)**	**Energy Capacity (MWh)**	**Power Subsystem Cost ($/kW)**	**Energy Storage Subsystem Cost ($/kWh)**
PHS	900-1400	5400-14000	1500-2700	250-270
CAES	135	2700	1250	60
Lead-acid Battery	20-50	250	4600-4900	920-980
Li-ion Battery	1-100	0.25-25	1085-1550	4340-6200
NaS Battery	50	300	3100-3300	520-550
Flywheel	20	5	1950-2200	7800-8800

2.9 Summary

In summary, due to the flexibility and capability of energy shifting, energy storage is gaining its popularity in power system applications. While several types of energy storage technologies are available today, the capital costs for energy storage are still high compared to conventional generators. As the needs for flexible generation resources increase in power system, energy storage will find more of its applications in power systems. In Table 2.2, a summary is presented for the available energy storage technologies discussed in this report.

Table 2.2 Summary for Available Energy Storage Technologies

Technology	Applications	Advantages	Challenges
Pumped Hydro Storage	• Load leveling/peak shaving • Backup generation • Ancillary services	• Developed and mature technology • High ramp rate and short transition time • Large power and energy capacities	• Geographical limitations • Negative environmental impacts
Compressed Air Energy Storage	• Load leveling/peak shaving • Backup generation • Ancillary services	• Low capital costs • Large power and energy capacities	• Geographically limitations • Require natural gas to drive the turbine in generation mode
Lead-acid Battery	• Ancillary services • Grid stabilization	• Most commercially mature battery technology	• Contains hazardous metal • Limited life cycle • Low power density • Self-discharge issues
Li-ion Battery	• Power quality services • Ancillary services	• High power density • Long cycle life • High round-trip efficiency	• High costs • Sensitive to over temperature and over discharge
NaS Battery	• Power quality services • Ancillary services	• Long discharge time at rated power • High power density • Good scaling potential	• Require high-temperature operating conditions
Flywheel	• Frequency regulation • Transient stability • Power quality services	• High power density • Fast respond time • High round-trip efficiency	• Limited energy capacity • High costs

3. Energy Storage Literature Review

For many years, energy storage has been used in a variety of applications in power systems, such as peak shaving, load leveling, price-arbitrage, integration of renewable resources, transmission congestion mitigation, and transmission expansion deferral. In this chapter, previous studies on different applications of bulk energy storage are reviewed and discussed.

3.1 Peak Shaving and Load Leveling

Peak shaving and load leveling [23]-[27] are two traditional applications of energy storage. In the case of peak shaving, energy stored during low-demand hours is used to supply demand during on-peak hours so that the peak load is reduced. Peak shaving can reduce the dispatch of the expensive "peaking" units and improve the system load factor. In the case of load leveling, the same process is used except that the goal is to flatten the load profile rather than simply shaving the peak load. In [23], a dc optimal power flow (OPF) model was used to study the peak shaving value of pumped hydro storage. By applying pumped hydro storage in peak shaving, $47 million was saved in system operating costs for the Arizona interconnection system. With this savings in total operating costs, the payback period for pumped storage was estimated to be about 15 years. In [24], the load-leveling value of pumped hydro and battery energy storage was studied. Based on the results from an economic dispatch model, the work in [24] demonstrated the effectiveness of pumped hydro storage in load leveling, which could lead to savings of $22 million per year. However, because of the high capital costs, using battery energy storage for load leveling was shown to be not economical.

3.2 Price-arbitrage Applications

Price arbitrage is another important application for energy storage. In the case of price arbitrage, the profit of energy storage is maximized by buying power in low-price hours and selling in electricity markets during high-price hours. In [28], a study was conducted to analyze the price-arbitrage value of energy storage participated in PJM markets. The study evaluated variation in the price-arbitrage value of energy storage under the impact of different factors, such as fuel prices, transmission constraints, and generation mixes. The study showed that energy storage may reduce the price differences between off-peak and on-peak hours, which may consequently reduce the benefits that energy storage gained from price arbitrage. Based on this result, the paper also pointed out that the value of energy storage is not limited to price-arbitrage opportunities and that other services provided by energy storage should also be considered when investing in energy storage. In [29], the application of a Sodium-Sulfur battery and a flywheel in the New York City region was studied. The results demonstrated that there was a strong economic case for batteries to participate in the electricity market within New York City, by price arbitrage and for flywheels to participate as well, by providing frequency regulation services. The paper also showed that the round trip efficiency played an important role in the cost-benefit analysis for energy storage. In [30], a stochastic simulation methodology was developed to evaluate the impact of energy storage integration into a system with wind resources. The energy

storage was assumed to be controlled by the Independent System Operator (ISO), with the goal of maximizing the total social surplus in the system. The study demonstrated the benefits of energy storage in systems with deepening penetration of wind resources, such as reducing the wholesale purchase payments by buyers and providing improvements in system reliability.

3.3 Integration of Renewable Resources

With the increasing integration of intermittent renewable resources, the need for flexible generation is greater than ever. Under such circumstances, with a peak shaving, load leveling, or price-arbitrage strategy, the full benefits of energy storage may not be realized. Furthermore, existing energy markets are designed primarily based on the characteristics of conventional generators; such market designs do not acknowledge the service that storage provides. Future energy markets may be redesigned to provide compensation associated to the flexibility provided by storage, i.e., the ability to shift MWs across hours. Thus, examining the economic potential of energy storage from the aforementioned aspects does not reflect the full "money on the table" that storage provides.

To exploit the full benefits of energy storage in systems with renewable energy, many studies have been focused on the application of energy storage to facilitate the integration of high levels of intermittent renewable resources. Under high levels of renewable penetration, large quantities of operating reserves and regulation reserves are needed to balance the variation in generation and deviation in grid frequency. Under such circumstances, the rapid-response characteristic and the ability to store and shift MWs will make energy storage a valuable reserve and regulation resource in power systems. In [31], a stochastic scheduling tool was used to study the impact of pumped hydro storage on the Irish power system under high wind penetration levels. The results demonstrated that, with pumped hydro storage in the system, more wind could be integrated into the grid and the system total costs could be reduced by more than 40%. However, with current wind penetration target in the Irish grid, the savings in total system costs will not be enough to justify the costs to build new pumped hydro storage facilities.

In [32], a two-stage stochastic method was proposed to determine the inter-temporal reservoir targets for pumped hydro storage in a system with significant wind generation. The first-stage of the method determined the weekly reservoir targets by using a stochastic unit commitment model, while the second-stage scheduled the daily reservoir usage through a rolling-horizon stochastic unit commitment. The results showed that the proposed method was able to provide more efficient and economical schedules for pumped hydro storage than the traditional weekly refill method.

The work in [33] evaluated the benefits of energy storage in enhancing renewable dispatchability using a stochastic security-constrained unit commitment model. The results illustrated that, with pumped hydro storage in the system, the total operation costs and corrective action costs are reduced while the dispatchability of wind generation was improved.

In [34], the impact of significant wind penetration on investments in compressed air energy storage was studied. A stochastic electricity market model was proposed to evaluate the economic value of compressed air energy storage. The results demonstrated that

compressed air energy storage can be a competitive investment option under high penetration levels of renewables. Sensitivity analysis was performed to study the impact of capital costs and storage size on investment in CAES. In [35], a security-constrained unit commitment model was implemented to study the impact of CAES on systems with wind integration. Results showed that CAES could reduce system total cost and replace the more expensive "peaking" units in the system.

Reference [36] used a security-constrained unit commitment model to study the impact of battery energy storage on systems with different levels of wind penetration. The results showed that, with batteries installed in the system, the expensive units were dispatched less and the system total costs were reduced. By locating batteries at different locations, results showed that locating a battery near to wind farms may had better effects than locating a battery away from wind farms.

While most of the previous work has formulated the problems from the viewpoint from a centralized entity, the work proposed in [37] was based on the assumption that the energy storage was owned by a generation company. In [37], a stochastic unit commitment model was presented to maximize the profits of a generation company who operated a wind farm and a pumped hydro storage. The generation company was assumed to be a risk-neutral agent. With uncertainties in market prices and wind generation, the results demonstrated that the co-optimization of wind farm and pumped hydro storage could increase profits and decrease the penalties for imbalances in wind generation that the company paid.

The study on the value of energy storage in providing frequency regulation services can be found in [38]-[41]. In [38], a control scheme was proposed to coordinate wind generators and a flywheel energy storage system to provide frequency regulation services. The results showed that the proposed scheme reduced grid frequency deviation and increased the profits for wind generators and flywheels.

In [39], a multi-time-scale framework was proposed to study the value of flywheel and battery energy storage systems over different time horizons. The proposed framework evaluated the benefits of energy storage in primary control, secondary frequency regulation, and economic dispatch. The results demonstrated the effectiveness of energy storage in providing primary and secondary frequency regulation and reducing the total frequency regulation costs in the system.

In [40], the performance and economic value of flywheels in providing frequency regulation services were studied. A strategy of coordinating flywheel with a hydro plant to provide frequency regulations was proposed. The results illustrated that the proposed scheme could improve the quality of frequency regulation services that the flywheel provided as well as increase the profits of the flywheel.

In [41], a test facility was built to evaluate the benefits of batteries in providing frequency regulation services. The results demonstrated that batteries are effective at providing frequency regulation services and a full-scale demonstration facility was decided to be built based on the promising results.

3.4 Review of Other Applications

Besides the aforementioned applications, energy storage can also be used to mitigate transmission line congestion [42], [43] and to defer investments in transmission [44], [45]. In [42], a security-constrained unit commitment model was used to determine the short-term scheduling of a PV/battery system. By locating energy storage on the "load" side of the congested line, the congestion on transmission line was significantly mitigated during peak-load hours. In [44], a mixed-integer linear programming model considering investments in transmission and energy storage was proposed. The results demonstrated that the integration of energy storage in the system could defer the building of new transmission lines and reduce total system investment costs.

4. Review of Unit Commitment

In this chapter, the concept of unit commitment is reviewed and a generic formulation for unit commitment is presented. Previous studies on deterministic unit commitment are reviewed and the merits and drawbacks for deterministic unit commitment are discussed. The concept of stochastic unit commitment is introduced. The advantages and challenges associated with stochastic unit commitment are discussed.

4.1 Overview of Unit Commitment

Power systems face variations in demand every day. Though load profiles have daily patterns, load can also fluctuate largely in real time. With the objective of meeting power demand at minimum costs, unit commitment (UC) plays a significant role in power system operation and planning. Unit commitment is a decision making process to schedule the on/off status for generators over a defined period [46]. The aim of unit commitment is to find the most cost-effective combination of generators to reliably supply electric power to customers with minimum production costs. Unit commitment is generally modeled as a mix integer program (MIP) subject to a set of network and security constraints. Due to the large scale of real-world power systems and the non-convexities of MIP, unit commitment is a complicated optimization problem with high computational complexity.

Unit commitment problems are generally solved on a daily-basis or longer in power system operation. However, some Independent System Operators (ISO) also solve unit commitment problems on a shorter time interval basis. In California ISO, a short-term unit commitment is solved every hour to designate short- and medium- start units. The short-term unit commitment looks ahead three hours beyond the trading hour [47]. A generic unit commitment problem can be formulated as

Minimize:

$$\sum_{t=1}^{T}\sum_{g\in\Omega_G}(c_g P_{gt} + c_g^{NL}u_{gt} + c_g^{SU}v_{gt} + c_g^{SD}w_{gt}) \tag{4.1}$$

Subject to:

$$\sum_{\forall g(n)}^{g\in\Omega_G} P_{gt} + \sum_{\delta^+(n)} P_{mt} - \sum_{\delta^-(n)} P_{mt} = d_{nt}, \forall n, t \tag{4.2}$$

$$P_{mt} = B_m(\theta_{mt}^+ - \theta_{mt}^-), \forall m, t \tag{4.3}$$

$$-P_m^{Max} \le P_{mt} \le P_m^{Max}, \forall m, t \tag{4.4}$$

$$P_g^{Min}u_{gt} \le P_{gt} \le P_g^{Max}u_{gt}, \forall g \in \Omega_G, t \tag{4.5}$$

$$\sum_{q=t-UT_g+1}^{t} v_{gq} \le u_{gt},\ \forall g, t \in \{UT_g, \dots, T\} \tag{4.6}$$

$$\sum_{q=t-DT_g+1}^{t} w_{gq} \le 1 - u_{gt},\ \forall g, t \in \{DT_g, \dots, T\} \tag{4.7}$$

$$v_{gt} - w_{gt} = u_{gt} - u_{g,t-1},\ \forall g, t \tag{4.8}$$

$$P_{gt} - P_{g,t-1} \le R_g^+u_{g,t-1} + R_g^{SU}v_{gt},\ \forall g, t \tag{4.9}$$

$$P_{gt-1} - P_{g,t} \le R_g^-u_{g,t} + R_g^{SD}w_{gt},\ \forall g, t \tag{4.10}$$

$$r_{gt} \leq P_g^{Max} u_{gt} - P_{gt}, \ \forall g, t \tag{4.11}$$

$$r_{gt} \leq R_g^+, \qquad \forall g, t \tag{4.12}$$

$$\sum_{\forall g} r_{gt} \geq \alpha \tag{4.13}$$

$$u_{gt}, \in \{0,1\}, \ \forall g, t \tag{4.14}$$

$$0 \leq v_{gt} \leq 1, 0 \leq w_{gt} \leq 1, \ \forall g, t \tag{4.15}$$

In the above formulation, equation (4.1) is the objective function minimizing operating costs, no-load costs, startup costs, and shutdown costs. Constraint (4.2) is the nodal balance constraint imposing the Kirchhoff's law at each node. Constraint (4.3) represents the dc power flow on each line and (4.4) is the line-flow limit for each transmission line. Constraint (4.5) is power output lower and upper bounds for each generator. Variable u_{gt} is a binary variable indicating the commitment status of a generator. If a generator is on, $u_{gt} = 1$ and the output for that generator is constrained by its minimum and maximum output levels. If generator is off, $u_{gt} = 0$ and the output for that generator is forced to be zero. Constraints (4.6)-(4.7) are the minimum up and minimum down time constraints for each generator. Constraint (4.8) guarantees the startup (shutdown) variables to take on value 1 if a generator is started up (shutdown). Startup and shutdown variables are forced to take on binary solutions when unit commitment variables are binary variables, even though the startup and shutdown variables are modeled as continuous variables [69]. Constraints (4.9)-(4.10) are inter-temporal ramp rate constraints. The change in output for any generator should not exceed its hourly ramp rate or its startup/shutdown ramp rate if the generator is started/shutdown in period *t*. Constraints (4.11) to (4.13) are the spinning reserve constraints in the system. Constraints (4.11) indicates that if a generator is on, then the maximum spinning reserve it can provide is the difference between its maximum capacity and its current output level. Constraint (4.12) guarantees that the spinning reserve provided by a generator is no greater than its ramp rate limits. Constraint (4.13) is the total reserve requirement in the system.

4.2 Deterministic Unit Commitment Methods

Traditionally, unit commitment is solved with deterministic loads and uses certain criteria to determine the required reserves in the system. Such methods focus on analyzing the reserve requirements based on deterministic criteria, such as loss of the largest generator in the system or system import change. In [48], the authors proposed a post-stage methodology to assess the efficiencies of spinning reserve requirements determined by unit commitment. A risk index was used to evaluate if the spinning reserves scheduled were too conservative. The method was demonstrated to be effective in reducing excess spinning reserves in the system. In [49], a "System Well-being Analysis" was proposed to evaluate the system capacity reserves. By incorporating factors such as unit forced outage rates and outage replacement rates, the system health and margin indices were determined. These "system well-being indices" were used in system planning to determine the system capacity reserves. Similar work can also be found in [50], where the "system well-being indices" were used to assess the reserve requirements in system operation. In [51], a unit commitment problem with transmission and environmental constraints was proposed. In

this model, deterministic requirements were used to schedule the reserves in the system. The unit commitment model was solved by an augmented Lagrangian relaxation algorithm.

Today, deterministic unit commitment methods can be solved for large-scale and practical problems within required time windows. However, one drawback with these methods is that the scheduling of reserves in the system may not be economical and efficient, since these methods use rules based on operating experiences rather than systematic analysis. Another drawback is that these methods only consider certain expected operating conditions. In some cases, real-time conditions may significantly deviate from the expected conditions and inadequate generation may occur in the system [52].

4.3 Stochastic Unit Commitment

Compared to deterministic unit commitment, stochastic unit commitment is a relative new approach, not in terms of research but in terms of implementation. Stochastic programming endogenously incorporates uncertainty, typically represented by a set of uncertain scenarios, which often relies on pre-sampling of discrete uncertainty realizations. Results obtained with stochastic programming are robust with respect to multiple possible realizations of uncertainties modeled within the mathematical program, not only for the expected one. In [53], a stochastic unit commitment formulation is used to address the demand uncertainties and generator outages.

Most stochastic unit commitment problems are formulated as a two-stage scenario based stochastic program. In a two-stage stochastic program, a set of decisions are made in the first-stage, which cannot be changed within the second-stage. In the second-stage, random events may occur and recourse decisions are made to compensate any negative effect that the random events have. These recourse actions, which are determined by the second-stage decision variables, are generally linked to the first-stage decisions. The optimal policy from such a model is the first-stage decisions and a set of correction actions corresponding to each random event [54]. The scenario used for the first-stage is generally referred to as the base scenario. In a stochastic unit commitment problem, the first-stage decisions generally are generation dispatch and commitment status. For the second-stage, depending on the different assumptions and formulations, decisions can be only generation dispatch [55], or both generation dispatch and commitment status (the commitment status of fast start units are allowed to differ between the second-stage decisions and the first-stage decisions) [32].

To compare the differences between deterministic unit commitment and stochastic unit commitment, two figures are shown in Figure 4.1 (a) and (b). In Figure 4.1 (a), each purple hexagon represents the solution for each time period and the blue dashed circles are the reserves scheduled for each period. With deterministic unit commitment, only one state is modeled in each time interval and the transition between each state is constrained by hourly ramp rate constraints for generators, as well as minimum up and down time restrictions. However, for stochastic unit commitment, multiple scenarios are modeled in each time period as shown in Figure 4.1 (b). The purple hexagons in Figure 4.1 (b) represent base scenarios, where the blue circles are the second-stage scenarios with uncertainties incorporated, such as wind forecast errors or system element failures. The transitions between base scenarios are constrained by hourly ramp rate limits, and the second-stage

scenarios are linked to the first-stage by short-term ramp rate constraints such as 10-minute ramp rate constraints.

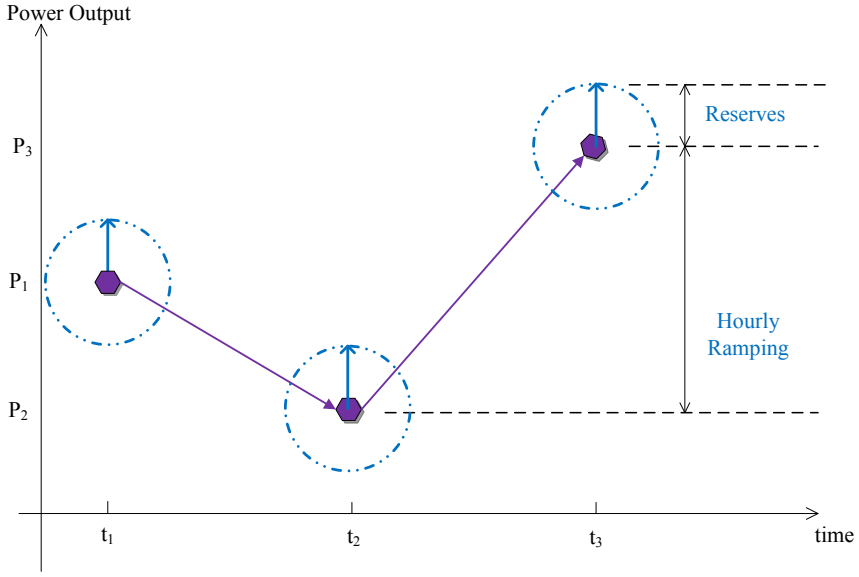

(a) Deterministic Unit Commitment

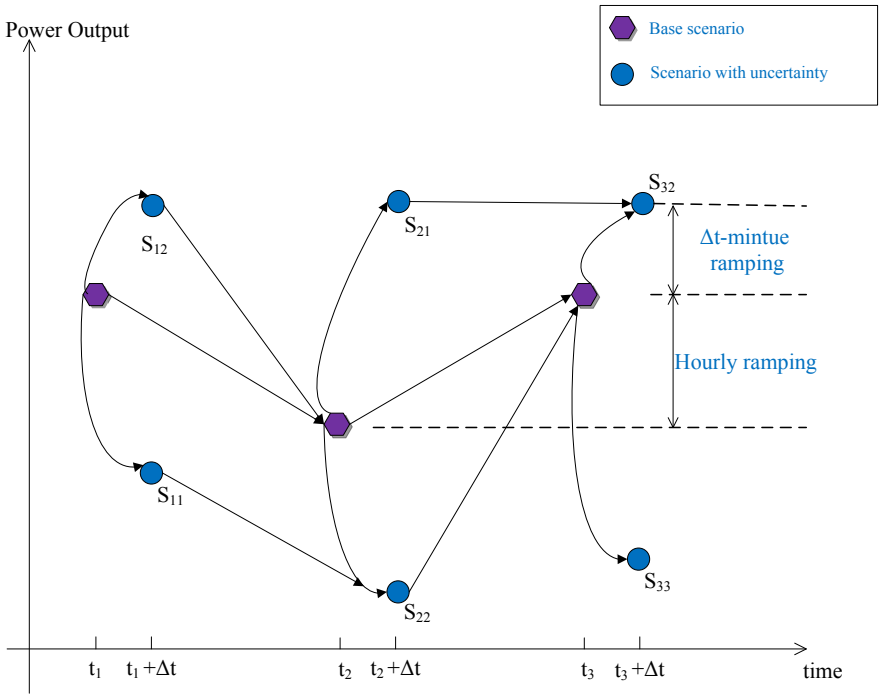

(b) Stochastic Unit Commitment

Figure 4.1 Comparison of Deterministic Unit Commitment and Stochastic Unit Commitment

The scenarios in stochastic unit commitment can be modeled to represent different uncertainties. In [60] and [61], scenarios were modeled as single transmission line and generator contingencies. In [62], scenarios were used to represent uncertainties in demand and wind generation. Reserve requirements, which are meant to satisfy N-1 compliance, can be modeled either implicitly or explicitly in stochastic unit commitment. Implicit modeling of such reserve requirements relies on deterministic policies, which are generally obtained from operating experiences. For an explicit approach, the loss of major system elements is endogenously modeled as scenarios. This is similar to an extensive form of security-constrained unit commitment (SCUC) [56], [57], where discrete failures of networks elements are explicitly considered. Sometimes the failures of single element in the system are also modeled along with other uncertainties, such as volatile wind generation in stochastic unit commitment [58]. Such an approach can account for different uncertainties and ensure the N-1 reliability of the system at the same time. However, it may significantly increase the computational complexity of the problem to the point that it is nearly impossible to solve for large-scale systems.

By simultaneously considering multiple realizations of uncertainties, stochastic unit commitment has been proved to be more reliable and cost effective than deterministic unit commitment in many applications. In [53], the authors demonstrated that stochastic unit commitment can provide significant cost savings in managing demand uncertainty and generator outage compared to a deterministic unit commitment model. In [63], a two-stage stochastic unit commitment was proposed to determine reserve requirements in the presence of wind generation. The results showed that the proposed stochastic method provided more efficient reserve schedules and reduced system total costs compared to deterministic unit commitment.

Despite its attractive advantages, two major challenges exist with stochastic unit commitment. One is the selection of scenarios and determination of their corresponding probabilities, as it is a difficult task to use only a few realizations to accurately represent a large set of uncertain events. In [63], a scenario reduction approach was proposed to select scenarios for stochastic unit commitment. The proposed method was able to capture the time-series relations of wind generation and explicitly select scenarios that may have significant impact on the solution. In [64], two scenario reduction methods were proposed for portfolio management, namely the simultaneous backward reduction and fast forward reduction methods. The backward reduction method deletes one scenario in every iteration, while the fast forward method selects one scenario in each iteration. In [66], the faster variants of the methods introduced in [64] were developed, where filtration distance was incorporated to improve the reliability of the method.

The other challenge associated with stochastic unit commitment problems is its computational complexity. While the industry still solves a deterministic unit commitment formulation today, algorithms for stochastic unit commitment are receiving increased attention and advances in techniques are being made. In [63], the authors used a Lagrange relaxation procedure to deal with the non-anticipativity constraints that bind the decisions in the first-stage to be consistent (for slow units) with the second-stage, the recourse stage. In [65], the authors proposed the use of Benders' decomposition as a mechanism to improve performance. Benders' decomposition is a row-generation technique that creates a master problem and a sub-problem and adds feasibility and optimality cuts to the master

problem based on whether the chosen master solution is feasible against the scenarios that are not captured in the master problem. The primary strength in Benders' decomposition is that the master problem often requires less memory initially but there is no guarantee that, after multiple iterations, the master problem grows in size to the extent that it is as difficult to solve as the original problem. In [67], the authors developed a progressive hedging framework and applied it to large-scale models with up to 100 scenarios; this work is being supported by the U.S. Department of Energy (DOE) Advanced Research Projects Agency-Energy (ARPA-E) Green Electricity Network Integration (GENI) program. The progressive hedging algorithm is a heuristic since it cannot guarantee a global optimal solution for MIPs; however, as [67] has shown, it performs rather well for large-scale stochastic unit commitment by producing a feasible solution with a small optimality gap.

5. Economic Assessment of Bulk Energy Storage with Significant Wind Penetration

In this chapter, a stochastic unit commitment model is used to evaluate the short-term profitability of conventional generators and energy storage under different renewable penetration levels. The formulation of stochastic unit commitment is presented, which also takes into account the cost of ramping for the conventional generators. A brief review of wind scenario modeling techniques is presented and a wind scenario modeling approach is described. The short-term profitability of conventional generators and energy storage units are compared under increasing renewable penetration levels to identify the impact on the attractiveness of bulk energy storage in comparison to conventional generators.

5.1 Background and Motivation

Traditionally, conventional generators (CG) have been used as the solution to compensate variability and uncertainty in renewable generation. However, under high levels of renewable resources, the role of conventional generators will transition from primarily supplying energy to providing reserves and backup generation for intermittent renewable resources. As a result, conventional generators will be operating at low output levels or be used as standby generation. At low operating levels, most conventional generators will have higher average costs and lower marginal costs as shown by Figure 5.1. As the locational marginal prices (LMPs) reflect the marginal cost of the "marginal unit" in the system, the LMPs in the system are likely to decrease. On the other hand, since the fuel costs of wind generation can be considered to be zero, the increase in penetration of renewable resources is expected to further drive down energy prices, which may decrease the profits that conventional generators receive on top of having an increase in average costs and a reduction in the overall utilization of the generator. Under high levels of variable resources, conventional generators may have to frequently adjust their outputs to provide system operating reserve and frequency regulation services. This imposed ramping requirement on conventional generators may degrade the efficiency and increase the emissions per MWh of conventional generators. The above factors may substantially decrease the incentive to invest in conventional generation under high levels of renewable penetration.

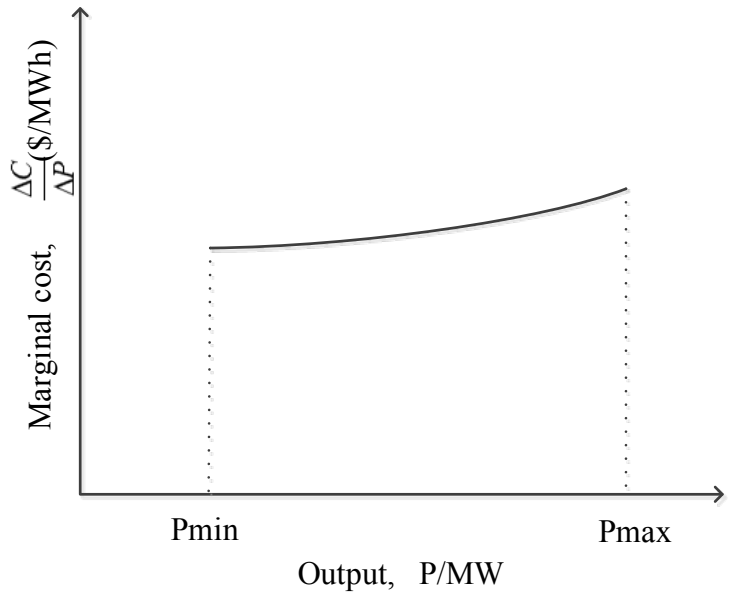

(a) Generator Marginal Cost Curve

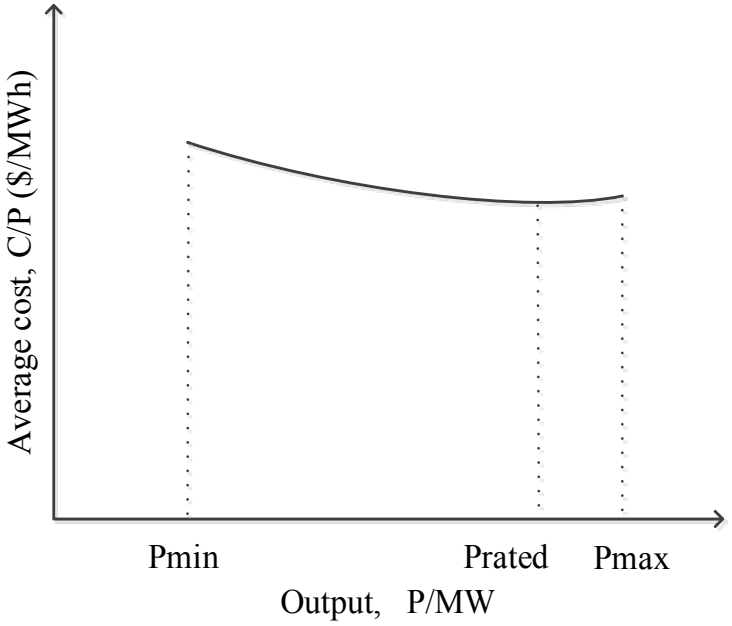

(b) Generator Average Cost Curve

Figure 5.1 Typical Conventional Generator Cost Curves

With the stringent fleet challenges introduced by renewable resources, the need for flexible resources in power systems is higher than ever. Since energy storage can absorb excess clean energy and shift it to hours when scheduled generation cannot meet demand, bulk energy storage has the potential to become competitive under high renewable penetration levels. Meanwhile, their fast ramping capability provides energy storage the ability to better manage the uncertainty and intermittency in renewable generation. Yet the primary

barrier with bulk energy storage is their high investment costs. California is the first US state to create an energy storage target [7]; note, however, that there is a specified MW target but no specified MWh target. In this chapter, studies are conducted to evaluate and compare the short-term profitability of conventional generators and energy storage under different renewable penetration levels.

5.2 Mathematical Formulation and Methodology

In this report, a two-stage stochastic unit commitment model, which takes into account multiple wind generation scenarios, is used. The model represents a traditional day-ahead generation scheduling problem with an hourly based interval. By using stochastic unit commitment, the uncertainties in wind generation are endogenously captured in the formulation.

5.2.1 Energy Storage Model

Pumped hydro storage and compressed air energy storage are included in this study, since they are the two most attractive large-scale options with low capital costs, low maintenance costs, and long life expectancies [68]. Since PHS and CAES are operated in similar ways, they can be modeled as shown in (5.1)-(5.5). The constraints include reservoir balance constraints (5.1), upper and lower bounds of power absorption and generation (5.2)-(5.3), initial and target reservoir levels (5.4), lower and upper bounds of the capacity of reservoir (5.5), and a binary variable indicating whether the PHS or CAES is in generation mode (z_{gkt}=1) or pumping/compression mode (z_{gkt}=0).

$$S_{gkt} = S_{gk,t-1} + P_{gkt}^{In}\eta_g^{In} - P_{gkt}^{Out}/\eta_g^{Out}, \forall g,k,t \tag{5.1}$$

$$L_g^{In}\left(1 - z_{gkt}\right) \le P_{gkt}^{In} \le U_g^{In}\left(1 - z_{gkt}\right), \forall g,k,t \tag{5.2}$$

$$L_g^{Out} z_{gkt} \le P_{gkt}^{Out} \le U_g^{Out} z_{gkt}, \forall g,k,t \tag{5.3}$$

$$S_{gk0} = S_{gkT}, \forall g,k \tag{5.4}$$

$$S_g^{Min} \le S_{gkt} \le S_g^{Max}, \forall g,k,t \tag{5.5}$$

$$z_{gkt} \in \{1,0\}, \forall g \in \{\Omega_C, \Omega_P\}, k, t \tag{5.6}$$

In the above formulation, it is assumed that the input power consumed during pumping mode can be varied continuously for pumped hydro storage. However, this is valid only for adjustable-speed pumped storage units. For traditional single-speed pumped hydro storage, input power consumed in pumping mode by each machine is fixed and water can only be pumped in blocks. A detailed discussion on the modeling of single-speed pumped hydro storage is presented in chapter 6. In this chapter, it is assumed that pumped hydro storage can have continuous power consumption in pumping mode and the above simplified model is used.

5.2.2 Stochastic Unit Commitment Model

A general stochastic unit commitment model is used in this paper, which is formulated as a mixed integer linear program (MILP). The model is assumed to be lossless. The objective function of the unit commitment model, which is shown in (5.7), is to minimize system total cost, which includes generator operating costs, no-load costs, startup costs, and ramping costs. The ramping cost terms in the objective function, $c_g^R(P_{gkt})$ and $c_g^R(P_{gkt}^{Out})$, are calculated using (5.12). The ramping cost terms represent the cost associated with generators during the 10-minute ramping process. Since generators may have different efficiencies when operating at a constant output compared to when they ramp, the term α is used to approximate the inefficiencies of generators during the ramping process. The complete unit commitment model is shown in (5.7)-(5.33).

Minimize

$$\sum_{k=1}^{K}\pi_k\sum_{t=1}^{T}\Big\{\sum_{g\in\Omega_G}\big[c_gP_{gkt}+c_g^R\big(P_{gkt}\big)\big]+\sum_{g\in\Omega_C}\big[c_gP_{gkt}^{Out}+c_g^R\big(P_{gkt}^{Out}\big)\big]+$$

$$\sum_{g\in\{\Omega_C,\Omega_G\}}\big[c_g^{NL}u_{gkt}+c_g^{SU}v_{gkt}\big]\Big\} \tag{5.7}$$

Subject to:

$$\sum_{\forall g(n)}^{g\in\Omega_G}P_{gkt}+\sum_{\forall g(n)}^{g\in\{\Omega_C,\Omega_G\}}\big(P_{gkt}^{Out}-P_{gkt}^{In}\big)+\sum_{\delta^+(n)}P_{mkt}-\sum_{\delta^-(n)}P_{mkt}=$$

$$d_{nkt}-\sum_{\forall g(n)}^{g\in\Omega_W}P_{gkt}^{Wind},\forall n,k,t \tag{5.8}$$

$$P_{mkt}=B_m(\theta_{mkt}^{+}-\theta_{mkt}^{-}),\forall m,k,t \tag{5.9}$$

$$-P_m^{Max}\le P_{mkt}\le P_m^{Max},\forall m,k,t \tag{5.10}$$

$$P_g^{Min}u_{gkt}\le P_{gkt}\le P_g^{Max}u_{gkt},\ \forall g\in\Omega_G,k,t \tag{5.11}$$

$$c_g^R\big(P_{gkt}\big)=\sum_{l=1}^{L}c_{gl}\big[\tfrac{(2l-1)\left(P_{gk,t}-P_{g0t}\right)}{2L}+P_{g0t}\big],\ \forall g\in\{\Omega_G,\Omega_C\},k,t \tag{5.12}$$

$$v_{g0t}-w_{g0t}=u_{g0t}-u_{g0,t-1},\ \forall g\in\{\Omega_C,\Omega_G\},k,t \tag{5.13}$$

$$\sum_{q=t-UT_g+1}^{t}v_{g0q}\le u_{g0t},\ \forall g\in\Omega_G,t\in\big\{UT_g,\dots,T\big\} \tag{5.14}$$

$$\sum_{q=t-DT_g+1}^{t}w_{g0q}\le 1-u_{g0t},\ \forall g\in\Omega_G,t\in\big\{DT_g,\dots,T\big\} \tag{5.15}$$

$$r_{gkt}\ge 0,\ \forall g\in\{\Omega_C,\Omega_G,\Omega_P\},k,t \tag{5.16}$$

$$r_{gkt}\le P_g^{Max}u_{gkt}-P_{gkt},\forall g\in\Omega_G,k,t \tag{5.17}$$

$$r_{gkt} \le R_g^{10+}, \forall g \in \Omega_G, k, t \tag{5.18}$$

$$r_{gkt} \le U_g^{Out} z_{gkt} - P_{gkt}^{Out} + P_{gkt}^{In}, \forall g \in \Omega_C, k, t \tag{5.19}$$

$$r_{gkt} \le U_g^{Out} - P_{gkt}^{Out} + P_{gkt}^{In}, \forall g \in \Omega_P, k, t \tag{5.20}$$

$$r_{gkt} \le \beta_g \eta_g^{Out} S_{gkt}, \forall g \in \{\Omega_C, \Omega_P\}, k, t \tag{5.21}$$

$$r_{gkt} \le \beta_g \eta_g^{In} S_{gk,t-1} + P_{gkt}^{In}, \forall g \in \{\Omega_C, \Omega_P\}, k, t \tag{5.22}$$

$$0 \le r_{gkt}^{NS} \le R_g^{NS}(1 - u_{gkt}), \forall g \in \{\Omega_G\}, k, t \tag{5.23}$$

$$P_{g0t} - P_{g0,t-1} \le R_g^{+} u_{g0,t-1} + R_g^{SU} v_{g0t}, \ \forall g \in \Omega_G, t \tag{5.24}$$

$$P_{g0,t-1} - P_{g0,t} \le R_g^{-} u_{g0,t} + R_g^{SD} w_{g0,t}, \ \forall g \in \Omega_G, t \tag{5.25}$$

$$-R_g^{10-} \le P_{gkt} - P_{g0,t} \le R_g^{10+}, \ \forall g \in \Omega_G, k, t \tag{5.26}$$

$$-R_g^{-} \le P_{g0,t}^{Out} - P_{g0,t-1}^{Out} \le R_g^{+}, \ \forall g \in \{\Omega_C, \Omega_P\}, k, t \tag{5.27}$$

$$-R_g^{10-} \le P_{gk,t}^{Out} - P_{g0,t}^{Out} \le R_g^{10+}, \ \forall g \in \{\Omega_C, \Omega_P\}, k, t \tag{5.28}$$

$$-R_g^{-} \le P_{g0,t}^{In} - P_{g0,t-1}^{In} \le R_g^{+}, \ \forall g \in \{\Omega_C, \Omega_P\}, k, t \tag{5.29}$$

$$-R_g^{10-} \le P_{gk,t}^{In} - P_{g0,t}^{In} \le R_g^{10+}, \ \forall g \in \{\Omega_C, \Omega_P\}, t \tag{5.30}$$

$$u_{gkt}, \in \{0,1\}, \ \forall g \in \Omega_G, k, t \tag{5.31}$$

$$z_{gkt} \in \{0,1\}, \forall g \in \{\Omega_C, \Omega_P\}, k, t \tag{5.32}$$

$$0 \le v_{gkt} \le 1, \ 0 \le w_{gkt} \le 1, \ \forall g, k, t \tag{5.33}$$

5.2.3 Power Flow Constraints and Startup and Shutdown Constraints

Nodal balance constraint is shown in (5.8), where bus injections are assumed to be positive and withdrawals negative. Line flow constraints are described in (5.9) and (5.10). Generator output limit constraint is shown in (5.11). Constraint (5.13) describes the relationships between unit commitment variables and startup and shutdown variables. The minimum up and down time constraints for conventional generators are shown in (5.14) and (5.15), which are similar to those introduced in chapter 4. Minimum up and down time constraints are not required for pumped hydro storage and compressed air energy storage, since they are considered to be fast units that can be turned on within one hour. Fast units

are defined to be the units that have minimum up and down time shorter or equal to one hour and can turn on within ten minutes, while slow units are generators with minimum up and down time longer than one hour.

5.2.4 System Spinning and Non-Spinning Reserve Constraints

The system spinning reserve requirements used in the above formulation follows the one that used in the California ISO system. It is required that the spinning reserve in the system should account for 50% of the system operating reserve. Operating reserve in the system should be greater than 5% of the hydro generation plus 7% of generation from other fuel types, or the single largest generator contingency in the system, whichever is greater [70].

Constraints (5.16) - (5.18) are spinning reserve requirements on conventional generators. Constraints (5.19) - (5.22) represent the spinning reserve requirements for pumped hydro storage and compressed air energy storage units. Constraint (5.19) indicates that, since a compressed air energy storage unit cannot transition from compression mode to generation mode within 10 minutes, the maximum spinning reserve it can provide is either P_{gkt}^{In} in compression mode, or $U_g^{Out} - P_{gkt}^{Out}$ in generation mode. Constraint (5.20) is only enforced for pumped hydro storage units. For a pumped hydro storage unit, it can turn on and ramp up to full capacity within less than ten minutes. Therefore, if a pumped hydro storage unit is in pumping mode, the maximum reserve it can provide is $U_g^{Out} + P_{gkt}^{In}$, which indicates that a pumped hydro storage unit can provide spinning reserve by stop pumping and transition to generation mode to provide power. If a pumped hydro storage unit is in generation mode, the maximum spinning reserve it can provide is $U_g^{Out} - P_{gkt}^{Out}$. Constraints (5.21) requires the spinning reserve provided by energy storage units in period *t* should be no greater than the energy stored by the end of period *t*. The parameter β_g is a coefficient converting energy into power. Constraint (5.22) guarantees that the spinning reserve provided by energy storage unit in period *t* is no greater than the energy stored by the end of period *t-1* plus the absorbing power during period *t*. The non-spinning reserve constraint for conventional generators is shown in (5.23).

5.2.5 Ramp Rate Constraints

The ramp rate constraints for conventional generators are shown in (5.24) – (5.26), where constraint (5.24) and (5.25) are inter-temporal ramp rate constraints, and constraint (5.26) is 10-minute ramp rate constraint. Ramp rate constraints for pumped hydro storage and compressed air energy storage units are shown in (5.27)-(5.30). Constraints (5.27) and (5.29) are inter-temporal ramping constraints for energy storage. And constraints (5.28) and (5.30) are 10-minute ramp rate constraints for energy storage.

5.2.6 Modeling of Ramp Rate Constraints and Uncertainties

While stochastic unit commitment can provide robust solutions, the multiple scenarios incorporated and the large number of constraints that couple the scenarios together make stochastic unit commitment a very computational challenging problem. Therefore, the accuracy and computation complexity should be balanced in the formulation of stochastic

unit commitment. A figure describing the modeling of ramp rate and uncertainties in this work is shown in Figure 5.2. The purple hexagons in Figure 5.2 represent base scenarios with actual wind forecast, while the blue circles represent wind scenarios with forecast errors. To accurately capture the ramp rate requirements in presence of intermittent wind generation, generator ramp rate constraints should be modeled between any base scenarios and scenarios with wind forecast errors. However, the combinatorial nature of this approach will significantly increase the number of constraints and the computational complexity of the problem. Therefore, to strike a balance between accuracy and computational complexity, hourly ramp rate constraints are only enforced between base case scenarios, i.e., only between the purple hexagons in Figure 5.2. And the 10-minute ramp rate constraints are only enforced between the base case and the second-stage scenarios in the same time interval, i.e., between hexagon and any purple circles in the same time interval *t*. It is assumed that if the system has enough flexibility in generation to manage transitions described in Figure 5.2, the system will also have enough flexibility to meet all the other ramping requirements that are omitted in this formulation.

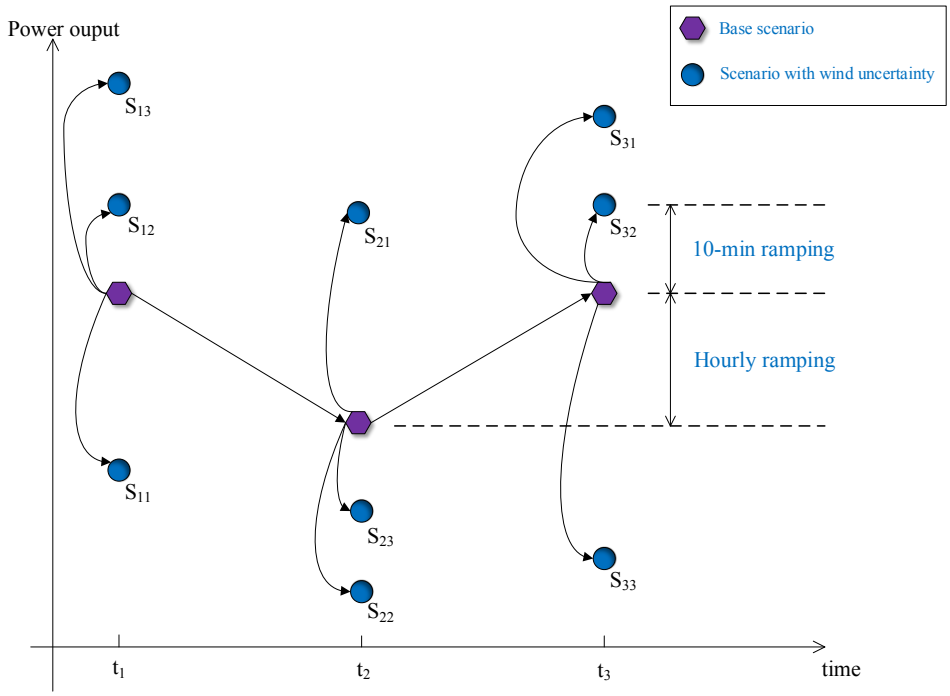

Figure 5.2 Modeling of Ramp Rate Constraints and Wind Uncertainties

5.3 Renewable Modeling

5.3.1 Brief Review on Wind Forecast Methods

Wind scenario generation can be performed by using different wind forecast models. Numeric weather prediction (NWP) is a physical model using weather data and advanced meteorological techniques for wind forecasting [72]-[73]. Due to the large computational burden of NWP, it is usually used for day-ahead forecast. Statistical models, such as

autoregressive integrated moving average (ARIMA) and their variants, [74]-[75], can also be used in wind scenario generation. Such models use historical data, pattern identification, and mathematical approaches to produce forecast. The implementation of such models, for wind scenario generation, is discussed in [76]. Spatial correlation models take the spatial relationship of different wind farms into account. The spatial correlation method is usually combined with other methods, such as the method combing fuzzy logic and spatial correlation, [77], and the ANFIS-based method using spatial correlation, [78].

5.3.2 Wind Scenario Generation

In this work, wind forecast data for different wind farms was obtained from NREL Wind Integration Datasets [79]. The method described in [80] was implemented to generate wind scenarios. One thousand wind scenarios were generated using Monte-Carlo simulation. For each time period *t*, the wind forecast error was assumed to follow a truncated Gaussian distribution $N(0,\sigma^2)$ with zero mean and variance σ^2. A truncated normal distribution with $a \le x \le b$ can be expressed as

$$p_X(x) = \begin{cases} 0 & x < a \\ \dfrac{\frac{1}{\sigma}\phi(\frac{x-\mu}{\sigma})}{\frac{1}{\sigma}\Phi\left(\frac{b-\mu}{\sigma}\right) - \frac{1}{\sigma}\Phi(\frac{a-\mu}{\sigma})} & a \le x \le b \\ 0 & x > b \end{cases} \tag{5.34}$$

where $\phi(x)$ is the probability density function for standard normal distribution and$\Phi(x)$is its cumulative distribution function. The truncation process is expressed as

$$P_w = P_{aw} - \varepsilon_w P_w^{cap}, \;\; \varepsilon_w^{min} \le \varepsilon_w \le \varepsilon_w^{max} \tag{5.35}$$

where P_w is the generated wind output, P_{aw} is the forecasted wind generation obtained from NREL Wind Datasets, P_w^{cap} is the maximum capacity for the corresponding wind farm, and ε_w is the forecast error following a truncated Gaussian distribution $N(0,\sigma^2)$ with $\varepsilon_w^{min} \le \varepsilon_w \le \varepsilon_w^{max}$. The minimum and maximum error ε_w^{min} and ε_w^{max} are determined as

$$\varepsilon_w^{min} = \begin{cases} -3\sigma & ,if\ Indx_{min} < P_w^{cap} \\ \dfrac{P_w}{P_w^{cap}} - 1 & ,if\ Indx_{min} \ge P_w^{cap} \end{cases} \tag{5.36}$$

$$\varepsilon_w^{max} = \begin{cases} 3\sigma & ,if\ Indx_{max} \ge 0 \\ \dfrac{P_w}{P_w^{cap}} & ,if\ Indx_{max} < 0 \end{cases} \tag{5.37}$$

where

$$Indx_{min} = P_{aw} + 3\sigma P_w^{cap} \tag{5.38}$$

$$Indx_{max} = P_{aw} - 3\sigma P_w^{cap} \quad (5.39)$$

Equations (5.36)-(5.39) truncate the distribution of forecast error such that 1) the forecast errors were within three standard deviations of the corresponding distribution; 2) the resulted wind generation was between zero and the maximum capacity of the wind generator. In [81] and [82], the typical forecast error for day-ahead forecasting was reported to be 10% to 20%. To reflect the practical forecast error reported in literature, σ was chosen to create an error of roughly 16%.

Due to the computational complexity and time limitations, including a large number of scenarios in stochastic unit commitment is not practical. A scenario reduction technique was used to reduce the number of scenarios to a predetermined number. In this paper, a backward reduction method introduced in [83] and [64] was employed to select ten scenarios out of one thousand to be used within the stochastic unit commitment. The backward reduction technique deletes the scenarios that have the minimum distance of the scenario pair. The probability of deleted scenarios is allocated to the remaining scenario.

5.4 Methodology

The methodology used in this work is described as follows. In the first step, Monte-Carlo simulation is performed to generate wind scenarios. A thousand wind scenarios are generated and ten scenarios are selected and used in the stochastic unit commitment problem. In the second step, the stochastic unit commitment is solved for different renewable penetration levels. In the third step, the resulting unit commitment solutions are tested against one-thousand wind scenarios (via Monte-Carlo simulations) to determine if the solutions can satisfy load under all wind scenarios for the corresponding penetration levels. After the wind scenario analysis, N-1 contingency analysis, combined with selected wind scenarios, is conducted to test if the system can withstand the loss of any single element while compensating for potential wind deviations as well. A flow chart summarizing the methodology is shown in Figure 5.3.

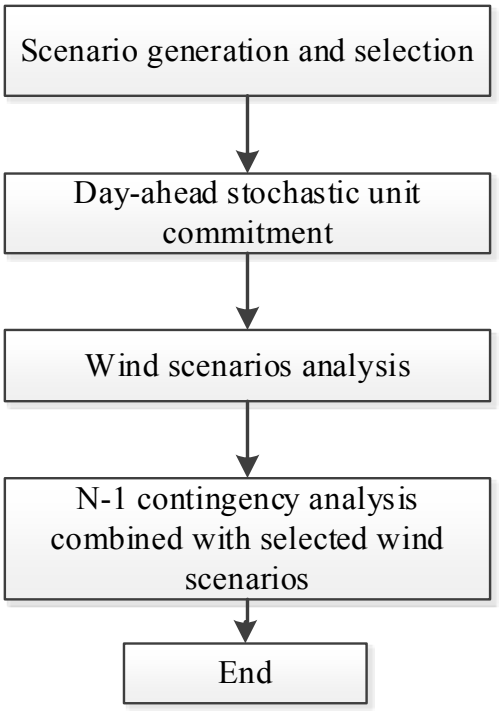

Figure 5.3 Day-Ahead Generation Scheduling Flowchart

5.4.1 Mathematical Formulation of Wind Scenario Analysis

Once day-ahead stochastic unit commitment is solved, generation dispatch, commitment status, spinning reserves, and non-spinning reserves are determined. Wind scenario analysis is then conducted to test the unit commitment solutions against all the wind scenarios generated from Monte-Carlo simulation. The purpose of wind scenario analysis is to test if the day-ahead solutions can supply the system demand under wind uncertainties. With scheduled generation dispatch and commitment status, operating reserves are dispatched in wind scenario analysis to address the deviations in wind generation from its forecasted value. If violations (e.g. involuntary load shedding) are reported, security corrections should be performed to correct such violations in the system. In this work, a price of $3000/MW was used to approximate the costs to correct such violations. Wind scenario analysis is formulated as a dc OPF problem with objective to minimize total operating costs, ramping costs, and security correction costs. The objective function of the dc OPF is shown in (5.40). The complete formulation of the constraints is presented in (5.41) - (5.50).

Minimize:

$$\sum_{g\in\Omega_G}\left[c_g P_g + c_g^R\left(P_g\right)\right] + \sum_{g\in\Omega_C}\left[c_g P_g^{Out} + c_g^R\left(P_g^{Out}\right)\right] + \sum_{n=1}^{NB} c_n^v\, s_n \tag{5.40}$$

Subject to:

$$P_g^{Min} u_{g0t} \le P_g \le P_g^{Max} u_{g0t}, \forall g \in \Omega_{Gs} \tag{5.41}$$

$$P_{g0t} - r_g \le P_g \le P_{g0t} + r_g, \forall g \in \Omega_{Gs} \tag{5.42}$$

$$0 \le P_g \le P_g^{Max}, \forall g \in \Omega_{Gf} \tag{5.43}$$

$$P_{g0t} - R_g^{10-} \le P_g \le P_{g0t} + R_g^{10+} u_{g0t} + R_g^{NS}(1 - u_{g0,t-1}), \forall g \in \Omega_{Gf} \tag{5.44}$$

$$\sum_{\forall g(n)}^{g\in\Omega_G} P_g + \sum_{\forall g(n)}^{g\in\{\Omega_P,\Omega_C\}}\left(P_g^{Out} - P_g^{In}\right) + \sum_{\delta^+(n)} P_m - \sum_{\delta^-(n)} P_m$$

$$= d_n - \sum_{\forall g(n)}^{g\in\Omega_W} P_g^{Wind} - s_n + w_n, \forall n \tag{5.45}$$

$$c_g^R\left(P_g\right) = \sum_{l=1}^{L} c_{gl}\left[\frac{(2l-1)\left(P_g - P_{g0t}\right)}{2L} + P_{g0t}\right], \forall g \in \{\Omega_G, \Omega_C\} \tag{5.46}$$

$$P_m = B_m(\theta_m^+ - \theta_m^-), \forall m \tag{5.47}$$

$$-P_m^{Max} \le P_m \le P_m^{Max}, \forall m \tag{5.48}$$

$$0 \le s_n \le d_n \tag{5.49}$$

$$0 \le w_n \le \sum_{\forall g(n)}^{g\in\Omega_W} P_g^{Wind} \tag{5.50}$$

Constraints (5.41) - (5.44) represent the operating range for generators in wind scenario analysis. Constraint (5.41) is the minimum and maximum capacity for slow generators. Variable u_{g0t} in (5.41) is the base-scenario commitment status determined from day-ahead generation schedule. Constraint (5.41) indicates that the commitment status for a slow unit in wind scenario analysis should be the same as the one in the stochastic unit commitment. The operating range for a slow generator is its scheduled generation plus and minus its scheduled reserve, which is shown in (5.42). Variable P_{g0t} is the scheduled dispatch for generator g in base scenario. Since fast generators can be started within ten minutes, their lower generation bounds are assumed to be zero in wind scenario analysis. The maximum output level for fast generators in wind scenario analysis are assumed to be the minimum of its capacity or scheduled dispatch plus 10-minute ramp rate (or non-spinning reserve ramp rate). The constraints on operating range for fast units are shown in (5.43) and (5.44). Nodal balance constraint is shown in (5.45). Variable s_n and w_n are slack variables representing nodal power balance violations and wind spillage at each bus. Constraint (5.46) represents the ramping costs incurred during the 10-minute ramping process.

Constraint (5.47) formulates the dc power flow on each line and (5.48) is the line-flow limit for each transmission line. Constraints (5.49) and (5.50) guarantee that s_n and w_n are non-negative variables and they cannot exceed the maximum load and wind generation at each bus respectively.

A flowchart showing the procedure used in wind scenario analysis is shown in Figure 5.4. Day-ahead solutions are first obtained from the stochastic unit commitment. Then dc OPF is performed to test the solutions against each wind scenario *k* in each time period *t*. Wind generation and system load is updated each time before dc OPF is solved. After all the wind scenarios are tested, results from each dc OPF are used to calculate system reliability metrics, such as expected costs for violations, expected wind spillage, and the number of violations during wind scenario analysis.

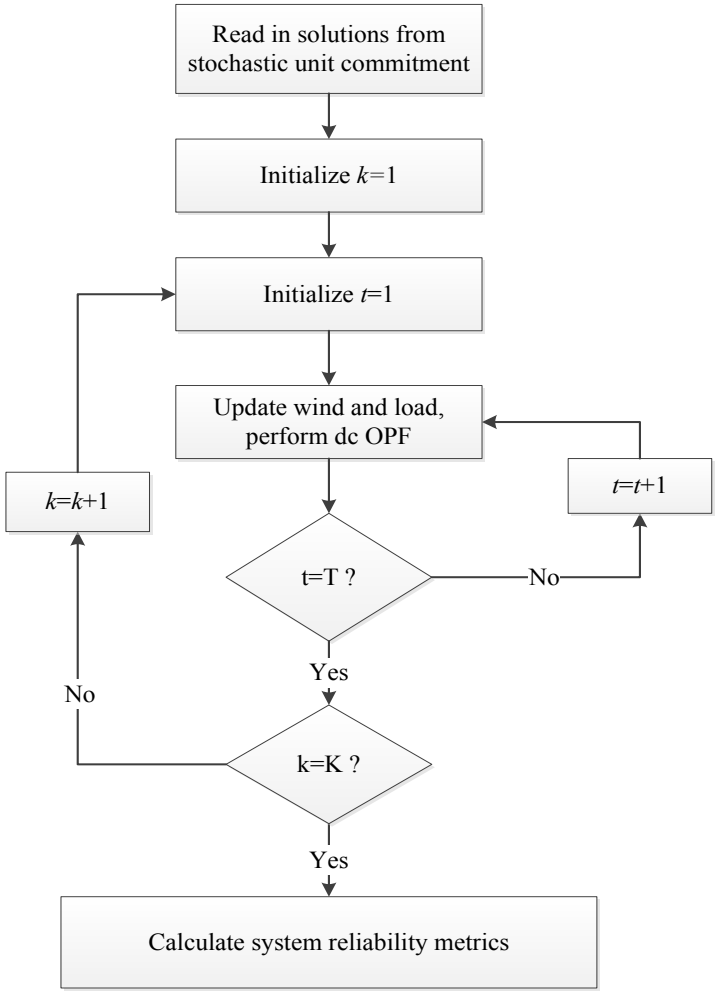

Figure 5.4 Flowchart for Wind Scenario Analysis

5.4.2 Mathematical Formulation of N-1 Contingency Analysis

N-1 contingency analysis simulates the post-contingency operating condition within ten minutes of the occurrence of a single transmission line or generator outage in the system. N-1 contingency analysis is performed combined with the selected wind scenarios to test if the system can withstand the loss of a single transmission line or generator under wind uncertainties. Similar to wind scenario analysis, N-1 contingency analysis is formulated as a dc OPF problem, of which the objective is to minimize system operating costs, ramping costs, and security corrections costs. The complete formulation is shown in (5.51)-(5.61).

Minimize:

$$\sum_{g\in\Omega_G}\left[c_g P_g + c_g^R\left(P_g\right)\right] + \sum_{g\in\Omega_C}\left[c_g P_g^{Out} + c_g^R\left(P_g^{Out}\right)\right] + \sum_{n=1}^{NB} c_n^v\, s_n \tag{5.51}$$

Subject to:

$$P_g^{Min} u_{g0t} N_g^C \le P_g \le P_g^{Max} u_{g0t} N_g^C, \forall g \in \Omega_{Gs} \tag{5.52}$$

$$(P_{g0t} - r_g) N_g^C \le P_g \le (P_{g0t} + r_g) N_g^C, \forall g \in \Omega_{Gs} \tag{5.53}$$

$$0 \le P_g \le P_g^{Max} N, \forall g \in \Omega_{Gf} \tag{5.54}$$

$$\left(P_{g0t} - R_g^-\right) N_g^C \le P_g \le \left[P_{g0t} + R_g^+ u_{g0t} + R_g^{NS}\left(1 - u_{g0,t-1}\right)\right] N_g^C, \forall g \in \Omega_{Gf} \tag{5.55}$$

$$\sum_{\forall g(n)}^{g\in\Omega_G} P_g + \sum_{\forall g(n)}^{g\in\{\Omega_P,\Omega_C\}}\left(P_g^{Out} - P_g^{In}\right) + \sum_{\delta^+(n)} P_m - \sum_{\delta^-(n)} P_m$$

$$= d_n - \sum_{\forall g(n)}^{g\in\Omega_W} P_g^{Wind} - s_n + w_n, \forall n \tag{5.56}$$

$$c_g^R\left(P_g\right) = \sum_{l=1}^{L} c_{gl}\left[\frac{(2l-1)\left(P_g - P_{g0t}\right)}{2L} + P_{g0t}\right], \forall g \in \{\Omega_P, \Omega_C\} \tag{5.57}$$

$$P_m = B_m N_m^C (\theta_m^+ - \theta_m^-), \forall m \tag{5.58}$$

$$-P_m^{Max} N_m^C \le P_m \le P_m^{Max} N_m^C, \forall m \tag{5.59}$$

$$0 \le s_n \le d_n \tag{5.60}$$

$$0 \le w_n \le \sum_{\forall g(n)}^{g\in\Omega_W} P_g^{Wind} \tag{5.61}$$

The constraints used in N-1 contingency analysis include output limits for generators (5.52)-(5.55), nodal power balance constraints (5.56), ramping costs constraint (5.46), dc power line flow constraint (5.58), transmission line thermal limit constraint (5.59), and constraints on voluntary load shedding and wind spillage variables (5.60), (5.61). Except

constraints (5.52)-(5.55), (5.58) and (5.59), all the other constraints are identical to those used in wind scenario analysis. The parameter N_g^G in (5.52)-(5.55) is a contingency index parameter indicating whether if generator g is in contingency condition in contingency scenario c. Similarly, the parameter N_m^L in constraints (5.58) and (5.59) is the contingency index parameter indicating whether transmission line m is in contingency condition in contingency scenario c. A flowchart describing the procedures used in N-1 contingency analysis is shown in Figure 5.5.

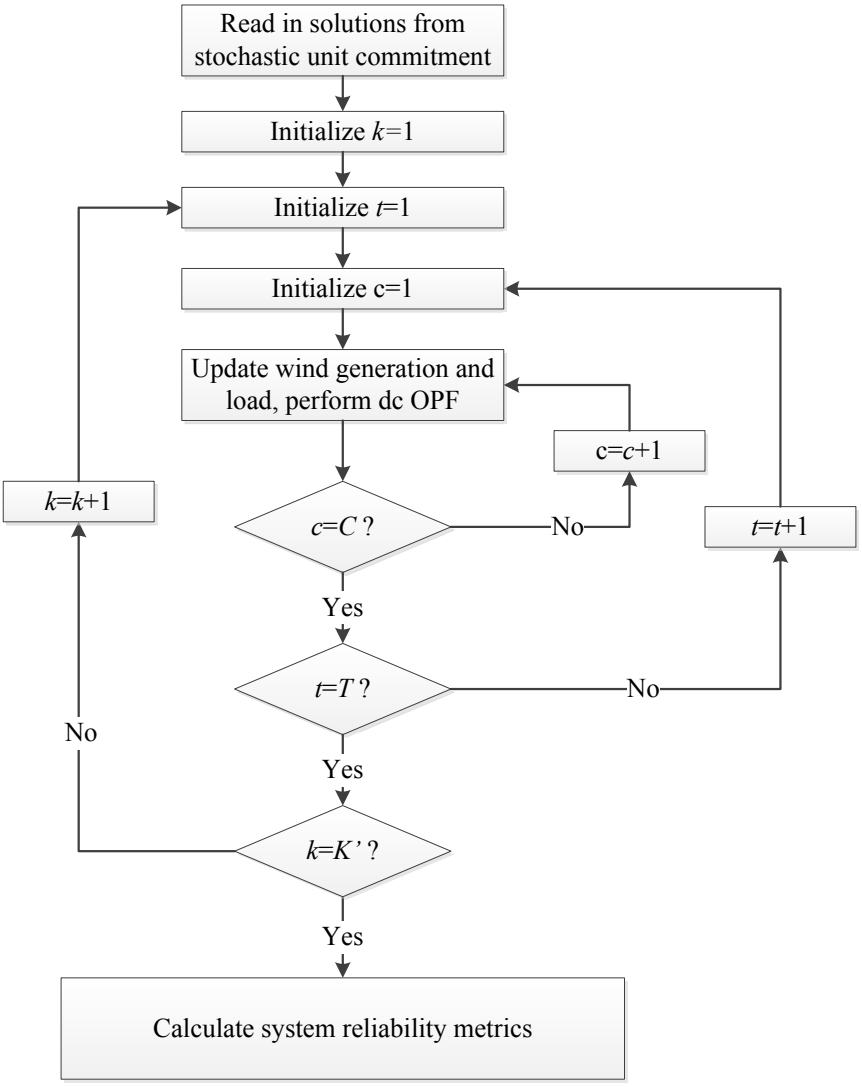

Figure 5.5 Flowchart for N-1 Contingency Analysis

5.5 Numerical Results

A modified RTS96 one-zone model [84], [85] was used to conduct the study. The original one-zone model has 32 generators, 24 buses and 17 loads. The total generation capacity in the system is 3402 MW, while the system peak load is 2850 MW. The six hydro generators in the system were replaced with one oil-fired and one coal-fired generator; the total

generation capacity remained the same as before. The ramping coefficient α was assumed to be 0.05. Wind penetration levels from 30% to 70% with 10% increments were studied, where the wind penetration level is defined as the ratio of total daily wind generation to the total system daily demand.

As wind penetration levels increase, it is imperative to accurately model the correlations of the renewable production. Under high wind penetration levels, the geographical spreading of wind farms is likely to increase. Since wind speed has relative weak correlation for long distances [63], geographical diversity will attenuate the system-wide wind forecast uncertainty. To represent the smoothing effect resulting from the widely dispersed wind farms, wind generation was not scaled up using a multiplier as penetration levels increase. Instead, for each 10% penetration increment, a wind farm with different wind profile and wind scenarios was added. Wind data for January 3rd was collected from NREL Wind Integration Datasets. The original 10-min wind data was averaged into hourly data and was used as the predicted wind power output in the simulation. Wind spillage was allowed in the unit commitment model.

5.5.1 Impact of Increasing Wind Penetration Levels on Conventional Generators

The primary interest in this subsection is to quantify the economic efficiencies of conventional generators under high wind penetration levels. The day-ahead stochastic unit commitment problem was solved for increasing wind penetration levels and the results are presented in Table 5.1. The first column in Table 5.1 shows the targeted wind penetration levels. As wind spillage is allowed, the actual wind generation dispatched in the system is presented in Table 5.2. Since the test bed system has limited capability to accommodate large amounts of wind generation, the actual wind generation dispatched in the system is less than the targeted wind penetration levels. Although the actual wind dispatched in the system did not achieve the targeted penetration levels, the actual dispatched wind generation increases as the targeted wind penetration level increases. To accommodate more wind generation into the system, more flexible generation should be incorporated into the study. The results in the paper can be interpreted as the evaluation of economic efficiencies for conventional generators under increasing "actual" wind penetration levels.

In Table 5.1, four metrics are used to evaluate the economic efficiencies of conventional generators, namely the expected hourly average cost per unit, expected capacity factor per unit, expected hourly utilization rate per unit, and the total number of dispatched units in the system. The expected hourly average cost is calculated as

$$C_{EAC} = \sum_g \frac{\sum_t \sum_k (\frac{C_{gkt}^{Total}}{E_{gkt}})\pi_k}{\sum_t \sum_k t_{gkt}^{on}\pi_k} \Big/ N_g^{On} \tag{5.62}$$

where E_{gkt} and C_{gkt}^{Total} are the energy generated and total cost in hour t and scenario k for generator g respectively, and N_g^{On} the number of units dispatched in the system. Variable t_{gkt}^{on} takes on a value of 1 if generator g is online in period t scenario k, and 0 otherwise. The term C_{gkt}^{Total} is the total cost for generator g in each hour and scenario, which includes variable costs, no-load costs, startup costs, and ramping costs. The expected utilization rate is calculated as

$$U_{\%} = \sum_g \frac{\sum_t \sum_k (\frac{P_{gkt}}{P_{gkt}^{Max}}) \pi_k}{\sum_t \sum_k t_{gkt}^{on} \pi_k} \Big/ N_g^{On} \tag{5.63}$$

This metric is used to measure the hourly utilization levels of dispatched conventional generators.

As shown in Table 5.1, the expected hourly average cost for a conventional generator increases in general as the wind penetration level increases. This result is consistent with the typical fossil-fuel fired generator average cost curve as shown in Figure 5.1. Under high wind penetration levels, conventional generators will operate at low output levels and mainly be used as backup generation. Due to large fixed costs, fossil-fuel fired generators have higher average costs and lower marginal costs at low output levels. Note that, in market settings, there are uplift payments made to generators if they do not recover their costs across a day; such required side payments are expected to increase, which is also not desirable.

One thing to note in Table 5.1 is that the expected hourly average cost for 40% wind penetration level is higher than those in all the other penetration levels. This is due to the different wind farm profiles that are modeled in the system, which cause more expensive units to be dispatched in the 40% penetration level. Under high wind penetration levels, because of the geographical diversity of wind profiles, the expected hourly average costs for conventional generators may not necessarily increase monotonically. However, the results in Table 5.1 show that the expected average costs for conventional generators, in general, increase as more wind is integrated in the system. As the wind penetration level increases, both the capacity factor and expected hourly utilization rate for conventional generator decrease, which indicates that conventional generators are utilized less efficiently under high wind penetration levels.

To further illustrate the changes in utilization rates as wind penetration levels increase, histograms depicting the distribution of utilization rates for conventional generators in each hour and each scenario are shown in Figure 5.6 and Figure 5.7 for 30% and 70% wind penetration level respectively. The different colors in the two figures represent the hourly utilizations rates in different wind scenarios. Comparing the two figures, it can be found that under 70% wind penetration level, more generators are operated with utilization rates less than 20% and fewer generators have utilization rates larger than 80% compared to the case with 30% wind penetration level. And the number of generators with utilization rates greater than 90% is much smaller than that in the case with 30% penetration level. Therefore, the results demonstrated that as wind penetration level increases, more generators are operated at low output level and are not being utilized efficiently. This result is in consistent with the decrease in expected utilization rates and shows that the efficiency for conventional generators will decrease as wind penetration level increases.

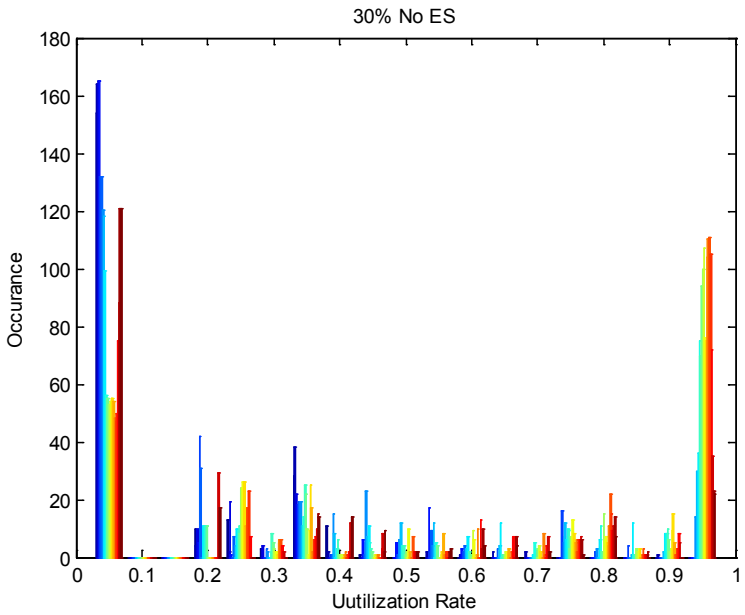

Figure 5.6 Histogram of Utilization Rates for Conventional Generators under 30% Wind Penetration Level

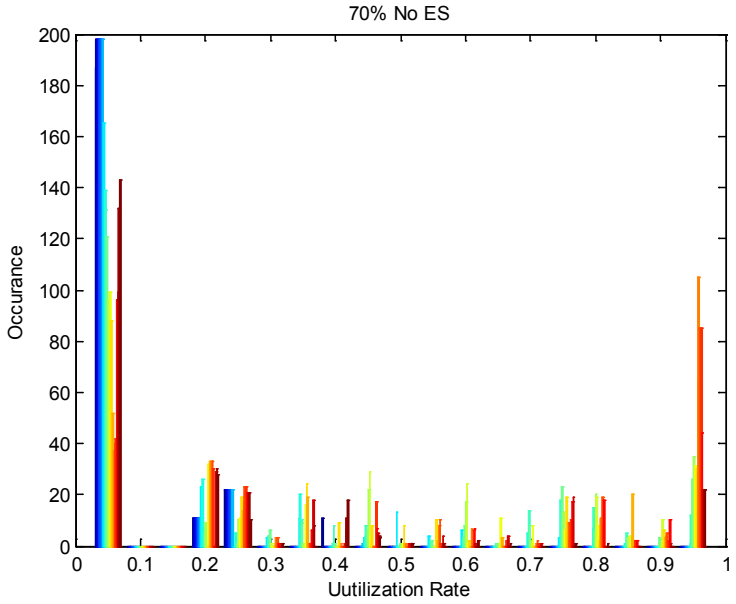

Figure 5.7 Histogram of Utilization Rates for Conventional Generators under 70% Wind Penetration Level

The total number of generators dispatched in the system for each penetration level is shown in the fourth column in Table 5.1. It can be found that more generators are dispatched in the system in higher wind penetration levels than when the penetration level is 30%. Under high wind penetration levels, the increased uncertainty and variability in renewable

generation requires more generators to be dispatched. However, to provide backup generation and ancillary services, these generators have to be operated with higher average costs, lower capacity factors, and lower hourly utilization rates, which indicate that conventional generators may have a decrease in profit under high renewable penetration levels.

Table 5.1. Expected Average Costs and Utilization of Conventional Generators

Wind Level%	Expected Hourly Average Cost Per Unit ($/MWh)	Expected Capacity Factor	Expected Hourly Utilization Rate	Number of Units Dispatched
30%	83.5	39.0%	65.5%	20
40%	88.5	30.3%	59.4%	23
50%	86.2	27.3%	58.1%	21
60%	86.8	25.2%	55.5%	21
70%	87.2	23.5%	54.8%	21

Table 5.2. Actual Wind Generation Dispatched in the System

Wind %	Without ES	With ES
30%	27%	29%
40%	35%	38%
50%	42%	45%
60%	45%	49%
70%	48%	51%

5.5.2 Economic Assessment of Energy Storage under High Wind Penetration Levels

Three energy storage units were included in the study, with one being compressed air energy storage and the other two pumped storage hydro. A summary of the parameters for the energy storage used in the study is presented in Table 5.3. The parameters for energy storage were obtained from [87] and [88].

Table 5.3. Energy Storage Parameters

Type	L_g^{Out}, L_g^{In} (MW)	U_g^{Out}, U_g^{In} (MW)	s_g^{Max} (MWh)	η_g^{In}	η_g^{Out}
CAES	0	100	1000	0.7	0.6
PHS	0	100	1000	0.8	0.8

The solution from stochastic unit commitment with energy storage is presented in Table 5.4 and the actual wind generation dispatched for each targeted wind penetration level is shown in Table 5.2. As wind penetration levels increase, the expected hourly average costs for conventional generators generally increase, while the expected capacity factors and

hourly expected utilization rates decrease. Comparing the results in Table 5.4 with those in Table 5.1, it can be found that, with energy storage in the system, the expected hourly average costs for conventional generators are lower compared to the cases without energy storage. Also, with energy storage, the expected capacity factors and hourly utilization rates are higher than those in the cases where energy storage is not included. The distribution of the hourly utilization rates for conventional generators with 30% wind penetration level is presented in Figure 5.8. Comparing Figure 5.8 and Figure 5.6, it can be noticed that with energy storage in the system, fewer generators are operated with hourly utilization rates lower than 60%, while the number of generators with hourly utilization rates greater than 90% is mostly the same in the two cases. This result demonstrates that energy storage can reduce the dispatch of generators with utilization rates.

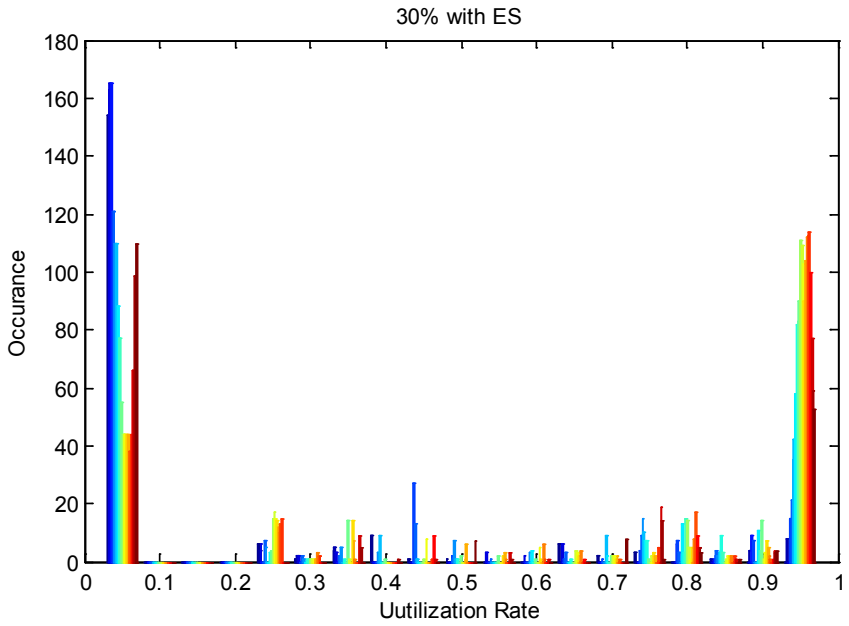

Figure 5.8 Histogram of Utilization Rates for Conventional Generators under 30% Wind Penetration Level with Energy Storage

Another observation can be made from the comparison is that by including energy storage, fewer generators are dispatched in the system. This result occurs because energy storage can store and shift excess wind power, which moderates the renewable generation in the system. Meanwhile, because energy storage has greater flexibility, it can provide more spinning and non-spinning reserves with higher quality than conventional generators. Therefore, with energy storage in the system, fewer conventional generators are needed as backup generation and the dispatched generators will have lower average costs and higher capacity factors and utilization rates. These important observations indicate that energy storage can improve the efficiency of conventional generators under high renewable penetration levels.

Table 5.4. Expected Average Costs and Utilization of Conventional Generators with Energy Storage

Wind Level %	Expected Hourly Average Cost Per Unit ($/MWh)	Expected Capacity Factor	Expected Hourly Utilization Rate	Number of Units Dispatched
30%	79.2	44.6%	82.6%	17
40%	79.9	38.5%	75.2%	17
50%	80.8	31.1%	69.7%	17
60%	80.3	27.2%	69.2%	17
70%	83.6	23.8%	63.6%	18

To further demonstrate the benefits of energy storage under high renewable penetration levels, the expected system total costs and expected generator daily profits for the case with and without energy storage are presented in Table 5.5. As wind penetration levels increase, the expected daily profits for conventional generators decrease in both the cases with and without energy storage. Since wind can be considered as a "free" energy with zero fuel cost, the increase of wind generation will decrease the LMPs in the system. At the same time, the average costs of conventional generators increase as wind integration levels increase. As a result, the profits for conventional generators will decrease as more wind generation is integrated in the system. Comparing the expected system total costs in the cases with and without energy storage, it can be found that the expected system total costs are lower when energy storage is integrated. The cost savings achieved by integrating energy storage is about 20% for each wind penetration level. These results again illustrate that the benefits of energy storage increase with the increase in renewable penetration levels.

Table 5.5. System Total Expected Costs and Generator Profits ($)

Wind Level %	Without Energy Storage		With Energy Storage		
	Expected System Total Cost	CG Expected Daily Profit	Expected System Total Cost	CG Expected Daily Profit	System Total Cost Savings
30%	656974	48552	532434	37529	19.0%
40%	566646	32711	449361	19588	20.7%
50%	447600	17684	359312	13582	19.7%
60%	418355	13963	330503	11920	21.0%
70%	377683	13491	294813	11179	21.9%

5.5.3 Results for Wind Scenario Analysis and N-1 Contingency Analysis

After the stochastic unit commitment was solved, wind scenario analysis and N-1 contingency analysis, combined with selected wind scenarios, were performed and the results are reported in Table 5.6. From Table 5.6, it can be found that both the expected

and maximum costs for correcting violations are lower in the cases with energy storage. Also, with energy storage in the system, the expected operating costs plus violation costs are lower than the cases without energy storage. These results show that energy storage can reduce the system operating costs as well as improve the reliability of the system. Similar results can also be observed for the number of violations, where the integration of energy storage significantly reduces the occurrence of violations in wind scenario analysis.

However, the wind spillage is large in both the cases with and without energy storage, which is a result of the limited capability of the system to accommodate intermittent renewable resources. Also, the wind spillage in wind scenario analysis is much higher than that in N-1 contingency analysis. The reason for the high wind curtailment in wind scenario analysis is that one thousand wind scenarios are generated through Monte-Carlo simulation and only ten scenarios are selected and used in the stochastic unit commitment. Therefore, in the wind scenario analysis, for a wind scenario that is not modeled within stochastic unit commitment, if the wind generation is severely different from the one used within stochastic unit commitment, the system may not have enough capability and flexibility to handle such large difference in wind generation. This is why the wind curtailment is much higher in wind scenarios analysis than that in N-1 contingency analysis. Meanwhile, another observation is that wind spillage is higher in the cases with energy storage. This is because the use of energy storage reduces the number of generators dispatched in the system. As the system only has limited number of fast units, more wind has to be shed in the cases when the flexibility of energy storage is maxed out or the reserve provided by energy storage cannot be delivered due to the congestion in the system.

Table 5.6. Results for Security Corrections with Wind Scenario Analysis and N-1 Contingency Analysis

Wind %	Wind Scenario Analysis				N-1 Combined with Selected Wind Scenarios			
	Cost for Violations ($K)	**Hourly Wind Spillage (MW)**	**Expected Violation Costs Plus Operating Cost ($)**	**Number of Violations**	**Cost for Violations ($K)**	**Hourly Wind Spillage (MW)**	**Expected Violation Costs Plus Operating Cost ($)**	**Number of Violations**
With Energy Storage								
30%	0.04 (41.6)	163.7 (834.2)	403233	1	1.6 (712.5)	3.7 (734.6)	13127	497
40%	0.2 (120.6)	194.2 (941.0)	346737	2	2.4 (748.8)	4.5 (989.0)	12294	624
50%	1.9 (353.6)	276.8 (1258.8)	290258	15	2.3 (904.4)	7.1 (1252.8)	10525	189
60%	1.9 (402.5)	422.6 (1721.6)	269804	11	1.7 (913.3)	11.0 (1669.6)	9295	262
70%	11.4 (1053.8)	589.1 (2360.7)	252258	49	1.0 (973.3)	15.4 (2309.0)	7693	179
Without Energy Storage								
30%	3.6 (255.9)	59.7 (479.4)	561413	43	4.5 (928.2)	1.0 (562.4)	19993	517
40%	6.8 (462.7)	98.1 (756.2)	485558	69	4.0 (794.3)	2.2 (804.2)	17332	469
50%	17.3 (681.4)	171.6 (1074.1)	392572	104	3.2 (1140.0)	4.3 (1067.9)	13702	235
60%	1.4 (354.9)	315.6 (1536.9)	349012	15	2.1 (1173.2)	8.1 (1484.7)	11680	163
70%	26.2 (1231.6)	468.1 (2175.9)	342917	119	1.9 (946.2)	12.3 (2124.2)	10448	147

[1] α (β): α represents the expected daily costs for violations (expected hourly wind spillage); β represents hourly maximum costs for violations (hourly maximum wind spillage).

5.6 Conclusions

As renewable penetration levels increase, conventional generators will have higher average costs, lower capacity factors, increased ramping, and decreasing utilization rates. These facts indicate that conventional generators will see lower profits and, hence, produce lower returns on investments as the renewable penetration levels increase. However, by integrating energy storage into the system, the average costs of conventional generators decrease, while fewer generators are dispatched in the system with higher capacity factors compared to the cases without energy storage. As such, energy storage improves the utilization of the conventional generators in the system. Furthermore, the benefits of energy storage have been shown to increase with the increasing level of renewables. While most forms of energy storage are still considered to be too expensive and not competitive with conventional generators, this paper shows that the attractiveness of conventional generators decreases as the renewable penetration levels increase whereas the attractiveness of energy storage increases with the increase in renewable resources. As a result, with new energy storage technologies, it is expected that there will be a break point where energy storage becomes competitive with conventional generating resources, resulting in increased deployment of energy storage technologies.

6. Evaluating the Benefits of Energy Storage in Real-time Operation

In this chapter, the real-time operation of energy storage under high renewable penetration levels will be analyzed. A study is conducted to identify the benefits of energy storage in providing regulation services in real-time operation under high renewable penetration levels. The real-time operation of energy storage is focused on flywheels.

6.1 Background and Motivation

In power systems, generation and load should match in order to maintain the target grid frequency and ensure the reliability and stability of the system. However, the exact match of generation and load can only be achieved for a short period of time and a normal frequency deviation is allowed. In the Eastern Interconnection (EI), the required standard deviation of frequency is 0.018 Hz from the nominal 60 Hz [89]. As load varies from minute to minute, it is a challenging task to balance load and generation continuously and instantaneously. Traditionally, the variation in load mainly results from the random turning on and off of different individual loads. With the increasing integration of renewable energy, the variability and uncertainty in renewable generation further increases the complexity and difficulty in mitigating the variation in load and maintaining the system frequency continuously.

Since energy storage provides energy shifting and fast ramping capabilities, energy storage is a competitive and attractive resource to regulate power system frequency by balancing load and generation in real-time operations. In this chapter, the benefit of energy storage in providing regulation services during real-time operations is evaluated. While most of the energy storage technologies can provide regulation reserve services, flywheels are one of the most attractive technologies in such applications, which is a result of its fast-ramping and quick respond capabilities. The response time for a flywheel unit can be as short as four milliseconds. Even though flywheels have limited energy capacity, its fast ramping capability and short response time provides flywheels great potential in regulating frequency and following AGC instructions in a real-time horizon. In this chapter, flywheels will be studied to identify the attractiveness of energy storage technologies in real-time operations.

6.2 Mathematical Framework

In this chapter, a two-stage framework is proposed to analyze the attractiveness of flywheel in providing regulation services in real-time operation. In the first-stage, a 15-minute real-time generation scheduling problem is formulated. In the second-stage, a real-time generation dispatch problem is modeled. The mathematical model for flywheel and the formulations used in the two stages are described in the following subsections.

6.2.1 Mathematical Model for Flywheel

The real-time model for a flywheel facility used in a dc OPF formulation is presented in (6.1)–(6.5). The formulation includes power absorbing limits (6.1), generation output

limits (6.2), energy balance constraint (6.3), reservoir capacity constraint (6.4), and initial and target reservoir level constraint (6.5). Since flywheels have high efficiencies that are generally above 90%, the efficiency coefficients are not included in the energy balance constraint (6.3).

$$0 \le P_{gt}^{In} \le U_g^{In}, \forall g, t \tag{6.1}$$

$$0 \le P_{gt}^{Out} \le U_g^{Out}, \forall g, t \tag{6.2}$$

$$S_{gt} = S_{g,t-1} + P_{gt}^{In} - P_{gt}^{Out}, \forall g, t \tag{6.3}$$

$$S_g^{Min} \le S_{gt} \le S_g^{Max}, \forall g, t \tag{6.4}$$

$$S_{g0} = S_{gT}, \forall g, t \tag{6.5}$$

Mandated by FERC order No. 890 issued in 2007, non-generation technologies are allowed to participate in the deregulated market for ancillary services [90]. Since flywheel has limited energy capacity, its primary application is to provide regulation reserves. Therefore, it is assumed in this report that flywheel units will only provide regulation reserves and not provide an energy product in the real-time operation.

6.2.2 Real-time Generation Scheduling Model

In the proposed framework, the first-stage represents a 15-minute generation scheduling problem, which is formulated as a lossless multi-period dc OPF model. In the real-time generation scheduling problem, a flywheel is considered as providing only regulation reserves. The real-time generation scheduling problem consists of three time periods, with each representing a 5-minute time interval. The objective of the dc OPF model is to minimize system total costs, which is shown in (6.6). The complete formulation is shown in (6.7)-(6.22).

Minimize

$$\sum_{g,t} c_g P_{gt} \tag{6.6}$$

Subject to:

$$\sum_{g \in g(n)} P_{gt} + \sum_{k \in \delta^+(n)} P_{kt} - \sum_{k \in \delta^-(n)} P_{kt} = d_{n,t} - \sum_{w \in w(n)} P_{wt}\ , \forall n, t \tag{6.7}$$

$$P_{kt} - B_k(\theta_{nt} - \theta_{mt}) = 0, \forall k, t \tag{6.8}$$

$$-P_m^{Max} \le\ P_{mt} \le P_m^{Max}, \forall t \tag{6.9}$$

$$P_{gt}\ + r_{gt}^{Ru} \le P_g^{Max}, \forall g, t \tag{6.10}$$

$$P_g^{Min} \leq P_{gt} - r_{gt}^{Rd}, \forall g, t \tag{6.11}$$

$$r_{gt}^{Ru} \leq R_g^{5+}, \forall g \in \Omega_G, t \tag{6.12}$$

$$r_{gt}^{Rd} \leq R_g^{5-}, \forall g \in \Omega_G, t \tag{6.13}$$

$$r_{gt}^{Ru} \geq 0, \forall g, t \tag{6.14}$$

$$r_{gt}^{Rd} \geq 0, \forall g, t \tag{6.15}$$

$$-R_g^{5-} \leq P_{gt} - P_{g,t-1} \leq R_g^{5+}, \forall g, t \tag{6.16}$$

$$r_{gt}^{Ru} \leq U_g^{Out} - P_{gt}^{Out} + P_{gt}^{In}, \forall g \in \Omega_{ES}, t \tag{6.17}$$

$$r_{gt}^{Rd} \leq U_g^{In} - P_{gt}^{In} + P_{gt}^{Out}, \forall g \in \Omega_{ES}, t \tag{6.18}$$

$$r_{gt}^{Ru} \leq 12(S_{g,t} - S_{Min}), \forall g \in \Omega_{ES}, t \tag{6.19}$$

$$r_{gt}^{Ru} \leq 12S_{g,t-1} - 12S_{Min} + P_{gt}^{In}, \forall g \in \Omega_{ES}, t \tag{6.20}$$

$$r_{gt}^{Rd} \leq 12\left(S_{Max} - S_{g,t}\right), \forall g \in \Omega_{ES}, t \tag{6.21}$$

$$r_{gt}^{Rd} \leq 12S_{Max} - (12S_{g,t-1} - P_{gt}^{Out}), \forall g \in \Omega_{ES}, \tag{6.22}$$

$$-\delta \leq P_{gt}^{Out} - P_{gt}^{In} \leq \delta, \forall g \in \Omega_{ES}, t \tag{6.23}$$

$$\sum_g r_{gt}^{Ru} \geq Reg^{up}, \forall t \tag{6.24}$$

$$\sum_g r_{gt}^{Rd} \geq Reg^{dn}, \forall t \tag{6.25}$$

In the above formulation, nodal balance constraint is shown in (6.7). Constraint (6.8) formulates the dc power flow on each line and (6.9) is the line-flow limit for each transmission line. Constraints (6.10)-(6.11) represent the operating range for generators. Constraint (6.10) implies that the sum of the power output and the scheduled up regulation reserve for each generator in each time period should be less or equal to the maximum capacity. Similarly, constraint (6.11) indicates that power output for each generator minus the scheduled down regulation reserve should be greater or equal to the minimum capacity in each time period. Constraints (6.12)-(6.13) require that the up and down regulation reserve should not exceed the ramp rate limits for each generator. Constraints (6.14)-(6.15) guarantee that all the regulation reserves are non-negative. The 5-minute ramp rate constraint is represented by (6.16). The constraints for the flywheel are shown in (6.17) - (6.22). Since flywheels have both fast ramping capability and short transition time, flywheels can stop consuming power to provide up regulation reserves and stop generating power to provide down regulation reserve. If a flywheel unit is in absorption mode, the

maximum reserve it can provide is $U_g^{Out} + P_{gt}^{In}$, which indicates that a flywheel unit can provide up regulation reserve by stop withdrawing power and transitioning to generation mode. If a flywheel unit is in generation mode, the maximum down regulation reserve it can provide is $U_g^{In} + P_{gt}^{Out}$, which indicates that a flywheel unit can stop generating and transition to absorption mode to consume the maximum amount of power. The above regulation requirements are modeled in constraints (6.17) and (6.18). Constraint (6.19) requires that up regulation reserve provided by flywheel should not exceed the energy that can be discharged during time period *t*. The coefficient 12 is the coefficient that converts energy to power, where it is assumed that the power output for flywheel is constant when the reserve is dispatched. Constraint (6.20) indicates that the maximum up regulation reserve is constrained by the energy stored by the end of period *t-1* plus the absorbing power in period *t*. Constraint (6.21) guarantees that if a flywheel unit is providing down regulation reserve in absorption mode, then the amount of energy absorbed should not exceed the maximum energy capacity of the flywheel. And constraint (6.22) indicates that the maximum down regulation reserve can be provided should be no greater than the maximum energy can be absorbed plus the generating power in period *t*.

Constraint (6.23) represents a proxy policy constraint on the operation of the flywheel. In the first-stage, the regulation reserve is scheduled for flywheel only based on the forecasted wind power. However, the actual wind generation in the second-stage may deviate from the forecasted wind generation in the first-stage. Without the proxy constraint, if the flywheel is scheduled to be generating at the maximum output in the first-stage, then flywheel may not be able to provide enough up regulation reserve in the second-stage when up regulation reserve is needed. With the proxy constraint, the power output for the flywheel is constrained within the range of $[-\delta, \delta]$ with the aim to ensure that the flywheel can provide both up and down regulation reserve in the second-stage real-time dispatch. In this report, the δ is chosen to be 5 MW, which is to ensure that the flywheel can provide both up and down regulation, and the flywheel can provide relative more up or down regulation reserve determined by the linear program.

The regulation reserve requirement is depended on the characteristics of different systems. In [91], it is reported that the regulation requirements in ISOs are typically 1% of the peak load. In this report, since the simulation is conducted under high levels of renewable penetration levels, both the up and down the regulation reserve requirement is assumed to be 2% of the peak load.

6.2.3 Real-time Dispatch Model

In the second-stage, a real-time dispatch model is used to dispatch the regulation reserves scheduled in the first-stage. The real-time dispatch model is solved to test if the scheduled regulation reserves can balance generation and load in real-time operation under different wind scenarios. The real-time dispatch problem is formulated as a multi-period dc OPF model, with each time interval to be 2.5 minutes. The objective of the real-time dispatch is to minimize the total operating costs and the costs of correcting involuntary load shedding, which is shown in (6.26).

$$\sum_t \left[\sum_{g\in\Omega_G} c_g P_{gt} + \sum_{g\in\Omega_{ES}} c_g P_{gt}^{ES} + \sum_{n=1}^{NB} c_n^v s_{nt}\right] \quad (6.26)$$

Subject to:

$$\sum_{\forall g(n)}^{g\in\Omega_G} P_{gt} + \sum_{\forall g(n)}^{g\in\Omega_{ES}} P_{gt}^{ES} + \sum_{\delta^+(n)} P_{mt} - \sum_{\delta^-(n)} P_{mt}$$

$$= d_{nt} - \sum_{\forall g(n)}^{g\in\Omega_W} P_{gt}^{Wind} - s_{nt} + w_{nt}, \forall n \quad (6.27)$$

$$P_{mt} = B_m(\theta_{mt}^+ - \theta_{mt}^-), \forall m \quad (6.28)$$

$$-P_m^{Max} \le P_{mt} \le P_m^{Max}, \forall m \quad (6.29)$$

$$P_g^{Min} \le P_{gt} \le P_g^{Max}, \forall g \in \Omega_G \quad (6.30)$$

$$\overline{P_{gt}} - \overline{r_{gt}^{Rd}} \le P_g \le \overline{P_{gt}} + \overline{r_{gt}^{Ru}}, \forall g \in \Omega_G \quad (6.31)$$

$$\overline{P_{gt}^{ES}} - \overline{r_{gt}^{Rd}} \le P_{gt}^{ES} \le \overline{P_{gt}^{ES}} + \overline{r_{gt}^{Ru}} \quad (6.32)$$

$$P_{gt}^{ES} = P_{gt}^{Out} - P_{gt}^{In} \quad (6.33)$$

$$0 \le P_{gt}^{Out} \le U_g^{Out} \quad (6.34)$$

$$0 \le P_{gt}^{In} \le U_g^{In} \quad (6.35)$$

$$S_{gt} = S_{g,t-1} + P_{gt}^{In} - P_{gt}^{Out} \quad (6.36)$$

$$S_{min} \le S_{gt} \le S_{max} \quad (6.37)$$

$$S_{g0} = \overline{S_0} \quad (6.38)$$

$$P_{gt}^{Out} \ge 0 \quad (6.39)$$

$$P_{gt}^{In} \ge 0 \quad (6.40)$$

$$0 \le s_{nt} \le d_{nt} \quad (6.41)$$

$$0 \le w_{nt} \le \sum_{\forall g(n)}^{g\in\Omega_W} P_{gt}^{Wind} \quad (6.42)$$

The complete formulation is shown in (6.26)-(6.42). Nodal balance constraint is shown in (6.27). Constraint (6.28) formulates the dc power flow on each line and (6.29) is the line-flow limit for each transmission line. Constraints (6.30)-(6.31) represent the operating range for generators. The variables with a bar above them are the solutions from the first-stage. Constraint (6.30) guarantees that the power output should be within the range of

minimum and maximum output. Constraint (6.31) indicates that the output for a generator should be in the range of its scheduled dispatch point plus and minus its scheduled up and down regulation reserve, $\overline{r_{gt}^{Ru}}$ and $\overline{r_{gt}^{Rd}}$ respectively. The constraints for flywheels are shown in (6.32)-(6.42). The variable P_{gt}^{ES} is the net output of a flywheel unit, which is the different between P_{gt}^{Out} and P_{gt}^{In} as shown in (6.33). Constraint (6.33) indicates that the output range for a flywheel unit should be the scheduled operating point plus and minus the scheduled regulation reserve. The minimum and maximum output limits on absorption mode and generation mode for flywheel are shown in (6.34) and (6.35) respectively. Constraint (6.36) is the energy balance constraint for flywheel and constraint (6.37) represents the energy capacity limits. The initial energy stored in flywheel is represented by (6.38). Constraints (6.39) and (6.40) guarantee that the variable P_{gt}^{out} and P_{gt}^{In} are non-negative. Constraints (6.39) and (6.40) guarantee that s_{nt} and w_{nt} are non-negative and they cannot exceed the actual load and maximum wind generation at each bus respectively.

6.3 Renewable Modeling

Similar to chapter 5, the method described in [80] was used to generate wind scenarios to be used in the real-time operation simulation. For each time period *t*, the wind forecast error was assumed to follow a truncated Gaussian distribution $N(0, \sigma^2)$ with zero mean and variance σ^2. The wind scenarios were generated to construct a scenario tree structure. An illustration of the scenario tree structure is shown in Figure 6.1. If each time period has a number of *NS* scenarios and the simulation has a number of *NT* periods, then the total number of scenarios in a scenario tree is NS^{NT}. The standard deviation was chosen such that the resulted forecast error is about 5% in the real-time operation [92].

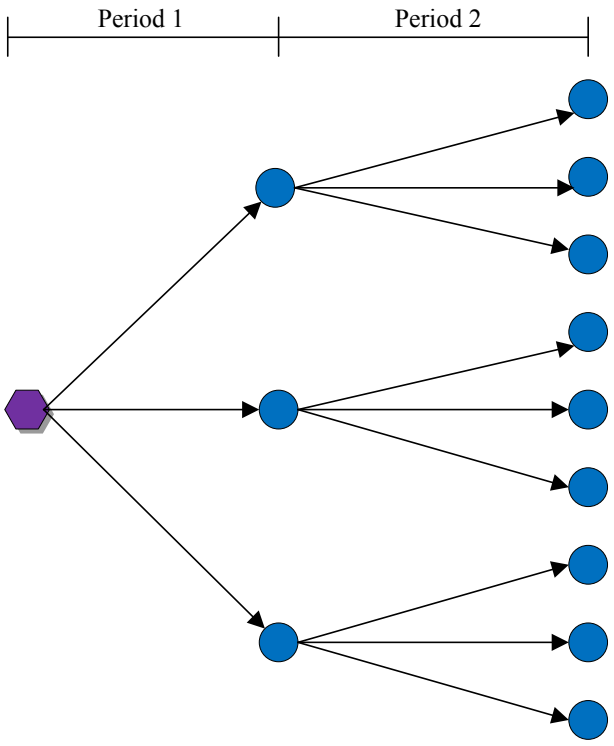

Figure 6.1. Illustration of the Scenario Tree Structure

6.4 Description of Methodology

The methodology used in this study is described as follows. In the first step, Monte-Carlo simulation is performed to generate four scenarios for each time period. Then a scenario tree is constructed using the generated scenarios. The resulted scenario tree has 4096 scenarios in total. In the second step, real-time generation scheduling problem is solved to determine the generation dispatch and the up and down regulation reserves for each generator and flywheel. After the solution is obtained from the first-stage, the real-time dispatch model is solved for all the wind scenarios in the scenario tree, one scenario at each time, to test if the scheduled generation and reserves can satisfy all the wind scenarios generated. If violations (e.g. involuntary load shedding) are reported, security corrections should be performed to correct such violations in the system so that the potential involuntary load shedding is not allowed.

6.5 Data Preparation

The RTS96 one-zone model [84], [85] was used as the test system. The one-zone model has 32 generators, 24 buses and 17 loads. The total generation capacity in the system is 3402 MW, while the system peak load is 2850 MW. The weekly and daily load information data is obtained from [84] and [85]. By using the weekly load to be 90% of the yearly peak load and the daily load to be 98% of the yearly peak load, the resulted system load is 2513.7 MW. The system load is assumed to remain the same during the 15 minutes of operation.

Wind penetration levels from 20% to 30% with 5% increments were studied, where the wind penetration level is defined as the ratio of total daily wind generation to the total system daily demand. Similar to chapter 5, to represent the smoothing effect resulting from the widely dispersed wind farms, for each 5% penetration increment, a wind farm with different wind profile and wind scenarios was added. Wind data was collected from NREL Wind Integration Datasets. The original 10-min wind data was interpolated into 2.5-minute and 5-minute data to be used in the real-time generation scheduling and real-time dispatch problem. Wind spillage was allowed in the simulation, which is to allow the optimization program to curtail wind generation when the system cannot accommodate all the wind generation modeled in the system. In the simulation, one flywheel unit is included in the system. The parameters used for the flywheel are obtained from [40] and a summary of the parameters used is presented in Table 6.1.

Table 6.1. Flywheel Parameters

Type	P_{min}^{Out}, P_{min}^{In} (MW)	P_{max}^{Out}, P_{max}^{In} (MW)	S_{min} (MWh)	S_{max} (MWh)
Flywheel	0	20	0.5	5

6.6 Result Analysis and Discussion

The system total cost and the wind spillage for the first-stage is reported in Table 6.2. In the first-stage, flywheel is considered as non-generating unit and only the regulation reserves are scheduled for the flywheel. Therefore, the system total costs and expected wind spillage are the same in the first-stage for the cases with and without flywheel. Only the scheduled up and down regulation reserves are different in the first-stage for the cases with and without flywheel.

Table 6.2. System Total Cost and Wind Spillage for the Real-time Generation Scheduling Problem

Wind %	Without Energy Storage		With Energy Storage	
	System Total Cost ($)	Wind Spillage (MW)	System Total Cost ($)	Wind Spillage (MW)
20%	30935.5	6.0	30935.5	6.0
25%	25885.8	1.1	25885.8	1.1
30%	23612.7	4.9	23612.7	4.9

In the second-stage, 15-minute dispatch model is solved for all the wind scenarios with and without flywheel, and the results are summarized in Table 6.3. Four metrics were used to evaluate the effectiveness of flywheel, namely the expected cost for violation, expected wind spillage, expected violation cost plus operating cost, and number of violations. As wind penetration levels increase, the ramping requirement becomes more stringent for generators. Since many conventional generators has relative slow ramping capability, the system has higher cost for violations and the number of violations in the system also increases as more wind generation is integrated, which is shown in Table 6.3.

With the flywheel in the system, the expected costs for correcting violations are reduced and the expected wind spillage is lower than the cases without the flywheel. Since the flywheel has fast ramping capability, it can provide a large quantity of regulation reserve in a short time period to mitigate the uncertainty in renewable generation. Meanwhile, the flywheel helps to reduce the expected violation costs plus operating cost in the system. With 20% wind penetration level, the cost savings by using flywheel is about two thousand dollars. Although this saving may seem small, the cost is only for 15 minutes of operation. As the operation horizon increases and once a larger system is tested, the cost saving from integrating flywheel is expected to increase. As wind penetration level increases, the savings in operating cost plus violation cost decreases. As more wind generation is integrated, the capacity of flywheel in the system remains the same. Therefore, with higher renewable penetration levels while the capacity of the flywheel remains the same, the flexibility of flywheel is maxed out and cannot provide as much benefits as it can in the lower renewable penetration levels.

For the maximum expected cost for violations, they are higher in the cases with the flywheel. This result is due to the fact that only the regulation reserves are scheduled for flywheel in the first-stage. In the second-stage, as a finer 2-5minute time interval is used, some scheduled reserve for flywheel may not be able to be dispatched, which is a result of the lack of energy or the energy level is at its maximum capacity.

Table 6.3. Results for 15-minute Real-time Dispatch Model with and without Flywheel

With Flywheel				
Wind %	Expected Cost for Violations ($Thousand)	Expected Wind Spillage (MW)	Fifteen-minute Expected Violation Costs Plus Operating Cost ($)	Number of Violations
20%	5.9 (35)	6.3 (36.1)	98075	3.5
25%	8.6 (37)	3.4 (26.3)	104480	4.8
30%	9.7(40)	5.4 (35.9)	106401	5
Without Flywheel				
Wind %	Expected Cost for Violations ($Thousand)	Expected Wind Spillage (MW)	Fifteen-minute Expected Violation Costs Plus Operating Cost ($)	Number of Violations
20%	6.2 (31)	6.6 (36.1)	100133	3.5
25%	8.7 (33)	3.5 (26.3)	105155	4.8
30%	9.8 (38)	5.6 (35.9)	106975	4.8

6.7 Conclusions

As wind penetration level increases, the power system requires higher flexibility in real-time operation to mitigate the uncertainty in renewable generation. Under high renewable penetration levels, the system will have increased cost for violations and higher number of violations. Due to the fast ramping and quick-respond capabilities of flywheels, flywheels can provide a high quantity of regulation reserve in a short period of time. As shown in the study, by providing fast regulation reserves, flywheels are able to reduce the expected cost for violations as well as reduce wind spillage in the system.

7. Conclusions

In this report, existing bulk energy storage technologies are reviewed and the attractiveness of bulk energy storage in transmission systems with high levels of renewable resources is evaluated.

Pumped hydro storage and compressed air energy storage technologies have the largest power ratings and energy capacities, as well as the lower capital costs, which make them the most attractive bulk energy storage options. For pumped hydro storage, it is the most widely used energy storage by far, which consists of around 99% of the installed energy storage capacity worldwide. For battery energy storage technologies, they have less site restrictions compared to pumped hydro storage and compressed air energy storage. However, the main drawbacks for batteries are their degradation effects caused by charging and discharging and their high capital costs. For flywheels, they have high efficiency and fast response times. As such, flywheels have characteristics that match well with the needs of frequency regulation applications. However, the barriers for flywheels are that they have limited energy capacity and high capital costs.

To study the short-term profitability of conventional generators and energy storage units under increasing renewable penetration levels, a stochastic unit commitment model is proposed in this report. Pumped hydro storage and compressed air energy storage are included in the study. To capture the impact of high penetration levels of renewable resources in the system, a ramping cost term is introduced in the stochastic unit commitment to represent the costs associated with the 10-minute ramping process. One thousand wind scenarios are generated through Monte-Carlo simulations based on the assumptions that the errors in wind forecast follow a truncated normal distribution. A backward reduction method is applied to select ten scenarios to be included in the stochastic unit commitment.

The results show that, as renewable penetration level increases, the increased uncertainty and variability in renewable generation requires more generators to be dispatched. Under such circumstances, the role of conventional generators will transition to primarily provide backup generation and ancillary services. As a result, conventional generators will have increased average costs, decreased capacity factors, decreased utilization rates, and increased ramping. As wind can be considered as a “free” energy with zero fuel cost, the increase of wind generation will decrease the LMPs in the system. Therefore, conventional generators will have decreased profits on top of increased average costs.

With energy storage in the system, conventional generators have lower expected hourly average costs, higher expected capacity factors, and higher hourly utilization rates compared to the cases without energy storage. The integration of energy storage also decreases the number of dispatched units in the system, which improves the efficiencies for conventional generators. Energy storage can shift energy and provide flexible ancillary services, thereby reducing the requirements for conventional generators to be operated as backup generation while also operating at low operating levels. With energy storage in the system, the total system costs are also reduced compared to the cases without energy storage. Meanwhile, the results from wind scenario and N-1 contingency analysis demonstrate that the integration of energy storage can improve the reliability of the system,

as energy storage can reduce the costs for security corrections and decrease the number of violations in the system.

The benefit of energy storage in real-time operation is also demonstrated in this report. Flywheel energy storage technologies are investigated in order to evaluate the effectiveness of energy storage in mitigating uncertainty in renewable generation. The study has shown that, under high levels of renewable penetration levels, flywheels can reduce the costs for violations as well as reduce wind spillage in the system. By providing large quantities of fast ramping regulation reserves, energy storage technologies provide an attractive resource in the future power grid with high renewable penetration levels.

The economic assessment of bulk energy storage conducted in this report has demonstrated the effectiveness of bulk energy storage in systems with high renewable penetration levels. As more renewable resources are integration in the system, the attractiveness of energy storage will increase while the attractiveness of conventional energy storage decreases. Therefore, the increase in renewable penetration level may provide more incentives for investors to invest in energy storage in the future.

References

[1] Global Wind Energy Council, "Global wind report: annual market update 2012," April 2013. [Online]. Available: http://www.gwec.net/wp-content/uploads/2012/06/Annual_report_2012_LowRes.pdf

[2] World Wind Energy Association,"2012 Half-year report," [Online]. Available: http://www.wwindea.org/webimages/Half-year_report_2012.pdf

[3] Earth Techling, "Global solar, wind energy growth continues to impress," [Online]. Available: http://www.earthtechling.com/2013/07/global-solar-wind-energy-growth-continues-to-impress/

[4] Energy Information Administration, "Most states have renewable portfolio standards," February 2012. [Online]. Available: http://www.eia.gov/todayinenergy/detail.cfm?id=4850

[5] Energy Information Administration, "Existing capacity by energy source," 2011. [Online]. Available: http://www.eia.gov/electricity/annual/html/epa_04_03.html

[6] Sandia National Laboratories, "DOE/EPRI 2013 Electricity storage handbook in collaboration with NEECA," July 2013. [Online]. Available: http://energy.gov/oe/downloads/doeepri-2013-electricity-storage-handbook-collaboration-nreca-july-2013

[7] California Public Utilities Commission, "CPUC sets energy storage goals for utilities," [Online]. Available: http://docs.cpuc.ca.gov/PublishedDocs/Published/G000/M079/K171/79171502.PDF

[8] Electric Power Research Institute, "Electricity energy storage technology options – a white paper primer on applications, costs, and benefits," December 2010. [Online]. Available: http://www.electricitystorage.org/images/uploads/static_content/technology/resources/ESA_TR_5_11_EPRIStorageReport_Rastler.pdf

[9] U.S. Department of Energy, "Grid energy storage," December 2013. [Online]. Available: http://energy.gov/sites/prod/files/2013/12/f5/Grid%20Energy%20Storage%20December%202013.pdf

[10] National Hydropower Association, "Challenges and opportunities for new pumped storage development," [Online]. Available: http://www.hydro.org/wp-content/uploads/2012/07/NHA_PumpedStorage_071212b1.pdf

[11] Electric Power Research Institute, "MISO energy storage study phase 1 report," Power Delivery & Utilization, February 2012. [Online]. Available: http://www.epri.com/abstracts/Pages/ProductAbstract.aspx?ProductId=000000000001024489

[12] General Commission, "Texas dispatchable wind 1, LLC," [Online]. Available: http://www.generalcompression.com/index.php/tdw1.

[13] Xtreme Power, “About Xtreme power,” [Online]. Available: http://www.xtremepower.com/about

[14] Alaska Energy Wiki, “Lead-acid batteries,” [Online]. Available: http://energy-alaska.wikidot.com/lead-acid-batteries

[15] Torresol Energy, “Gemasolar,” [Online]. Available: http://www.torresolenergy.com/TORRESOL/gemasolar-plant/en

[16] Torresol Energy, “Central-tower technology,” [Online]. Available: http://www.torresolenergy.com/TORRESOL/central-tower-technology/en

[17] Ivanpah Solar Electric Generating System, “Ivanpah project facts,” [Online]. Available: http://ivanpahsolar.com/about

[18] Highveiw Power Storage, “Cryo energy storage,” [Online]. Available: http://highview-power.com/wordpress/?page_id=8

[19] Electricity Storage Association, “Liquid air energy storage (LAES),” [Online]. Available: http://www.electricitystorage.org/technology/tech_archive/laes_storage

[20] Institution of Mechanical Engineers, “Electricity storage,” [Online]. Available: https://custom.cvent.com/2A4273FF30A84F3194B3668DAC5E13F7/files/d6022910c6e749d5908ef249bfa2d640.pdf

[21] J. A. Suul, “Variable speed pumped storage hydropower plants for integration of wind power in isolated power system,” [Online]. Available: http://www.intechopen.com/books/renewable-energy/variable-speed-pumped-storage-hydropower-plants-for-integration-of-wind-power-in-isolated-power-syst

[22] Department of Energy, “DOE global energy storage database,” [Online]. Available: http://www.energystorageexchange.org/

[23] J. R. Ruggiero and G. T. Heydt, “Making the economic case for bulk energy storage in electric power systems,” *North American Power Symposium*, September 2013.

[24] R. J. Kerestes, G. F. Reed, and A. R. Sparacino, “Economic analysis of grid level energy storage for the application of load leveling,” *IEEE Power and Energy Society General Meeting*, July 2012.

[25] K. Aoki, M. Itch, T. Satoh, K. Nara, and M. Kanezashi, “Optimal long-term unit commitment in large scale systems including fuel constrained thermal and pumped-storage hydro,” *IEEE Transactions on Power Systems*, vol. 4, no. 3, pp. 1065-1063, August 1989.

[26] G. H. McDaniel and A. F. Garbrielle, “Dispatching pumped storage hydro,” *IEEE Transactions on Apparatus and Systems*, vol. PAS-85, no. 5, pp. 465- 461, May 1966.

[27] B. Y. Lee, Y. M. Park, and K. Y. Lee, “Optimal generation planning for a thermal system with pumped-storage based on analytical production costing model,” *IEEE Transactions on Power Systems*, vol. PWRS-2, no. 2, May 1987.

[28] R. Siohansi, P. Denholm, T. Jenkin, and J. Weiss, "Estimating the value of electricity storage in PJM: arbitrage and some welfare effects," *Energy Economics*, vol. 32, no. 2, pp. 269-277, March 2009.

[29] R. Walawalkar, J. Apt, and R. Mancini, "Economics of electric energy storage for energy arbitrage and regulation in New York," *Energy Policy*, vol. 35, issue 4, pp. 2558-2568, November 2006.

[30] G. Gross, A. Dominguez-Garcia, C. Singh, and A. Sprintson, "Integration of storage devices into power systems with renewable energy sources," PSERC Publication 12-24, September 2012. [Online]. Available: http://www.pserc.wisc.edu/documents/publications/reports/2012_reports/gross_pserc_project_s-40_2012.pdf

[31] A. Tuohy, M. O'Malley, "Impact of pumped storage on power system with increasing wind penetration," *IEEE Power & Energy Society General Meeting*, July 2009.

[32] J. P. Deane, E. J. Mckeogh, and B. P. O. Gallachoir, "Derivation of intertemporal targets for large hydro energy storage with stochastic optimization," *IEEE Transactions on Power Systems*, vol. 28, no. 3, pp. 2147-2155, August 2013.

[33] M. E. Khodayar and M. Shahidehpour, "Enhancing the dispatchability of variable wind generation by coordination with pumped-storage hydro units in stochastic power systems," *IEEE Transactions on Power Systems*, vol. 28, no. 3, pp. 2808-2818, August 2013.

[34] D. J. Swider, "Compressed air energy storage in an electricity system with significant wind power generation," *IEEE Transactions on Energy Conversion*, vol. 22, no. 1, pp. 95-102, March 2007.

[35] H. Daneshi, A. K. Srivastava, and A. Daneshi, "Generation scheduling with integration of wind power and compressed air energy storage," *IEEE Transmission and Distribution Conference and Exposition*, April 2010.

[36] H. Daneshi and A. K. Srivatava, "Impact of battery energy storage on power system with high wind penetration," *IEEE Transmission and Distribution Conference and Exposition*, May 2012.

[37] J. Garcia-Gonzalez, R. M. R. Muela, L. M. Santos, and A. M. Gonzalez, "Stochastic joint optimization of wind generation and pumped-storage units in an electricity market," *IEEE Transactions on Power Systems*, vol. 23, no. 2, pp. 460-469, May 2008.

[38] A. A. Thatte, F. Zhang, and L. Xie, "Coordination of wind farms and flywheels for energy balancing and frequency regulation," *IEEE Power and Energy Society General Meeting*, July 2011.

[39] L. Xie, A. A. Thatte, and Y. Gu, "Multi-time-scale modeling and analysis of energy storage in power system operations," *Energytech*, May 2011.

[40] N. Lu, M. R. Weimar, Y. V. Makarov, F. J. Rudolph, S. N. Murthy, and J. Arseneaux, "An evaluation of the flywheel potential for providing regulation

services in California," *IEEE Power and Energy Society General Meeting*, July 2010.

[41] H. J. Kunish, K. G. Kramer, and H. Dominik, "Battery energy storage another option for load-frequency-control and instantaneous reserve," *IEEE Transactions on Energy Conversion*, vol. EC-1, no. 3, pp. 41-45, September 1986.

[42] B. Lu and M. Shahidehpour, "Short-term scheduling of battery in a grid-connected PV/battery system," *IEEE Transactions on Power Systems*, vol. 29, no. 2, pp. 1053-1051, May 2005.

[43] M. E. Khodayar, L. Abreu, and M. Shahidephour, "Tranmission-constrained intrahour coordination of wind and pumped-storage hydro units," *IET Generation, Transmission, and Distribution*, vol. 7, no. 7, pp. 755-765, October 2012

[44] Z. Hu, F. Zhang, and B. Li, "Transmission expansion planning considering the deployment of energy storage systems," *IEEE Power and Energy Society General Meeting*, July 2012.

[45] K. A. Zach and H. Auer, "Bulk energy storage versus transmission grid investments: bringing flexibility into future electricity systems with high penetration of variable RES-electricity," *9th International Conference on the European Energy Market (EEM)*, May 2012.

[46] ISO New England, "Unit commitment and dispatch," May 2013. [Online]. Available: http://www.iso-ne.com/support/training/courses/wem201/01_wem201_unit_commitment_and_dispatch_coutu.pdf

[47] California ISO, "Market process," [Online]. Available: http://www.caiso.com/market/Pages/MarketProcesses.aspx

[48] H. B. Gooi, D. P. Mendes, K. R. W. Bell, and D. S. Kirschen, "Optimal scheduling of spinning reserve," *IEEE Transactions on Power Systems*, vol. 14, no. 4, pp. 1485-1483, November 1999.

[49] R. Billinton and R. Karki, "Capacity reserve assessment using system well-being analysis," *IEEE Transactions on Power Systems*, vol. 14, no. 2, pp. 433-438, May 1999.

[50] M. Foruhi-Firuzabad and R. Billinton, "Generating unit commitment using a reliability framework," *Proceedings of 1999 IEEE Canadian Conference on Electrical and Computer Engineering*, May 1999.

[51] S. J. Wang, S. M. Shahidehpour, D. S. Kirschen, S. Mokhtari, G. D. Irisarri, "Short-term generation scheduling with transmission and environmental constraints using an augmented lagrangian relaxation," *IEEE Transactions on Power Systems*, vol. 10, no. 3, pp.1294-1301, August 1995.

[52] D. Bertsimas, E. Litvinov, X. A. Sun, J. Zhao, and T. Zheng, "Adaptive robust optimization for the security constrained unit commitment problem," *IEEE Transactions on Power Systems*, vol. 28, no. 1, pp. 52-53, February 2013.

[53] S. Takriti, J. R. Birge, and E. Long, "A stochastic model for the unit commitment problem," *IEEE Transactions on Power Systems*, vol. 11, no. 3, pp. 1497-1507, August 1996.

[54] A. Shapiro and A. Philpott, "A tutorial on stochastic programming," [Online]. Available: http://stoprog.org/stoprog/SPTutorial/TutorialSP.pdf

[55] S. A. H. Bahreyni, M. A. Khorsand, and S. Jadid, "A stochastic unit commitment in power systems with high penetration of smart grid technologies," *2012 2nd Iranian Conference on Smart Grid (ICSG)*, May 2012.

[56] J. M. Arroyo and F. Galiana, "Energy and reserve pricing in security and network-constrained electricity markets," *IEEE Transactions on Power Systems*, vol. 20, no. 2, pp. 634-643, May 2005.

[57] T. Alvey, D. Goodwin, X. Ma,D. Streiffert, and D. Sun, "A security-constrained bid-clearing system for the New Zealand wholesale electricity market," *IEEE Transactions on Power Systems*, vol. 13, no. 2, pp. 340–346, May 1998.

[58] J. Wang, M. Shahidehpour, and Z. Li, "Security-constrained unit commitment with volatile wind power generation," *IEEE Transactions on Power Systems*, vol. 23, no. 3, pp. 1319-1327, August 2008.

[59] A. Botterud, et al., "Wind power trading under uncertainty in LMP markets," *IEEE Transactions on Power Systems*, vol. 27, no. 2, pp. 894-893, May 2012.

[60] F. Bouffard, F. D. Galiana, and A. J. Conejo, "Market-clearing with stochastic security- Part I: formulation," *IEEE Transactions on Power System*, vol. 20, no. 4, pp. 1818-1816, November 2005.

[61] F. Bouffard, F. D. Galiana, and A. J. Conejo, "Market-clearing with stochastic security- Part II: case studies," *IEEE Transactions on Power System*, vol. 20, no. 4, pp. 1818-1816, November 2005.

[62] F. Bouffard and F. D. Galiana, "Stochastic security for operations planning with significant wind power generation," *IEEE Power and Energy Society General Meeting*, July 2008.

[63] A. Papavasiliou, S. S. Oren, and R. P. O'Neil, "Reserve requirements for wind power integration: a scenario-based stochastic programming framework," *IEEE Transactions on Power System*, vol. 26, no. 4, pp. 2197-2206, November 2011.

[64] N. Gröwe-Kuska, H. Heitsch, and W. Römisch, "Scenario reduction and scenario tree construction for power management problems," in *Proc. IEEEE Power Tech Conf.,* Bologna, Italy, vol. 3, pp. 23-26, June 2003.

[65] J. Wang, M. Shahidephour, and Z. Li, "Security-constrained unit commitment with volatile wind power generation," *IEEE Transactions on Power Systems*, vol. 23, no. 3, pp. 1319-1327, August 2008.

[66] H. Heitsch and W. Romisch, "Scenario tree reduction for multistage stochastic programs," *Computational Management Science*, vol. 6, no. 2, pp. 117-133, May 2009.

[67] S. M. Ryan, R. J.-B. Wets, D. L. Woodruff, C. Silva-Monroy, and J.-P. Watson, "Toward scalable, parallel progressive hedging for stochastic unit commitment," University of California Davis. [Online]. Available: http://www.math.ucdavis.edu/~rjbw/mypage/Stochastic_Optimization_files/FGRWWW12_ph_1.pdf

[68] T. Das, V. Krishnan, Y. G, and J. D. McCalley, "Compressed air energy storage: state space modeling and performance analysis," *IEEE Power and Energy Society General Meeting*, July 2011.

[69] K. W. Hedman, M. C. Ferris, R. P. O'Neil, E. B. Fisher, and S. S. Oren, "Co-optimization of generation unit commitment and transmission switching with N-1 reliability," *IEEE Transactions on Power Systems*, vol. 25, no. 2, pp. 1052-1064, May 2010.

[70] California ISO, "Spinning reserve and non-spinning reserve," Settlements Guide, January 2006. [Online]. Available: http://www.caiso.com/docs/2003/09/08/2003090815135425649.pdf

[71] D. Milborrow, "Forecasting for scheduled delivery," Windpower Monthly, December 2003. [Online]. Available: http://www.windpowermonthly.com/article/955591/forecasting-scheduled-delivery

[72] L. Landberg, "A mathematical look at a physical power prediction model," *Wind Energy*, vol.1, no. 1, pp. 23-28, September 1998.

[73] J. S. Hong, "Evaluation of the high-resolution model forecasts over the Taiwan are during GIMEX," *Weather and Forecasting*, vol. 18, no. 5, pp. 836-846, October, 2003.

[74] W. Guoyang, X. Yang, and W. Shasha, "Discussion about short-term forecast of wind speed on wind farm," *Jilin Electric Power*, vol. 181, no. 5, pp. 21-24, 2005.

[75] K. Lalarukh and Z. Yasmin, "Time series models to simulate and forecast hourly averaged wind speed in Quetta, Pkasitan," *Solar Energy*, vol. 61, no. 1, pp. 23-32, July 1997.

[76] A. Papavasiliou, S. S. Oren, and R. P. O'Neil, "Reserve requirements for wind power integration: a scenario-based stochastic programming framework," *IEEE Transactions on Power Systems*, vol. 26. no. 4, pp. 2197-2206, November 2011.

[77] I. G. Damousis, and P. Dokopoulos, "A fuzzy expert system for the forecasting of wind speed and power generation in wind farms," *ICPICA*, pp.63-69, May 2001.

[78] C. W. Potter and M. Negnevitsky, "Very short-term wind forecasting for Tasmanian power generation," *IEEE Transactions on Power Systems*, vol. 21, no. 2, pp. 965-972, May 2006.

[79] National Renewable Energy Laboratory, "Wind integration datasets," 2006. [Online]. Available: http://www.nrel.gov/electricity/transmission/wind_integration_dataset.html

[80] CAISO, "Integration of renewable resources: technical appendices for California ISO renewable integration studies – version 1," October 2010. [Online]. Available: http://www.caiso.com/282d/282d85c9391b0.pdf

[81] W. Yuan-Kang and H. Jing-Shan, "A literature review of wind forecasting technology in the world," in *Proc. IEEE Power Tech*, pp. 504 -509, Jul. 2007.

[82] S. Fan, J. R. Liao, R. Yokoyama, L. Chen, and W. Lee, "Forecasting the wind generation using a two-stage network based on meteorological information," *IEEE Transactions on Energy Conversion*, vol. 24, no. 2, pp. 474-482, June 2009.

[83] J. Dupacová, N. Gröwe-Kuska, and W. Römisch, "Scenario reduction in stochastic programming: An approach using probability metrics," *Math. Program*, Series A, vol. 3, pp. 493–511, February 2003.

[84] University of Washington, "Power systems test case archive," Dept. Elect. Eng., 1999. [Online]. Available: http://www.ee.washington.edu/research/pstca/rts/pg tcarts.htm

[85] J. M. S. Pinheiro, C. R. R. Dornellas, M. Th. Schilling, A. C. G. Melo, and J. C. O. Mello, "Probing the new IEEE reliability test system (RTS-96): HL-II Assessment," *IEEE Transactions on Power Systems*, vol. 13, no. 1, pp. 171-176, February 1998.

[86] T. Aigner and T. Gjengedal, "Detailed wind power production in northern Europe," in *Proc. Renewable Energy Conf. 2010*, Yokohoma, July 2010.

[87] Sandia National Laboratories, "Characteristics and technologies for long- vs. short-term energy storage: A study by the DOE energy storage systems program," SAND2001-0765, March 2001. [Online]. Available: http://prod.sandia.gov/techlib/access-control.cgi/2001/010765.pdf

[88] Sandia National Laboratories, "Energy storage system cost update: A study by the DOE energy storage systems program," SAND2011-2730, April 2011. [Online]. Available: http://prod.sandia.gov/techlib/access-control.cgi/2011/112730.pdf

[89] North American Electric Reliability Corporation, "Balancing and frequency control," January 2011. Available: http://www.nerc.com/docs/oc/rs/NERC%20Balancing%20and%20Frequency%20Control%20040520111.pdf

[90] Y. V. Makaror, "Wide-area storage and management system to balance intermittent resources in the Bonneville Power Administration and California ISO control areas," Pacific Northwest National Laboratory, June 2008. [Online]. Available: http://www.pnl.gov/main/publications/external/technical_reports/PNNL-17574.pdf

[91] M. L. Lazarewicz, "Integration of flywheel-based energy storage for frequency regulation in deregulated markets," *IEEE Power and Energy Society General Meeting*, July 2010.

[92] Pacific Gas and Electric, "Renewable generation model – results and model demonstration," October 2010. [Online]. Available: http://www.cpuc.ca.gov/NR/rdonlyres/7462FECF-81A3-490A-AAE7-56AB0A7D8EFE/0/PGECPUCWorkshopOct22v8Final.ppt